



# University of HUDDERSFIELD

## University of Huddersfield Repository

Ahmad, Shamsuddeen A.

Formulation and Analysis of Drug-Silica and Drug-Polymer Based Systems

### Original Citation

Ahmad, Shamsuddeen A. (2021) Formulation and Analysis of Drug-Silica and Drug-Polymer Based Systems. Doctoral thesis, University of Huddersfield.

This version is available at <http://eprints.hud.ac.uk/id/eprint/35544/>

The University Repository is a digital collection of the research output of the University, available on Open Access. Copyright and Moral Rights for the items on this site are retained by the individual author and/or other copyright owners. Users may access full items free of charge; copies of full text items generally can be reproduced, displayed or performed and given to third parties in any format or medium for personal research or study, educational or not-for-profit purposes without prior permission or charge, provided:

- The authors, title and full bibliographic details is credited in any copy;
- A hyperlink and/or URL is included for the original metadata page; and
- The content is not changed in any way.

For more information, including our policy and submission procedure, please contact the Repository Team at: [E.mailbox@hud.ac.uk](mailto:E.mailbox@hud.ac.uk).

<http://eprints.hud.ac.uk/>

# **Formulation and Analysis of Drug-Silica and Drug-Polymer Based Systems**

**Shamsuddeen Abdullahi Ahmad**

A thesis submitted to the University of Huddersfield in partial fulfilment of the requirements  
for the degree of Doctor of Philosophy

The University of Huddersfield

May 2021

## Abstract

Three mesoporous silica excipients (Syloid<sup>®</sup> silicas AL-1 FP, XDP 3050 and XDP 3150) were formulated with three model drugs known for their poor aqueous solubility, namely phenylbutazone, indomethacin and imipramine in an attempt to enhance the extent and rate of their dissolution. Although other forms of mesoporous silica have been investigated in previous studies, the effect of inclusion with these specific Syloid<sup>®</sup> silica-based excipients with phenylbutazone, indomethacin and imipramine are unknown. This work reports a significant enhancement for both the extent and rate of drugs release for all three forms of Syloid<sup>®</sup> silica at 1:1, 2:1 and 1:3 drug:silica ratios over a period of 45 minutes. An explanation for this increase was determined to be conversion from crystalline to the amorphous form and an enhanced drug loading ability within the pores. Differences between the release profiles of the three silicas was concluded to be a consequence of the physicochemical differences between the three forms. Overall, this study confirms that Syloid<sup>®</sup> silica-based excipients can be used to enhance dissolution, and potentially therefore bioavailability, for compounds with poor aqueous solubility, such as phenylbutazone, indomethacin and imipramine. In addition, it has been confirmed that drug release can be carefully tailored based on the choice of Syloid<sup>®</sup> silica and desired release profile.

The second part of this study investigated the effect of microwave heating through the application of microwave differential thermal analysis to eight model pharmaceutical compounds and a set of four model excipients. Benzocaine, haloperidol, ibuprofen, indomethacin, ketoprofen, naproxen, imipramine and phenylbutazone were analysed, along with four excipients, namely  $\beta$ -cyclodextrin, D-mannitol, stearic acid and Syloid<sup>®</sup> silica (XDP 3050) using microwave differential thermal analysis. Samples were heated by microwave irradiation at 5 °C/min to a minimum of 160 °C, held isothermally and then slowly cooled to room temperature. Thermal profiles were analysed and compared with data obtained using differential scanning calorimetry (DSC), x-ray powder diffraction (XRD) and hot stage microscopy (HSM). Overall, it was found that the process of microwave heating produced different thermal profiles to those seen using traditional, conductive heating. Investigating differences in thermal profiles can be a useful way to consider the effect of microwave induced heating on formulations which can, in turn, help guide formulation choices.

The latter part of this study describes the analysis and characterisation of polyvinylalcohol (PVA)-based hydrogel polymer beads, developed for the embolisation of vessels, specifically

focussing on the quantitative and qualitative aspects of water within such beads in the absence and presence of a model drug, namely imipramine. The utilisation of Microwave differential thermal analysis (MWDTA) for the characterisation of bound water within the polymer beads was unsuccessful because there was no cooling system and as a result, most of the water evaporated during the measurement. Following successful incorporation within the beads, thermogravimetric analysis (TGA) permitted determination of the total water content within the beads (96.8 %) and differential scanning calorimetry (DSC) indicated the water within the beads was apportioned as 15.8 % non-freezing, 25.1 % loosely bound and the remaining 55.9 % unbound. In the presence of drug, the size of the beads decreased with an average diameter reduction from 121.4  $\mu\text{m}$  to 78.5  $\mu\text{m}$ , coupled with a reduced total water content of 95.4 %, coupled with a reduced percentage of loosely bound water. This study confirms the ability of TGA and DSC to characterise the differing types of water within the beads and indicates the relative changes in water content in the presence of model drugs.

## **Acknowledgements**

Firstly, I would like to express my profound gratitude to my supervisors Prof. Laura Waters and Dr Gareth M.B. Parkes for all their support and guidance throughout my PhD, without whom it would not have been possible to complete the work. I would once more like to thank Prof. Laura Waters for her endurance, encouragement, motivation, dedication and immense knowledge that you have provided me, I could not have achieved this without you.

I would like to thank the University of Huddersfield for providing me with a tuition fee-waiver scholarship and Tertiary Education Trust Fund (TETFund) through Sokoto state university for giving me the living expenses funds to pursue doctoral degree at the school of applied sciences.

I would also like to thank members of our research group for sharing their great deal of knowledge, including the hardworking undergraduate students I have had the opportunity to work with, you made my journey productive and enjoyable. I would like to thank the team of technicians in the School of Applied Sciences for their endless support and assistance. I would personally like to appreciate Dr Gage Ashton and Dr Jim Rooney for their guidance and advice in solving many instrumental issues.

To my parents and siblings, thank you for supporting me throughout the period of this research and my life in general. Finally, to my wife, Maryam, I owe you everything for your unfaltering love, tolerance and support, and for making the last three years a truly enjoyable time to reflect upon.

## Table of Contents

Chapter 1: Introduction .....	1
1.1. Strategies to enhance dissolution .....	3
1.1.1. Hot melt extrusion (HME).....	4
1.1.2. Particle size reduction.....	5
1.1.3. Solvent evaporation technique.....	6
1.2. Formulation development and drug dissolution .....	7
1.2.1. Dissociation constant (pKa).....	9
1.2.2. Solid state and their effects on dissolution.....	10
1.3. Common techniques used in the analysis of pharmaceutical formulations .....	11
1.3.1. High performance liquid chromatography (HPLC) .....	11
1.3.2. Ultraviolet (UV) spectrophotometry.....	12
1.3.3. Infrared (IR) spectroscopy.....	14
1.4. Microwave formulation .....	15
1.4.1. Microwave theory .....	16
1.4.2. Microwave heating versus conventional heating.....	18
1.4.3. Microwave differential thermal analysis (MWDTA) .....	20
1.4.4. Thermal runaway.....	23
1.4.5. Heating of poorly coupling materials.....	24
1.4.6. Description of MWDTA instrument.....	24
1.5. Previous thermal analysis (TA) techniques .....	27
1.5.1 Differential thermal analysis (DTA).....	28
1.5.2 Differential scanning calorimetry (DSC).....	29
1.5.3 Thermogravimetric analysis (TGA).....	29
1.5.4. Hot stage microscopy (HSM).....	30
1.6. Transarterial Chemoembolisation (TACE) and DC Bead™ .....	31
1.6.1. Composition of DC Bead.....	32
1.6.2. DC Bead Chemistry.....	33
1.6.3. Drug loading and elution.....	35
1.7. Bound water analysis .....	36

1.8. Project aims.....	37
Chapter 2: Materials and methods .....	39
2.1 Materials .....	39
2.2 Methods.....	46
2.2.1 Preparation of physical mixtures of drugs- silicas .....	46
2.2.2. Microwave formulation.....	46
2.3 Characterisation methods.....	47
2.3.1 <i>In vitro</i> dissolution studies.....	47
2.4 Solid state characterisation .....	48
2.4.1 Differential scanning calorimetry (DSC) for solid-state characterisation.....	48
2.4.2 X-ray diffraction (XRD).....	49
2.4.3 Fourier transform infrared (FT-IR).....	49
2.4.4 Scanning electron microscopy (SEM).....	49
2.5. Preparation of binary mixtures of drugs-excipients.....	49
2.5.1. Microwave differential thermal analysis (MWDTA) of pharmaceutical compounds	50
2.5.2 Differential scanning calorimetry (DSC).....	50
2.5.3 Hot-stage microscopy (HSM).....	51
2.6. Imipramine loading into beads.....	51
2.6.1 Optical microscopy, bead sizing and water content estimation .....	51
2.7 Thermogravimetric analysis (TGA).....	52
2.8 Differential scanning calorimetry (DSC).....	52
Chapter 3: Microwave formulations of phenylbutazone (PhB), indomethacin (IMC) and imipramine hydrochloride (Imi) using three mesoporous silica excipients (Syloid <sup>®</sup> silicas AL- 1 FP, XDP 3050 and XDP 3150).....	54
3.1. Introduction.....	54
3.2. Results and discussion .....	56
3.2.1. Solid state characterisation of PhB formulation.....	56
3.2.1.1. Differential scanning calorimetry (DSC) .....	56
3.2.1.2. X-ray diffraction (XRD).....	61
3.2.1.3. Fourier transform infrared spectroscopy (FT-IR).....	65
3.2.1.4. Scanning electron microscopy (SEM).....	68
3.2.2. <i>In vitro</i> phenylbutazone release.....	71

3.2.3. Solid state characterisation of IMC.....	76
3.2.3.1 Differential scanning calorimetry (DSC) .....	76
3.2.3.2 X-ray diffraction (XRD).....	80
3.2.3.3 Fourier transform infrared spectroscopy (FT-IR).....	83
3.2.3.4. Scanning electron microscopy (SEM).....	86
3.2.4. <i>In vitro</i> indomethacin release.....	88
3.2.5. Solid state characterisation of Imipramine formulations .....	92
3.2.5.1 Differential scanning calorimetry (DSC) .....	92
3.2.5.2 X-ray diffraction (XRD).....	96
3.2.5.3 Fourier transform infrared spectroscopy (FT-IR).....	100
3.2.5.4. Scanning electron microscopy (SEM).....	103
3.2.6. <i>In vitro</i> imipramine release.....	105
3.3. Conclusions.....	109
Chapter 4. Microwave differential thermal analysis (MWDTA) of pharmaceutical compounds .....	111
4.1. Introduction.....	111
4.2. Results and discussion .....	113
4.2.1. MWDTA of silicon carbide (SiC).....	113
4.2.2. MWDTA of pharmaceutical compounds.....	114
4.2.2. Differential scanning calorimetry (DSC) of pharmaceutical compounds.....	125
4.2.3. X-ray diffraction (XRD) of pharmaceutical compounds .....	131
4.2.4. Hot stage microscopy (HSM) of pharmaceutical compounds .....	134
4.3. MWDTA of excipients .....	142
4.3.1. DSC for excipients.....	146
4.3.3. XRD for excipients.....	148
4.3.4. HSM for excipients.....	150
4.4. MWDTA of benzocaine and pharmaceutical excipients .....	153
4.4.1. DSC of benzocaine and pharmaceutical excipients .....	158
4.4.2. XRD of benzocaine and pharmaceutical excipients.....	161
4.4.3. HSM of benzocaine-excipient formulations.....	163
4.5. MWDTA of indomethacin and pharmaceutical excipients .....	167



4.5.1. DSC for IMC and pharmaceutical excipients.....	173
4.5.2. XRD of indomethacin and pharmaceutical excipients.....	178
4.5.3. HSM for IMC with excipients.....	180
4.6. Conclusions.....	184
Chapter 5: The DSC and TGA approach to study bound water restrained by polymer beads (DC Bead <i>MI</i> <sup>TM</sup> ).....	186
5.1. Introduction.....	186
5.2. Results and discussion .....	188
5.2.1. Drug loading evaluations.....	188
5.2.2 Optical microscopy.....	188
5.2.3 Water content analysis.....	190
5.2.3.1 Thermogravimetric analysis (TGA) .....	190
5.2.3.2 Differential scanning calorimetry (DSC) .....	191
5.3. Conclusions.....	193
Chapter 6: Conclusions and Future work.....	195
6.1. Conclusions.....	195
6.2. Future work.....	198
References.....	200

## List of Figures

Figure 1. 1. Mesoporous Syloid® silica (Biopharma-asia, 2020) .....	2
Figure 1. 2. The schematic illustration of Hot Melt extrusion process [26] .....	5
Figure 1. 3. The Biopharmaceutical Classification System (BCS) [50] .....	8
Figure 1. 4. Electric and magnetic field components in microwaves (Kappe et al., 2012a). ..	17
Figure 1. 5. Dipolar polarisation mechanism. Dipolar molecules try to align with an oscillating electric field (Kappe et al., 2012a).....	18
Figure 1. 6. Conventional heating (A) and microwave heating (B) highlighting the differing nature of the process (Kostas et al., 2017).....	19
Figure 1. 7. Illustration of thermal runaway under microwave heating i.e. where the temperature of the material rises rapidly even though the amount of microwave power is unchanged (Bedford, 2011).....	23
Figure 1. 8. Schematic diagram of MWDTA instrument .....	25
Figure 1. 9. Schematic diagram of the microwave components of the MWDTA instrument (G. Parkes, P. Barnes, et al., 2000). .....	26
Figure 1. 10. Heat-Assisted / MWDTA Sample cell – design (G. Parkes, P. Barnes, et al., 2000). .....	27
Figure 1. 11. Schematic of a typical DTA instrument (Wagner, 2013).....	28
Figure 1. 12. Available DC bead™ with their size ranges and colour (Swaine, 2018). .....	33
Figure 1. 13. DC Bead™ unloaded (A) and DC Bead™ loaded with doxorubicin (Dox) illustrating the intense colour change from blue to red (B) (Swaine, 2018).....	34
Figure 1. 14. DC bead™ mode of loading with doxorubicin (dox) and subsequent displacement of water through an ion exchange mechanism (Swaine, 2018). .....	35
Figure 1. 15. USP Type II dissolution apparatus (Swaine, 2018).....	36
Figure 2. 1. An example of the temperature and power profile for microwave formulation of indomethacin and Syloid® silica XDP 3050 (1:1). .....	47
Figure 2. 2. Dissolution apparatus used for analysing formulations.....	48
Figure 3. 1. DSC profiles for phenylbutazone (PhB) along XDP 3050 based physical mixtures (PM) and microwave formulations (MWF). (a) Pure PhB, (b) PM 1:1 (c) PM 2:1 (d) PM 1:3 (e) MWF 1:1 (f) MWF 2:1 and (g) MWF 1:3.....	56
Figure 3. 2. DSC profiles for phenylbutazone (PhB) along XDP 3150 based physical mixtures (PM) and microwave formulations (MWF). (a) Pure PhB, (b) PM 1:1 (c) PM 2:1 (d) PM 1:3 (e) MWF 1:1 (f) MWF 2:1 and (g) MWF 1:3.....	58
Figure 3. 3. DSC profiles for phenylbutazone (PhB) along AL1 FP based physical mixtures (PM) and microwave formulations (MWF). (a) Pure PhB, (b) PM 1:1 (c) PM 2:1 (d) PM 1:3 (e) MWF 1:1 (f) MWF 2:1 and (g) MWF 1:3.....	59
Figure 3. 4. XRD patterns for (a) PhB, (b) XDP 3050, (c) PM 1:1, (d) PM 2:1, (e) PM 1:3 (f) MWF 1:1, (g) MWF 2:1 and (h) MWF 1:3. ....	61
Figure 3. 5. XRD patterns for (a) PhB, (b) XDP 3150, (c) PM 1:1, (d) PM 2:1, (e) PM 1:3 (f) MWF 1:1, (g) MWF 2:1 and (h) MWF 1:3. ....	63
Figure 3. 6. XRD patterns for (a) PhB, (b) AL1 FP, (c) PM 1:1, (d) PM 2:1, (e) PM 1:3 (f) MWF 1:1, (g) MWF 2:1 and (h) MWF 1:3. ....	64

Figure 3. 7. FT-IR analysis of (a) PhB (b) XDP 3050, (c) MWF 1:1, (d) MWF 2:1, and (e) 1:3 drug-XDP 3050 formulations .....	65
Figure 3. 8. FT-IR analysis of (a) PhB (b) XDP 3150, (c) MWF 1:1, (d) MWF 2:1, and (e) 1:3 drug-XDP 3150 formulations .....	66
Figure 3. 9. FT-IR analysis of (a) PhB (b) AL1 FP, (c) MWF 1:1, (d) MWF 2:1, and (e) 1:3 drug-AL1 FP formulations.....	67
Figure 3. 10. Scanning electron microscope (SEM) images of (a) PhB, (b) XDP 3050 (c) XDP 3150, and (d) AL1 FP at x500 magnification .....	68
Figure 3. 11. SEM images at x500 of (a) PM of PhB and XDP 3050 (1:1), (b) PM of PhB and XDP 3050 (2:1), (c) PM of PhB and XDP 3050 (3:1). (d), PM of PhB and XDP 3150 (1:1), (e) PM of PhB and XDP 3150 (2:1), (f) PM of PhB and XDP 3150 (1:3). (g) PM of PhB and AL1 FP (1:1), (h) PM of PhB and AL1 FP (2:1), and (i) PM of PhB and AL1 FP (1:3). .....	69
Figure 3. 12. SEM images at x500 of (a) MWF of PhB and XDP 3050 (1:1), (b) MWF of PhB and XDP 3050 (2:1), (c) MWF of PhB and XDP 3050 (3:1). (d), MWF of PhB and XDP 3150 (1:1), (e) MWF of PhB and XDP 3150 (2:1), (f) MWF of PhB and XDP 3150 (1:3), (g) MWF of PhB and AL1 FP (1:1), (h) MWF of PhB and AL1 FP (2:1), and (i) MWF of PhB and AL1 FP (1:3). .....	70
Figure 3. 13. Release profiles for phenylbutazone (PhB), Syloid <sup>®</sup> XDP 3050 based formulations using microwave at 1:1, 2:1 and 1:3 drug to silica ratios. Each data point represents the mean of triplicate results ( $\pm$ SD).....	71
Figure 3. 14. Release profiles for phenylbutazone (PhB), Syloid <sup>®</sup> XDP 3150 based formulations using microwave at 1:1, 2:1 and 1:3 drug to silica ratios. Each data point represents the mean of triplicate results ( $\pm$ SD).....	73
Figure 3. 15. Release profiles for phenylbutazone (PhB), Syloid <sup>®</sup> AL1 FP based formulations using microwave at 1:1, 2:1 and 1:3 drug to silica ratios. Each data point represents the mean of triplicate results ( $\pm$ SD).....	75
Figure 3. 16. DSC profiles for indomethacin (IMC) along XDP 3050 based physical mixtures (PM) and microwave formulations (MWF). (a) Pure IMC, (b) PM 1:1 (c) PM 2:1 (d) PM 1:3 (e) MWF 1:1 (f) MWF 2:1 and (g) MWF 1:3.....	76
Figure 3. 17. DSC profiles for indomethacin (IMC) along XDP 3150 based physical mixtures (PM) and microwave formulations (MWF). (a) Pure IMC, (b) PM 1:1 (c) PM 2:1 (d) PM 1:3 (e) MWF 1:1 (f) MWF 2:1 and (g) MWF 1:3.....	78
Figure 3. 18. DSC profiles for indomethacin (IMC) along AL1 FP based physical mixtures (PM) and microwave formulations (MWF). (a) Pure IMC, (b) AL1 FP (c) PM 1:1 (d) PM 2:1 (e) PM 1:3 (f) MWF 1:1 (g) MWF 2:1 and (h) MWF 1:3 .....	79
Figure 3. 19. XRD patterns for (a) IMC, (b) XDP 3050, (c) PM 1:1, (d) PM 2:1, (e) PM 1:3 (f) MWF 1:1, (g) MWF 2:1 and (h) MWF 1:3. ....	80
Figure 3. 20. XRD patterns for (a) IMC, (b) XDP 3150, (c) PM 1:1, (d) PM 2:1, (e) PM 1:3 (f) MWF 1:1, (g) MWF 2:1 and (h) MWF 1:3. ....	81
Figure 3. 21. XRD patterns for (a) IMC, (b) AL1 FP, (c) PM 1:1, (d) PM 2:1, (e) PM 1:3 (f) MWF 1:1, (g) MWF 2:1 and (h) MWF 1:3. ....	82
Figure 3. 22. FT-IR analysis of (a) IMC (b) XDP 3050, (c) MWF 1:1, (d) MWF 2:1, and (e) 1:3 drug-XDP 3050 formulations .....	83
Figure 3. 23. FT-IR analysis of (a) IMC (b) XDP 3150, (c) MWF 1:1, (d) MWF 2:1, and (e) 1:3 drug-XDP 3150 formulations .....	84

Figure 3. 24. FT-IR analysis of (a) IMC (b) AL1 FP, (c) MWF 1:1, (d) MWF 2:1, and (e) 1:3 drug-AL1 FP formulations.....	85
Figure 3. 25. SEM images at x500 of (a) IMC (b) PM of IMC and XDP 3050 (1:1), (c) PM of IMC and XDP 3050 (2:1), (d) PM of IMC and XDP 3050 (3:1). (e), PM of IMC and XDP 3150 (1:1), (f) PM of IMC and XDP 3150 (2:1), (g) PM of IMC and XDP 3150 (1:3), (h) PM of IMC and AL1 FP (1:1), (i) PM of IMC and AL1 FP (2:1), and (j) PM of IMC and AL1 FP (1:3).	86
Figure 3. 26. SEM images x500 of (a) MWF of IMC and XDP 3050 (1:1), (b) MWF of IMC and XDP 3050 (2:1), (c) MWF of IMC and XDP 3050 (3:1), (d), MWF of IMC and XDP 3150 (1:1), (e) MWF of IMC and XDP 3150 (2:1), (f) MWF of IMC and XDP 3150 (1:3), (g) MWF of IMC and AL1 FP (1:1), (h) MWF of IMC and AL1 FP (2:1), and (i) MWF of IMC and AL1 FP (1:3).	87
Figure 3. 27. Release profiles for pure indomethacin (IMC) and indomethacin Syloid® XDP 3050-based formulations at 1:1, 2:1 and 1:3. Each data point represents the mean of triplicate results ( $\pm$ SD).	88
Figure 3. 28. Release profiles for pure indomethacin (IMC) and indomethacin Syloid® XDP 3150-based formulations at 1:1, 2:1 and 1:3. Each data point represents the mean of triplicate results ( $\pm$ SD).	90
Figure 3. 29. Release profiles for pure indomethacin (IMC) and indomethacin Syloid® AL1 FP-based formulations at 1:1, 2:1 and 1:3. Each data point represents the mean of triplicate results ( $\pm$ SD).	92
Figure 3. 30. DSC profiles for imipramine (Imi) along XDP 3050 based physical mixtures (PM) and microwave formulations (MWF). (a) Pure Imi, (b) PM 1:1 (c) PM 2:1 (d) PM 1:3 (e) MWF 1:1 (f) MWF 2:1 and (g) MWF 1:3.....	93
Figure 3. 31. DSC profiles for imipramine (Imi) along XDP 3150 based physical mixtures (PM) and microwave formulations (MWF). (a) Pure Imi, (b) PM 1:1 (c) PM 2:1 (d) PM 1:3 (e) MWF 1:1 (f) MWF 2:1 and (g) MWF 1:3.....	94
Figure 3. 32. DSC profiles for imipramine (Imi) along AL1 FP based physical mixtures (PM) and microwave formulations (MWF). (a) Pure Imi, (b) PM 1:1 (c) PM 2:1 (d) PM 1:3 (e) MWF 1:1 (f) MWF 2:1 and (g) MWF 1:3.....	95
Figure 3. 33. XRD patterns for (a) Imi, (b) XDP 3050, (c) PM 1:1, (d) PM 2:1, (e) PM 1:3 (f) MWF 1:1, (g) MWF 2:1 and (h) MWF 1:3. ....	97
Figure 3. 34. XRD patterns for (a) Imi, (b) XDP 3150, (c) PM 1:1, (d) PM 2:1, (e) PM 1:3 (f) MWF 1:1, (g) MWF 2:1 and (h) MWF 1:3. ....	98
Figure 3. 35. XRD patterns for (a) Imi, (b) AL1 FP, (c) PM 1:1, (d) PM 2:1, (e) PM 1:3 (f) MWF 1:1, (g) MWF 2:1 and (h) MWF 1:3. ....	99
Figure 3. 36. FT-IR analysis of (a) Imi (b) XDP 3050, (c) MWF 1:1, (d) MWF 2:1, and (e) 1:3 drug-XDP 3050 formulations .....	100
Figure 3. 37. FT-IR analysis of (a) Imi (b) XDP 3150, (c) MWF 1:1, (d) MWF 2:1, and (e) 1:3 drug-XDP 3150 formulations .....	101
Figure 3. 38. FT-IR analysis of (a) Imi (b) AL1 FP, (c) MWF 1:1, (d) MWF 2:1, and (e) 1:3 drug-AL1 FP formulations.....	102
Figure 3. 39. SEM images (x500) of (a) Imi (b) PM of Imi and XDP 3050 (1:1), (c) PM of Imi and XDP 3050 (2:1), (d) PM of Imi and XDP 3050 (3:1), (e), PM of Imi and XDP 3150 (1:1), (f) PM of Imi and XDP 3150 (2:1), (g) PM of Imi and XDP 3150 (1:3), (h) PM of Imi and AL1 FP (1:1), (i) PM of Imi and AL1 FP (2:1), and (j) PM of Imi and AL1 FP (1:3).....	103

Figure 3. 40. SEM images x500 of (a) MWF of Imi and XDP 3050 (1:1), (b) MWF of Imi and XDP 3050 (2:1), (c) MWF of Imi and XDP 3050 (3:1), (d), MWF of Imi and XDP 3150 (1:1), (e) MWF of Imi and XDP 3150 (2:1), (f) MWF of Imi and XDP 3150 (1:3), (g) MWF of Imi and AL1 FP (1:1), (h) MWF of Imi and AL1 FP (2:1), and (i) MWF of Imi and AL1 FP (1:3). .....	105
Figure 3. 41. Release profiles for pure imipramine (Imi) and imipramine Syloid® XDP 3050-based formulations at 1:1, 2:1 and 1:3. Each data point represents the mean of triplicate results ( $\pm$ SD). .....	106
Figure 3. 42. Release profiles for pure imipramine (Imi) and imipramine Syloid® XDP 3150-based formulations at 1:1, 2:1 and 1:3. Each data point represents the mean of triplicate results ( $\pm$ SD). .....	107
Figure 3. 43. Release profiles for pure imipramine (Imi) and imipramine Syloid® AL1 FP-based formulations at 1:1, 2:1 and 1:3. Each data point represents the mean of triplicate results ( $\pm$ SD). .....	108
Figure 4. 1. Microwave differential thermal analysis (MWDTA) of silicon carbide (SiC) heating at 5 °C/min to 300 °C then cooled at -5 °C/min to 30 °C. .....	114
Figure 4. 2. Temperature and associated power profile for benzocaine heated at 5 °C/min to 160 °C and then cooled to 40 °C .....	115
Figure 4. 3. Microwave differential thermal analysis (MWDTA) of benzocaine heating at 5 °C/min to 160 °C for the first and second run (FR and SR) and cooling at -5 °C/min to 40 °C in both cases. .....	116
Figure 4. 4. Microwave differential thermal analysis (MWDTA) of haloperidol heating at 5 °C/min to 200 °C for the first (FR) and second (SR) run then cooling at 5 °C/min to 40 °C in both cases. .....	117
Figure 4. 5. Microwave differential thermal analysis (MWDTA) of indomethacin heating at 5 °C/min to 200 °C for the first (FR) and second (SR) run then cooled at 5 °C/min to 40 °C in both cases. .....	119
Figure 4. 6. Microwave differential thermal analysis (MWDTA) of ketoprofen heated at 5 °C/min to 160 °C then cooled to 40 °C for the first (FR) and second (SR) run. .....	120
Figure 4. 7. Microwave differential thermal analysis (MWDTA) of phenylbutazone heated at 5 °C/min to 160 °C then cooled to 40 °C for the first (FR) and second run (SR). .....	121
Figure 4. 8. Microwave differential thermal analysis (MWDTA) of ibuprofen heated at 5 °C min <sup>-1</sup> to 160 °C then cooled to 40 °C for the first (FR) and second (SR) run. .....	122
Figure 4. 9. Microwave differential thermal analysis (MWDTA) of naproxen heating at 5 °C/min to 200 °C for the first and second run (FR and SR) and cooling at 5 °C/min to 40 °C in both cases. .....	123
Figure 4. 10. Microwave differential thermal analysis (MWDTA) of imipramine heating at 5 °C/min to 180 °C for the first and second run (FR and SR) and cooling at 5 °C/min to 40 °C in both cases. .....	124
Figure 4. 11. DSC thermograms of; (a) Benzocaine first run (FR) and (b) Benzocaine second (SR) .....	126
Figure 4. 12. DSC thermograms of; (a) Haloperidol first run (FR) and (b) Haloperidol second run (SR), .....	127
Figure 4. 13. DSC thermograms of; (a) Indomethacin first run (FR), and (b) Indomethacin second run (SR). .....	128

Figure 4. 14. DSC thermograms of; (a) phenylbutazone first run (FR), (b) phenylbutazone second (SR), (c) ketoprofen first run (FR), (d) ketoprofen second run (SR), (e) Ibuprofen first run (FR), and (f) Ibuprofen second run (SR) .....	129
Figure 4. 15. DSC thermograms of; (a) naproxen first run (FR), (b) naproxen second (SR), (c) imipramine first run (FR), (d) imipramine second run (SR).....	130
Figure 4. 16. XRD patterns of; (a) benzocaine first run (FR), (b) benzocaine second (SR), (c) haloperidol first run (FR), (d) haloperidol second run (SR), (e) indomethacin first run (FR) and (f) indomethacin second run (SR).....	131
Figure 4. 17. XRD patterns of; (a) phenylbutazone first run (FR), (b) phenylbutazone second (SR), (c) ketoprofen first run (FR), (d) ketoprofen second run (SR), (e) ibuprofen first run (FR) and (f) ibuprofen second run (SR) .....	133
Figure 4. 18. XRD patterns of; (a) naproxen first run (FR), (b) naproxen second (SR), (c) imipramine first run (FR) and (d) imipramine second run (SR).....	134
Figure 4. 19. Microscope images and optical data of a sample of benzocaine heated from 30 to 160 °C as a function of temperature.....	135
Figure 4. 20. Microscope images and optical data of a sample of haloperidol heated from 30 to 200 °C as a function of temperature.....	136
Figure 4. 21. Microscope images and optical data of a sample of indomethacin heated from 30 to 200 °C as a function of temperature.....	137
Figure 4. 22. Microscope images and optical data of a sample of phenylbutazone heated from 30 to 160 °C as a function of temperature.....	138
Figure 4. 23. Microscope images and optical data of a sample of ketoprofen heated from 30 to 160 °C as a function of temperature.....	139
Figure 4. 24. Microscope images and optical data of a sample of ibuprofen heated from 30 to 160 °C as a function of temperature.....	140
Figure 4. 25. Microscope images and optical data of a sample of naproxen heated from 30 to 200 °C as a function of temperature.....	141
Figure 4. 26. Microscope images and optical data of a sample of imipramine heated from 30 to 200 °C as a function of temperature.....	142
Figure 5. 1. Size (A) and volume (B) distribution of bland DC Bead <i>MI</i> , 10 mgmL <sup>-1</sup> , 25 mgmL <sup>-1</sup> , and 50 mgmL <sup>-1</sup> drug loaded beads.....	189
Figure 5. 2. Microscope images of DC Bead <i>MI</i> after loading overnight. A) Bland beads. B) 10 mgmL <sup>-1</sup> loading. C) 25 mgmL <sup>-1</sup> loading. D) 50 mgmL <sup>-1</sup> loading. The scale bar is 500 µm. ....	190
Figure 5. 3. A TGA sample profile for beads alone (solid line) and imipramine with beads (dashed line) indicating the associated mass loss from water.....	191
Figure 5. 4. DSC profiles for water, DC Bead <i>MI</i> and DC Bead <i>MI</i> drug loaded.....	192

## List of Tables

Table 2. 1: The physicochemical properties of the Syloid® silicas used in this study (Grace, September, 2015; Laura J Waters et al., 2018). .....	40
Table 2. 2: Physicochemical properties of the chemicals used.....	40
Table 4. 1: Physicochemical data and DSC peak values for the melting ( $T_m$ ) and recrystallisation ( $T_r$ ) of eight compounds and four excipients.....	125
Table 4. 2: A summary of DSC peak values for the melting ( $T_m$ ) and recrystallisation ( $T_r$ ) of benzocaine with four excipients.....	158
Table 4. 3: A Summary of DSC peak values for melting ( $T_m$ ) and recrystallisation temperatures ( $T_r$ ) of indomethacin with four excipients. ....	174
Table 5. 1: Drug structure and loading amount and efficiency in 1 mL of DC Bead <i>MI</i> (n=3) .....	188
Table 5. 2: Data for bead sizes and estimated water fraction in beads .....	189

## Abbreviations

API	Active pharmaceutical ingredients
ATR	Attenuated total reflection
AMPS	Acrylamido methyl propane sulfonate
BET	Brunauer-Emmett-Teller
BJH	Barrett, Joyner and Halenda
BZ	Benzocaine
Cu	Copper
DSC	Differential scanning calorimetry
D-man	D-mannitol
DTA	Differential thermal analysis
DDED	Drug delivery embolization device
DTGA	Differential thermogravimetric analysis
Dox	Doxorubicin
DEB	Drug eluting beads
FR	First run
FDA	Food and drug administration
FTIR	Fourier transform infrared spectroscopy
HPLC	High performance liquid chromatography
Halo	Haloperidol
HSM	Hot stage microscopy
IBU	Ibuprofen
IMC	Indomethacin
IMI	Imipramine
IVIVC	<i>In vitro in vivo</i> correlation
Keto	Ketoprofen
Log P	Logarithm of the Partition Coefficient



MWDTA	Microwave differential thermal analysis
MWs	Microwaves
MWF	Microwave formulation
$M_w$	Molecular weight
NMR	Nuclear magnetic resonance
NPX	Naproxen
PHBU	Phenylbutazone
PM	Physical mixing
PVA	Polyvinyl alcohol
PEG	Polyethylene glycol
PBS	Phosphate buffer saline
RLI	Reflected light intensity
SA	Stearic acid
SYL	Syloid
SiC	Silicon carbide
SD	Standard deviation
SR	Second run
SEM	Scanning electron microscopy
TGA	Thermogravimetric analysis
TETFund	Tertiary education trust fund
TA	Thermal analysis
$\tan \delta$	Loss tangent
TACE	Transarterial chemoembolisation
$T_g$	Glass transition
$T_m$	Melting temperature
$T_r$	Recrystallisation temperature
USP	United states pharmacopeia
UV	Ultraviolet radiation
XRD	X-ray diffraction
$\beta$ -CD	Beta-cyclodextrin

$\epsilon'$	Dielectric constant
$\epsilon''$	Dielectric loss
$\Delta T$	Temperature difference
$\Lambda$	Wavelengths

## **Publications and Conference presentations arising from this thesis**

### **Publications**

1. Enhancing the dissolution of phenylbutazone using Syloid<sup>®</sup> based mesoporous silicas for oral equine applications. Laura J. Waters, John P. Hanrahan, Joseph M. Tobin, Catherine V. Finch, Gareth M.B. Parkes, Shamsuddeen A. Ahmad. Journal of Pharmaceutical Analysis, 8(3), 181-186: ISSN: 2095-1779, 2018
2. Predicting the suitability of microwave formulation using microwave differential thermal analysis (MWDTA). Laura J. Waters, Shamsuddeen, A. Ahmad, and Gareth M.B. Parkes. Journal of Thermal Analysis and Calorimetry, 136(4), 1-10: ISSN: 1588-2926, 2019

### **Contributions**

1. Introduction, materials, methods, data acquisition and results analysis
2. Introduction, materials, methods data acquisition and data analysis

### **Published material in thesis**

1. Chapter 1: Section 1.0, 1.1 and 1.2.

Chapter 2: Section 2.1, 2.3.1, 2.4.2 and 2.4.3

Chapter 3: Section 3.1, 3.2, 3.2.1, 3.2.2.3, 3.2.2.4 and 3.3

2. Chapter 1: Section 1.5

Chapter 2: Section 2.1, 2.2.1, 2.2.2, 2.5.1 and 2.5.3,

Chapter 4: Section 4.1, 4.2.2, 4.2.3 and 4.2.5,

Section 4.4, 4.4.1 and 4.4.3

Section 4.6

## **Conference Presentations**

1. Microwave thermal analysis (MWTA) of indomethacin interactions with some pharmaceutical excipients. 10<sup>th</sup> International PharmSci Conference. University of Greenwich, London, 2019.
2. Novel technique for investigating thermal transitions of API-excipients interaction using microwave thermal analysis (MWTA). The pharmaceutical analysis research awards and careers symposium. Royal Society of Chemistry, London, UK, 2019.

## **Contributions**

1. Introduction, materials, methods, data acquisition and data analysis
2. Introduction, materials, methods data acquisition and data analysis

## **Chapter 1: Introduction**

Mesoporous silica materials have been used as carriers for oral delivery of poorly water-soluble drugs since their emergence in 1970. The pore diameter of these materials is between 2 – 50 nm which gives them the name ‘‘Mesoporous’’, they are arranged in a crystallographic sense meaning the mesopores are identical in size and organised in a uniform manner in the silica matrix which itself is amorphous [1]. They have a high surface area as one of their unique advantages, adjustable particle size, flexible morphology, large pore volume, excellent biocompatibility, facile surface functionalisation and biodegradation [2]. These excellent properties make the silica materials appropriate for a wide range of applications in drug delivery and development, catalysis, as an adsorbent in environmental studies and chromatography [3-5].

A large number of drugs exhibit poor solubility, causing lots of challenges in formulation, and in some cases, because of this, drug candidates are rejected during the development processes [6]. Poor solubility results in low level bioavailability of drugs and therefore improving the oral bioavailability without affecting the pharmaceutical activity and stability creates one of the challenges in the pharmaceutical industry. Several traditional strategies to modify drug release have been developed over the years including gelatin/non-gelatin capsules [7], co-solvents, solid dispersions, salt formations, lipid-based formulations [8, 9], mesoporous silica materials [10, 11], liposomes [12], inclusion complexes such as cyclodextrins [13], polymers [14] and many others such as nanocarriers [15]. Such formulations have successfully created a wide variety of drug release profiles with a range of positive impacts such as reducing dosing intervals or side effects, in some cases increasing bioavailability and generally increasing patient compliance. However, even with the strategies previously considered, some drugs continue to present formulation issues and still require the development of a suitable modified release formulation to enhance their drug release profiles. Compared with these strategies,

silica-based substances have attracted lots of attention as novel drug carriers due to their textural and structural features, as can be seen in Figure 1.1.

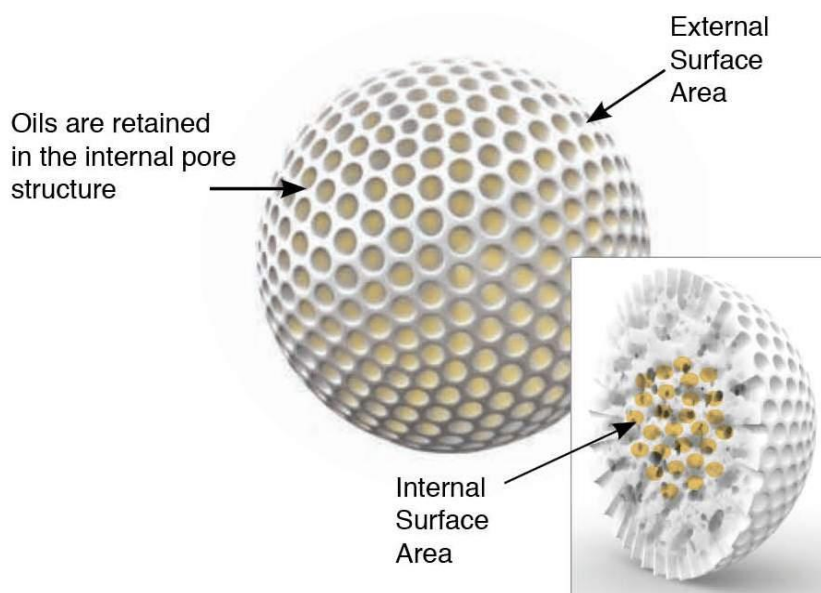


Figure 1. 1. Mesoporous Syloid® silica [16]

One particular category of mesoporous silicas where only very limited studies have been conducted to date is regarding Syloid® silica-based formulations. These forms of silica have a highly developed network of mesopores that provide access to the large surface area, i.e. a combination of a high adsorption capacity, along with a desirable pore size and surface morphology. For these reasons, these silicas tend to be used to improve the flow properties of pharmaceuticals where liquid ingredients can be converted into free-flowing powders. Although these properties are beneficial, their suitability to enhance dissolution has only briefly been considered (by publication) for two forms of Syloid® silica (244 and AL-1FP) with two model drugs, namely indomethacin [17] and itraconazole [18]. Interesting, for both compounds an enhancement in the rate, and extent of dissolution was observed in both studies. Yet surprisingly, other forms of Syloid® silica have not yet been considered even though they may provide a plethora of advantages for drug-loading formulations.

## **1.1. Strategies to enhance dissolution**

Appropriate excipients have to be incorporated into formulations with suitable processing techniques in order to utilise mesoporous silica materials in oral drug delivery of poorly water-soluble drugs. The growing number of research papers concentrating on the formulation of these systems is an indication of the growing interest in these drug delivery systems. Following an earlier report by Linnell et al., several strategies have attempted to use conventional methods to incorporate materials with poorly water-soluble drugs. Methods such as an immersion method and melting of drug molecules into the silica has been reported [19]. Unfortunately, this strategy is economically challenging, laborious and non-automatic on an industrial scale but rather suitable for small sample batches. Another issue is that in the filtration method [20], there is a high risk of crystallisation on the surfaces of the particles. Regarding the adsorption method [21], small drug particles on the surface of large excipients has been a successful strategy for low-dose drugs. Other options such as reduction of particle size to nanoscale [22], generation of amorphous forms and co-crystallisation [23], physical mixtures and microwave oven heating [6], spray drying and solid dispersions [24] as well as the use of buffers [25] have all been previously reported for the formulation of poorly water soluble drugs with mesoporous silica.

A limited number of studies have attempted to use other drug carriers to incorporate materials with poor water solubility, such as mannitol formulated with indomethacin and nifedipine as reported by Saffari et al. [22] and found that an improved product was the result of this method. Loratadine was also formulated with cyclodextrin derivatives and cyclodextrin was demonstrated to enhance the dissolution rate and oral bioavailability of the drug [26]. One study has successfully enhanced dissolution through the creation of a solid dispersion with polyethylene glycol (PEG) 8000 [27]. However, there is still a clear need for developing

alternative formulations that can achieve an even greater enhancement in release of active compounds. Other techniques reported include;

### **1.1.1. Hot melt extrusion (HME)**

Among several methods used to produce solid dispersions, HME is one of them. In this technique, the polymer matrix and the active pharmaceutical ingredients (API) are combined to produce a physical mixture at the same time accompanied by heating cycle which produces a homogeneous dispersion [28]. In order to employ this method, certain parameters need to be considered as they contribute significantly to the standard of the final formulation. These parameters include barrel design, die geometry, temperature, screw speed, feed rate and shear force [29]. The schematic illustration of this technique is shown in Figure 1.2. HME technique offers several benefits over other conventional methods, such as, fewer processing steps, solvent free and it is one step. This method can improve the bioavailability by dispersing the API at the molecular level because compression is not required. However, despite several advantages, this technique has some certain limitations that could restrict its use in the pharmaceutical industry including the possible exclusion of thermo-labile drugs due to high processing temperatures involved and the requirement of the high energy input when compared to other amorphous formulation techniques [28, 30]. This technique has gained popularity because it has successfully been applied to manufacture various pharmaceutical drug delivery systems such as nanocrystals [31], granules [32], topical and transdermal delivery systems [33] and solid-lipid nanoparticles [34].



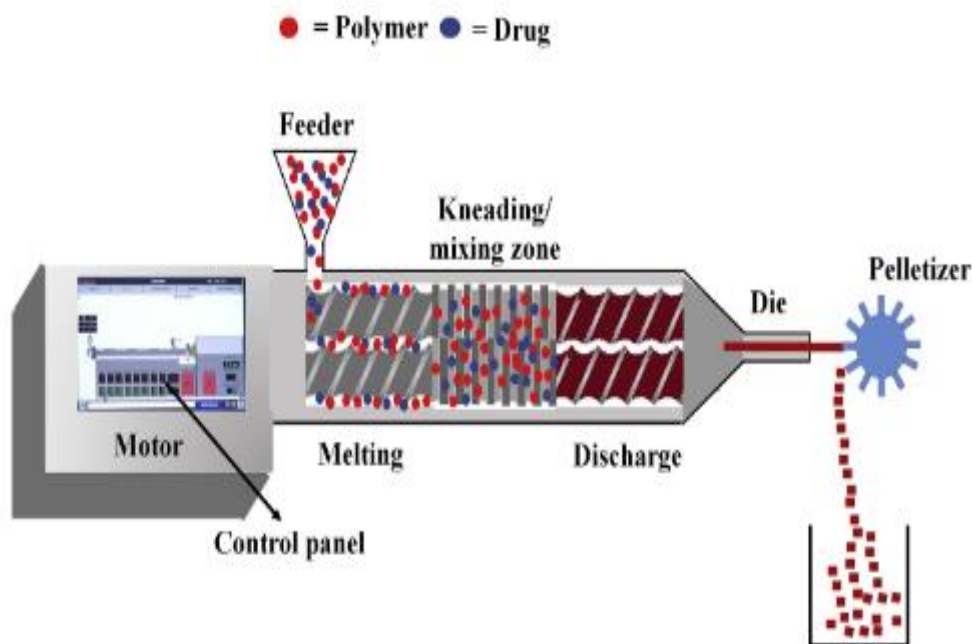


Figure 1. 2. A schematic illustration of hot melt extrusion process [33]

### 1.1.2. Particle size reduction

Essentially, dissolution is related to particle size because reducing the particle size will provide a larger surface area which will result in an enhanced dissolution rate owing to the improved solvation of the solute [24]. The technique of particle size reduction is classified in bottom-up and top-down approaches, depending on the substance to start with. Some of the advantages of the bottom-up technique include its processing time which is very short, low cost and better size control when compared to the top down approach [35].

In confined liquid impinging, drug particles are mixed rapidly and produced in a confined mixing chamber using two liquid streams of solution containing drug and anti-solvent [36]. Precipitation occurs in this process, due to super saturation by introducing a solution and anti-solvent in the chamber at the crossing of the micro-channels. Several factors can affect the narrow size distribution and ultra-fine particle disposition such as the liquid concentration, temperature, reactants flow rate, jet velocity and operating parameters of the jets geometry [37]. The micronised method to improve the solubility and permeability of low aqueous

solubility drugs including griseofulvin, felodipine and digoxin has been successfully proven [38]. Using mechanical pulverisation while jet milling, the micronised drug particles can be obtained, pin milling and ball milling are utilised commonly also. Agglomeration of drug particles can sometimes result through micronisation which by reducing the available surface area can decrease the dissolution rate. Though, to avoid such issues, surface active agents have been applied previously [39].

### **1.1.3. Solvent evaporation technique**

Drug and a carrier are dissolved in a solvent to form a homogenous solution followed by evaporation of the solvent in this technique [40]. For thermo-labile drugs, this is a technique of choice [41]. The solvent evaporation method for solid dispersion was developed by Nakamura and Tachibana in 1965 to solubilise polyvinylpyrrolidone and  $\beta$ -carotene using chloroform as a solvent. By solidification rate, the physical state of the API in the resultant solid dispersion is determined [42]. By rapid evaporation of the solvent, fast solidification guarantees the amorphous content of drug [43].

Several approaches have been used previously in removing the solvent using this technique including heating on plate [44], rotary evaporation, vacuum drying, freeze drying and spray drying [39, 40]. Most commonly used solvents in this technique include water, methanol, methylene chloride, acetone, and ethyl acetate. However, most of these organic solvents are toxic in nature which is a major drawback of the technique [40]. Other limitations of this method include high cost of production and protection against explosion, environmental issues, physical instability of the solid dispersion developed as a result of solvent residue among others [43].

These techniques have limitations including: solvent residues using the solvent technique, thermal instability using the melting technique, the low *in-vivo-in-vitro* correlation, the

recrystallisation of the API in the developing process, and drug precipitation in dissolution media owing to super saturation [43], all of these limitations can result in a decreased dissolution rate.

## **1.2. Formulation development and drug dissolution**

Traditionally, drug delivery has been administered in various forms including infusion, inhalation, topical application and injection [44]. The most preferred route of drug administration is the oral delivery route which accounts for more than a 60 % share of the worldwide drug delivery market. The high degree of patient compliance and convenience of the drug administration make it the most appropriate and frequent route of drug delivery [45]. This delivery route is not free from challenges which can result in poor bioavailability [46]. The main factors affecting the oral delivery of various existing drugs are poor solubility and intrinsic dissolution rate (i.e., mass of the drug dissolved per unit time and area). New chemical entities, about 40 % of them generated via discovery of drug, display poor water solubility [45]. In most cases, such compounds are classified in Class II or IV as per the biopharmaceutical classification system (BCS) [47] and in most cases their oral delivery results in poor bioavailability, lack of dose proportionality and erratic absorption [48]. Another factor that affects the oral bioavailability of many drugs is poor gastrointestinal permeability. Compounds with high membrane permeability but low solubility are classified as BCS Class II drugs [49]. Solubility among the physicochemical properties is of prime importance in drug development as low water solubility limits the efficacy of drugs. Molecules of the drug need to dissolve and permeate through the gastrointestinal tract (GIT) in order to achieve optimal success with oral administration [49]. Combining these two factors, namely, permeability and solubility describes the basis of BCS. In order to understand the physicochemical and biopharmaceutical properties of drugs, the BCS is the main tool, it is utilised when developing products and in

decision making [36, 39, 47]. Four different drug groups are classified according to BCS as illustrated in Figure 1.3.

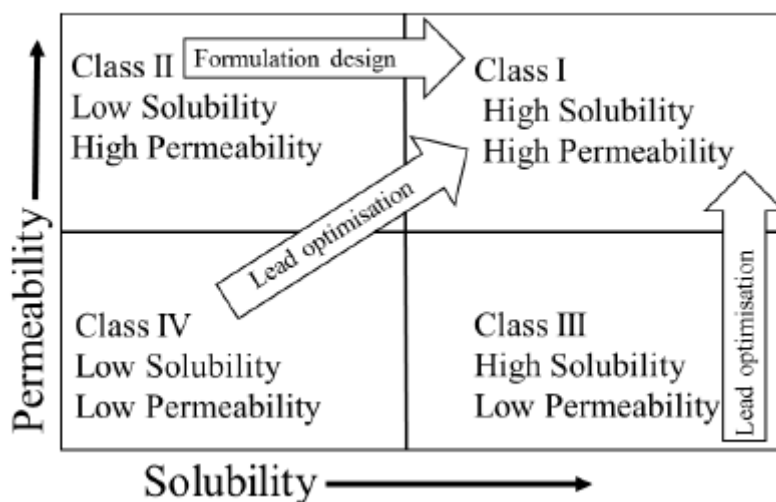


Figure 1. 3. The Biopharmaceutical Classification System (BCS) [47]

The definitions for the BCS according to Alam et al., [49] and Langham [50] are;

1. A drug substance is considered as highly soluble if the highest dose strength of the immediate product release is soluble in 250 mL or less of aqueous media pH range of 1 – 7.5.
2. A drug substance is considered as highly permeable when the absorption extent in humans is 90 % or more of the dose administered based on a weight – balance discovery or when compared with an intravenous dose reference.
3. A drug substance is considered as rapidly dissolving if no less than 85 % of the amount of the drug substance dissolves in 30 min using USP apparatus I at 100 rpm or USP apparatus II at 50 rpm in a volume of less than or equal to 900 mL in any of the following media: 1 N HCl, a pH 6.8 buffer or a pH 4.5 buffer, or simulated intestinal fluids.

In gastrointestinal fluids, drugs need to dissolve to permeate the gut wall, pass through the liver without being inactivated and reach the systematic blood circulation in order to produce a response pharmacologically which requires adequate aqueous solubility [46]. As a result, dissolution rate is often the most important factor in controlling a drugs bioavailability.

### **1.2.1. Dissociation constant (pKa)**

At different pH values, the extent of ionisation of an ionisable drug molecule can be described by the drug's pKa (acid dissociation constant). The pKa is a very essential chemical parameter in drug discovery. This is because in pharmaceutical formulations it helps in determining the ionisation profile of a material and predict the behaviour of drugs and their pharmacokinetic properties such as charge interaction with the target site, distribution in tissue and the permeability through biological membranes [51, 52]. On some essential physicochemical properties such as solubility and lipophilicity, the pKa can reveal an impact on such properties which could in turn affect the absorption and dissolution rate of the drug from the gastrointestinal tract [53].

A neutral complex is formed when an ionisable drug is combined with a counter ion, this is straightforward to administer and allows the refinement of its physicochemical properties. Utilising different species of ionisation of a drug can produce a series of compounds with the goal of enhancing the solubility and dissolution rate of drug [52]. Moreover, the choice of excipients for a drug, also in view of its medical administration, must always account for the physicochemical parameters of the drug.

The variables of the pKa are of great importance since the drugs transport into the cells and across membranes is a function of physicochemical properties. The amount of material found in the unionised form and ionised form is a function of its pKa and of the pH of the surrounding medium [52]. As a result of this, the absorption of the drug with the pH is influenced

accordingly. The ionised form normally has greater aqueous solubility while the unionised form is more lipophilic [54]. Several approaches has been reported for pKa determination including potentiometric titration which depends on the molecule possessing high aqueous solubility [55] and capillary electrophoresis which involves measurement of the mobility of different ionised species eluted through a capillary under the influence of an electric field [56].

### **1.2.2. Solid state and the effect on dissolution**

The most influential factor once the drug substance has been identified is the solid-state selection when considering the development of a solid drug formulation. A variety of forms may exist in the solid state and each form will have different physicochemical properties including stability, dissolution rate, surface energy, crystal habit, density, compressibility and flowability [57]. Two substances that have the same chemical composition, but the lattice structure is different, are said to be polymorphs and the phenomenon is known as polymorphism [39, 40]. Pharmaceutical companies have invested much time and money into the determination of polymorph stability hierarchy because of the effect that the solid state has on a drug and its properties.

The majority of commercially available drugs are marketed in the lowest energy crystalline form because it is the most stable form thermodynamically. When considering the wide range manufactured, and long period of storage for both the bulk drug substance and final product, this is of exceptional importance, because it is essential to be able to guarantee that the performance of the drug is not affected after such treatment [50]. Compounds when condensed into an ordered pattern form crystals. They must possess a high degree of mobility for ordering to occur. When a sample is in liquid form, these conditions occur, in the vapour state or in an amorphous matrix [57]. To enhance the dissolution of poorly water-soluble drugs, lots of consideration has been given to co-crystals. These are defined as a crystalline substance comprising of at least two or more different components [58].

Unlike crystalline substances, amorphous materials are high energy substances lacking a crystal lattice. These materials are highly soluble and usually have a faster dissolution rate than their crystalline counter parts, and so to enhance the bioavailability of poor aqueous solubility compounds, as a strategy, they offer an alternative [57]. Amorphous materials tend to change structure with time because they are thermodynamically unstable, first by relaxation and ultimately by crystallisation. Lots of formulations are made in an amorphous form against the risk of change upon storage [59].

### **1.3. Common techniques used in the analysis of pharmaceutical formulations**

There are several techniques used in the analysis of pharmaceutical formulations, the most commonly used ones include the following;

#### **1.3.1. High performance liquid chromatography (HPLC)**

In the pharmaceutical industry chromatographic techniques are used often to assess safety, efficacy and quality of drug formulations. In the chromatography method, the sample components are distributed between the mobile phase (liquid or gas) and stationary phase (solid or liquid) [60, 61]. The separation may be based on ion-exchange, adsorption or partition, or based on other differences in the physicochemical properties of the molecule. Among various types of chromatographic techniques used in pharmaceutical analysis, HPLC is the most used because it has many advantages such as low detection limit, good accuracy, high sensitivity, specificity and obvious separation effect [62].

HPLC is used for separating mixtures, either to analyse the mixture or to separate required products from others in a reaction mixture. It can also be used to find the relative amounts of different components in a mixture. This form of separation usually occurs when the sample interacts with the mobile and stationary phases. The various parts of the sample are separated

based on their polarities i.e. samples having different levels of affinity for the mobile phase, resulting in migration through the column at different speed [63].

HPLC works on the same principle as paper chromatography, a liquid called the mobile phase moves through the solid stationary phase. If a mobile phase is more polar than the stationary phase, the more polar component of a mixture will tend to move more quickly than the less polar one [64].

In HPLC, the stationary phase is a solid packed into a column, this column contains silica particles to which hydrocarbons are attached making the stationary phase non-polar. In this technique, the liquid is forced through the column by high pressure pumps. The reservoir holds the solvent, and two solvents can be mixed in any proportion to give a mixture, the liquid phase must be of a suitable polarity for the separation that is being done. A good example is water which is very polar and ethanenitrile which is less polar. The pump produces a pressure of 15000 kPa i.e. 150 times that of the atmosphere [63]. If a single sample is to be run, it is injected into the solvent stream in the injection port. Alternatively, several samples can be run in succession by loading them into an auto sampler which will run them in order without any human intervention. The pumps force the mixed solvents through the column and the solvent emerges from the column carrying the separated components of the mixture which then passes into the detector. The time that each component takes to pass through the column is called retention time and can be used to help identify compounds [64].

### **1.3.2. Ultraviolet (UV) spectrophotometry**

UV-visible spectrophotometry gives information about electronic transitions in atoms and molecules. Spectra are produced when electrons in molecules or atoms move from a lower energy level to higher energy level. In doing so, the absorbed energy is equal to the gap between



the two levels. Transition metal compounds and organic dyes are coloured and absorbed in the visible regions while those that absorb only in the ultraviolet region are colourless [65].

A typical UV-vis spectrophotometer consists of a light source, a monochromator and a detector. There are two light sources inside the UV-vis spectrophotometer, one giving out visible light and the other one ultraviolet. A Deuterium lamp is usually the light source which emits the electromagnetic radiation in the UV region of the spectrum. A second source of light is tungsten which is used for wavelengths in the visible region. The monochromator contains a diffraction grating that splits the beam of light into its constituent wavelengths. Different wavelengths correspond to different colours (about 700 nm for red and 400 nm for blue). Wavelengths shorter than about 350 nm are called ultraviolet, shorter wavelengths have higher energy [66, 67].

The source produces white light that includes all wavelengths or colours. The instrument scans through the spectrum, sending different wavelengths of light through the sample in sequence, this is done by the grating which rotates. A single wavelength passes into the modulator which consists of a rotor with mirrors on it, this splits the light into two beams. One beam passes through the sample cell while the other passes through the reference cell for a double beam instrument. Both sample and the reference beam are directed by mirrors on to a detector which compares their intensities and sends a signal proportional to the ratio of their intensities to the computer that controls the instrument. The logarithm of this ratio gives a quantity called absorbance which is a measure of how much light is being absorbed by the sample at that wavelength [66].

UV spectra are usually run on solutions as light does not normally pass through **some** solid samples. To run the spectrum in a UV spectrophotometer, solvent is placed in a cuvette to act as a blank (a reference), the cuvette may be made of glass or plastic if only the visible region

of the spectrum is required. Quartz cuvettes are needed for work in the ultraviolet range because glass and plastic absorb UV light. A solution of the sample is placed in the second cuvette, the blank and the sample are placed in the sample holders. The lid is closed to prevent the light from the laboratory from interfering in the spectrum. The wavelength required and scanning speed are selected before scanning [66, 68].

### **1.3.3. Infrared (IR) spectroscopy**

IR spectroscopy helps analysts to identify the functional groups present in a compound. It helps in finding the structure of a compound. Almost any molecule having covalent bonds, whether inorganic or organic, absorbs several frequencies of electromagnetic radiation in the IR region of the electromagnetic spectrum (EMS) [69]. This region lies at wavelengths longer than those associated with visible light, which is found from approximately 400 - 800 nm ( $1 \text{ nm} = 10^{-9}$ ), but lies at wavelengths shorter than those associated with microwaves which are larger than 1 mm. Most bonds absorb energy in the IR region of the EMS which corresponds to heat, such as OH, C=O, NH, C-H, C=C which absorb at a particular frequency and this allows compounds to be identified. IR spectra are a plot absorbance against wavenumbers measured per centimetre ( $\text{cm}^{-1}$ ) which are proportional to the frequency [65].

All IR instruments have a source of IR radiation which is a coil of wire surrounded by a ceramic capsule which is heated electrically so that it gives out IR radiation (heat) over a whole range of frequencies. The IR radiation goes by a series of mirrors into the sample which is placed in an appropriate holder. The radiation not absorbed by the sample arrives at the detector. Modern IR instruments use a device called an interferometer which consists of a beam splitter and a pair of mirrors at right angles to one another, this produces what is called an interferogram from the source radiation [70]. The interferogram holds information about the intensity of all IR radiation at all frequencies simultaneously, which passes to the sample and then to detector. The interferogram that arrives at the detector can be decoded by a mathematical technique

called Fourier transformation, which gives the intensity of the IR radiation at each frequency separately. The transformation is handled by the computer and produces a graph of percentage transmission against wave number [71].

The sample is placed on a sample holder which is a crystal made of diamond or germanium, the IR beam is directed into the sample by a mirror and it is reflected back from the upper surface of the sample before being guided into the detector by a second mirror, this process is called attenuated total reflection (ATR). In running the instrument, after switching on the instrument, the blank is run with no sample in place, this is to find the absorption of the air which must be subtracted from the sample [72]. A little sample is placed on the ATR crystal, less than a milligram (mg) of solid sample is required, the tool crunch is used to squash the sample to ensure a good contact with the surface of the crystal. For most samples, no preparation is required, details of the scan are entered into the computer and the spectrum of the sample is obtained within a few seconds. The wave numbers of the most significant peaks can be labelled on to the spectrum for data interpretation [70].

#### **1.4. Microwave formulation**

In contrast to the use of microwave radiation as an analytical tool, a comparatively large volume of research has been undertaken to investigate the effects (and potential benefits) of using microwaves in a formulation capacity. For example, it has been shown that microwave radiation can affect the viscosity and gelatinisation of industrially utilised starch [73], be applied to synthesise novel maize protein-based functional materials [74], curing composites [75], enhancing rates of reaction [76] and considered for biodiesel production [77]. Possibly the most researched area of microwave-based formulation is regarding pharmaceutical applications where the limited physicochemical properties of compounds can be a significant barrier to the development of new medicines thus requiring intervention to enhance their properties. Two fundamental properties of ensuring the success of a drug are solubility and

permeability as these will ultimately dictate drug absorption within the body and therefore efficacy. Microwave treatment has been shown to enhance both the physicochemical and pharmacokinetic properties of pharmaceutical preparations, such as the solubility of efonidipine hydrochloride ethanolate [78], the formation of cocrystals [79], the solubility of nanocomposites [80], the dissolution of gemfibrozil [81], through modifying drug release characteristics [82], increased yields [83] or controlling drug delivery profiles [84]. Not long ago, a procedure based on sustained-release solid dispersion was proposed for ibuprofen [85]. Microwave irradiation is a well-known method for heating and drying pharmaceutical powders [86]. Previous work within the Huddersfield research group has highlighted the benefits of using microwave processing for pharmaceutical compounds with the presence of excipients to create unique products including combinations of ibuprofen with stearic acid and polyvinylpyrrolidone along with fenofibrate and mesoporous silicas [87, 88]. An interesting, and very recent, application of microwave irradiation is the concept of amorphisation within the tablet, i.e. creating the amorphous form of the drug in its final dosage form directly before administration [89].

Overall, microwave radiation has been previously employed for the analysis of compounds through the use of microwave differential thermal analysis (MWDTA), and separately, to formulate products that possess unique physicochemical properties that can be advantageous, especially in the pharmaceutical industry. However, as yet, there has been no consideration for the use of MWDTA to investigate pharmaceutical compounds that are to be subjected to microwave irradiation during formulation to fully understand if such a process will be suitable and identify the interactions that will occur.

#### **1.4.1. Microwave theory**

Almost twenty years ago a new technique was described for the first time, namely microwave differential thermal analysis (MWDTA), that combined the advantages of microwave heating

with the benefits of differential temperature measurement to probe the thermal properties of materials [90]. The features governing the successful application of microwaves in thermal analysis (TA) of pharmaceutical compounds and the physical principles behind it are not well known in the pharmaceutical industry, possibly because pharmaceutical compounds have not been previously studied in this way [91].

Microwaves (MWs) are a form of electromagnetic energy found in the electromagnetic spectrum with a frequency ranging from 300 MHz - 300 GHz; a region that is found in between the radio waves and infrared waves with a wavelength from 1 cm - 1 m [92]. Microwaves have electric and magnetic field components (Fig. 1.4) and for most analysis related to the MW in the electromagnetic field, it is the electric field component that is of relevance for wave-material interactions, the magnetic component is mainly only of relevance for interactions with transition metal oxides [93].

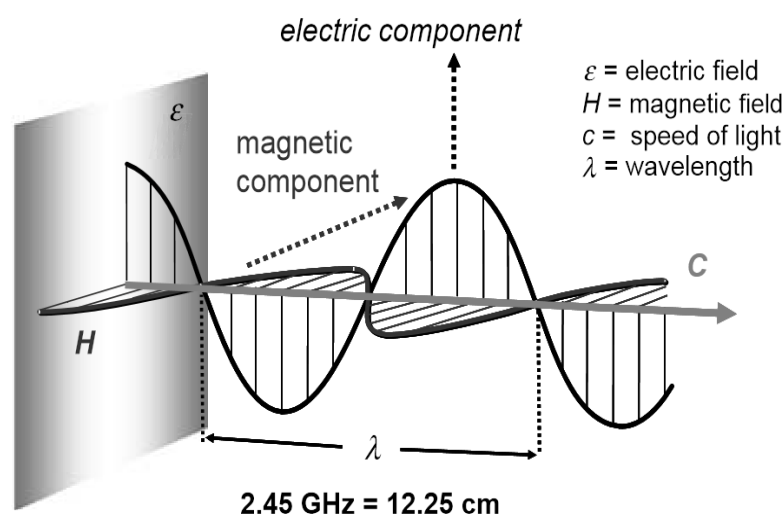


Figure 1. 4. Electric and magnetic field components in microwaves [91].

Heating a material with the electric field component of the MW occurs due to two main mechanisms; which efficiently generate rapid volumetric heating (Fig. 1.5) as a result of microwave contact with ions or polar molecules; ionic conduction and dipole rotation [93, 94]. Interactions that occur as polar molecules aim to realign themselves with the speedily vibrating

electric field component of the microwave are a result of the dipolar polarisation mechanism (Fig. 1.4) [91, 93]. As the electric field vibrates, the dipole attempts to realign itself with the vibrating electric field and in the process, energy is lost in the form of heat during the aforementioned event through dielectric loss ( $E''$ ) and molecular friction. The amount of heat induced by this process is directly related to the capacity of the substance to align itself with the frequency of the applied electric field [93]. In this research, this becomes relevant for heating microwave absorbing compounds, such as pharmaceutical drugs and their excipients.

An ionic conduction mechanism (Ohmic heating) is the second heating mechanism. During this mechanism, dissolved charged atoms (usually ions such as electrons) in a sample rotate back and forth under the effect of the microwave field, they then come into collision with their neighbouring atoms or molecules. A motion or agitation is caused as a result of the collision, thereby creating heat [93].

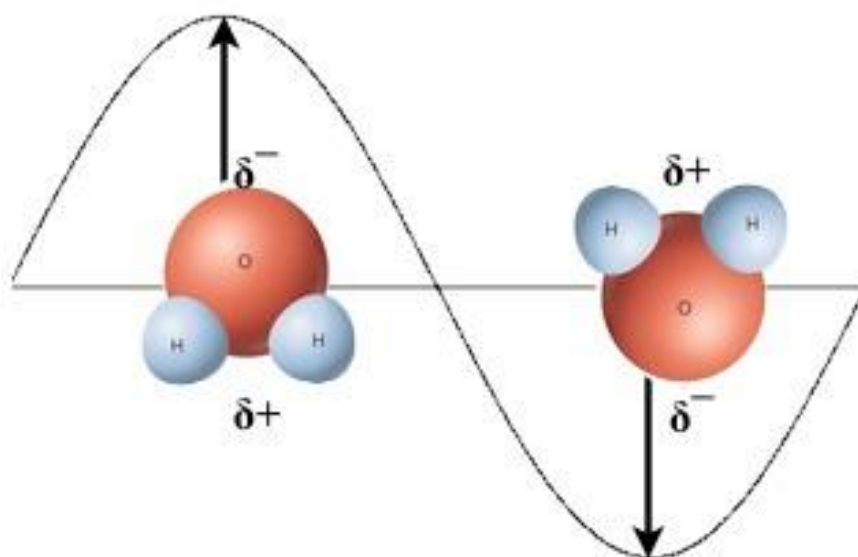
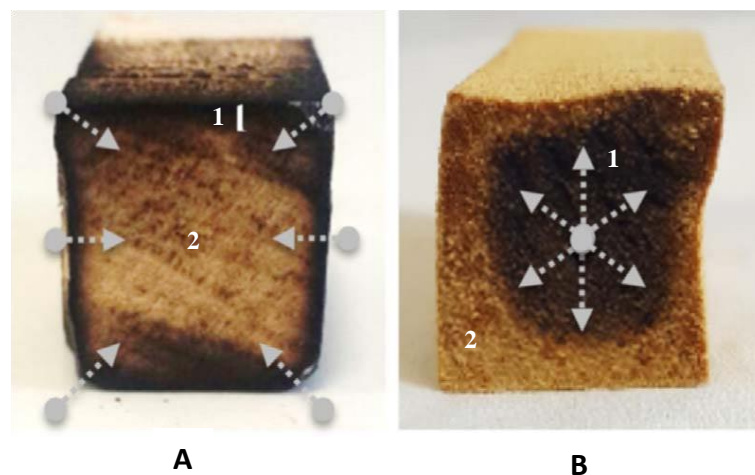


Figure 1. 5. Dipolar polarisation mechanism. Dipolar molecules try to align with an oscillating electric field [91]

#### 1.4.2. Microwave heating versus conventional heating

The limited thermal response using conventional heating is avoided using microwave heating as there is direct interaction of the material with microwave energy. However, more

importantly, microwave heating provides a unique means of investigating thermal transitions based on the associated changes in the dielectric properties of the materials. These thermally induced changes, such as melting or decomposition, are then analysed based on the microwave power profiles obtained [95]. In a conventional heating system, heat is transferred from the outside of the material by radiation, convection or conduction and is then transferred to the cooler part of the material by thermal conduction as illustrated in Fig. 1.6A (hotter region). This system of heating is inefficient, relatively slow and depends on the thermal conductivity of a substance. On the contrary, microwave heating transfers electromagnetic energy into heat energy. Rather than a form of thermal heating, MW heating can, therefore, be described as a form of energy conversion; as electromagnetic energy is converted into thermal energy [93]. Microwaves can penetrate through any material that has a dipole moment and deposit energy. Thus, rather than an external source of the material in conventional heating, the heat can be produced throughout the volume of the material. Fig. 1.6B (cooler region) illustrates this type of heating as the interior of the material is heated to a remarkably higher temperature than the exterior region, contrary to conventional heating [92].



**1 = hotter region 2=cooler region**

Figure 1. 6. Conventional heating (A) and microwave heating (B) highlighting the differing nature of the process [92]

In conventional heating (Fig. 1.6A), heat is transferred from the outside of the material inwards by conduction. Overheating can occur on the outside whilst still maintaining a cooler inner region. On the contrary, for microwave heating (B), microwaves penetrate the material and heat volumetrically. Energy is then uniformly dissipated throughout the material [92]. The benefits of microwave heating compared with conventional heating include high heating efficiency, no overheating at the surface, rapid volumetric heating, better and rapid process control and energy saving. As such, this has been considered to be a useful method that could be applied for the drying of wet materials [95, 96].

Microwave irradiation is a well-established technique of accelerating and improving chemical reactions because it provides the energy directly to the reactant. As a result, heat transfer is more effective than in conventional heating and the reaction can be completed in a much shorter period [97]. Thus, microwave irradiation is one of the best techniques for reducing the reaction time and obtaining a higher yield, for example in the production of biodiesel. In comparison with conventional heating, using microwaves improves the speed of the reaction and makes the separation process easier [93]. Instead of conventional heating, microwave heating has been utilised to change the crystalline nature of a drug as reported by Kerc and Kofler, [98] when felodipine and silicon dioxide were used as a model drug and excipient. Furthermore, this form of heating has been successfully applied in many studies including bioenergy [92] and biochemical processing for bioethanol production via fermentation [99].

#### **1.4.3. Microwave differential thermal analysis (MWDTA)**

Although the use of microwaves has broadened vastly since the discovery of its heating capabilities, its use in thermal analysis is not widely mentioned, other than the work of Karmazsin *et al.* [100] which led to the work of Barnes, Parkes and Bond [101] and the later related work of Nesbitt *et al.* [102]. Typically, transitions are observed using MWDTA within the order of 10's or 100's of degrees unlike in conventional thermal analysis where they are



observed in the order of a few degrees when using similar techniques such as DSC, making the transition very noticeable. Increases in sensitivity of this technique allow transitions, such as dehydration to be very easy to determine which is an added advantage. This is because water couples more strongly to microwave radiation and when the water is lost, the MW power required for the instrument to reach the setpoint changes remarkably. This is, therefore, a very useful technique, for example for the identification of water in pharmaceutical samples [103]. TA techniques are well-established methods for the analysis and characterisation of a wide range of materials. These analyses have seen a rapid growth in the range of their applications in recent years, particularly in the field of material sciences, nanotechnology, drug discovery and polymers. A limited field of thermal analysis involves microwave – based techniques [95, 104, 105]. Clearly, there is a need to develop an understanding of how changes in such materials affect their interaction with microwave energy. With the advances detailed in this research, MWDTA is considered to be potentially suitable not only to monitor the changes mentioned earlier but also to provide data comparative to conventional thermal techniques such as DSC and DTA.

The ability to provide information on thermally induced transformations in materials is one particular benefit of the microwave technique for studying all forms of thermal reactions and processing. When a material is subjected to microwave radiation there are two important parameters that dictate the nature of the interaction, namely the dielectric constant ( $\epsilon'$ ) and the dielectric loss factor ( $\epsilon''$ ). The former considers the way a material is polarised by the electric field and the latter the conversion from radiation to heat [95]. The relative extent of microwave heating of any given material can be determined by a term called the 'loss tangent' ( $\tan \delta$ ) defined as the ability of a material to absorb and convert electromagnetic energy into heat at a given frequency and temperature. The loss tangent is also the ratio of dielectric constant and dielectric loss expressed by the equation:

$$\tan \delta = \varepsilon'' / \varepsilon'$$

Where  $\varepsilon''$  is the dielectric loss factor and  $\varepsilon'$  is the dielectric constant of the material. Materials can be classified into three types according to their interactions with microwaves: microwave - insulators/transparent (e.g. ceramics and glass) where the microwaves pass through the material without any losses, microwave-conducting (e.g. metals) in which the microwave does not penetrate and instead is reflected, or microwave-absorbing (e.g. polar molecules such as water and drugs) where the microwaves are absorbed and converted into heat [106]. In general, materials can be classified as high ( $\tan > 0.5$ ), medium ( $0.1 - 0.5$ ) and low microwave absorbing ( $< 0.1$ ) compounds. A reaction medium with high  $\tan \delta$  is needed for rapid heating [91]. A low-value  $\tan \delta$  does not preclude material from being used in a microwave-heated reaction; additives can be used to achieve rapid heating of the material of low  $\tan \delta$  value. For example, poorly coupling compounds e.g. pharmaceutical drugs and excipients can be mixed with a subsector (e.g. alumina or SiC) or used with a 'heat assisted' sample cell (Fig.1.10) [104, 106]. Materials with higher values of  $\tan \delta$  will attain higher temperatures than those with lower values of  $\tan \delta$ , leading to a thermal gradient within the material that is unique to microwave heating. The  $\tan \delta$  is dependent on both the temperature of the sample and the frequency of the microwave radiation [104].

This form of analysis has been successfully applied to a range of materials including decompositions, dehydration and phase changes [95] and can provide qualitative and quantitative information on solid-state processes [104]. Furthermore, MWDTA can make a valuable contribution to the investigation of the so-called 'microwave effect', these are anomalies that occur when certain materials are heated in a microwave field [107] as well as reveal fine detail through the use of derivative plots of either the applied power or the temperature [101]. In recent years a variety of studies have investigated the application of

MWDTA to both a range of materials, such as ceramics [108], and a range of more complex analytical systems [102].

#### 1.4.4. Thermal runaway

One disadvantage emerges from the way that the terms  $\epsilon'$  and  $\epsilon''$  (and subsequently  $\tan \delta$ ) are reliant both on the substance and crucially, the temperature. For a few substances, their capacity to couple with microwave energy can increase sharply with temperature, potentially leading to unwanted 'thermal runaway' effects (Fig. 1.7). MWDTA is ideally suited to investigate this phenomenon. A large number of solids have low dielectric losses, and these losses increase with temperature. As the temperature increases,  $\tan \delta$  rapidly increases and the temperature then rises exponentially. The temperature can only be stabilised if heat can be removed at a rate that equals the rise, or by restricting the microwave power [103].

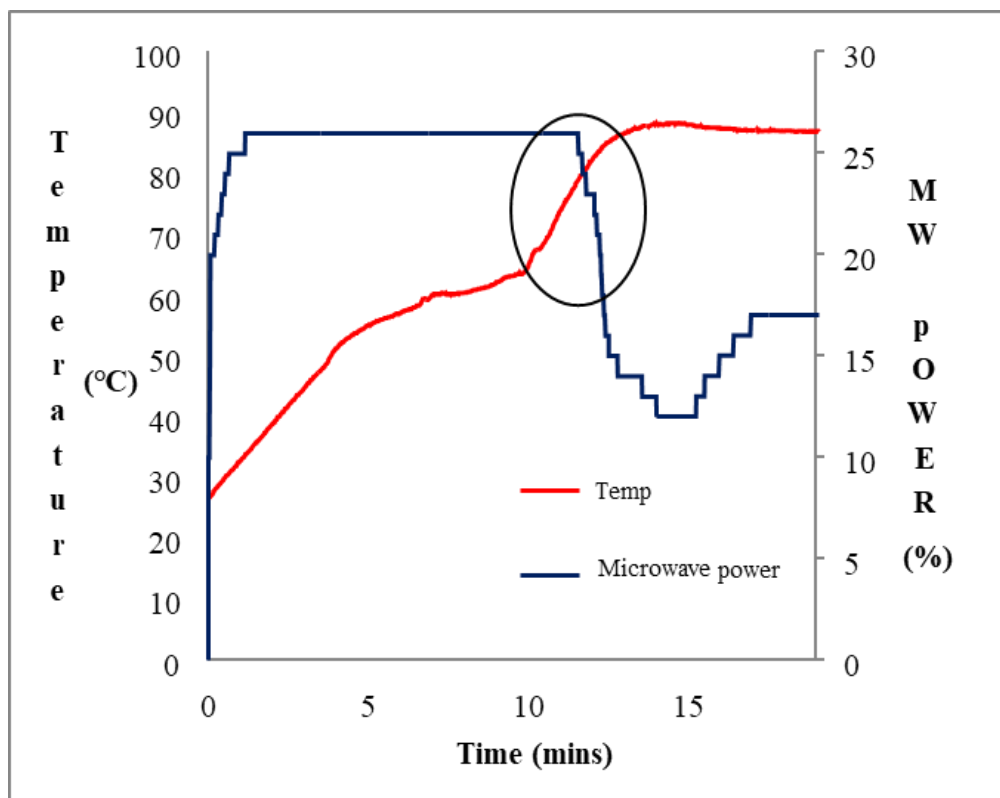


Figure 1. 7. Illustration of thermal runaway under microwave heating i.e. where the temperature of the material rises rapidly even though the amount of microwave power is unchanged [58]

Due to the chance of thermal runaway and the potential heating abilities of microwaves, the actual amount of energy applied if the sample is heated to a higher temperature can destroy the sample. Microwaves do not have adverse effects on the actual material being heated, they just facilitate this process, allowing a faster and a more uniform heating process [58].

#### **1.4.5. Heating of poorly coupling materials**

Various materials do not heat by any of the systems discussed already and therefore require an assistant medium in order to raise their temperature when only utilising microwaves as a heating source. The medium most normally used in these cases is known as a susceptor and is a material which is able to absorb electromagnetic radiation and convert it into heat resulting in the surrounding area heating via conduction. Commonly, the required amount of susceptor is mixed with the material of interest creating countless heating sources or ‘intimate furnaces’ which heat the material from several points within and around its volume [103].

The advantage of this arrangement is, although the sample is heating via conduction, (as in a conventional method) the material and heating sources are touching therefore nearly eliminating thermal mass. In addition to this, the applied power or heating rate required to heat a material can be modified by either adding or removing susceptible material. The main disadvantage of this technique occurs if the material is not thoroughly mixed or the percentage of the susceptor is too high. As a result, localised hot spots can occur prompting thermal runaway, and/or inaccurate temperature measurements as illustrated in Fig. 1.4 [103].

#### **1.4.6. Description of MWDTA instrument**

The apparatus (Fig. 1.8), described in detail elsewhere [95], is based on a single mode system which is tuned to set up a standing wave with a maximum in the electric field component (E) coinciding with the location of the sample.

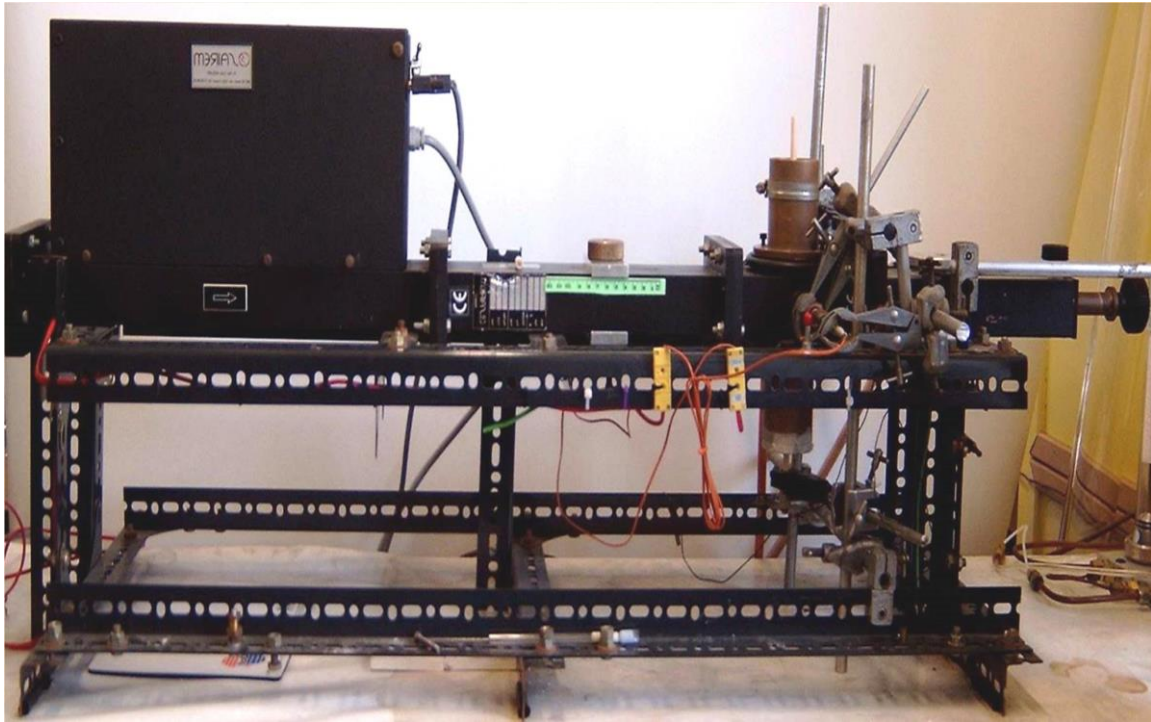


Figure 1. 8. Schematic diagram of MWDTA instrument

The microwave power, which can be varied in 1 W steps to 300 W (Fig. 1.8), is supplied by a very stable switch-mode, narrowband 2.45 GHz generator manufactured by Sairem, the generator is under computer control. The microwaves are passed from the generator, via a water-cooled circulator used to absorb any reflected power, to a launcher incorporated into a brass waveguide (Type 340, internal dimensions 86 mm\_43 mm) to prevent damage to the magnetron by reflected waves. The sample is located in a section of the waveguide which has four circular ports, the two larger of which are vertical (diameter 50 mm) and allow insertion and removal of the sample cell, while the two smaller are horizontal (diameter 15 mm) and provide access for temperature measurement devices.

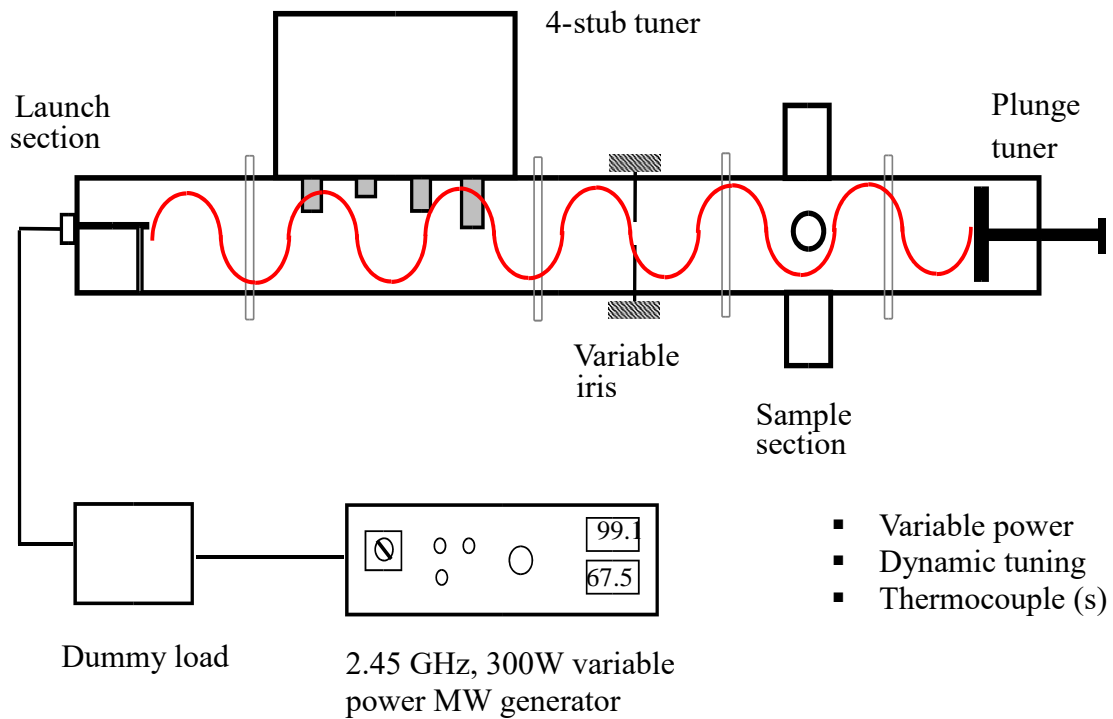
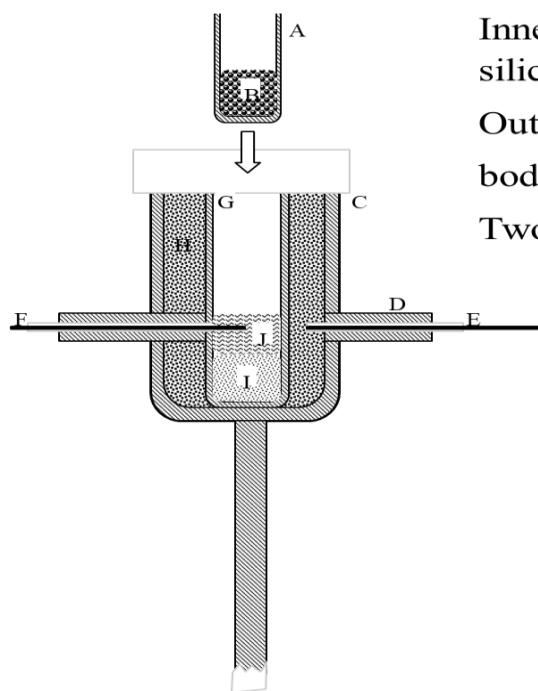


Figure 1. 9. Schematic diagram of the microwave components of the MWDTA instrument [104].

Tuning is supplied by three components. Firstly, a 'short circuit' or 'plunge tuner' which can be utilised to alter the internal length of the waveguide, secondly, a variable iris, consisting of a thin copper sheet with a rectangular orifice (50 mm\_25 mm) which can be traversed over a range of 6 cm, and thirdly an automated four-stub tuner. This latter device provides continuous 'fine-tuning' via the vertical movement of four brass rods in the waveguide and compensates for any small alterations in the system tuning produced by the sample and cell as they are heated.



Inner, removable, 6 mm silica sample cell.

Outer, SiC filled, silica body (reference).

Two thermocouples (MWTA)

Heat-Assisted / MWTA Cell – the benefits.

- Sample sizes: 5 to 50 mg.
- Cell body contributes most (but not all) of the heating → any sample can be analysed.
- $\Delta T$  → sensitive detection of thermal events.

Figure 1. 10. Heat-Assisted / MWDTA Sample cell – design [104].

### 1.5. Previous thermal analysis (TA) techniques

Enhancing research and development throughput is one of the biggest challenges facing the pharmaceutical industry. The pharmaceutical industry depends heavily on thermal analysis (TA), along with X-ray diffraction (XRD) and spectroscopic methods to perform in-depth physical and chemical characterisations of active pharmaceutical ingredients (API) as well as inactive ingredients (excipients) that go into pharmaceutical products. Solid-state characterisation lays the basis for formulation development and assists in science-driven rational decisions in the development of a stable drug product that can be manufactured with a reasonable shelf-life. TA techniques allow one to deduce physical and chemical properties as a function of temperature [109]. Differential scanning calorimetry (DSC), thermal (hot stage) microscopy (HSM), differential thermal analysis (DTA) and thermogravimetric analysis (TGA) are the most widely used thermal analytical methods for pharmaceuticals. A collection and correlation of data from complementary techniques are often required (i.e. not just a single

analytical technique) to draw conclusions, in order to gain an in-depth understanding of the nature of thermal transitions [110].

### 1.5.1 Differential thermal analysis (DTA)

DTA is a thermal technique similar to DSC, it is used to measure the temperature difference between samples under study and an inert reference substance while both are heated at the same linear rate [111, 112]. The temperature difference ( $\Delta T$ ) is plotted as a function of sample temperature or time. The DTA signal provides information on the physical and chemical transformations of the sample such as crystallisation, sublimation, dehydration, decomposition and melting [113]. It also allows the detection of an exothermic or endothermic event.

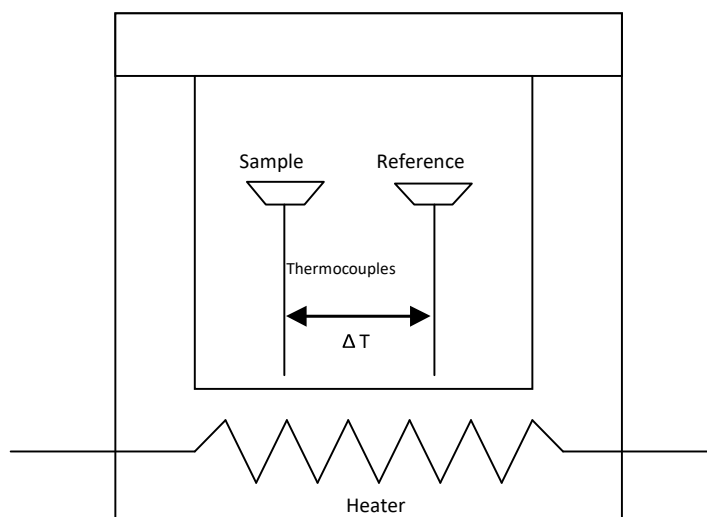


Figure 1. 11. Schematic of a typical DTA instrument [109]

In DTA, the temperature is continuously compared between the reference and the sample. Experimentally, this is achieved using a single heat source, which contains a sample holder that holds two similar and symmetrical areas for sample placement. The thermocouples (or any other temperature measuring device) in these areas are similar. The sample under study is placed in one holder, and a thermally inert reference substance (usually silicon carbide, empty pan or alumina) is placed in the other, then both holders are subjected to an equivalent temperature heating or cooling rate. The difference in temperature ( $\Delta T$ ) between the sample



and the reference is measured by two thermocouples (Fig. 1.11) that are coupled back to back in the sample and in an inert reference as a function of time or temperature [109].

### **1.5.2 Differential scanning calorimetry (DSC)**

DSC is the most commonly employed thermal analysis method due to its simplicity, speed and availability. It works in a similar way to DTA, except that it is a calorimetric method so the difference in temperature is not recorded but rather energy. DSC measures the heat flow that occurs in a sample under study when the sample is heated, held isothermally or cooled at constant temperature [114]. This method provides quantitative information on physical transitions and chemical reactions a substance may undergo, including; melting, crystallisation behaviour and supercooling, the glass transition of amorphous materials, decomposition, reaction enthalpies and quantification through peak areas [109, 114, 115]. To construct DSC measurements, the sample is placed into a small aluminium crucible. The reference is also an aluminium pan usually empty, they both have pierced lids [116]. To have good reproducibility and to protect the measuring cell, nitrogen, air or helium are usually used as purging gas at the rate of about 50 mL/min. The sample size is usually 4 to 10 mg and the temperature range up to about 600 °C [109].

There are variations in the type of DSC instruments available and in this research; a heat-flux DSC was used. In the heat-flux system, the difference in heat flow is measured as the sample and the reference are heated in one furnace and heat flows into the sample and reference through thermocouples [115].

### **1.5.3 Thermogravimetric analysis (TGA)**

TGA is another thermal technique in which the difference in weight of a sample is measured as a function of time or sample temperature as it is subjected to a controlled temperature program in a controlled atmosphere [117]. Based on the rate at which sample mass changes with respect to time or temperature, a differential thermogravimetric (DTGA) curve can be

obtained [118]. A mass difference occurs when the sample under study loses material in one of several ways or interacts with the surrounding atmosphere. This produces steps in the TGA curve or peaks in the DTGA curve. These effects can cause the sample to lose or gain mass and produce steps in the curve. Such processes include oxidation of metals in oxygen or air, oxidative decomposition of organic substances in air or oxygen [109], thermal decomposition of a sample in an inert atmosphere which is also known as pyrolysis [118, 119].

TGA is mostly utilised to investigate degradation temperatures, absorbed content of materials, levels of inorganic and organic parts contained in a material and also analyse solvent residue. A thermobalance is used in TGA, with this type of balance the position of the sample in the furnace remains the same even if the weight changes [109].

#### **1.5.4. Hot stage microscopy (HSM)**

The best properties of microscopy and thermal analysis have been combined by HSM as an analytical technique to facilitate the characterisation of the physical properties of a substance as a function of temperature. The significance of supporting thermal analysis techniques has been previously reported [120], and with the coupling of HSM to the aforementioned thermal techniques, it offers greater possibilities for the characterisation of materials due to high-resolution colour cameras and image manipulation software that the technique possesses [121]. In the pharmaceutical industry, HSM is used to verify transitions observed using other thermal techniques. Solid-state characterisation of bulk drugs can be investigated using HSM [122], dehydration in which bubbles emanate from the crystals, evolution of crystal forms, particle characteristics such as shape and size, phase transitions, decomposition (if discolouration occurs or gases evolved), and other physio-chemical properties can all be observed using HSM [110, 123].

In summary, all current conventional TA methods use electrical furnaces as a source of heating where the heat passes from the furnace wall to the surface then through the sample by conduction. Unfortunately, this process of heat transfer produces temperature gradients within the sample that reduces the resolution of data produced. This project seeks to overcome this drawback through the application of microwave differential thermal analysis (MWDTA) to yield more useful and more reliable thermal analysis data for pharmaceutical compounds.

### **1.6. Transarterial Chemoembolisation (TACE) and DC Bead™**

The 5<sup>th</sup> most widespread cancer is hepatocellular carcinoma (HCC) with a global occurrence of some 500,000 new cases per year, three quarters of those cases being in Asia. The type of therapy that a patient will receive is determined according to a staging system classified by the development of the cancer [124]. At the present time, the therapy of choice for sufferers at the early stage is liver transplant or resection of the tumour. Resection is no longer considered for patients with intermediate or advanced disease and lots of alternative therapies including chemotherapy, palliative or embolisation treatments are available [125]. Due to their quality of life supremacy, less-invasive procedures are finding favour and this includes methods such as radiofrequency, cryoablation and transarterial chemoembolisation (TACE). Among these techniques, two new clinical trials at random have revealed that TACE results in remarkable survival benefits over palliative care in the treatment of intermediate stage HCC in both Asian and European patient populations [126, 127].

For over 30 years, transarterial chemoembolisation (TACE) has been practiced in patients [128] and explains the delivery target of chemotherapeutic agents followed by subsequent injection of embolic particles to hypervascular liver tumours through a catheter placed in the tumour supplying arteries [129, 130]. TACE can be categorised into conventional TACE (cTACE) and drug-eluting bead TACE (DEB-TACE). cTACE is very often carried out by emulsifying chemotherapeutic agents with Lipiodol and then infusing this emulsion through the catheter

prior to distribution of embolic substance, while on the contrary, a single distribution system of drug loadable microspheres is used by DEB-TACE to achieve co-delivery of drug and embolic agent, which both block the chosen vessels and provides controlled drug release [131, 132]. Drug eluting beads have emerged as a substitute to cTACE more recently [133].

The most commonly used and well characterised DEB is DC Bead, which is a microspherical, cleared drug delivery embolisation device (DDED) used for the treatment of hypervascular tumours as well as arterio-venous malformations [124, 128, 134]. The device was developed in 2002 and manufactured by Biocompatibles UK Ltd, for the advancement of diagnosis and treatment of cancer, with an objective of standardising the TACE procedure for patient benefits and also providing handling advantages [128].

#### **1.6.1. Composition of DC Bead**

The DC bead is composed of a sulfonate-modified polyvinyl alcohol hydrogel, which permits subsequent delivery and loading of a variety of positively charged chemotherapeutic drugs including irinotecan, doxorubicin and mitoxantrone [124, 135-137]. The beads are available in numerous sizes ranging from 100 – 300  $\mu\text{m}$ , 300 – 500  $\mu\text{m}$  and 500 – 700  $\mu\text{m}$  with the former two being the most popular for the embolisation of tumours [135]. Lewis et al., reported a rapid uptake of doxorubicin by the smallest bead size (100 – 300  $\mu\text{m}$ ), in which a complete loading was attained before the first sampling point at 10 min. The uptake is slower with increasing bead size as a result of a decrease in bead surface area as the size increases. Thus, drug loading is proportional to the surface area of bead [124]. The beads are supplied in a 10 mL coded glass vial with a rubber stopper and aluminium cap as shown in Figure 1.10. Each vial contains 6 mL of packing solution (phosphate buffer saline) and 2 mL of beads, intended for one patient use.



Figure 1. 12. Available DC bead™ with their size ranges and colour [134].

### 1.6.2. DC Bead Chemistry

The drug of choice is taken up by the bead via an ion exchange mechanism [137]. The beads change colour when loaded with certain chromatic drugs as illustrated in Figure 1.12. The high-water content (> 95 %) beads, enables the diffusion of water soluble drugs into the network structure [132]. When the drug molecule is positively charged, it may interact with the sulfonate groups reversibly by an ion exchange mechanism to take over the position of the sodium counter ion from the 2-acrylamido-2-methyl propane sulfonate (AMPS) and secure the drug into the structure of the hydrogel by ionic interaction.

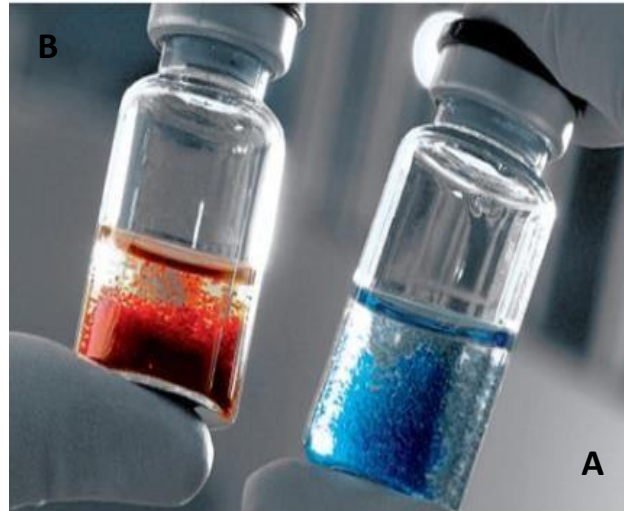


Figure 1. 13. DC Bead™ unloaded (A) and DC Bead™ loaded with doxorubicin (Dox) illustrating the intense colour change from blue to red (B) [134]

The proof of this interaction is illustrated in Figure 1.14, which demonstrates clearly the displacement of water from the hydrogel shell. Initially the beads enlarge in size as they are reconstituted in water prior to drug loading, but then decrease as water is replaced from the hydrogel and the drug molecule is sequestered from the solution [124, 138]. The water content in the hydrogel decreases with increasing drug content during loading, which is accompanied by an increase in resistance to compression force of the hydrogels. The water content and the compressibility were proven by Lewis et al. [124] to return to the level of the unloaded DC bead upon elution of all drug from the delivery device.

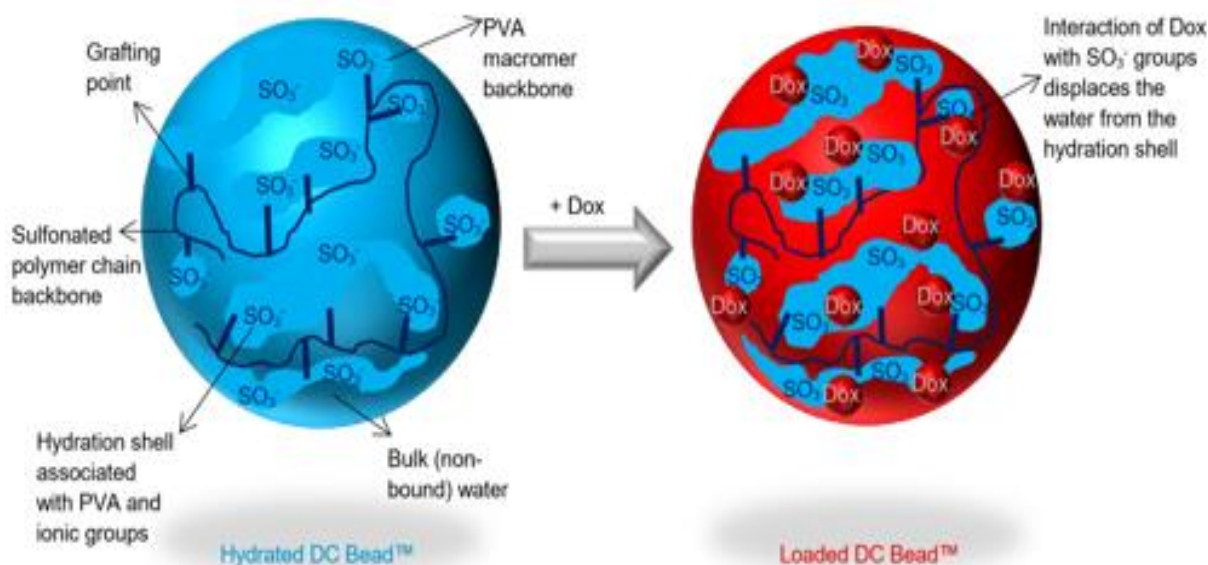


Figure 1. 14. DC bead™ mode of loading with doxorubicin (dox) and subsequent displacement of water through an ion exchange mechanism [134].

### 1.6.3. Drug loading and elution

Due to the relative increase in the surface area to volume ratio, the rate of intake of a particular drug increases with decreasing bead size. As seen in Figure 1.13A, when the drug is isolated into the structure of the bead, it is likely to change colour if the drug itself is coloured, a good example is seen in Figure 1.14 for doxorubicin which is red or irinotecan which is straw yellow, yielding a turquoise colour and mitoxantrone which is intense blue when loaded into the blue beads as Lewis et al. reported [132].

The process of extracting the drug from the bead may therefore be expressed as a function of not only the composition and ionic strength of the elution medium but also dependent upon the type and degree of drug-bead and drug-drug interactions. Again, the bead size is an essential determinant of the rate of elution, as the surface area to volume ratio comes into play. The release rate can be determined by a variety of different elution methods *in vitro*; the easiest one is the USP II equipment in which all of the drug can be eluted very quickly by selection of a suitable elution medium under sink conditions (Figure 1.15). This apparatus, while essential from a development of the product and quality control perspective, did not offer an insight into

how quickly the drug might be released *in vivo* [132]. Other different types of apparatus including flow through cells (USP IV) have been reported, which have been illustrated by *in-vitro-in vivo* (IVIVC) correlations to better estimate the fraction of drug that is released into the systematic circulation following drug eluting bead (DEB) administration [137, 139].

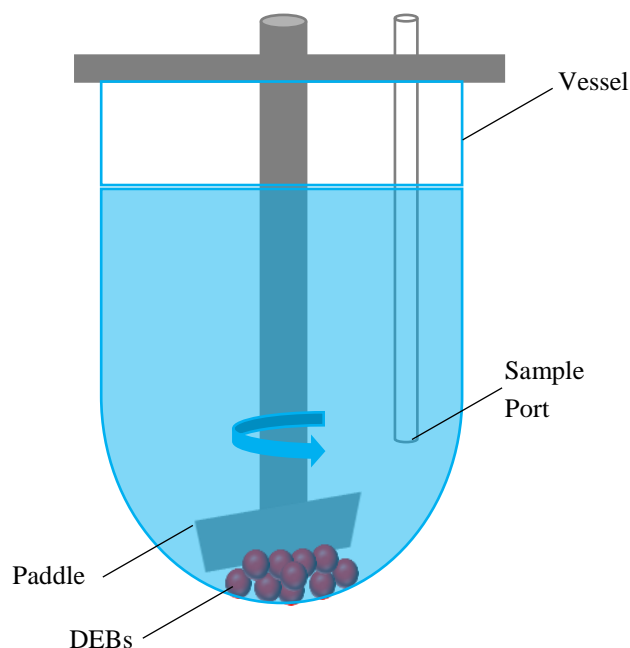


Figure 1. 15. USP Type II dissolution apparatus [134]

It was reported that using high performance liquid chromatography (HPLC), doxorubicin (dox) does not change chemical structure before and after loading, i.e. the drug does not degrade. Moreover, it was found that dox elutes in phosphate buffer (PBS) and plasma, but does not release in water as the rate of release is dependent upon the concentration of salt, i.e. a far more substantial amount of drug was eluted from beads at higher salt concentrations [137].

### 1.7. Bound water analysis

Drug-eluting beads (DEBs) are known to contain a high percentage of water, essential to their physical structure and therefore suitability to be used in drug delivery. Traditionally the water content within such beads is calculated based upon a simple size decrease calculation or solid content measurement. This process is based upon several assumptions, such as that the volume



decrease is a consequence of water content and is potentially neither accurate nor precise. Furthermore, the water within the beads can be considered to be in one of three forms with regards to its interaction with the solid polymer content: tightly bound, loosely bound or unbound. Until now it has not been possible to easily quantify the total water content as well as these three individual amounts, thus prompting the method developed within this study.

Among several strategies to calculate the amount of water content within polymer hydrogels [140], particular attention was paid to thermal analysis techniques such as differential scanning calorimetry (DSC) and thermogravimetric analysis (TGA), since the behaviour of the water content can easily be identified by these methods through phase transitions [141]. Through vaporisation, thermogravimetric analysis can be used to calculate the total water content in a hydrogel [142], while using DSC, it was hypothesised that the three forms of water (tightly bound, loosely bound or unbound with regards to their interaction with the solid polymer content) can be calculated quantitatively from the enthalpies of melting and crystallisation of water associated with the polymer [140]. Besides thermal methods, interactions between water and different hydrogels have been investigated using nuclear magnetic resonance (NMR) [143], spectroscopic techniques [144, 145], dielectric methods [146], viscometry [147] and by means of computer simulations as carried out by Mazeau and Rinaudo [148].

In summary, several strategies have been adopted to estimate the amount of bound water within polymers including poly (2-methacryloyloxyethyl phosphorylcholine) (PMPC), in this study, we pay particular attention to DC beads as a large number of studies have been concerned with PMPC co-polymers.

## **1.8. Project aims**

This research considers the suitability of using Syloid<sup>®</sup> silica excipients as a novel formulation system to enhance the extent and rate of dissolution of model drugs and investigate the

application of thermal analysis, particularly MWDTA, on such compounds. A secondary aim is to consider the potential of thermal analysis to investigate water content within bead-based formulations. This will be approached based on the following objectives.

1. To investigate the suitability of using three types of Syloid<sup>®</sup> silica-based excipients to quantify their potential to enhance the rate of dissolution of drugs and determine the causes of any enhancements observed. These forms of silicas have a highly developed network of mesopores that provide access to the large surface area, a desirable pore diameter, pore volume and surface morphologies.
2. To use thermal analysis, particularly MWDTA on model pharmaceutical compounds to investigate the potential application of this form of thermal analysis on such compounds as an indicator of the suitability of microwave-based formulation methods.
3. As previously discussed, polymers such as those considered in this study contain three distinct types of water. Little is known about their relative ratios, yet their composition will undoubtedly affect their behaviour. Therefore, the third aim of this study is to portray the potential of thermal analysis, particularly MWDTA, TGA and DSC to quantify and characterise the water present within polymer beads, including the incorporation of model drug to exemplify the effect of drugs on the relative water profiles.

## Chapter 2: Materials and methods

### 2.1 Materials

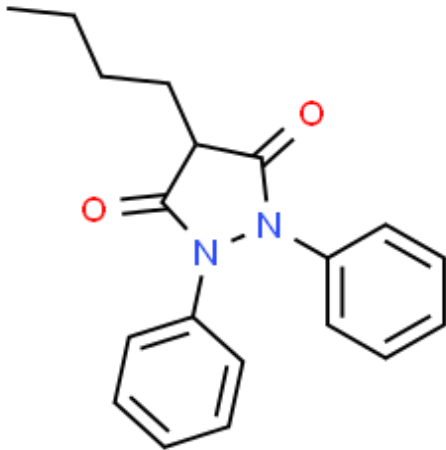
Indomethacin ( $\gamma$ -form), benzocaine (BZ), D-Mannitol (D-man), haloperidol (Halo), ibuprofen (Ibu), ketoprofen (Keto), phenylbutazone (PhB), naproxen (NPX),  $\beta$ -Cyclodextrin ( $\beta$ -CD or Beta-CD), stearic acid (SA), potassium phosphate dibasic and potassium phosphate monobasic (both  $\geq 99\%$ ) were purchased from Sigma Aldrich (Dorset, UK). Imipramine hydrochloride (Imi) ( $>99\%$ ) was purchased from Tokyo Chemical Industry Ltd. (Oxford, UK). Polymer beads 70-150  $\mu\text{m}$  (DC BeadMI™) were kindly donated by Biocompatible UK Ltd., a BTG International group company (Camberley, UK). Syloid® silicas (AL-1 FP, XDP 3050 and XDP 3150) were kindly donated by Glantreo Ltd, Cork, Ireland and W. R. Grace & Co, Maryland, USA. These compounds were selected based on their dielectric properties (dielectric constant, dielectric loss and loss tangent) as materials interact differently with the microwaves based on these properties. The higher the loss tangent the better the conversion of microwave energy into heat and the more effective the microwave heating. These compounds were assumed to have either a high, medium or low tangent (i.e.  $\tan > 0.5$ ,  $\tan > 0.1 - 0.5$  and  $\tan < 0.1$ ). Table 2.1 provides a summary of the physicochemical properties of the Syloid® silicas, the data presented was determined using nitrogen gas sorption isotherms. These were measured at 77 K using a Micromeritics TriStar II surface area analyser (Micromeritics, Norcross, GA, USA). Samples were pre-treated by heating at 200 °C under nitrogen for 12 hours. The surface area was measured using the Brunauer-Emmett-Teller (BET) method. The pore volume and pore diameter data was calculated using the Barrett, Joyner and Halenda (BJH) method [149]. Specific surface areas were calculated from the measured relative pressure in the range of  $P/P_0 = 0.01$  to  $P/P_0 = 0.3$ . Mesoporous volumes were estimated from the volume of nitrogen adsorbed after the micropores have been filled until after condensation into the mesopores was complete. Of particular interest is the range of surface areas and pore volumes exhibited by the

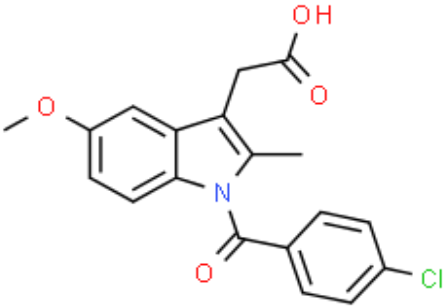
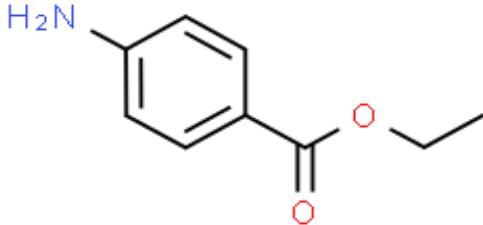
three Syloid<sup>®</sup> silicas as based on previous research, such properties may influence dissolution, for example, pore size has been known to effect drug release profiles for other mesoporous systems [150]. The materials were stored appropriately to avoid degradation and de-ionised water was used throughout the experiments. Physicochemical properties, along with chemical structures, are presented in Table 2.2.

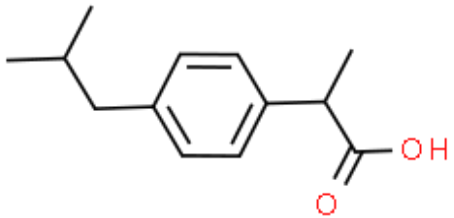
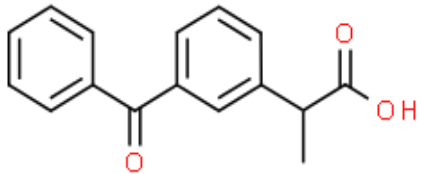
Table 2. 1: The physicochemical properties of the Syloid<sup>®</sup> silicas used in this study [11, 151].

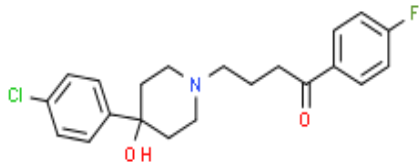
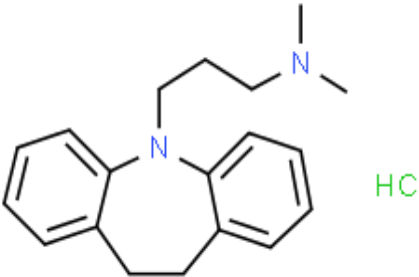
Name	Average Particle Size (µm)	Shape	Surface Area (m <sup>2</sup> g <sup>-1</sup> )	Pore Volume (cm <sup>3</sup> g <sup>-1</sup> )	Pore Diameter (Å)
AL-1 FP	7.5 – 10	Irregular	605	0.40	26
Syloid XDP 3050	48 – 66	Irregular	320	1.70	229
Syloid XDP 3150	120 – 170	Irregular	320	1.70	200

Table 2. 2: Physicochemical properties of the chemicals used

<b>Phenylbutazone</b>		Structure
Abbreviation	PhB	
Molecular weight	308.37 g mol <sup>-1</sup>	
Melting point	105 – 108 °C	
Log P	3.16	
Charge	Neutral	
pKa	4.50	
Solubility	0.034 mg/mL at 23 °C	
BCS	Class II	

<b>Indomethacin</b>		
Abbreviation	IMC	
Molecular weight	357.79 g mol <sup>-1</sup>	
Melting point	158 – 161 °C	
Log P	4.27	
Charge	Anionic	
pKa	4.50	
Solubility	0.00094 mg/mL at 25 °C	
BCS	Class II	
<b>Benzocaine</b>		
Abbreviation	BZ	
Molecular weight	165.19 g mol <sup>-1</sup>	
Melting point	88 – 92 °C	
Log P	1.95	
Charge	Cationic	
pKa	2.80	
Solubility	1.310 mg/mL at 25 °C	
BCS	Class II	

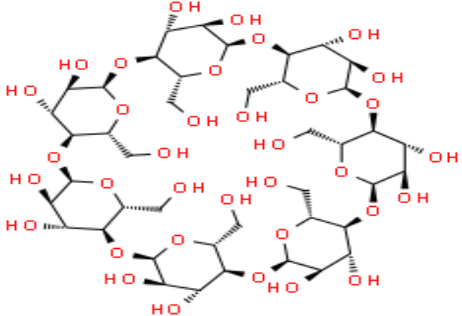
<b>Ibuprofen</b>		
Abbreviation	IBU	
Molecular weight	206.28 g mol <sup>-1</sup>	
Melting point	75 – 78 °C	
Log P	3.72	
Charge	Anionic	
pKa	4.40	
Solubility	0.021 mg/mL at 25 °C	
BCS	Class II	
<b>Ketoprofen</b>		
Abbreviation	KETO	
Molecular weight	254.28 g mol <sup>-1</sup>	
Melting point	91 – 93 °C	
Log P	2.81	
Charge	Anionic	
pKa	4.45	
Solubility	0.051 mg/mL at 22 °C	
BCS	Class II	

<b>Haloperidol</b>		
Abbreviation	HALO	
Molecular weight	357.86 g mol <sup>-1</sup>	
Melting point	152 °C	
Log P	4.30	
Charge	Cationic	
pKa	8.66	
Solubility	0.014 mg/mL at 25 °C	
BCS	Class II	
<b>Imipramine hydrochloride</b>		
Abbreviation	IMI	
Molecular weight	316.87 g mol <sup>-1</sup>	
Melting point	189 °C	
Log P	4.80	
Charge	Cationic	
pKa	9.20	
Solubility	0.47 mg/mL at 25 °C	
BCS	Class I	

<b>Naproxen</b>		
Abbreviation	NPX	
Molecular weight	230.26 g mol <sup>-1</sup>	
Melting point	154 – 156 °C	
Log P	3.18	
Charge	Anionic	
pKa	4.30	
Solubility	0.016 mg/mL at 25 °C	
BCS	Class II	
<b>Stearic acid</b>		
Abbreviation	SA	
Molecular weight	284.48 g mol <sup>-1</sup>	
Melting point	67 – 70 °C	
Log P	8.22	
Charge	Anionic	
<b>D-mannitol</b>		
Abbreviation	D-MAN	
Molecular weight	182.17 g mol <sup>-1</sup>	
Melting point	165 – 167 °C	
Log P	-3.10	
Charge	Anionic	



<b>Beta-cyclodextrin</b>	
Abbreviation	BETA-CD
Molecular weight	1134.98 g mol <sup>-1</sup>
Melting point	290 °C
Log P	-2.3
Charge	Neutral



Structure, molecular weight, melting point, dissociation constants, solubility and Log P were generated from chemspider [152, 153].

The majority of drugs are either weak organic acids or weak organic bases or their salt. The degree to which these compounds are ionised in solution is highly dependent on the pH. Phenylbutazone and indomethacin have low aqueous solubility because they are weak acids with pKa values falling in the range of 4.50 – 5.0 while the pKa of imipramine is 9.20, a weaker acid than phenylbutazone and imipramine. These compounds released hydrogen ions (H<sup>+</sup>) upon dissociation. The more H<sup>+</sup> are released, the more acidic the solution becomes, and this will inhibit the solubility of these drugs because weak acids dissolve to a greater extent when in mild basic conditions. A phosphate buffer pH 7.0 was used to improve the solubility of these compounds because acidic buffers may lead to slowing down of drug release [154]. Silica matrices are freely soluble at a pH 5.0 – 8.0, whereas some polymer matrices such as Eudragit<sup>®</sup> polymer is only soluble in an acid environment up to pH 5.0 [155]. The solubility is pH dependent and increases with increasing pH, this can be related by the following equations:

$$\text{pKa} = -\log\text{Ka} \quad (1.1)$$

$$\text{Ka} = \frac{[\text{H}^+][\text{A}^-]}{[\text{HA}]} \quad (1.2)$$

[H<sup>+</sup>] = Hydrogen ions

[A<sup>-</sup>] = Ionised drug

[HA] = Unionised drug

## **2.2 Methods**

### **2.2.1 Preparation of physical mixtures of drugs- silicas**

Physical mixtures of phenylbutazone, were prepared by mixing the drug with Syloid® silica XDP 3050 in a Turbula mixer (Turbula T10B) for 10 min at 72 revs per min. Different ratios of drug: silica (1:1, 2:1, and 1:3) were prepared for comparison. This process was repeated with the replacement of XDP 3050 with XDP 3150 and AL-1 FP to produce a total of three unique drug-Syloid® silica mixtures. The procedure was repeated for indomethacin and imipramine with the same silicas at the same ratios of 1:1, 2:1, and 1:3 drugs to excipient mass ratio. The reason for these ratios was to investigate solid-state interactions between the drugs and excipients because the comparison of thermal curves of single components with their physical mixtures will provide an insight into the solid-state interaction, behaviour and modification of the resultant products compared with the components as a consequence of the method utilised for complex preparation. The powders were stored in screw-capped glass vials in a desiccator until required after the mixing process.

### **2.2.2. Microwave formulation**

A known mass (30 - 80 mg) of the physically mixed phenylbutazone, indomethacin and imipramine with syloid XDP 3050 at 1:1, 2:1 and 1:3 drugs to excipient mass ratios were transferred into a quartz crucible and placed in the microwave. The microwave heating system was operated and controlled by software previously published [95]. The software was set to continuously modify the microwave power such that the samples were heated at 5 °C/min to the melting temperature of each drug from 25 to 160 °C or from 25 – 200 °C (as exemplified in Fig. 2.1 for indomethacin), depending upon the sample under analysis. The formulations were held isothermally for 5 min and then cooled over a period of 60 – 80 min under an air atmosphere utilising a microwave power of 30 to 45 W. This process was repeated with the

replacement of XDP 3050 with XDP 3150 and AL-1 FP to produce a total of three unique drug-Syloid<sup>®</sup> silica formulations at the same ratios of 1:1, 2:1, and 1:3 drugs to excipient.

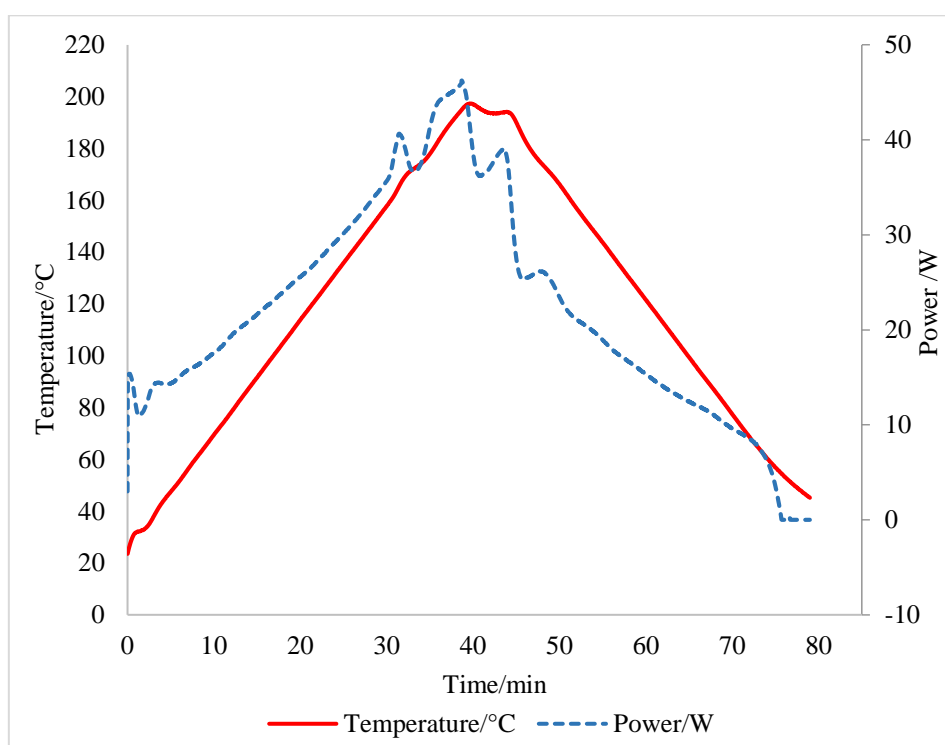


Figure 2. 1. An example of the temperature and power profile for microwave formulation of indomethacin and Syloid<sup>®</sup> silica XDP 3050 (1:1).

## 2.3 Characterisation methods

### 2.3.1 *In vitro* dissolution studies

To assess drug release from the Syloid<sup>®</sup> silica formulations, dissolution analysis was carried out using the USP type II (paddle method). This was a fully automated assembly, comprising a dissolution bath (Pharmatest DT 70), peristaltic pump and UV visible spectrophotometer (Cecil 3021, series 3000). Formulated samples with a total drug content (based upon suitable calibrations using calibration data) of 22.50 mg for phenylbutazone, 21.60 mg for indomethacin and 54.0 mg for imipramine were placed in 900 mL of pH 7.0 phosphate buffer, stirred at 75 rpm and at  $37.0 \pm 0.5$  °C, maintaining sink conditions throughout the duration of the experiment. Samples were taken by an auto-sampling system every 5 min equipped with  $\mu$ m filters over a period of 45 min and returned to the original solution. The solution was measured

by UV spectrophotometry (set at a wavelength ( $\lambda$ ) of 282, 280 and 284 nm for PhB, IMC and Imi) to calculate the drug concentration released using a standard calibration plot for the drugs, as exemplified in Figure 2.2. All the samples were analysed in triplicate to determine mean drug release percentages and associated error limits. Drug release from Syloid<sup>®</sup> silica formulations were compared with pure drugs for comparison.



Figure 2. 2. Dissolution apparatus used for analysing formulations.

## 2.4 Solid state characterisation

### 2.4.1 Differential scanning calorimetry (DSC) for solid-state characterisation

Differential scanning calorimetry (DSC) was performed using a Mettler Toledo DSC 1 equipped with chiller cooling apparatus. Samples of pure drugs, physical mixtures as well as their formulations were scanned individually using a mass ranging from 4 to 10 mg in sealed aluminium pans heated at a rate of 10 °C/min under a nitrogen flow of 80 mL/min from 25 to 160 °C or from 25 to 200 °C depending upon the sample under analysis. The resultant profiles were obtained, analysed and compared.

#### **2.4.2 X-ray diffraction (XRD)**

Powder X-ray diffraction data were collected on a Bruker D<sub>2</sub>-Phaser instrument equipped with a Cu K $\alpha$ <sub>1</sub> radiation source at 30 kV and 10 mA current at a scanning range of 5 – 100 for 4 min. The drugs and excipients were scanned individually followed by their physical mixtures and formulations. Diffraction patterns were obtained and compared.

#### **2.4.3 Fourier transform infrared (FT-IR)**

For stability, functional group identification, drug-drug, and drug-excipient bonding information, a Nicolet-380 Fourier Transform Infrared spectrometer (FT-IR) with an ATR crystal was used to record the infrared spectrum of pure drugs and their formulations. Powdered samples were placed directly onto the diamond crystal and the anvil lowered to ensure that samples were in full contact with the diamond. Each spectrum was obtained in the range of 400 – 4000 cm<sup>-1</sup> with 2 cm<sup>-1</sup> resolution.

#### **2.4.4 Scanning electron microscopy (SEM)**

The morphology of the prepared samples was characterised using scanning electron microscopy (SEM), (JEOL JSM-6060LV, Japan) with gold-plating using a sputter coater (SC7620) prior to imaging. The procedure involved mounting the samples to a specimen stub and coating the surface of the material in an ultrathin layer of gold to inhibit accumulation of electrostatic charges, making the surface of the sample electrically conductive.

#### **2.5. Preparation of binary mixtures of drugs-excipients**

Two compounds were selected for further analysis, namely benzocaine, and indomethacin, prepared along with the four distinct excipients (XDP 3050, D-man, Beta-CD and SA). Initially, a total mass of 500 mg benzocaine (BZ) and 500 mg Syloid<sup>®</sup> XDP 3050 silica was transferred into a 25 mL glass jar, i.e. to create a 1:1 (BZ: XDP) mixture. The sample was placed in a Turbula mixer (Turbula T10B) for 10 min at 72 rpm to achieve a homogeneous

mixture and then removed and allowed to settle for 2 min. The procedure was repeated for the same mass of drug with a further three excipients:  $\beta$ -CD, D-man and SA, at the same ratio of 1:1 (BZ:  $\beta$ -CD, BZ:D-man and BZ:SA) drug to excipient mass ratio. This process was repeated with the replacement of BZ with Indo. This ratio was selected to maximise observable changes in the behaviour of the resultant products compared with the components.

### **2.5.1. Microwave differential thermal analysis (MWDTA) of pharmaceutical compounds**

Microwave thermal analysis of benzocaine (BZ), haloperidol, ibuprofen, indomethacin, ketoprofen, naproxen, imipramine and phenylbutazone, together with binary mixtures of benzocaine (BZ), and IMC with four excipients,  $\beta$ -cyclodextrin, D-mannitol, Syloid XDP (3050) and stearic acid, were performed using a known amount of each sample (30–90 mg) using a system previously published [104]. A known mass of each sample was placed into a quartz cell and heated at  $5\text{ }^{\circ}\text{C min}^{-1}$  from 25 to 160  $^{\circ}\text{C}$  or from 25 to 200  $^{\circ}\text{C}$ , depending upon the sample under analysis. The sample was held isothermally for 5 min and then cooled over a period of 70–90 min. All experiments were carried out under an air atmosphere utilising a microwave power of 30 W.

### **2.5.2 Differential scanning calorimetry (DSC)**

DSC analysis was conducted using a DSC 1 apparatus (Mettler Toledo) containing 5–8 mg samples in sealed aluminium pans. Samples were heated at a scanning rate of  $10\text{ }^{\circ}\text{C min}^{-1}$  under a nitrogen flow of  $80\text{ mL min}^{-1}$  from 25 to 160  $^{\circ}\text{C}$  or from 25 to 200  $^{\circ}\text{C}$ , depending upon the sample, and then cooled to 30  $^{\circ}\text{C}$ . The eight model pharmaceutical compounds were analysed individually, as well as the binary mixtures of BZ, and IMC with the four excipients (BZ: XDP, BZ:  $\beta$ -CD, BZ:D-man and BZ:SA), the resultant curves were analysed and data compared with that obtained with MWDTA and HSM.

### **2.5.3 Hot-stage microscopy (HSM)**

Particle morphology and visible changes (as a consequence of heating samples) were examined using hot-stage microscopy (HSM). An Olympus (SZ-CTV, Japan) polarising light microscope equipped with in-house constructed hot stage and software was used. A small amount of each sample was transferred into a quartz crucible, placed on the hot stage and heated at  $5\text{ }^{\circ}\text{C min}^{-1}$  from 25 to 160  $^{\circ}\text{C}$  or from 25 to 200  $^{\circ}\text{C}$ , depending upon the sample, and then cooled to 30  $^{\circ}\text{C}$ . Photomicrographs of the samples were collected at temperatures corresponding to any changes noticed in the sample as a function of temperature under a magnification of 4.5.

## **2.6. Imipramine loading into beads**

Polymer beads were supplied in saline solution and the majority of the packing salt solution was removed with a pipette to leave a slurry of beads. The beads were then washed five times with 5 mL deionised water per wash. The washed beads were centrifuged in a 10 mL screw cap, plastic tube at 3000 rpm for 5 minutes, allowed to settle for 2 minutes, and excess water was removed by first using a syringe followed by filter paper to remove residual surface water. Imipramine hydrochloride solution (10 mg/mL) was added into samples of beads under study with a volume of 1 mL, 2.5 mL, and 5 mL to target 10, 25, and 50 mg/mL loadings via an ion exchange mechanism to consider approximately below, equal and above saturation followed by occasional gentle agitation and left for 8 hours. The residual solution was diluted, and the UV absorbance was measured using UV-Vis spectrophotometry at 250 nm and compared with a standard plot to determine the amount of drug remaining in solution (and hence by subtraction that loaded into the beads).

### **2.6.1 Optical microscopy, bead sizing and water content estimation**

Optical microscopy and measurement of bead sizes were carried out using a BX50 microscope and a 10x dry objective. (Olympus UK Ltd, Essex, England). The eyepiece graticule used to

measure the beads was verified using a calibrated graticule placed on the microscope stage (Graticules Ltd, Kent, England). A monolayer of bead sample was placed in a Petri dish on the microscope stage and using the 10x objective and eyepiece graticule, the diameter of 200 individual beads was measured. The bead sizing data was entered into a spreadsheet and the size histograms generated using Prism 6 (GraphPad Software, Inc., La Jolla, CA). Based on the size change of beads and the assumption that size decrease is a consequence of water displaced from beads by the drug, the water content in drug loaded beads was calculated as follows:

$$\text{Water content} = \frac{\text{Volume of water in bland beads} - \text{Volume of water loss after drug loading}}{\text{Volume of drug loaded beads}} \times 100 \%$$

## **2.7 Thermogravimetric analysis (TGA)**

A Mettler Toledo (TGA) was used to investigate the total water content of the beads. Samples were filtered to remove excess water, ranging from 4 – 16 mg, placed on an aluminium holder and heated from 25 to 120 °C with a nitrogen carrier gas flow of 80 mL/min and a heating rate of 1 °C/min. Weight loss as a function of temperature change was recorded with the total loss equated to the water content within the beads (n=3) both with and without the presence of drug.

## **2.8 Differential scanning calorimetry (DSC)**

Differential scanning calorimetry (DSC) was performed using a Mettler Toledo DSC 1 equipped with chiller cooling apparatus. Samples of water, beads (filtered to remove excess water) and drug with beads ranging from 4 to 10 mg in sealed aluminium pans were heated at a rate of 1 °C/min under a nitrogen flow of 80 mL/min from -20 to 20 °C (n=3). Using this data, it was possible to quantify the amount of water within the beads that was able to undergo the freezing process, i.e. was not tightly bound to the polymer structure. This assumed that 'bound' water would not contribute to the peak observed within the DSC profile thus



subtracting the water associated with the peak observed with DSC from the total water content observed from TGA allowed calculation of the amount of tightly bound water within the beads.

### **Chapter 3: Microwave formulations of phenylbutazone (PhB), indomethacin (IMC) and imipramine hydrochloride (Imi) using three mesoporous silica excipients (Syloid<sup>®</sup> silicas AL-1 FP, XDP 3050 and XDP 3150)**

#### **3.1. Introduction**

Mesoporous silica has been shown to exhibit great potential to aid in the formulation of pharmaceutical compounds with poor aqueous solubility, as reviewed by Choudhari et al. [156]. As a drug carrier system, mesoporous silica can accommodate drugs that have been introduced through organic solvent immersion, incipient wetness impregnation or melted in [149]. Specific advantages of using excipients such as mesoporous silicas are their nonporous structures, high surface areas, clinical safety and large pore volumes [157]. Current opinion is that substantial progress has been made in recent years in the characterisation and development of mesoporous drug delivery systems although more work is needed regarding dissolution enhancement potential and related physicochemical properties [158]. There are several reasons for this need to continue exploring the possible use of mesoporous silica including practical considerations such as manufacturability to large-scale quantities (e.g. tonne) and regulation, as well as physicochemical considerations such as the possibility of re-adsorption onto the silica surface [158]. Adsorption of small drug particles on the surface of large excipients has been a successful strategy for low-dose drugs, poorly water-soluble drugs, targeted drug release [159], sustained drug delivery [160] and stability enhancement. This is mainly a result of improving the dissolution profile by increasing drug surface area or transformation of the drug from a crystalline to amorphous form [161], and its ability to be retained within the silica pores [162]. In many cases, the method of formulation can be critical in defining the properties of the resultant formulation. For example, silica-based drug delivery vehicles have been investigated to avoid hydrolysis of the active compound using supercritical CO<sub>2</sub> [163, 164], a formulation method known for its high drug-loading ability [165] amongst other advantages [166]. Several

other formulation methods have also been attempted, for example, to create liquid (also known as liquid-solid) formulations [167] and paediatric (solvent free) formulations [168]. Previously published studies have confirmed the application of conventional methods for formulation with mesoporous silicas [6]. Furthermore, there is clearly an interest in developing mesoporous silica formulations as evidenced by recent work to predict *in vivo* performance, for example, using *in silico* techniques [169], to overcome multi drug resistance [170] as well as to ameliorate toxic side effects [171].

This study investigates the suitability of using microwave formulations and three types of Syloid<sup>®</sup> silica-based excipients to quantify their potential to enhance the rate of dissolution of phenylbutazone, indomethacin and imipramine to determine the causes of any enhancements observed.

## 3.2. Results and discussion

### 3.2.1. Solid state characterisation of PhB formulation

#### 3.2.1.1. Differential scanning calorimetry (DSC)

DSC analysis was completed for PhB, PM and MWF of PhB with XDP 3050 silica at 1:1, 2:1 and 1:3 drug-silica ratios. Examples of the data obtained for the samples are presented in Figure 3.1. The analysis was used to monitor the presence of PhB in pure form and determine the interactions with syloid silica. Analysis of the  $\delta$ -polymorph of PhB in Figure 3.1 (a) showed the expected well defined, sharp melting peak of the crystalline drug with high intensity with corresponding fusion of 107.98 °C ( $\delta$ -form) as previously reported [172, 173]. This confirms the crystalline nature of the drug.

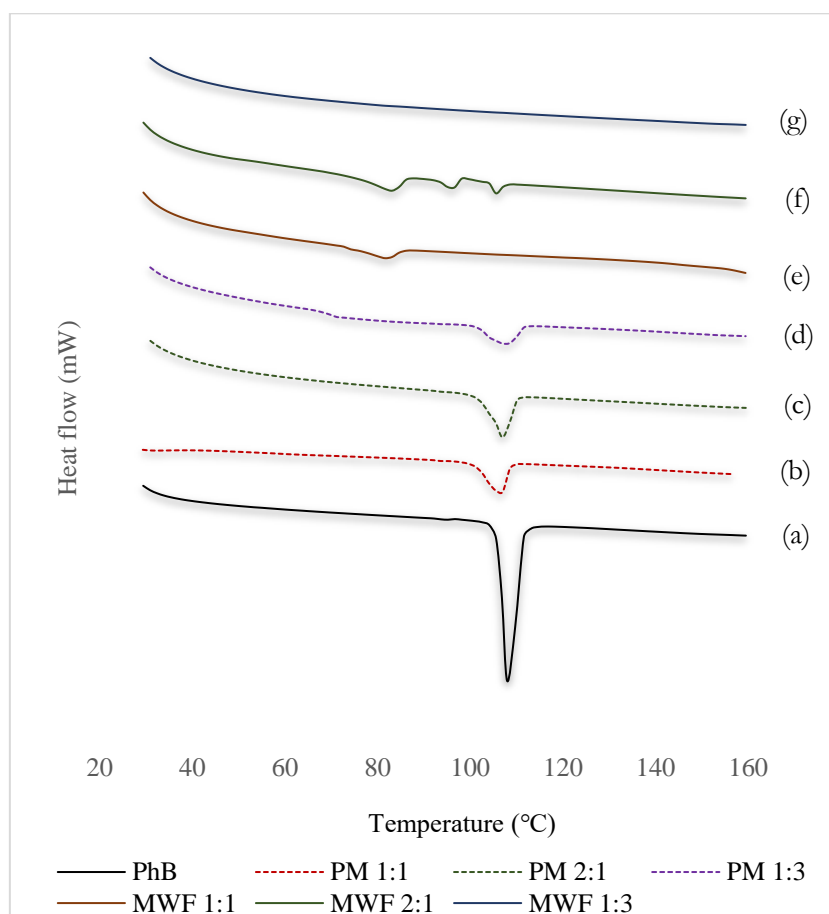


Figure 3. 1. DSC profiles for phenylbutazone (PhB) along XDP 3050 based physical mixtures (PM) and microwave formulations (MWF). (a) Pure PhB, (b) PM 1:1 (c) PM 2:1 (d) PM 1:3 (e) MWF 1:1 (f) MWF 2:1 and (g) MWF 1:3

Analysis of the physical mixture of PhB with the silica in Figure 3.1 (b), (c) and (d) at 1:1, 2:1 and 1:3 ratios did not reveal any changes other than reduction in the intensity of the peak thus implying that the drug had been converted from crystalline to partially amorphous form after physical mixture. In Figure 3.1 (e), a single broad melting peak with reduced intensity for the drug was observed at 81.64 °C thus confirming a shift to a lower temperature in comparison with the melting peak of the pure drug. This single melting peak indicated the presence of an  $\alpha$  polymorphic form of phenylbutazone [173] which implies that there is residual presence of the drug in crystalline state even after the formulation as previously reported [174]. At this ratio, the pore volume ( $1.70 \text{ cm}^3\text{g}^{-1}$ ) and pore diameter (229 Å) of the silica were unable to accommodate the whole content of the drug, possibly some of the drug may be inside the pores of the silica while some could be on the surface. Figure 3.1 (f) illustrates three polymorphic peaks for phenylbutazone at 83.13 °C for  $\alpha$ -form, 96.62 °C for  $\beta$ -form and 105.58 °C for  $\delta$ -form which shows the highest melting temperature [173]. The first two were broad with reduced intensity and shifted to a lower temperature in comparison to the most stable form ( $\delta$ -form), possibly indicating a transformation of the drug from a crystalline to a partially amorphous form during the formulation. The later peak was sharper with reduced intensity and occurred very close to the melting peak of the pure drug (107.98 °C); this implies the presence of drug molecules in a crystalline state after formulation, which suggests an incomplete drug inclusion. At this ratio (2:1), the pore volume ( $1.70 \text{ cm}^3\text{g}^{-1}$ ) of the silica was insufficient for hosting the extra phenylbutazone molecules. However, in Figure 3.1 (g), there was a complete disappearance of the drug-melting peak after the formulation, thus confirming the conversion of crystalline drug to amorphous form as a result of microwave formulation. A complete transformation of the drug to an amorphous form at this ratio (1:3) was the reason behind the 99.7 % ( $\pm 6.4$  %) drug release discussed earlier as seen in Figure 3.13.

DSC was undertaken for phenylbutazone formulated with Syloid® XDP 3150 and AL1 FP at the same ratios mentioned earlier. Figures 3.2 and 3.3 illustrate the DSC thermograms for XDP 3150 and AL1 FP based physical mixtures and microwave formulations along with pure PhB.

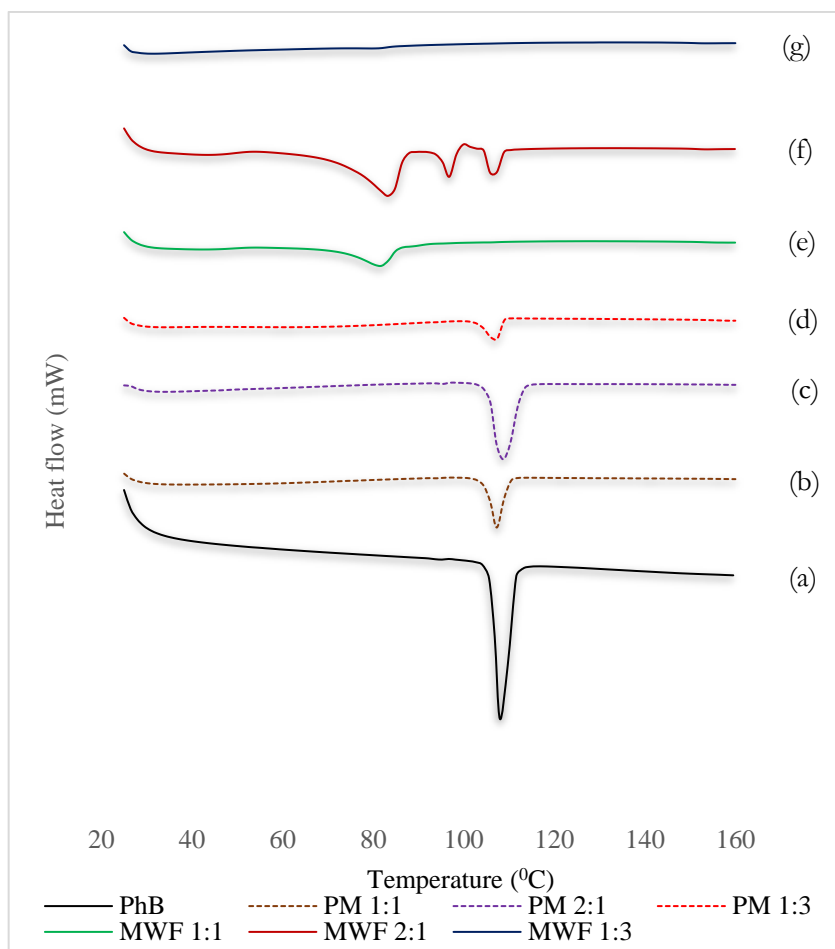


Figure 3. 2. DSC profiles for phenylbutazone (PhB) along XDP 3150 based physical mixtures (PM) and microwave formulations (MWF). (a) Pure PhB, (b) PM 1:1 (c) PM 2:1 (d) PM 1:3 (e) MWF 1:1 (f) MWF 2:1 and (g) MWF 1:3

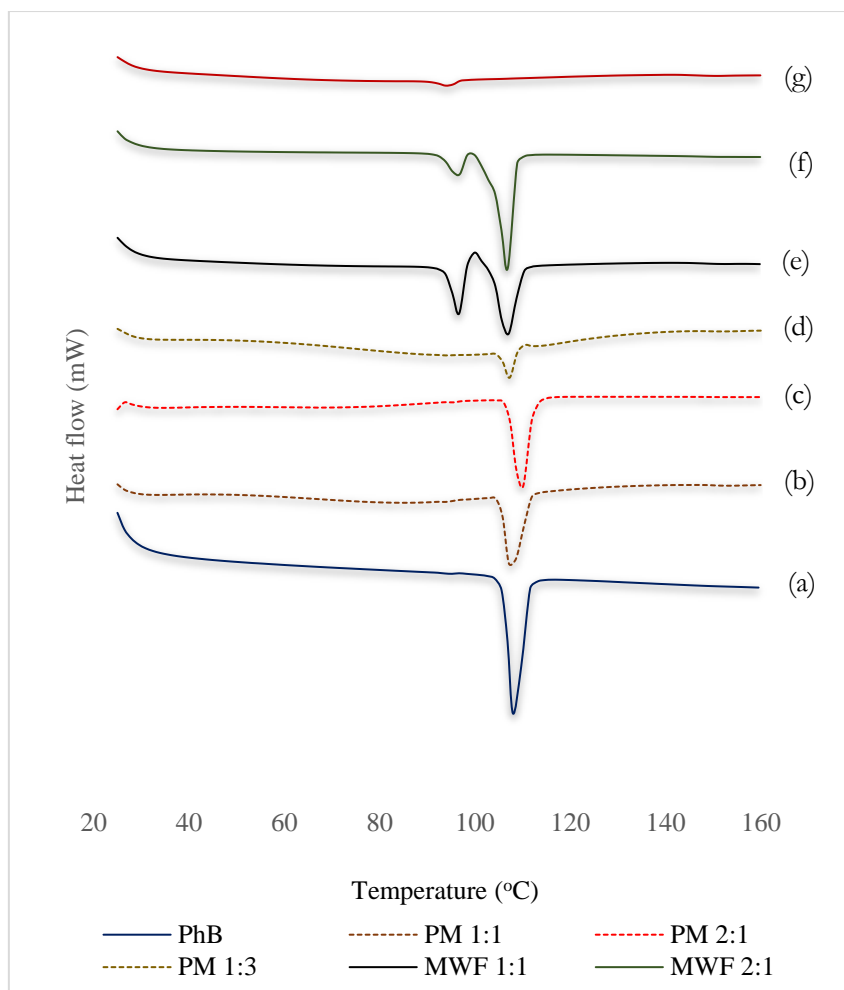


Figure 3. 3. DSC profiles for phenylbutazone (PhB) along AL1 FP based physical mixtures (PM) and microwave formulations (MWF). (a) Pure PhB, (b) PM 1:1 (c) PM 2:1 (d) PM 1:3 (e) MWF 1:1 (f) MWF 2:1 and (g) MWF 1:3

Physical mixtures in the two figures, showed similar characteristics to those observed in Figure 3.1 (b), (c) and (d). There was no significant difference between Figure 3.2 and 3.3 other than some small variations in the melting peaks of phenylbutazone of not more than  $\pm 1$  °C. Figure 3.3 (e) showed two well-defined, sharp endothermic peaks at 96.67 °C and 107.07 °C indicating a  $\beta$  and  $\delta$ -polymorph for phenylbutazone [175]. The former at the lower temperature, confirmed the presence of the partially-amorphous form of the drug while the latter was very close to the melting peak of the pure drug thus indicating the presence of some PhB molecules in a crystalline state after formulation. Possibly the small pore volume and diameter ( $0.23 \text{ cm}^3\text{g}^{-1}$  and  $26 \text{ \AA}$ ) could be the reason why the AL1 FP accepts the drug molecules beyond its capacity

even though an equal mass was used for physical mixing and therefore, drug molecules were deposited on the external surface of the silica. For the 2:1 ratio (Figure 3.3f), a peak with reduced intensity at 96.82 °C ( $\beta$ -form) for phenylbutazone was observed which shifted to a lower temperature compared with the melting peak of the  $\delta$ -form indicating a transition from a crystalline to partially amorphous form as a result of formulation. A sharp and well-defined peak with high intensity was recorded at 106.89 °C, close to the melting peak of the drug thus indicating the existence of drug molecules in a crystalline state, which suggests an incomplete inclusion complexation. At a 1:3 drug-silica ratio (Figure 3.3g), the high surface area of AL1 FP ( $605 \text{ m}^2\text{g}^{-1}$ ) could be the reason why the silica accommodated the major portion of the drug inside its pores, and the residual presence of the drug melting peak observed could be due to small pore volume and pore diameter of the syloid silica.



### 3.2.1.2. X-ray diffraction (XRD)

Following on from the DSC results discussed earlier, XRD investigations of the samples were conducted to support the studies. The X-ray diffraction (XRD) patterns of pure phenylbutazone and XDP 3050 based physically mixed and microwave formulations at 1:1, 2:1 and 1:3 are presented in Figure 3.4. Previous XRD studies using naproxen noted that the diminishment of peak intensities confirmed that the crystalline drug had molecularly dispersed within the mesoporous silica material [176], resulting in an amorphous formulation with an absence of characteristic peaks [88].

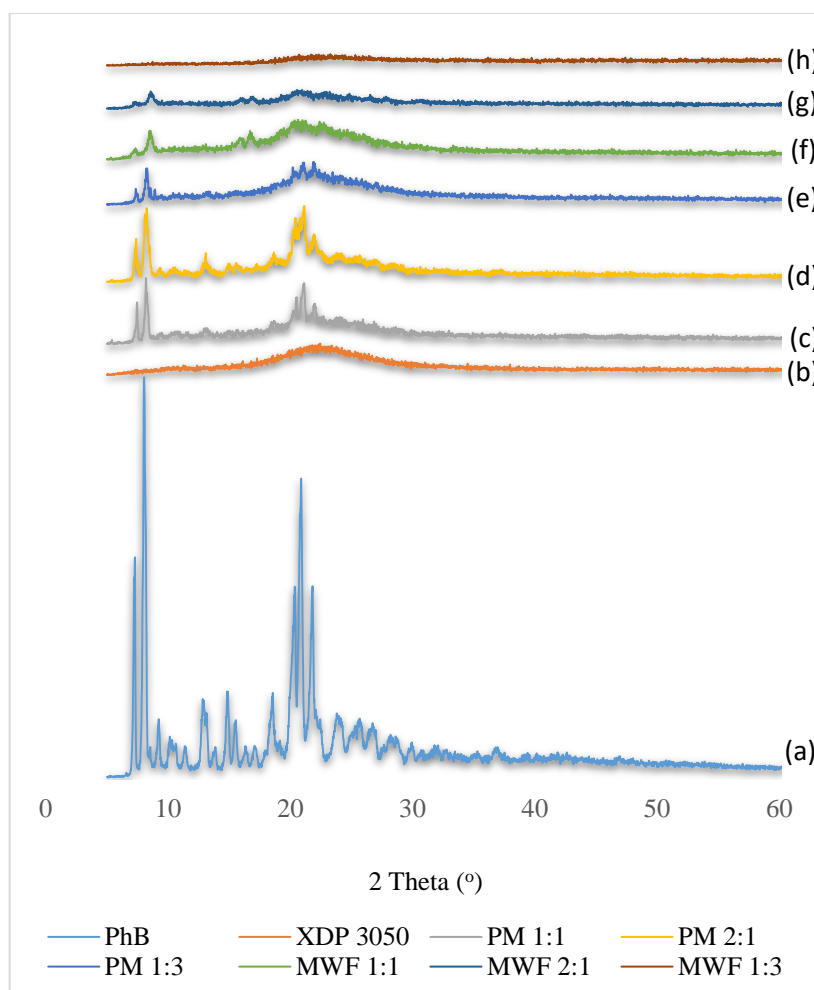


Figure 3. 4. XRD patterns for (a) PhB, (b) XDP 3050, (c) PM 1:1, (d) PM 2:1, (e) PM 1:3 (f) MWF 1:1, (g) MWF 2:1 and (h) MWF 1:3.

A similar result was observed in this work whereby the purely crystalline phenylbutazone that could be seen in Figure 3.4 (a) with sharp diffraction peaks at  $8.12^\circ$ ,  $12.95^\circ$ ,  $18.59^\circ$  and  $20.88^\circ$

in comparison with the featureless pattern for the syloid XDP 3050 silica (Figure 3.4b). Phenylbutazone peaks were still evident in the physical mixtures of 1:1, 2:1 and 1:3 drug-silica ratios (Figure 3.4c, d and e) even though the mixing process reduced them. In contrast, diffraction patterns for the samples formulated using microwave (Figure 3.4f, g) show small diffraction peaks with reduced intensity suggesting that the samples were largely non-crystalline.

In Figure 3.4h, the sample was converted to the amorphous form following formulation with the Syloid<sup>®</sup> XDP silica. As discussed earlier, from analysing the 1:1, 2:1 and confirming the entire drug had remained within the formulation, the presence of small peaks can be explained by a reduced concentration of drug in the former and a transformation to the amorphous form in the latter. In summary, XRD results are in good agreement with those reported using DSC. Figures 3.5 and 3.6 show the XRD patterns of XDP 3150 and AL1 FP based physical mixtures and microwave formulations at 1:1, 2:1 and 1:3 drug silica ratios. Sharp diffraction patterns with high intensity for the pure drug were observed in both the figures, which were discussed earlier while the absence of diffraction peaks in Syloid<sup>®</sup> XDP 3150 and AL1 FP indicates the amorphous nature of the two silicas.

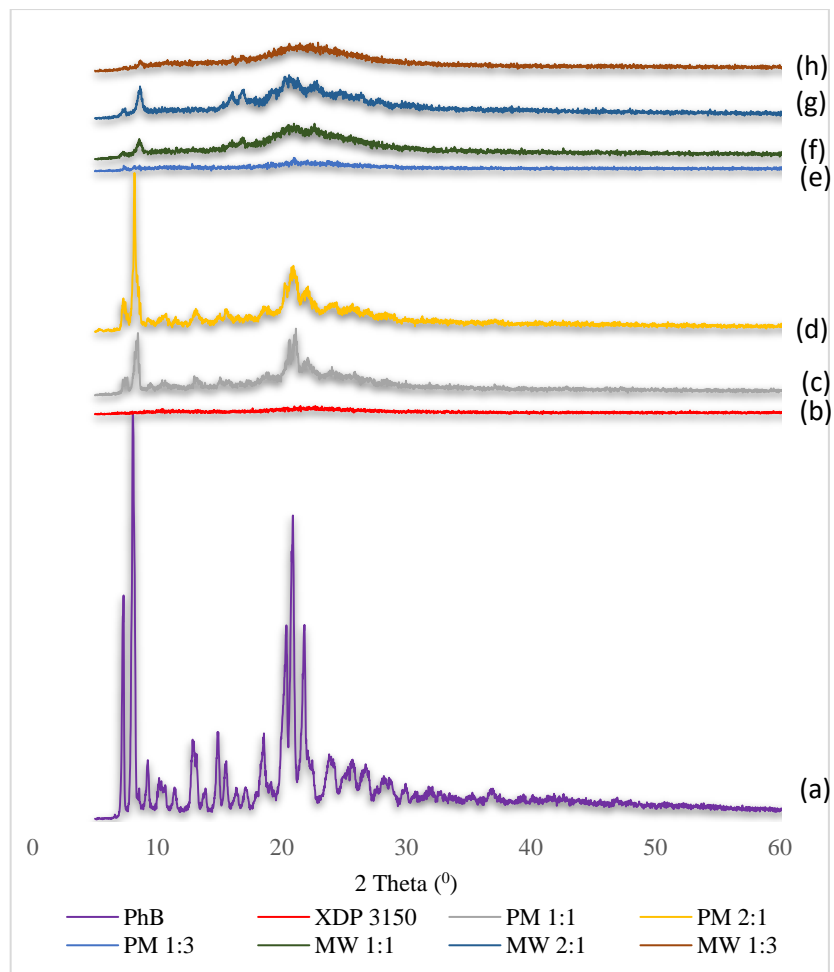


Figure 3. 5. XRD patterns for (a) PhB, (b) XDP 3150, (c) PM 1:1, (d) PM 2:1, (e) PM 1:3 (f) MWF 1:1, (g) MWF 2:1 and (h) MWF 1:3.

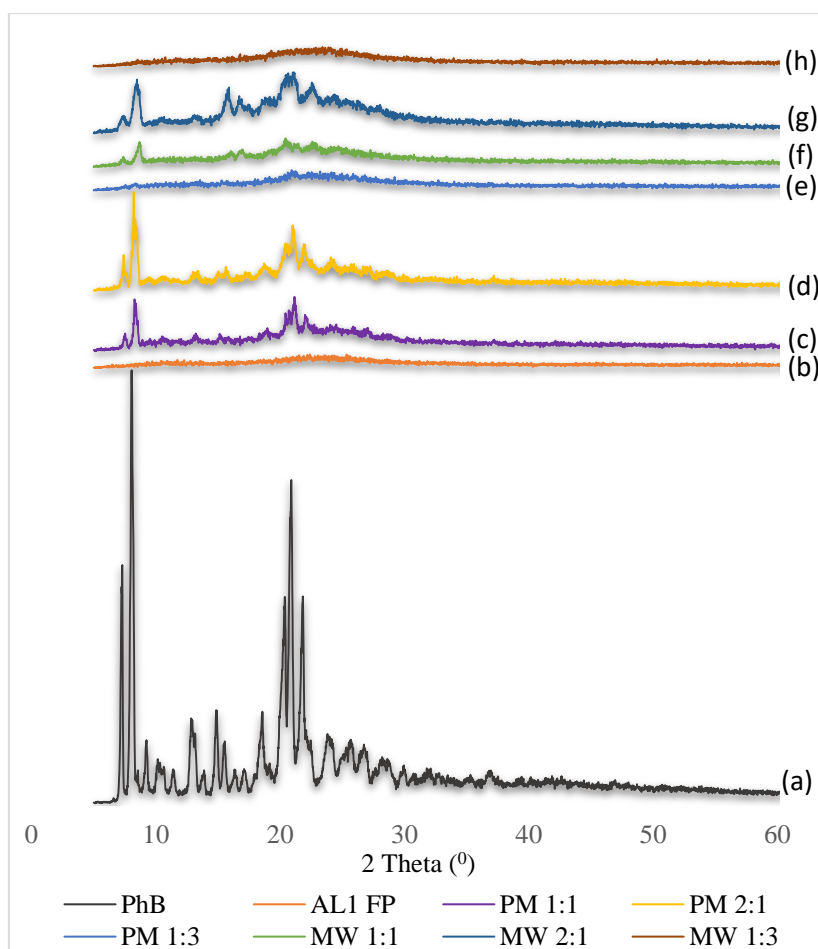


Figure 3. 6. XRD patterns for (a) PhB, (b) AL1 FP, (c) PM 1:1, (d) PM 2:1, (e) PM 1:3 (f) MWF 1:1, (g) MWF 2:1 and (h) MWF 1:3.

The characteristic diffraction peaks of crystalline phenylbutazone in the physical mixes with XDP3150 and AL1 FP were still evident with a higher intensity for the 2:1 ratio compared with 1:1. The diffraction peaks in 1:3 were not visible due to the three times mass of the silicas used in the physical mixing. The less intense peaks observed in the 1:1 ratio using the microwave formulation indicates that the crystalline drug, highly dispersed in the amorphous XDP and AL1 FP silicas, was brought to a less crystalline state due to the microwave energy applied during the formulation. In the 2:1 ratio, the diffraction peaks of the drug were more visible, a consequence of pore volumes ( $1.70$  and  $0.40 \text{ cm}^3\text{g}^{-1}$ ) and the large mass of the drug used for the formulation, indicating that the two silicas were unable to accommodate the whole content of the drug in their pores. There was a complete disappearance of diffraction peaks after the microwave formulations in 1:3 ratios. This confirms that the drug was no longer in a crystalline

state in such ratios, which provides proof of its actual inclusion within the silicas [177]. These results were in full agreement with DSC, confirming amorphisation was achieved using microwave formulation with each amorphous silica.

### 3.2.1.3. Fourier transform infrared spectroscopy (FT-IR)

FT-IR spectroscopy was utilised to monitor the presence of phenylbutazone and determine interactions with the three syloid (XDP 3050, XDP 3150 and AL1 FP) silicas. Figure 3.7, 3.8 and 3.9 all include the spectra for pure phenylbutazone, indicating the expected absorption bands at wavenumbers (with corresponding functional groups) of  $2922\text{ cm}^{-1}$  for C-H,  $1713\text{ cm}^{-1}$  for C=O and  $1290\text{ cm}^{-1}$  for C-N (aromatic amine) respectively.

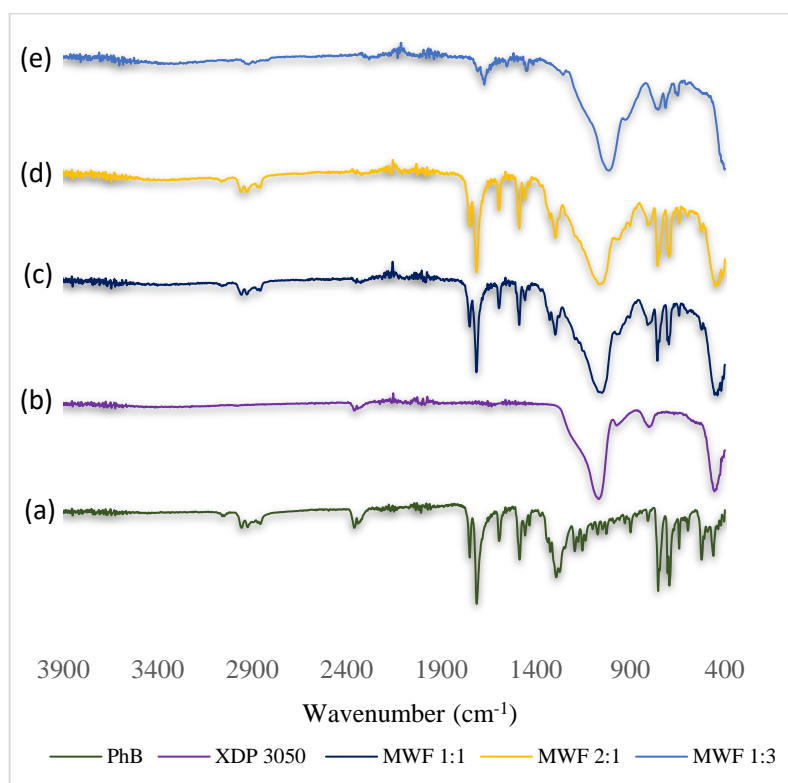


Figure 3. 7. FT-IR analysis of (a) PhB (b) XDP 3050, (c) MWF 1:1, (d) MWF 2:1, and (e) 1:3 drug-XDP 3050 formulations

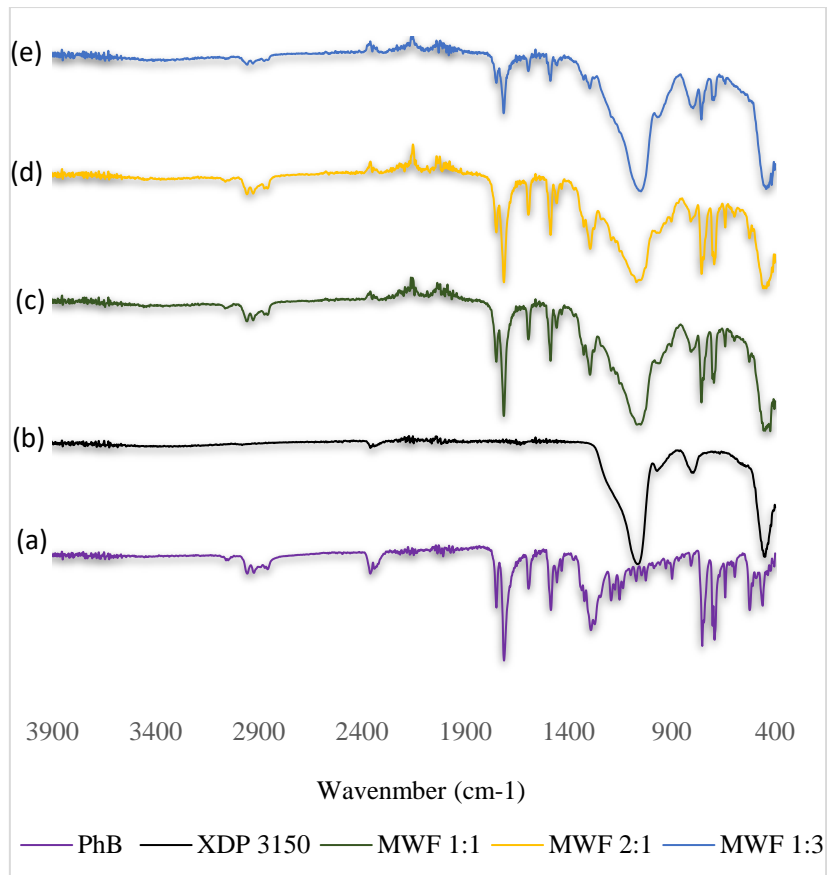


Figure 3. 8. FT-IR analysis of (a) PhB (b) XDP 3150, (c) MWF 1:1, (d) MWF 2:1, and (e) 1:3 drug-XDP 3150 formulations

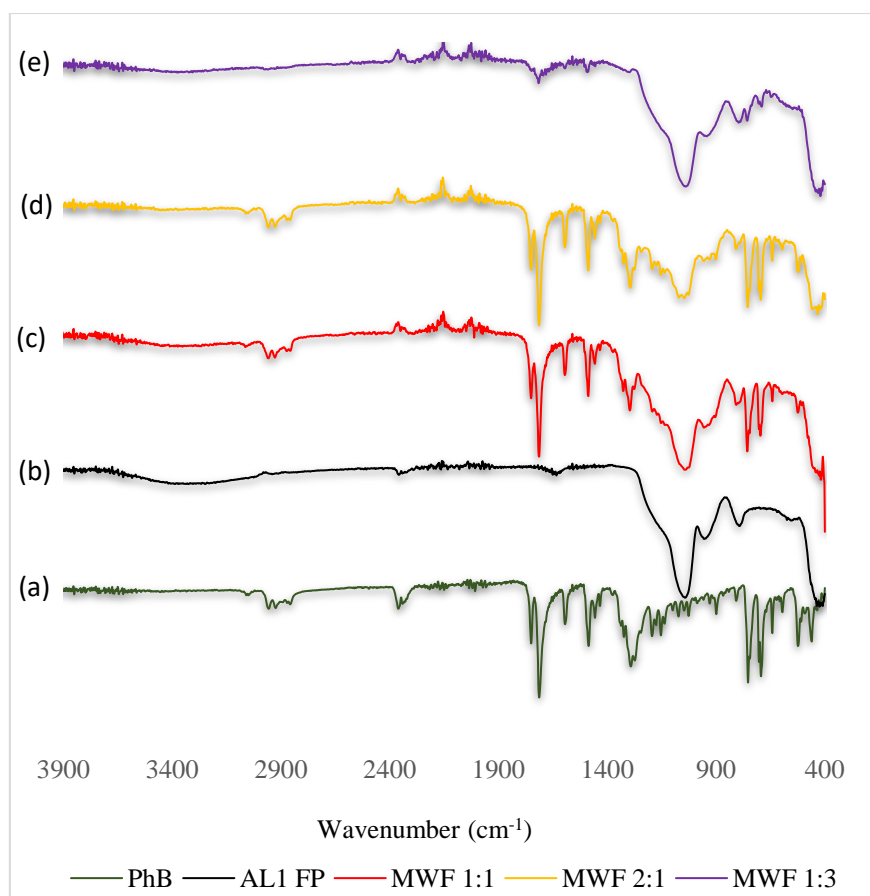


Figure 3. 9. FT-IR analysis of (a) PhB (b) AL1 FP, (c) MWF 1:1, (d) MWF 2:1, and (e) 1:3 drug-AL1 FP formulations

The three Syloids silicas were analysed using FT-IR spectroscopy and all displayed the expected intense and broad Si-O absorption band at 1064–1070  $\text{cm}^{-1}$  [178]. The absorption band at 962  $\text{cm}^{-1}$  corresponds to Si-OH bending. On the other hand, the symmetric stretching vibrations of Si-O-Si appeared at 788  $\text{cm}^{-1}$  and its bending vibration appeared at 453  $\text{cm}^{-1}$  [179].

The IR spectra for microwave formulations of phenylbutazone and the three syloid silicas (1:1 and 2:1 ratios) was reflected by the appearance of the characteristic intense peaks for drug and less intense peaks for the silicas. For the 1:3 ratio (i.e. having a higher silica content) in all the three phenylbutazone-silica formulated products, the results indicated a shift in the peaks, suggesting a successful interaction of the drug with the silicas. The microwave formulation method did not reveal any changes in the specific absorption bands for the drug, suggesting a lack of degradation because of the formulation process. Furthermore, the spectra did not display

any obvious additional peaks, thus indicating there had been no significant changes in the chemical structure or drug-silica interactions.

#### 3.2.1.4. Scanning electron microscopy (SEM)

Scanning electron microscopy (SEM) was used for solid-state characterisation of the drug-silica system; the technique allowed an in-depth investigation into the morphological aspect of the interacted mixtures obtained by the microwave formulation method. SEM displayed morphological changes, which are associated with the interaction between the drug and silica, and any existence of a single component in the formulation obtained.

Surface morphologies of the pure phenylbutazone (x500 magnification) and the three syloid silicas - XDP 3050, XDP 3150 and AL1 FP (x500 magnification) are presented in Figure 3.10. The drug's crystalline state, along with the disordered irregular shapes of AL 1 FP, XDP 3150, and XDP 3050 silicas were evident by SEM in the Figure.

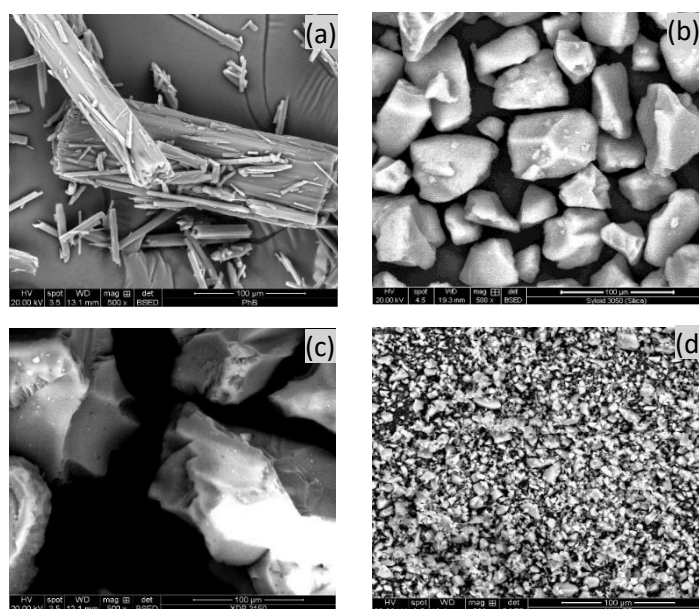


Figure 3. 10. Scanning electron microscope (SEM) images of (a) PhB, (b) XDP 3050 (c) XDP 3150, and (d) AL1 FP at x500 magnification



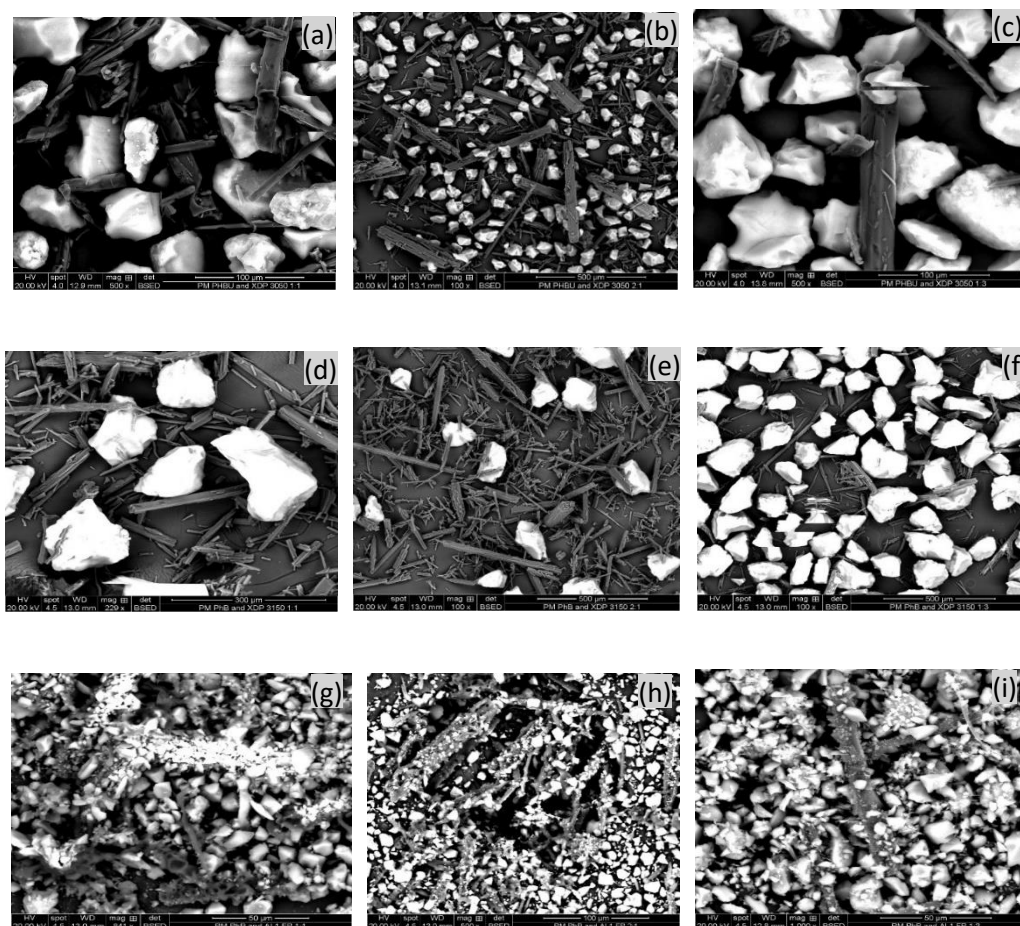


Figure 3. 11. SEM images at x500 of (a) PM of PhB and XDP 3050 (1:1), (b) PM of PhB and XDP 3050 (2:1), (c) PM of PhB and XDP 3050 (3:1). (d), PM of PhB and XDP 3150 (1:1), (e) PM of PhB and XDP 3150 (2:1), (f) PM of PhB and XDP 3150 (1:3). (g) PM of PhB and AL1 FP (1:1), (h) PM of PhB and AL1 FP (2:1), and (i) PM of PhB and AL1 FP (1:3).

Figure 3.11 displays nine images of the physical mixtures of phenylbutazone with three syloid silicas - XDP 3050, XDP 3150 and AL1 FP at 1:1, 2:1 and 1:3 (x500 magnifications) drug-silica ratios. It can be seen evidently in the images the needle-like crystals of the phenylbutazone and irregular shapes of the three silicas. This suggests that the drug and the silicas do not well together and remained separated at the microscopic level using physical mixing alone as the drug retained a crystalline structure.

Surface morphologies of phenylbutazone with three syloid-based microwave formulations at 1:1, 2:1 and 1:3 (x500 magnifications) drug-silica ratios are presented in Figure 3.12. The SEM images confirmed the significant effects of the microwave formulation process as the drug had

lost its crystalline structure. However, PhB could hardly be seen on the surface of AL 1 FP due to a larger surface area ( $605 \text{ m}^2\text{g}^{-1}$ ), smaller pore volume and pore diameter ( $\text{cm}^3\text{g}^{-1}$  and  $\text{\AA}$ ). For Syloid XDP 3150 and XDP 3050 based formulations, there was an even distribution of the former particles with phenylbutazone particles reduced in size while for the latter, possibly more of the drug has been molecularly dispersed on the surface as visible in the SEM images (Figure 3.12).

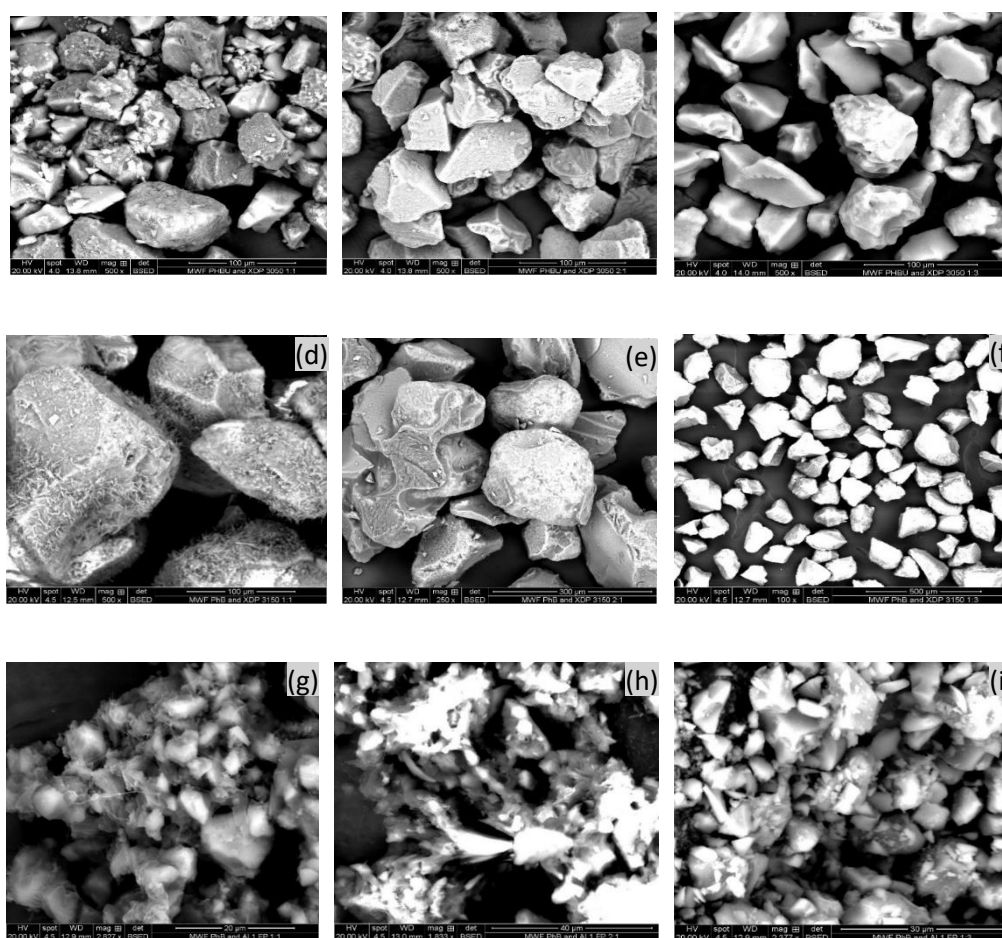


Figure 3. 12. SEM images at x500 of (a) MWF of PhB and XDP 3050 (1:1), (b) MWF of PhB and XDP 3050 (2:1), (c) MWF of PhB and XDP 3050 (3:1). (d), MWF of PhB and XDP 3150 (1:1), (e) MWF of PhB and XDP 3150 (2:1), (f) MWF of PhB and XDP 3150 (1:3), (g) MWF of PhB and AL1 FP (1:1), (h) MWF of PhB and AL1 FP (2:1), and (i) MWF of PhB and AL1 FP (1:3).

Overall, these results justified an enhancement in the dissolution profiles of phenylbutazone formulated with the syloid silicas using the microwave method discussed earlier, due to the

absence of any crystalline structures of the drug and possible dispersion of drug molecules on the surfaces of the silicas.

### 3.2.2. *In vitro* phenylbutazone release

In order to investigate the aim of enhancing phenylbutazone's dissolution rate using a microwave method, *in vitro* dissolution profiles of formulated products using three carriers were compared to those of pure drug. The dissolution profile of phenylbutazone, along with Syloid XDP 3050 at different ratios is displayed in Fig. 3.13 over a period of 45 min in pH 7.0 phosphate buffer. As can be seen, pure phenylbutazone that had not undergone the formulation process exhibited 12.4 % ( $\pm 0.3$  %) drug release after 5 min yet only increased to a maximum of 31.9 % ( $\pm 3.9$  %) release after 45 min. For many drugs, this low percentage of drug release after this time would be deemed unsuitably low and may limit bioavailability.

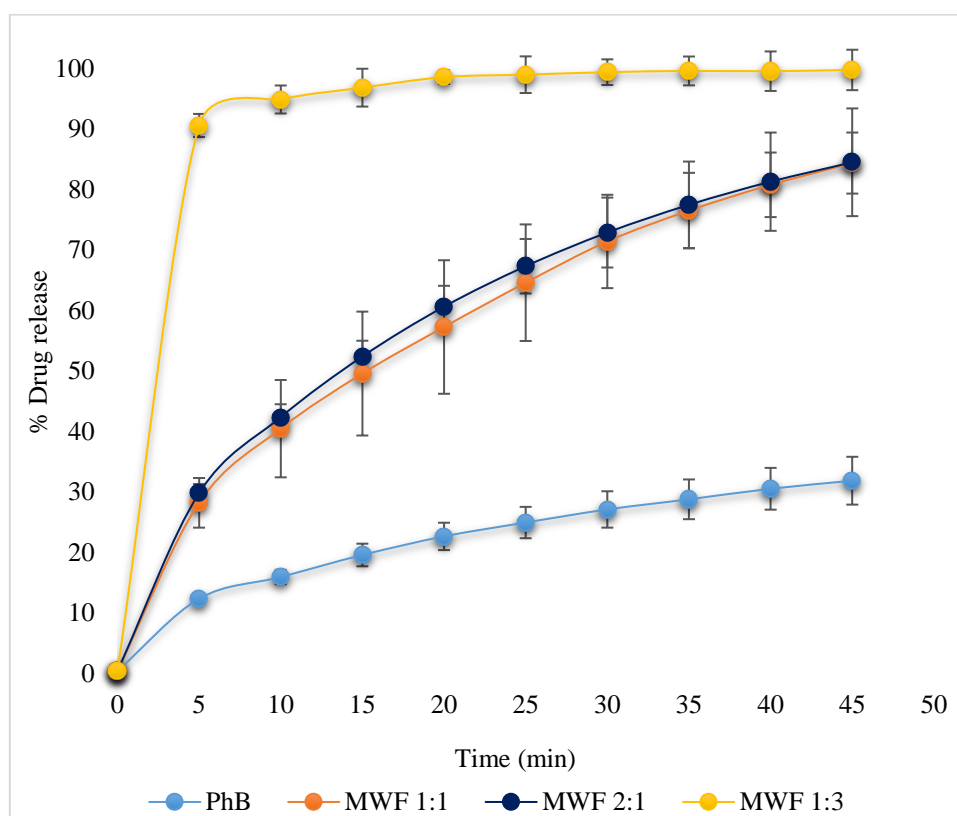


Figure 3. 13. Release profiles for phenylbutazone (PhB), Syloid<sup>®</sup> XDP 3050 based formulations using microwave at 1:1, 2:1 and 1:3 drug to silica ratios. Each data point represents the mean of triplicate results ( $\pm$ SD).

The XDP 3050 silica-based formulation exhibited a dramatic enhancement in percentage dissolution, confirming that the presence of silica contributed to the increase. Firstly, the 1:1 drug-silica ratio achieved a percentage release of 28.2 % ( $\pm 4.1$  %) after only 5 min, i.e. almost equal to the overall period observed for drug alone. After a period of 45 min, this value had increased to 84.3 % ( $\pm 5.0$  %), far higher than that seen for drug alone. Secondly, 2:1 showed a promising percentage release of 29.8 % ( $\pm 1.5$  %) after 5 min compared with 1:1, yet after a total of 45 min had not exceeded the former ratio to reach a maximum percentage release of 84.5 % ( $\pm 8.9$  %) i.e. almost similar to the 1:1 ratio discussed earlier. Finally, 1:3 was found to be the most successful drug-silica ratio for enhancing percentage release with an impressive 90.5 % ( $\pm 1.5$  %) released after 5 min, i.e. greater than the total seen for pure drug after 45 min, increasing to a maximum of 99.7 % ( $\pm 6.4$  %) release after 45 min. One reason for this impressive release is that the 1:3 formulation is with higher silica content and presents a large number of available pores when compared to the formulation with lower XDP 3050 content (i.e. 1:1 and 2:1). The chances of pore filling by the molten drug to full capacity in the 1:3 ratio is high and some phenylbutazone is being deposited on the surface of the XDP 3050, which resulted in an impressive release [19].

When determining why all three ratios improved the percentage drug release, following the microwave formulation of PhB-XDP 3050, it would appear that the transformation from crystalline to partially amorphous form as in the case of 1:1 and 2:1 ratios and completely amorphous for 1:3 ratio plays a key role. This was evidenced by the DSC, XRD and dissolution profiles of the formulated ratios. This is in agreement with other researchers and fits well with this research [180, 181].

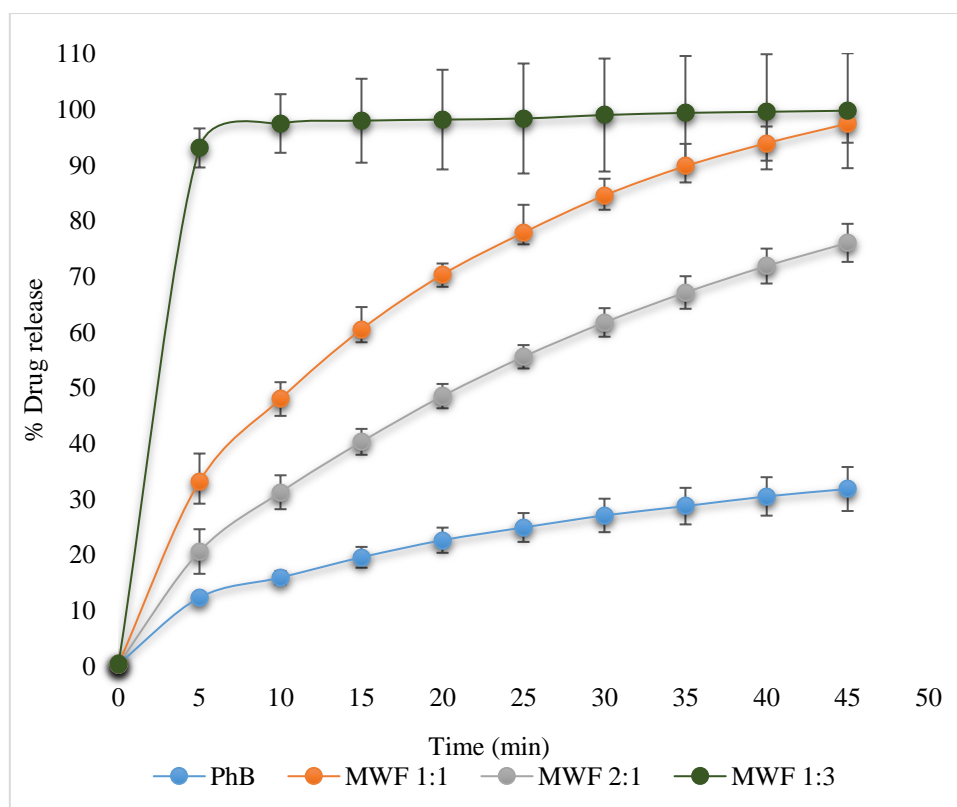


Figure 3. 14. Release profiles for phenylbutazone (PhB), Syloid® XDP 3150 based formulations using microwave at 1:1, 2:1 and 1:3 drug to silica ratios. Each data point represents the mean of triplicate results ( $\pm$ SD).

The release behaviour of phenylbutazone from Syloid® XDP 3150 is presented in Figure 3.14. Slow and steady drug release was evidenced for the 1:1 ratio, i.e. 33.2 % ( $\pm$  6.4 %) and 97.5 % ( $\pm$  5.3 %) after 5 and 45 min respectively. The 2:1 drug-silica ratio made little difference to the dissolution behaviour when compared to the aforementioned profiles yet was still significant in comparison with pure phenylbutazone, for example 20.6 % ( $\pm$  5.8 %) and 76.1 % ( $\pm$  7.9 %) was evidenced after 5 and 45 min respectively. As twice the mass of the drug was used during the formulation in comparison with the mass of silica, this was possibly because the pores of the silica were unable to accommodate the whole content of the drug. This anomaly was attributed to the pore diameter of the silica (200 Å) [6], in which some part of the drug may be inside the pores of the silica whilst some was on the surface. The 1:3 drug-silica ratio provided rapid drug release reaching 93.1 % ( $\pm$  3.5 %) after 5 min followed by continuous release to reach a maximum of 99.8 % ( $\pm$  5.2 %) after 45 min.

The findings showed that the dissolution profile of the 1:3 ratio containing higher silica content had the best drug release in comparison to 1:1 and 2:1 ratios with lower silica content. It is interesting to note that conversion from crystalline to amorphous form of the drug in the 1:3 ratio brought about the increase as evidenced in the DSC and XRD findings. Based on these findings, the physicochemical properties of the Syloid<sup>®</sup> XDP 3150 is best suited to formulate the drug using 1:1 and 1:3 drug-silica ratios, the drug is transported and uniformly distributed inside the pores of the silica as confirmed by the results of XRD and DSC (discussed earlier). The dissolution profile studies with the aforementioned silica provided a high increase compared with the pure drug, which could lead to a great enhancement in the oral bioavailability of phenylbutazone. Therefore, the microwave formulation technique is a potential method to overcome phenylbutazone's poor solubility and could lead to significant enhancement in the therapeutic effect.

Figure 3.15 displays the dissolution profile of the microwave technique employed with both phenylbutazone and AL 1 FP formulations. It can be seen that there was a remarkable enhancement of the dissolution rate compared with the pure drug. For the 1:3 drug-silica ratio 46.4 % ( $\pm 1.92$  %) of drug was released in 5 min followed by 97.6 % ( $\pm 2.4$  %) in 45 min. The 1:3 ratio was much faster than the 1:1 and 2:1 ratio. In 5 min, 23.5 % ( $\pm 3.5$  %) and 18.5 % ( $\pm 7.3$  %) of drug was released for the aforementioned while 78.8 % ( $\pm 8.8$  %) and 77.6 % ( $\pm 4.0$  %) was released after 45 min respectively. The different percentages of release occurred due to the different mass of AL1 FP used in this formulation. The AL1 FP silica employed, coupled with the microwave technique, were responsible for the improved dissolution profiles.

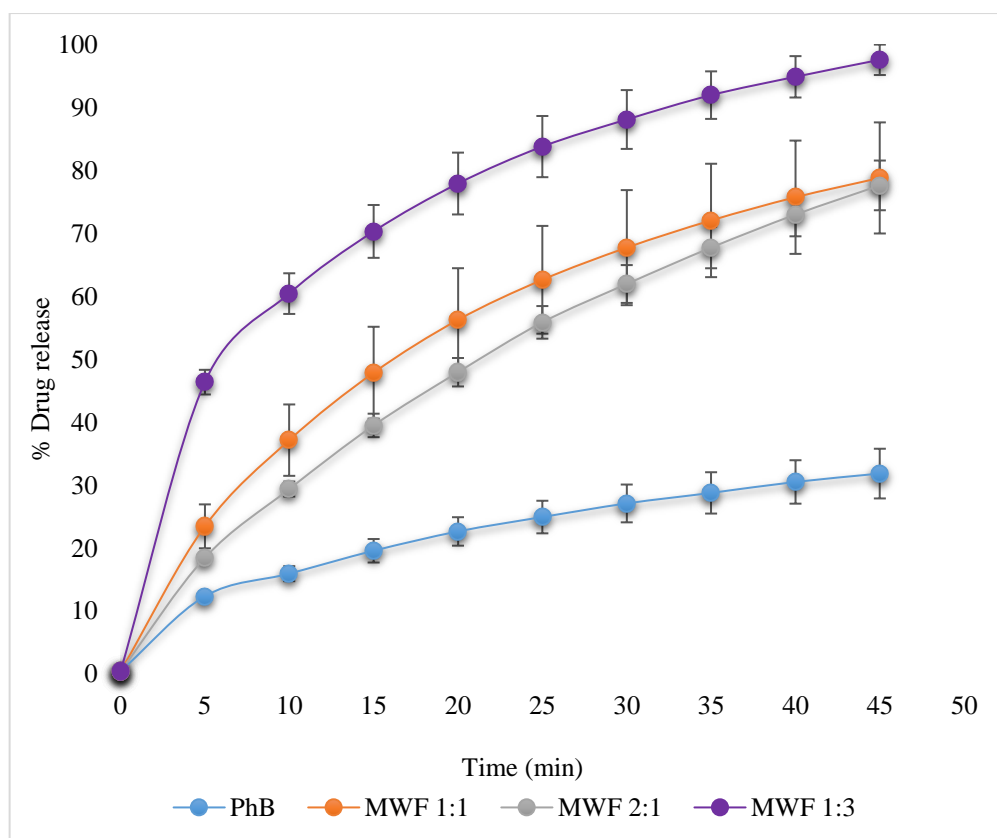


Figure 3. 15. Release profiles for phenylbutazone (PhB), Syloid® AL1 FP based formulations using microwave at 1:1, 2:1 and 1:3 drug to silica ratios. Each data point represents the mean of triplicate results ( $\pm$ SD).

All the three ratios have improved the percentage release following a microwave formulation method, it would appear that the transformation from the crystalline to partially amorphous form (as evidenced by DSC, XRD and dissolution profiles of processed samples) plays a key role. This has been the conclusion of other researchers, when investigating alternative mesoporous materials [182], and fits well with the results from this work. However, when considering why the three ratios did not facilitate the same increase in percentage release, it is more appropriate to consider amount of Syloid® AL1 FP used in making the physical mixture for the three ratios, this has been identified in Section 2.2.1.

### 3.2.3. Solid state characterisation of IMC

#### 3.2.3.1 Differential scanning calorimetry (DSC)

DSC analysis was applied to investigate the phase change during the formation of solid dispersions. As reported in Figure 3.16 (a), the thermal curve of pure indomethacin was characterised by a well-defined sharp melting peak at 160.7 °C in agreement with the melting point previously reported [183].

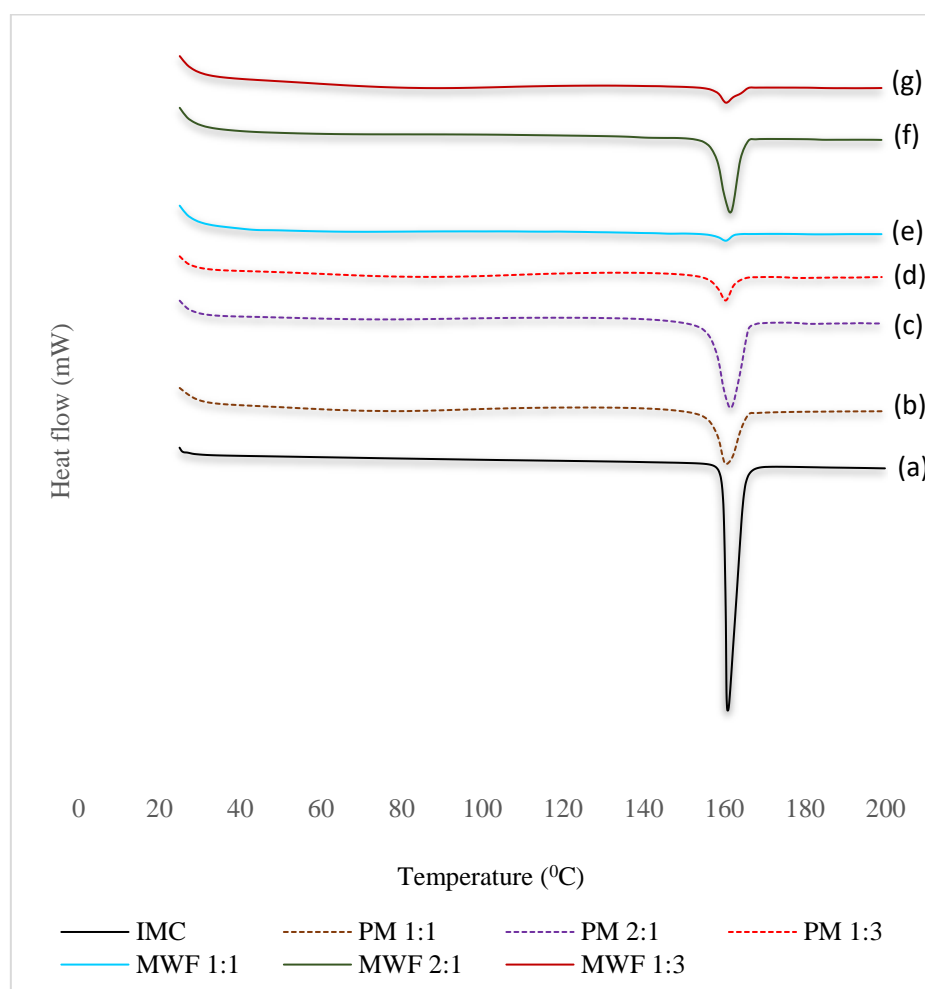


Figure 3. 16. DSC profiles for indomethacin (IMC) along XDP 3050 based physical mixtures (PM) and microwave formulations (MWF). (a) Pure IMC, (b) PM 1:1 (c) PM 2:1 (d) PM 1:3 (e) MWF 1:1 (f) MWF 2:1 and (g) MWF 1:3

In the thermal profile of physical mixtures 1:1, 2:1 and 1:3 (Figure 3.16 b, c and d), a small endothermic peak corresponding to the melting point of indomethacin was detectable, this event can be attributed to the transformation of indomethacin from crystalline to a partially



amorphous form during the programmed heating. After microwave formulation, there was a reduction in the size of the drug-melting peak for the three ratios, indicating a possible dispersion of drug into Syloid<sup>®</sup> XDP 3050 carrier as a result of microwave irradiation. The drug was embedded into the Syloid<sup>®</sup> XDP 3050 thereby bringing it to a less crystalline state in agreement with the XRD data discussed earlier. This result was compatible with indomethacin confinement into the mesoporous silica as previously reported [184] which resulted in amorphisation of the drug.

Figures 3.17 and 3.18 describe the DSC thermograms for Syloid<sup>®</sup> XDP 3150 and AL1 FP based physical mixtures and microwave formulations along with pure indomethacin at 1:1, 2:1 and 1:3 drug-silica ratios. Pure indomethacin was characterised by a single sharp melting peak at 160.7 °C as discussed in Figure 3.16. The DSC thermogram for AL1 FP in Figure 3.18 (b) showed a broad dehydration peak in the region of 70.0 °C to 133 °C which also appeared in its physical mixtures with the drug (Figure 3.18c and 3.18e) in 1:1 and 1:3 ratios. These events occurred ~ 30 °C higher than the boiling point of water indicating that the water molecules are held tightly within AL1 FP and therefore higher energy was required to overcome the hydrogen bonding because of intermolecular forces. The thermal peak of the drug in the physical mixtures showed slight variations in terms of size and broadening when compared with pure drug, indicating transformation from crystalline to a partially amorphous form.

For indomethacin formulated with XDP 3150 at three ratios, endothermic transitions corresponding to the drug were observed, the transitions were with reduced intensity and a broadened peak when compared with the transition of the pure drug. This phenomenon was attributed to the transition from the crystalline to amorphous form of indomethacin. DSC thermograms for AL1 FP formulated with indomethacin (Figure 3.18f) at a 1:1 ratio showed a glass transition ( $T_g$ ) at 56.1 °C,  $T_g$  of the mixtures was influenced by the compound compatibility and intermolecular interaction.

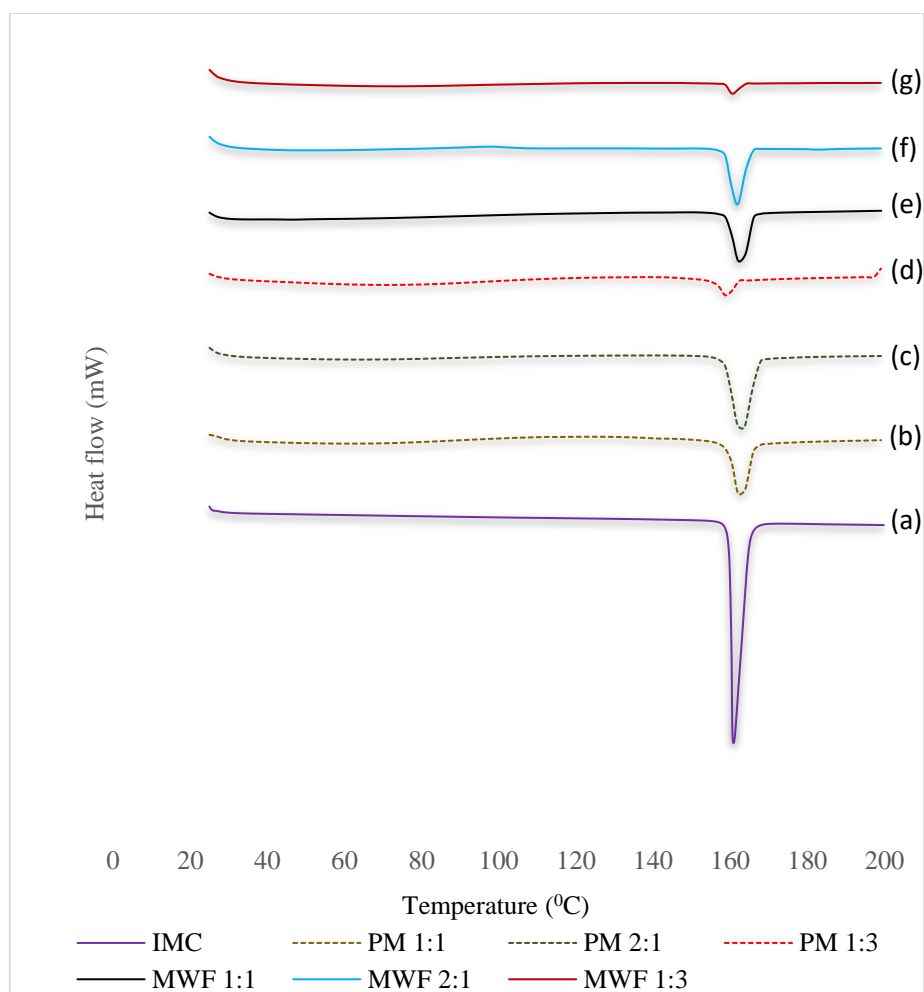


Figure 3. 17. DSC profiles for indomethacin (IMC) along XDP 3150 based physical mixtures (PM) and microwave formulations (MWF). (a) Pure IMC, (b) PM 1:1 (c) PM 2:1 (d) PM 1:3 (e) MWF 1:1 (f) MWF 2:1 and (g) MWF 1:3

The formulation prepared with a higher drug ratio (2:1) in Figure 3.18 (g) showed a glass transition ( $T_g$ ) at 48.8 °C followed by a broad exothermic transition possibly corresponding to a cross-linking reaction between the drug and the carrier at 114.9 °C initiated by heat or microwave irradiation during the formulation, it could also be a recrystallisation peak. A high peak intensity was observed at 158.3 °C, indicating that the small pore volume and pore diameter ( $0.40 \text{ cm}^3\text{g}^{-1}$  and  $26 \text{ \AA}$ ) could be the reason why the AL1 FP does not accept drug molecules beyond its capacity and therefore, the drug molecules are likely to be deposited on the surface of the AL1 FP. This has been the conclusion of other researchers, when investigating gemfibrozil with Syl-AL-1 and Syl-72 [177], and fits in well with the results of

this research. At the higher AL1 FP 1:3 ratio (Figure 3.18h), there was a complete disappearance of the melting peak of the indomethacin because enough pores were available to accommodate the molecules of the drug. All the Syloid<sup>®</sup> XDP 3050, 3150 and AL1 FP-indomethacin physical mixtures including formulations did not show any thermal transitions other than the thermal endotherm and glass transitions for the drug and dehydration for AL1 FP. This confirms the thermal stability of the product and absence of polymorphic transitions.

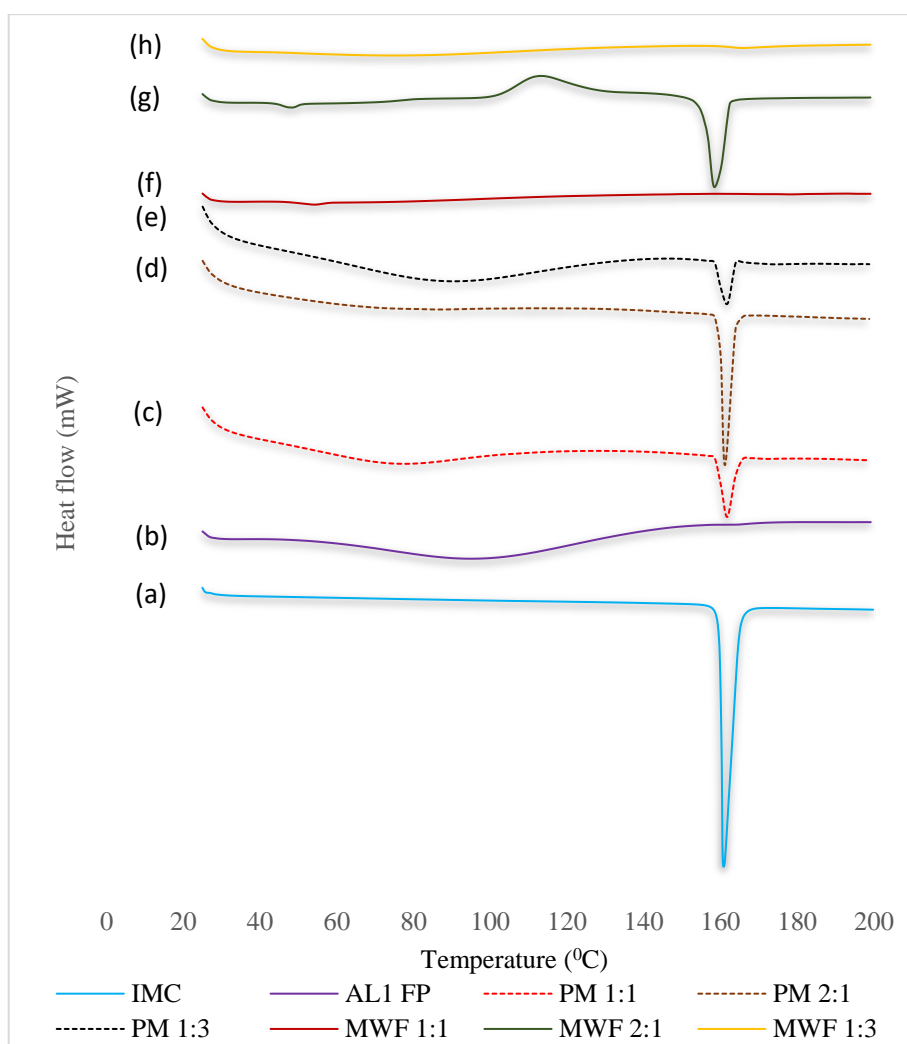


Figure 3. 18. DSC profiles for indomethacin (IMC) along AL1 FP based physical mixtures (PM) and microwave formulations (MWF). (a) Pure IMC, (b) AL1 FP (c) PM 1:1 (d) PM 2:1 (e) PM 1:3 (f) MWF 1:1 (g) MWF 2:1 and (h) MWF 1:3

### 3.2.3.2 X-ray diffraction (XRD)

To support the results of the DSC, indomethacin, Syloid<sup>®</sup> XDP 3050, XDP 3150 and AL1 FP, prepared physical mixtures as well as microwave formulations of the samples were analysed by XRD and the results are presented in Figures 3.19, 3.20 and 3.21. From the diffractions scanned, it is clear that indomethacin is a crystalline drug with high intensity diffraction peaks whereas all the Syloid<sup>®</sup> XDP 3050, XDP 3150 and AL1 FP carriers are completely amorphous.

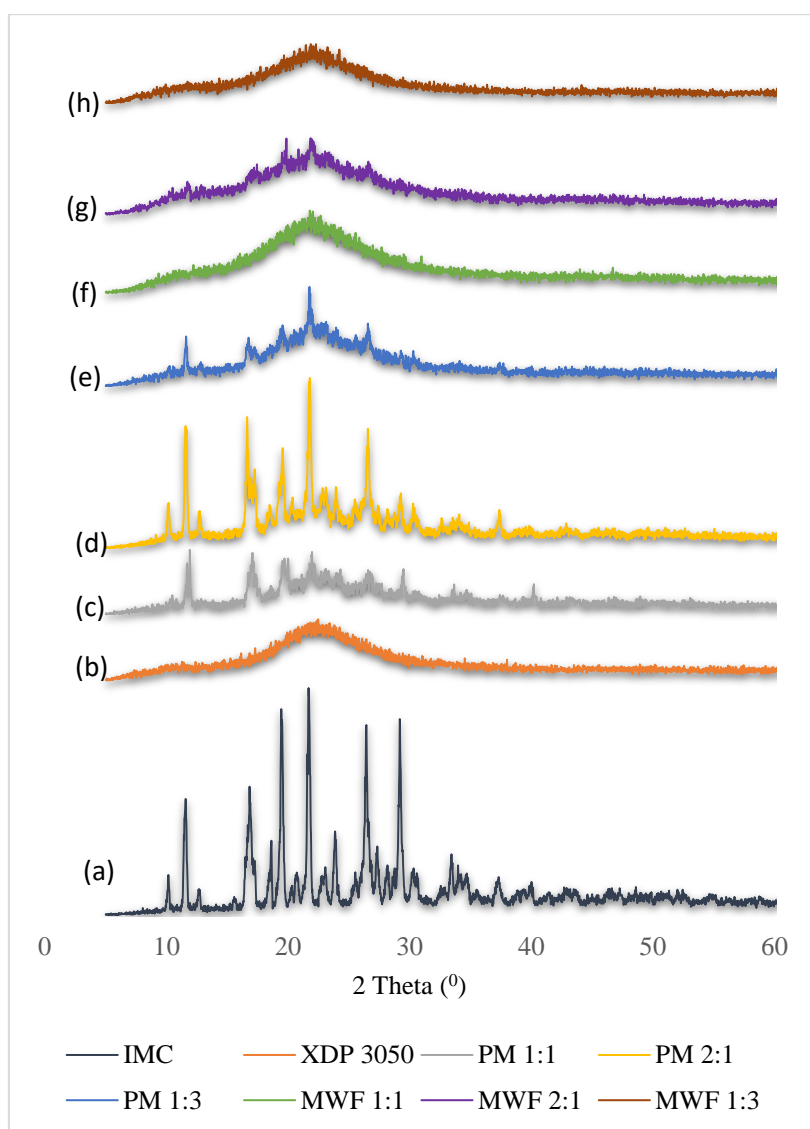


Figure 3. 19. XRD patterns for (a) IMC, (b) XDP 3050, (c) PM 1:1, (d) PM 2:1, (e) PM 1:3 (f) MWF 1:1, (g) MWF 2:1 and (h) MWF 1:3.

The diffractograms for the physical mixtures of indomethacin with the three Syloid<sup>®</sup> silicas at 1:1, 2:1 and 1:3 drug/silica ratios showed that the indomethacin crystalline peaks were

maintained in the physical mixtures indicating that the drug was still in a crystalline state, these results agree with the previous DSC results.

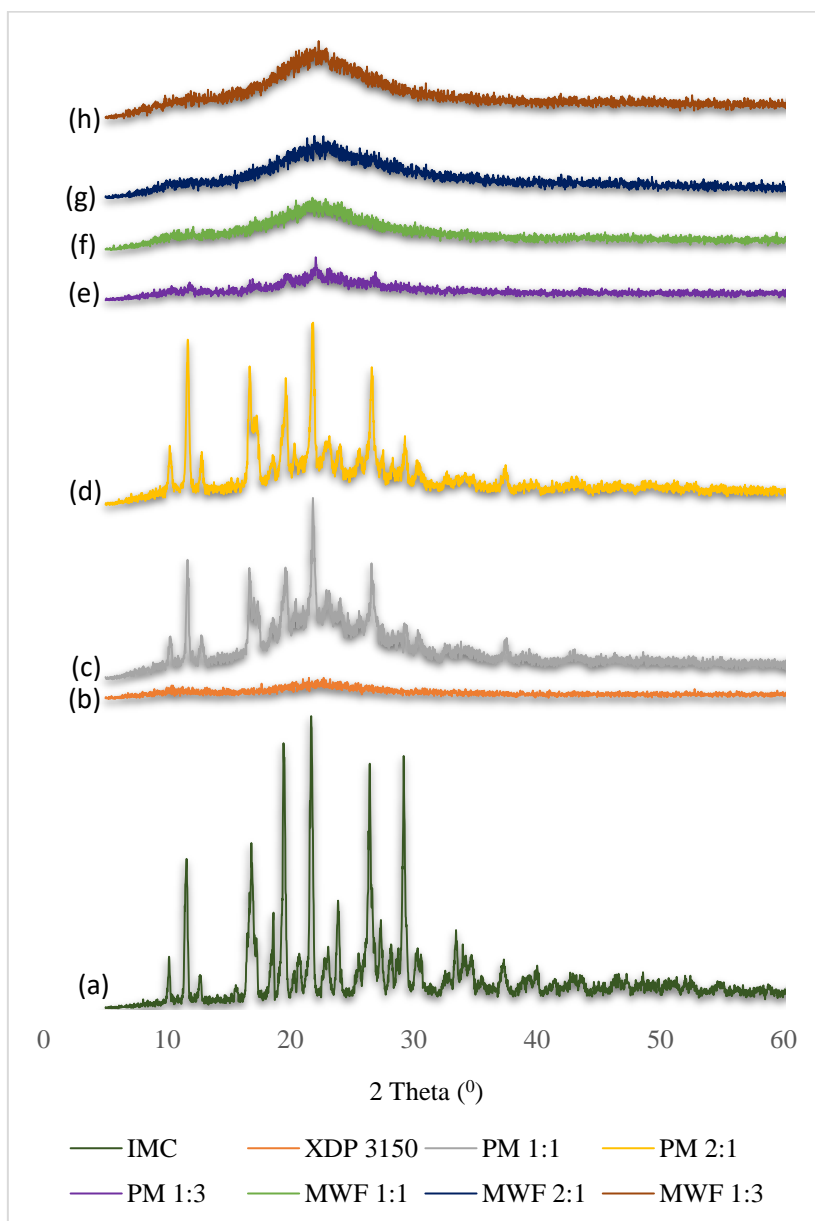


Figure 3. 20. XRD patterns for (a) IMC, (b) XDP 3150, (c) PM 1:1, (d) PM 2:1, (e) PM 1:3 (f) MWF 1:1, (g) MWF 2:1 and (h) MWF 1:3.

The microwave formulations of indomethacin with Syloid<sup>®</sup> XDP 3050, XDP 3150 and AL1 FP at a 1:1 ratio showed that the drug is completely amorphous and was no longer in a crystalline state even though this does not provide definitive proof of inclusion into the Syloid<sup>®</sup> silicas.

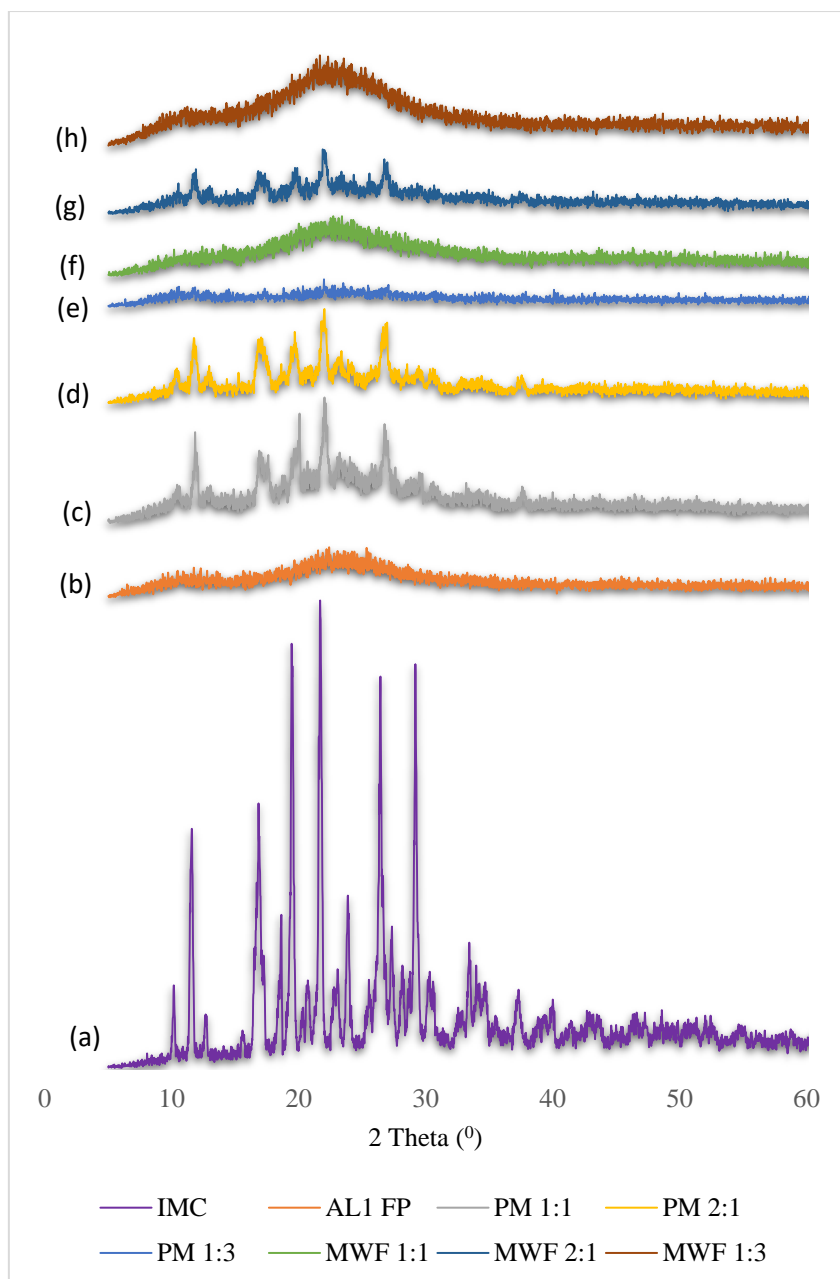


Figure 3. 21. XRD patterns for (a) IMC, (b) AL1 FP, (c) PM 1:1, (d) PM 2:1, (e) PM 1:3 (f) MWF 1:1, (g) MWF 2:1 and (h) MWF 1:3.

These results prove that the microwave formulation method is suitable for producing amorphous solid dispersions. This result fits well with the amorphous solid dispersion of a poorly water soluble drug (felodipine) prepared with different polymer matrices [185]. The 2:1 ratio showed small diffraction peaks for the drug, which is highly evidenced in the microwave formulation of the drug with AL1 FP, revealing the transition from crystalline to a partially amorphous state of indomethacin.

### 3.2.3.3 Fourier transform infrared spectroscopy (FT-IR)

FTIR was used to investigate the nature of the interaction-taking place between the carriers (Syloid<sup>®</sup> XDP 3050, 3150, AL1 FP at 1:1) and the active indomethacin. The spectrum of indomethacin, three Syloid<sup>®</sup> silicas as well as their formulations are shown in Figures 3.22, 3.23 and 3.24. The spectrum of the active drug (Figure 3.22a) showed an absorption band at 2930 cm<sup>-1</sup> for hydroxyl (O-H) stretching vibrations, 1690 cm<sup>-1</sup> for carbonyl (C=O), 1450 cm<sup>-1</sup> for phenyl groups (C=C) and 900 cm<sup>-1</sup> for the C-H vibrations of indomethacin [186].

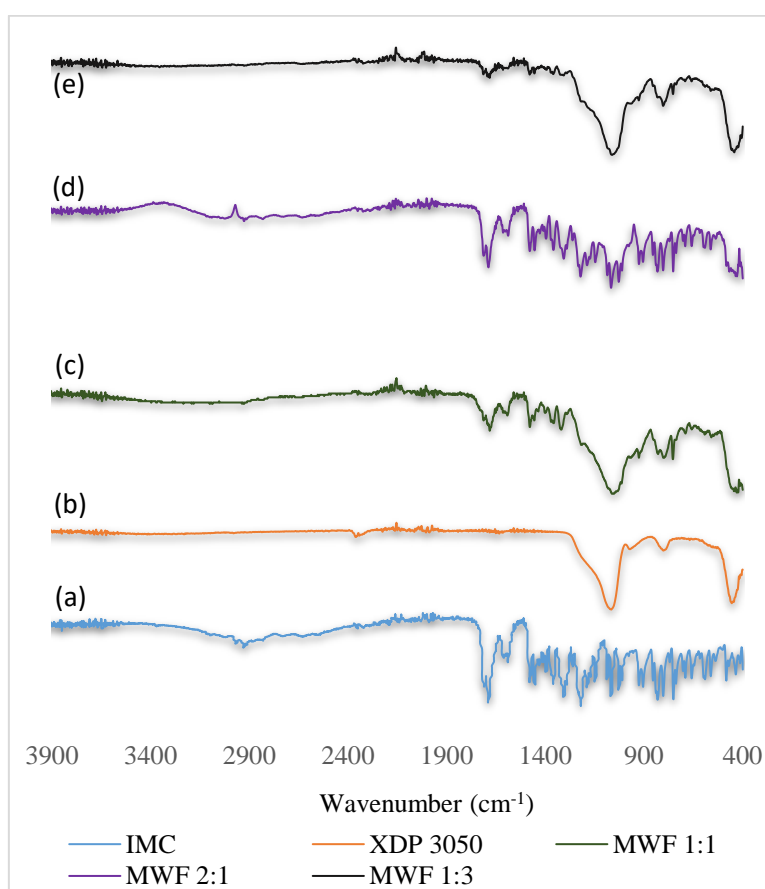


Figure 3. 22. FT-IR analysis of (a) IMC (b) XDP 3050, (c) MWF 1:1, (d) MWF 2:1, and (e) 1:3 drug-XDP 3050 formulations

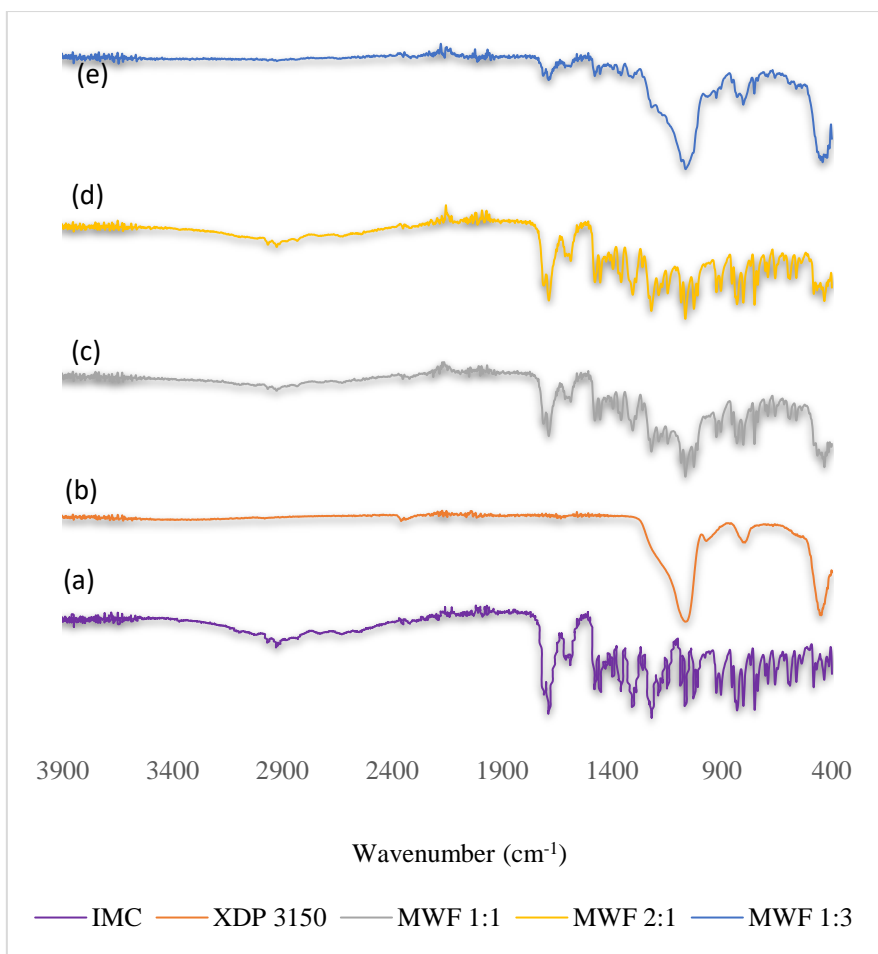


Figure 3. 23. FT-IR analysis of (a) IMC (b) XDP 3150, (c) MWF 1:1, (d) MWF 2:1, and (e) 1:3 drug-XDP 3150 formulations



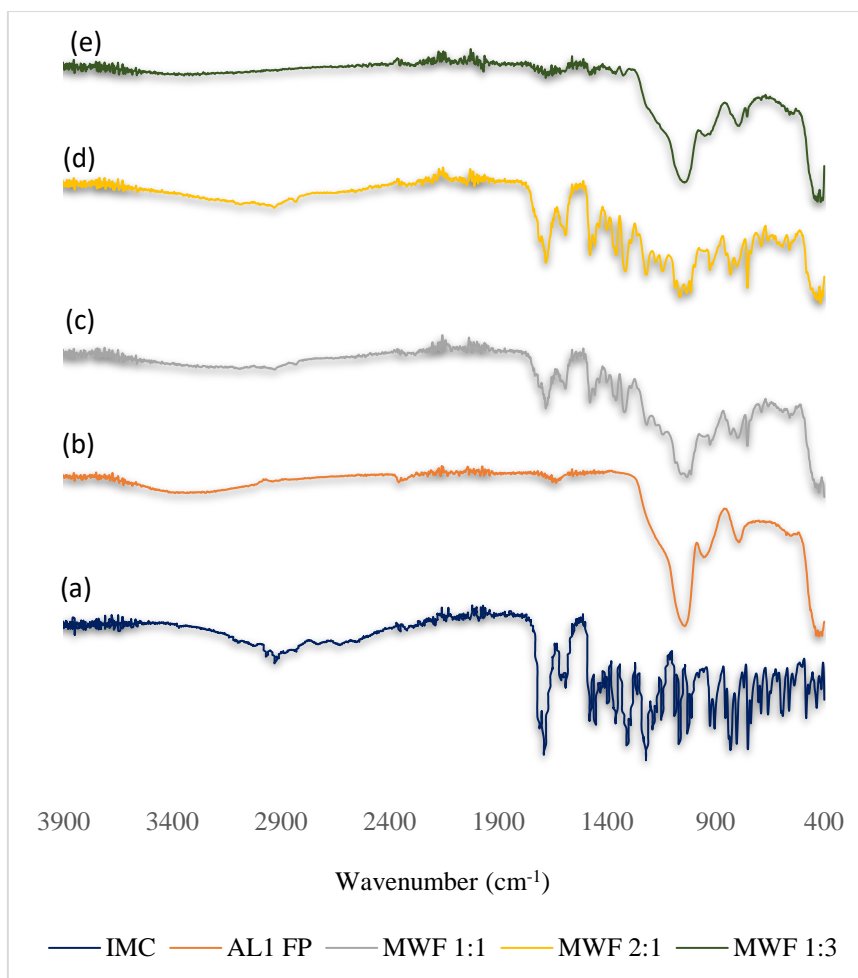


Figure 3. 24. FT-IR analysis of (a) IMC (b) AL1 FP, (c) MWF 1:1, (d) MWF 2:1, and (e) 1:3 drug-AL1 FP formulations

IR spectra of the three pure syloid silicas showed a broad band at  $1056\text{ cm}^{-1}$  corresponding to asymmetric (Si-O-Si) stretching,  $792\text{ cm}^{-1}$  for the symmetric Si-O-Si stretch and at  $447\text{ cm}^{-1}$  a bending vibration for Si-O-Si was observed, as previously reported [187]. Following microwave formulation of the active with the silicas at different ratios, characteristic stretching bands of the active drug were observed, narrow for the 1:1 ratio and intense for the 2:1 ratio due to the higher drug content. Moreover, the bands become broader and shifts in the 1:3 formulations are due to the high silica content. These observations possibly may be due to an interaction between drug-silica after the microwave formulation.

### 3.2.3.4. Scanning electron microscopy (SEM)

An in-depth study of the morphological aspect of single component and interacted mixtures was carried out with SEM. The findings are displayed in Figures 3.25 and 3.26 (x500 magnification). The drug crystalline state is evident while the disordered irregular shape and size of syloid silicas has been discussed in Figure 3.10. Differences in images of the physical mixtures of the drug with silicas at different ratios are insignificant as confirmed by the SEM (x500 magnification).

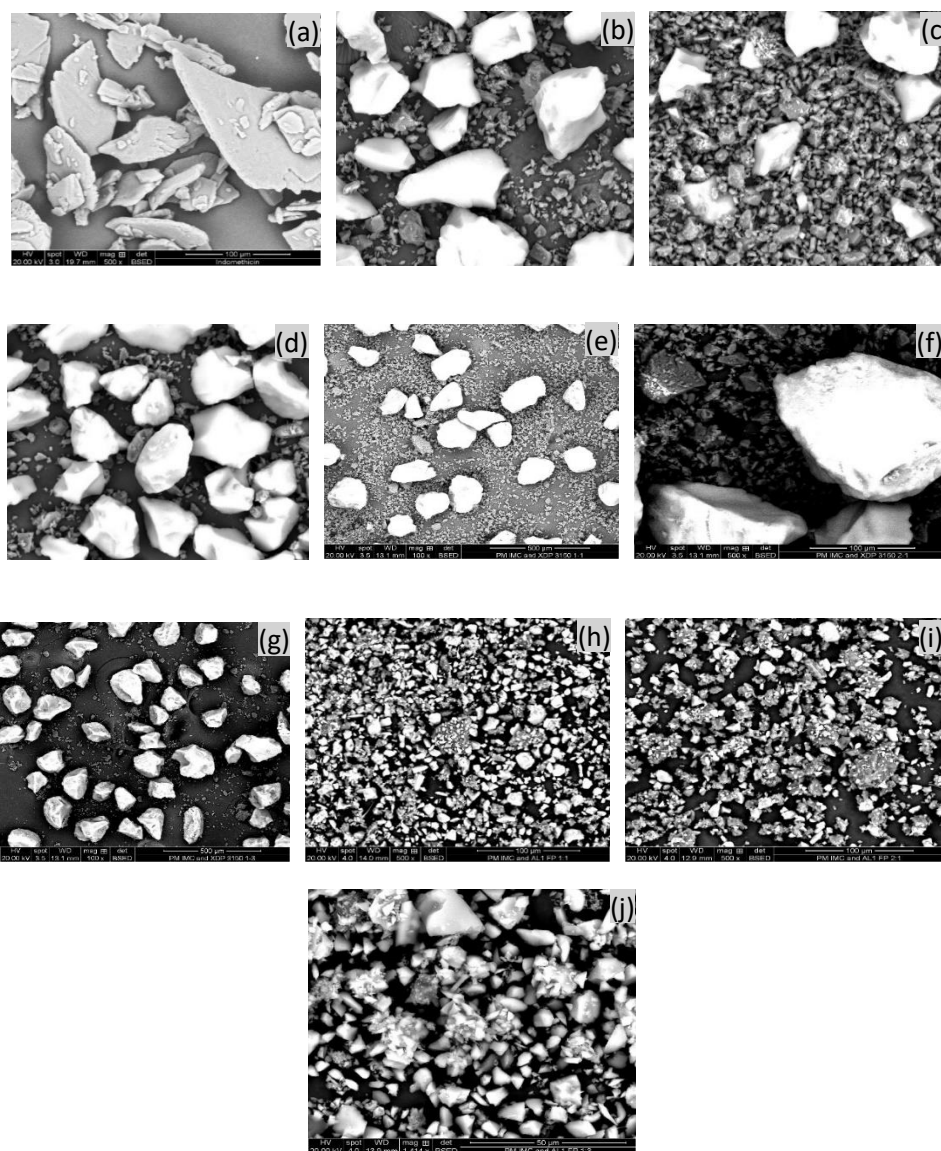


Figure 3. 25. SEM images at x500 of (a) IMC (b) PM of IMC and XDP 3050 (1:1), (c) PM of IMC and XDP 3050 (2:1), (d) PM of IMC and XDP 3050 (3:1). (e), PM of IMC and XDP 3150 (1:1), (f) PM of IMC and XDP 3150 (2:1), (g) PM of IMC and XDP 3150 (1:3), (h) PM of IMC and AL1 FP (1:1), (i) PM of IMC and AL1 FP (2:1), and (j) PM of IMC and AL1 FP (1:3).

However, the crystals of indomethacin on the surface of the syloid silicas were not evident after microwave formulation. For the 2:1 (x500 magnification) microwave formulation, there was a uniform appearance of some drug molecules on the surface of the silicas.

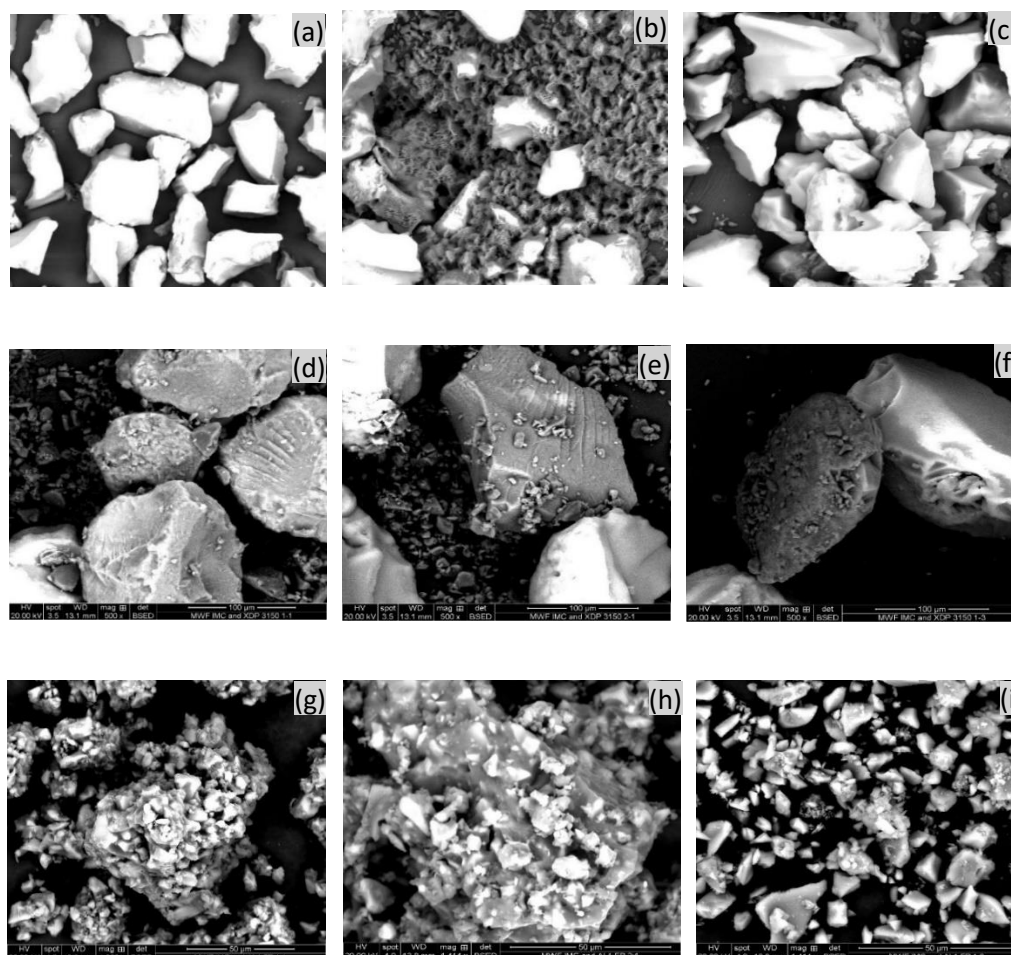


Figure 3. 26. SEM images x500 of (a) MWF of IMC and XDP 3050 (1:1), (b) MWF of IMC and XDP 3050 (2:1), (c) MWF of IMC and XDP 3050 (3:1), (d), MWF of IMC and XDP 3150 (1:1), (e) MWF of IMC and XDP 3150 (2:1), (f) MWF of IMC and XDP 3150 (1:3), (g) MWF of IMC and AL1 FP (1:1), (h) MWF of IMC and AL1 FP (2:1), and (i) MWF of IMC and AL1 FP (1:3).

These images confirmed the DSC and XRD results, where amorphous material was detected at a 1:1 drug-silica ratio, indicating a homogenised system while for the 2:1 ratio, there was the presence of partially amorphous drug on the surface of the silica due to the higher mass of the drug used in the formulation. Overall, these results confirmed that subjecting the drug to a

microwave formulation process can modify the proportion of crystalline drug and create a product that may contain a uniform dispersion of drug within the silica matrix.

### 3.2.4. *In vitro* indomethacin release

Dissolution studies were performed on pure indomethacin and microwave formulations of indomethacin with three syloid silicas at 1:1, 2:1 and 1:3 drug-silica ratios to investigate the influence of the silicas and microwave on the dissolution behaviour of the drug. The *in vitro* release profiles of indomethacin from syloid XDP 3050 at aforementioned drug-silica ratios along with pure indomethacin in phosphate buffer over a period of 45 minutes are presented in Figure 3.27.

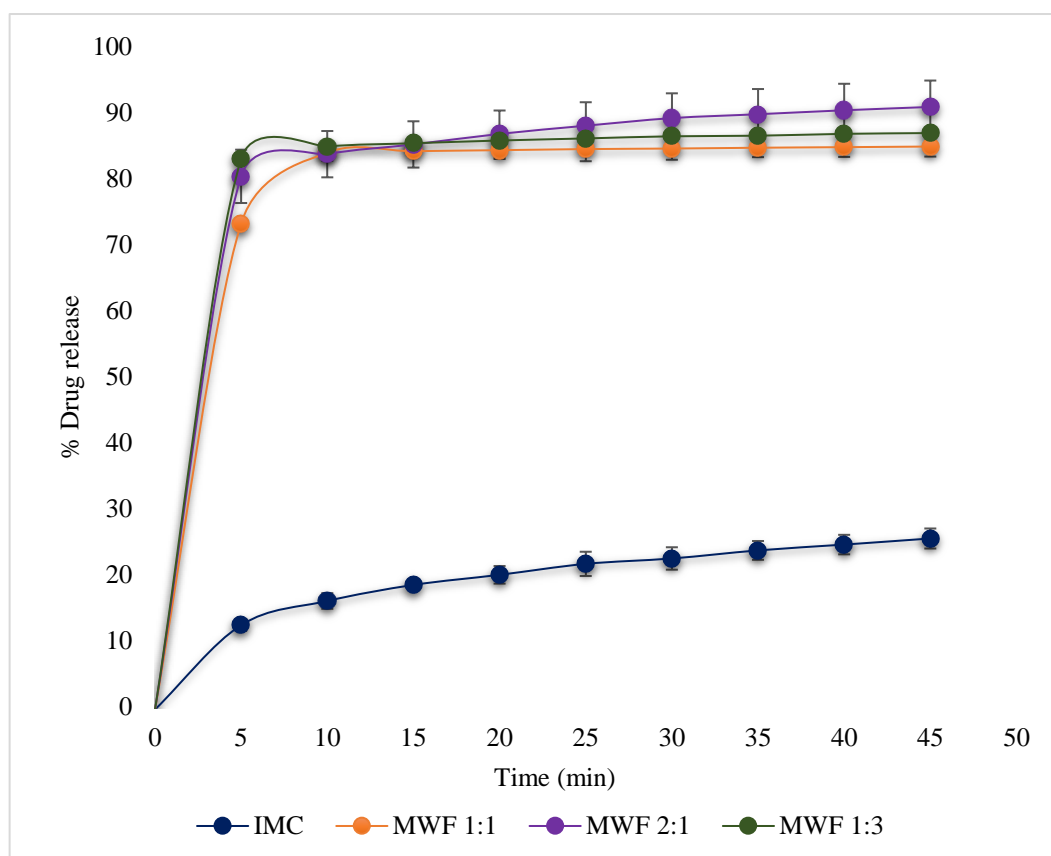


Figure 3. 27. Release profiles for pure indomethacin (IMC) and indomethacin Syloid® XDP 3050-based formulations at 1:1, 2:1 and 1:3. Each data point represents the mean of triplicate results ( $\pm$ SD).

These results highlight that pure indomethacin (that had not undergone the microwave formulation process) exhibited 12.4 % ( $\pm 0.8$  %) drug release after 5 minutes yet only increased to 22.4 % ( $\pm 1.7$  %) after 30 minutes and to a maximum of 25.5 % ( $\pm 1.5$  %) after 45 minutes. Syloid XDP 3050-based formulations exhibited a significant enhancement in the percentage release, confirming the formulation of the drug in the presence of syloid using the microwave method contributed to the increase. Formulation of a 1:1 drug-silica ratio achieved a percentage release of 80.3 % ( $\pm 0.1$  %) after only 5 minutes, while after 30 minutes, the value had increased to 84.6% ( $\pm 0.2$  %) and 84.8% ( $\pm 0.2$  %) at 45 minutes. The initial release was attributed to adsorption of the drug into the pores of the XDP 3050 silica [188]. However, a similar drug release profile was observed for the 2:1 drug-silica ratio whereby 83.0 % ( $\pm 4.0$  %) after 5 minutes was achieved. This was greater than the total seen for the pure drug after 45 minutes. The reason for this enhanced release has to do with the physicochemical properties of the syloid XDP 3050 [19], and the drug possibly was confined inside the pores and on the surface of the silica. This result fits well with the findings of other studies with mesoporous silica for the release of gemfibrozil [177]. Finally, the 1:3 ratio did show a promising percentage release of 82.8 % ( $\pm 10.5$  %) after 5 minutes compared with the 2:1, yet after a total of 45 minutes had exceeded further to reach a maximum percentage release of 86.9 % ( $\pm 0.4$  %). The IMC-XDP 3050 formulation with low silica content (i.e. in 2:1) showed greater drug release while the 1:1 and 1:3 formulations with higher silica content showed an opposite trend. The indomethacin molecules are well dispersed in the silica at higher drug content. In 2:1 ratio, the XDP 3050 partially amorphised the indomethacin by forming an incomplete inclusion complex, this is evidenced by the reduction in the melting peak intensity on DSC thermograms of the ratio (Fig. 3.16). For 1:1 and 1:3 ratios with higher XDP 3050 content, the amount of silica was enough for incorporating IMC, and the interaction of IMC and XDP 3050 was reduced, contributing improved redispersion of XDP 3050 nanoparticles [189].

Figures 3.28 and 3.29 display the dissolution studies of indomethacin formulated with Syloid XDP 3150 and AL1 FP at 1:1, 2:1 and 1:3 drug-silica ratios. XDP 3150 and drug (1:1) achieved a percentage release of 70.9 % ( $\pm 6.2$  %) after 15 minutes and attained a maximum release of 76.9 % ( $\pm 4.8$  %) after 45 minutes. The release profile achieved using the 2:1 ratio was greater than that obtained with 1:1, where a percentage release of 81.4 % ( $\pm 7.5$  %) was achieved in the first 15 minutes to a maximum of 83.4 % ( $\pm 7.2$  %) after 45 minutes. The greatest percentage release achieved using this silica is at a ratio of 1:3 with 90.3% ( $\pm 3.5$  %) and 92.2 % ( $\pm 3.0$  %) released after 15 and 45 minutes respectively.

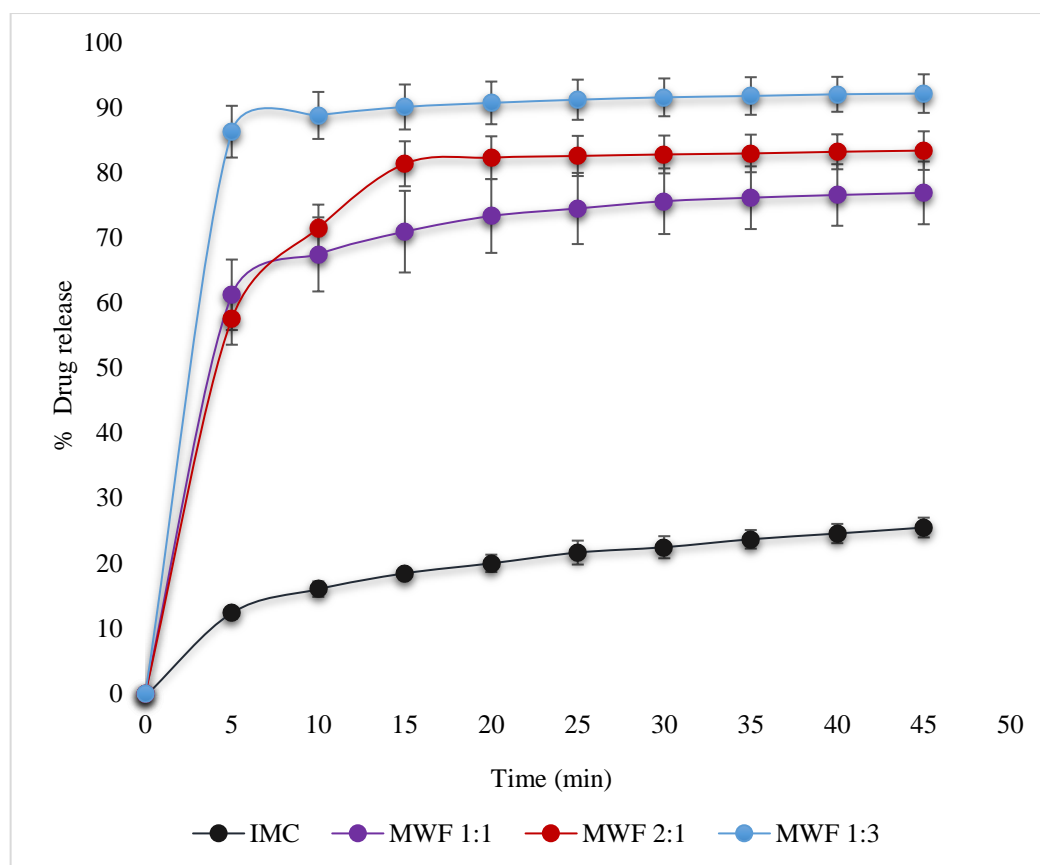


Figure 3. 28. Release profiles for pure indomethacin (IMC) and indomethacin Syloid® XDP 3150-based formulations at 1:1, 2:1 and 1:3. Each data point represents the mean of triplicate results ( $\pm$  SD).

Interestingly, when comparing the three ratios of IMC loading into XDP 3150 mesoporous silica carried out at low and high IMC amounts, it could be observed that for the same type of particles the faster IMC release profiles were obtained for formulations with the lowest amount

of drug i.e. 1:3 ratio [18]. This is also in very good agreement with both the DSC and XRD findings (Fig. 3.17g and Fig. 3.20g respectively). The results showed that the dissolution profile of the 1:3 ratio containing higher silica content had the best drug release in comparison to 1:1 and 2:1 ratios with lower silica content. This is due to conversion from the crystalline to partially amorphous form [190] of the drug in the 1:3 ratio brought about the increase. This silica displayed a different dissolution profile due to its different properties in comparison to the profiles of XDP 3050 previously discussed.

Lastly, dissolution profiles for indomethacin with Syloid<sup>®</sup> AL1 FP did not show such a promising percentage release of 43.0 % ( $\pm 0.7$  %) after 15 minutes for the 1:1 drug-silica ratio, 60.1 % ( $\pm 2.3$  %) for the 2:1 and 55.7 % ( $\pm 4.0$  %) for the 1:3. After a total of 45 minutes, the values were 52.2 % ( $\pm 0.7$  %), 76.7% ( $\pm 3.4$  %) and 66.7 % ( $\pm 2.0$  %) for the 1:1, 2:1 and 1:3 ratios respectively. The IMC release was faster for the 2:1 and 1:3 ratios, the drug release in the 1:1 ratio was slightly slower compared with the two previous ratios, but still faster significantly when compared to the pure IMC.

It was concluded that, the most influential physical parameter of the mesoporous silicas used in this project for enhancing drug release was the pore volume. The particle size highlighted in Table 2.1 was not found to have a major effect on the drug release kinetics but other studies have shown that larger particle size has been related to slower drug release rate [191, 192] . The much higher surface area of Syloid<sup>®</sup> AL1 FP ( $605 \text{ m}^2\text{g}^{-1}$ ) mesoporous silica did not display higher drug release for the three ratios analysed when compared to the Syloid<sup>®</sup> XDP 3050 and 3150 carriers with lower surface area ( $320 \text{ m}^2\text{g}^{-1}$ ). The AL1 FP has narrower pores than the XDP 3050 and 3150 which has been suggested to contribute to a lower release rate due to steric hindrance that block the drug from diffusing out of the pores [193].

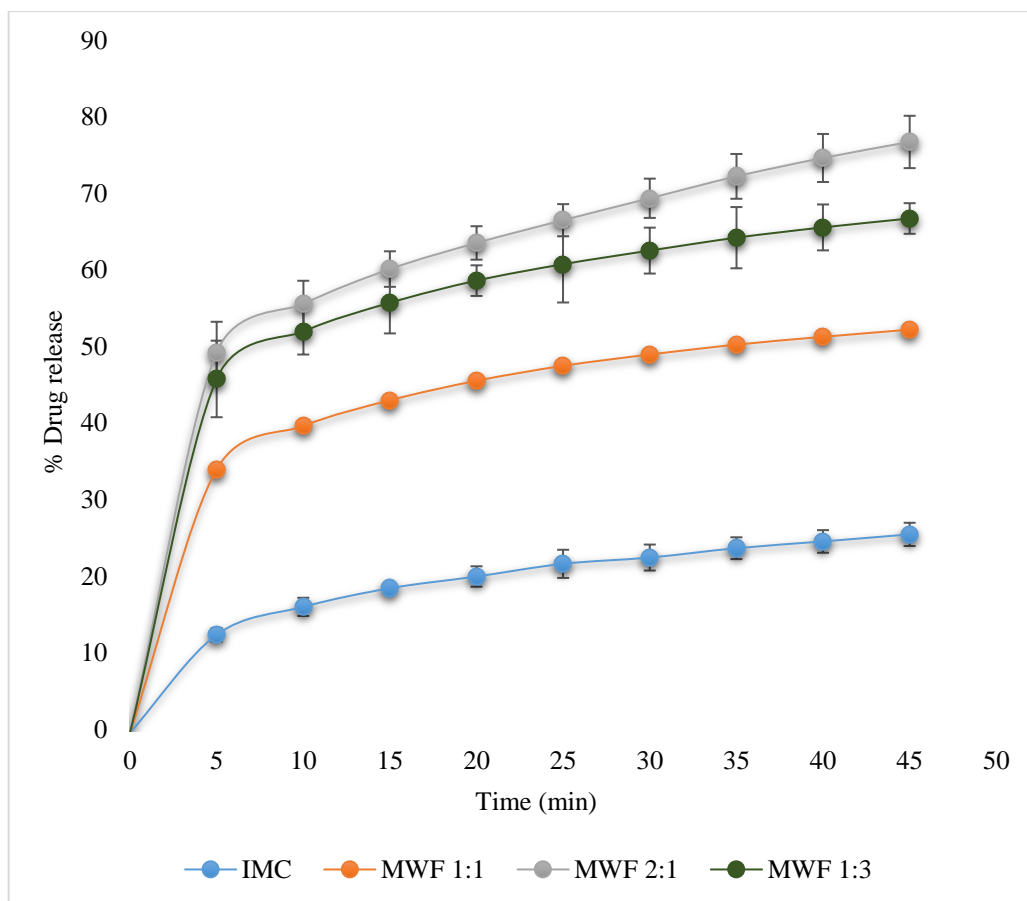


Figure 3. 29. Release profiles for pure indomethacin (IMC) and indomethacin Syloid® AL1 FP-based formulations at 1:1, 2:1 and 1:3. Each data point represents the mean of triplicate results ( $\pm$ SD).

### 3.2.5. Solid state characterisation of Imipramine formulations

#### 3.2.5.1 Differential scanning calorimetry (DSC)

The physical state of Imi entrapped in Syloid® XDP 3050, XDP 3150 and AL1 FP materials was analysed by DSC. As can be seen in Figure 3.30, crystalline imipramine exhibited a well-defined sharp endothermic peak at 175.3 °C corresponding to its melting in agreement with the melting point previously reported [194]. The characteristic peak of the drug appeared in the physical mixtures at all drug/silica ratios with little disparities in terms of melting peak broadening and depression, providing an insight about solid-state modifications and transition from crystalline to partially amorphous form of the drug.



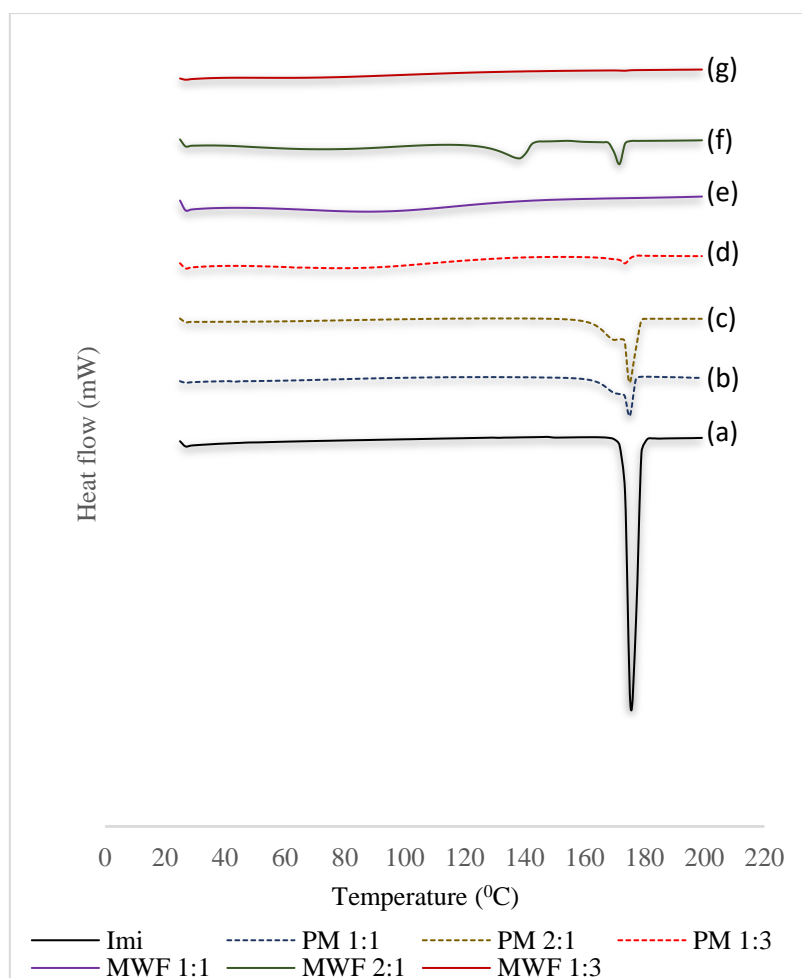


Figure 3. 30. DSC profiles for imipramine (Imi) along XDP 3050 based physical mixtures (PM) and microwave formulations (MWF). (a) Pure Imi, (b) PM 1:1 (c) PM 2:1 (d) PM 1:3 (e) MWF 1:1 (f) MWF 2:1 and (g) MWF 1:3

When imipramine was formulated with Syloid<sup>®</sup> XDP 3050 at 1:1 and 1:3 drug/silica ratios seen in Figure 3.30 (e) and (g), no sign of a melting peak for the drug could be observed, affirming the amorphous nature of imipramine within formulations and this was in good agreement with other XRD measurements (Figure 3.33 f). In contrast, two melting peaks of imipramine were detected, one broad at 138.7 °C and another small at 171.7 °C for the 2:1 drug/silica ratio. At this ratio, possibly even though not confirmed could be due to the pore volume of the XDP 3050 ( $1.70 \text{ cm}^3\text{g}^{-1}$ ) which is inadequate for accommodating the extra imipramine molecules, the residual drug molecules instead could have resided on the external surface of XDP 3050. DSC confirmed the presence of crystalline imipramine in this ratio following the formulation

process (despite a slight shift from 175.3 °C) and this is in good agreement with other XRD measurement (Figure 3.33f).

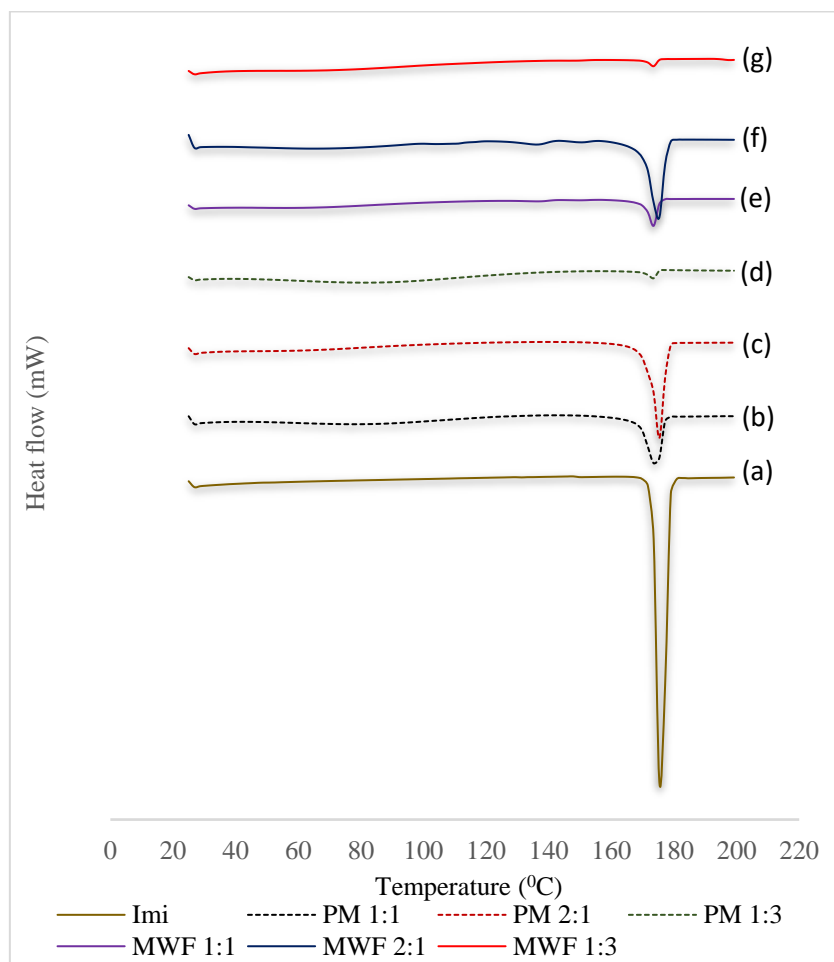


Figure 3. 31. DSC profiles for imipramine (Imi) along XDP 3150 based physical mixtures (PM) and microwave formulations (MWF). (a) Pure Imi, (b) PM 1:1 (c) PM 2:1 (d) PM 1:3 (e) MWF 1:1 (f) MWF 2:1 and (g) MWF 1:3

Figure 3.31 shows the DSC thermograms of pure Imi, physical mixtures and drug loaded Syloid<sup>®</sup> XDP 3150 at 1:1, 2:1 and 1:3 drug/silica ratios respectively. The melting endotherm of pure Imi has been discussed previously (Fig. 3.30), all the physical mixtures prepared showed characteristics of an imipramine melting endotherm without any polymorphic transition. However, there was a gradual decrease in the intensity of the melting peak with increasing XDP 3150 content as can be seen in 1:3 (Fig. 3.31d) drug to silica ratio. When the physically mixed and microwave-based formulations are compared, a decrease in melting peak

intensity of imipramine was more prominent in solid dispersions than the physically mixed formulations.

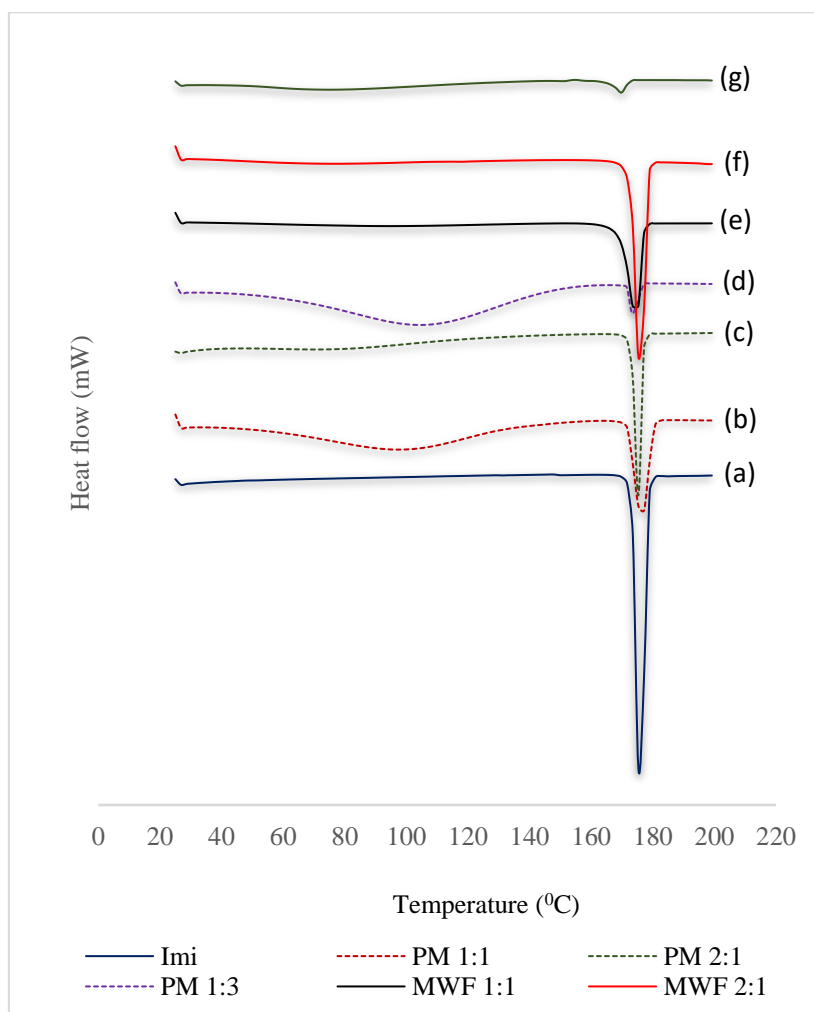


Figure 3. 32. DSC profiles for imipramine (Imi) along AL1 FP based physical mixtures (PM) and microwave formulations (MWF). (a) Pure Imi, (b) PM 1:1 (c) PM 2:1 (d) PM 1:3 (e) MWF 1:1 (f) MWF 2:1 and (g) MWF 1:3

The size reduction in terms of the melting endotherm and broadening was attributed to the transition from crystalline to partially amorphous form of imipramine and the drug molecules being dispersed in the XDP 3150 as previously reported [195, 196]. This size reduction was more evident in the 1:3 drug to silica ratio formulation due to the higher weight of the XDP 3150 in the formulations. The weight of the XDP 3150 has a significant effect on the thermal endotherm of imipramine as seen in the DSC results.

For Syloid<sup>®</sup> AL1 FP (Figure 3.32), the melting endotherm was more evident both in the physical mix products and microwave formulations, this was attributed to the small pore volume and diameter of the silica ( $0.40 \text{ cm}^3 \text{ g}^{-1}$  and  $26 \text{ \AA}$ ), the imipramine molecules are likely deposited on the surface of the AL1 FP as the DSC scans confirmed, the drug molecules were not accepted by the AL1 FP due to its small capacity [181]. Based on the results of Syloid<sup>®</sup> XDP 3050, 3150 and AL1 FP, it can be concluded that pore volume has an effect on imipramine loading.

### **3.2.5.2 X-ray diffraction (XRD)**

Following on from the scans using DSC, i.e. the implication that possibly the products had increased in amorphous content on formulation, X-ray powder diffraction (XRD) analysis of pure imipramine, the physical mixtures and microwave-based formulations with Syloid<sup>®</sup> XDP 3050, XDP 3150 and AL1 FP at ratios of 1:1, 2:1 and 1:3 were carried out to confirm this. Figure 3.33 (a) displays the XRD patterns of pure imipramine with diffraction peaks appearing at  $12.2^\circ$ ,  $16.0^\circ$ ,  $18.2^\circ$ ,  $19.8^\circ$ ,  $23.8^\circ$ , thus confirming the crystalline state expected for the drug in comparison with the featureless patterns for the Syloid<sup>®</sup> XDP 3050 (Figure 3.33b), 3150 (Figure 3.34b) and AL1 FP (Figure 3.35b). All the physical mixtures prepared with either XDP 3050, XDP 3150 and AL1 FP displayed peaks, indicating imipramine was still in a crystalline state. In contrast, the XRD patterns for the 1:1 product formulated utilising microwave radiation (Figure 3.33f, 3.34f and 3.35f) indicated small peaks of imipramine suggesting possibly that the formulation was partially amorphous.

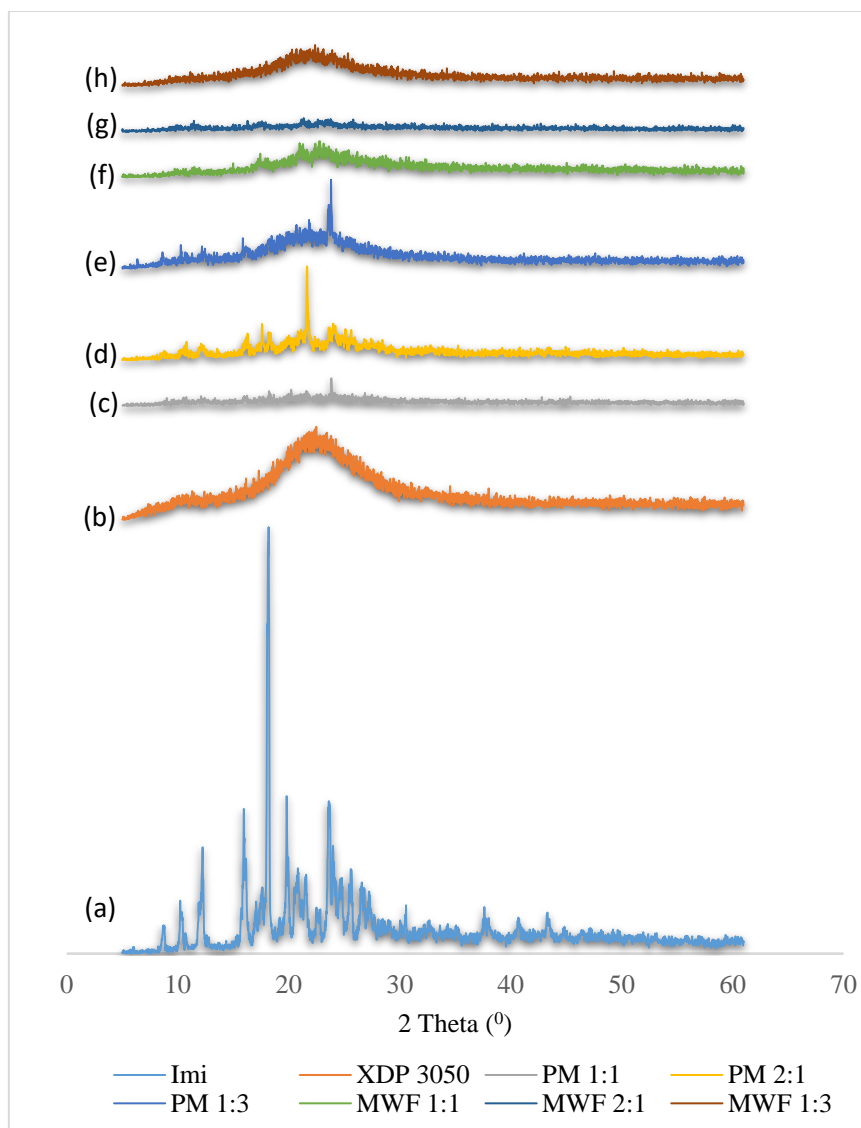


Figure 3. 33. XRD patterns for (a) Imi, (b) XDP 3050, (c) PM 1:1, (d) PM 2:1, (e) PM 1:3 (f) MWF 1:1, (g) MWF 2:1 and (h) MWF 1:3.

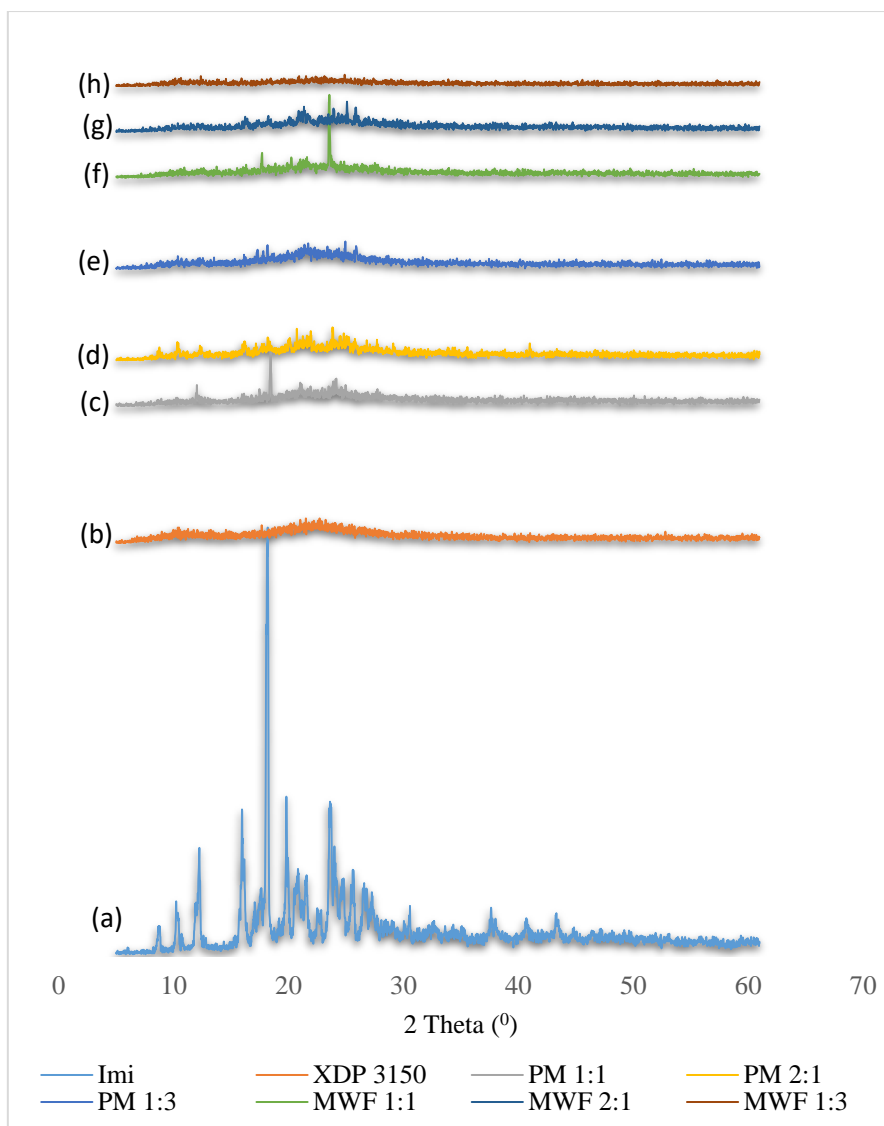


Figure 3. 34. XRD patterns for (a) Imi, (b) XDP 3150, (c) PM 1:1, (d) PM 2:1, (e) PM 1:3 (f) MWF 1:1, (g) MWF 2:1 and (h) MWF 1:3.

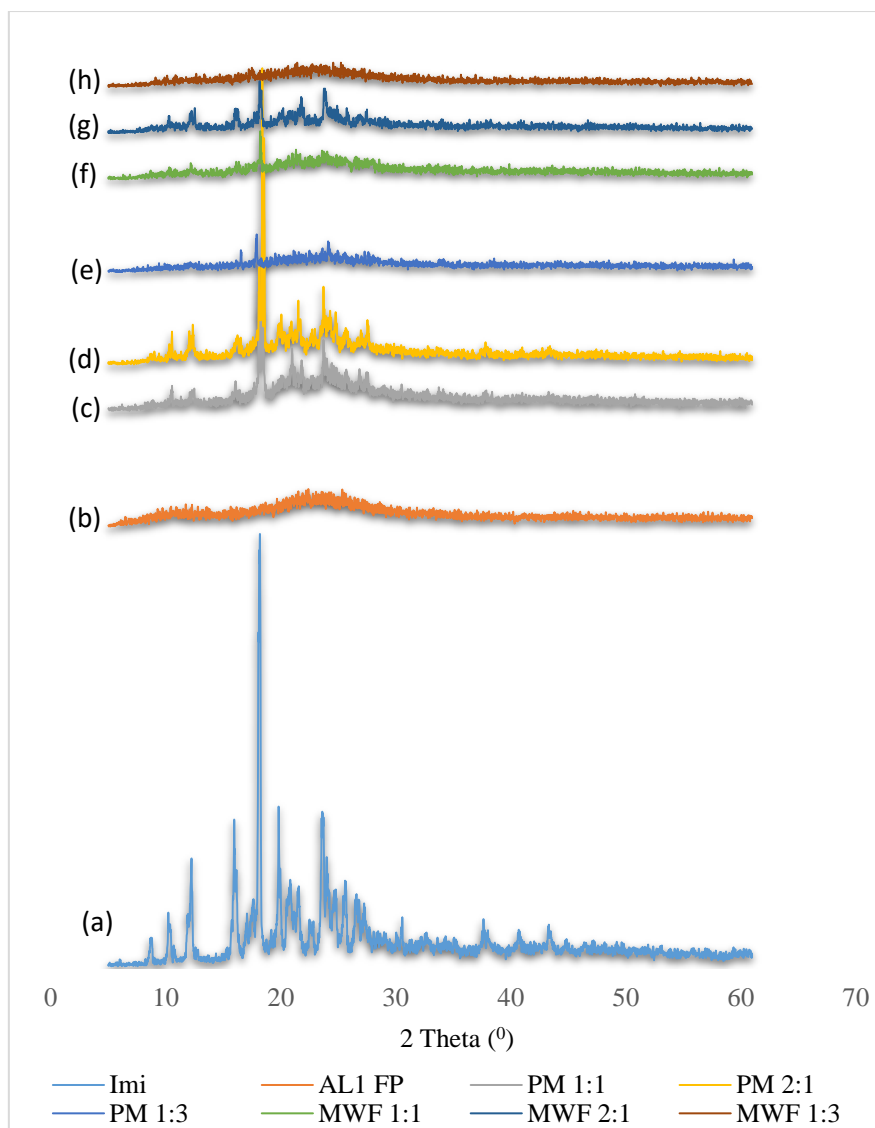


Figure 3. 35. XRD patterns for (a) Imi, (b) AL1 FP, (c) PM 1:1, (d) PM 2:1, (e) PM 1:3 (f) MWF 1:1, (g) MWF 2:1 and (h) MWF 1:3.

These findings are in agreement with those reported on artemether [195], gemfibrozil [181] and fenofibrate [197] where other forms of silica and formulation processes were adopted. However, diffraction peaks were absent in the 1:3 drug to silica ratio products due to the higher silica content, thus confirming that the imipramine had been converted from a crystalline to amorphous form upon microwave heating. Due to the high silica content, a partial crystalline peak of imipramine was evident in the 2:1 drug to silica ratio-based products. In summary, these results were in full agreement with the DSC results reported, confirming an amorphous product was created using microwave formulation with the three amorphous silicas.

### 3.2.5.3 Fourier transform infrared spectroscopy (FT-IR)

As previously reported, FTIR has been utilised to investigate the incorporation of aminopropyl groups on the surface of mesoporous silica nanoparticles [198]. Figures 3.36 – 3.38 display the FTIR profiles for imipramine with Syloid<sup>®</sup> XDP 3050, XDP 3150 and AL1 FP at 1:1, 2:1 and 1:3 drug-silica ratios.

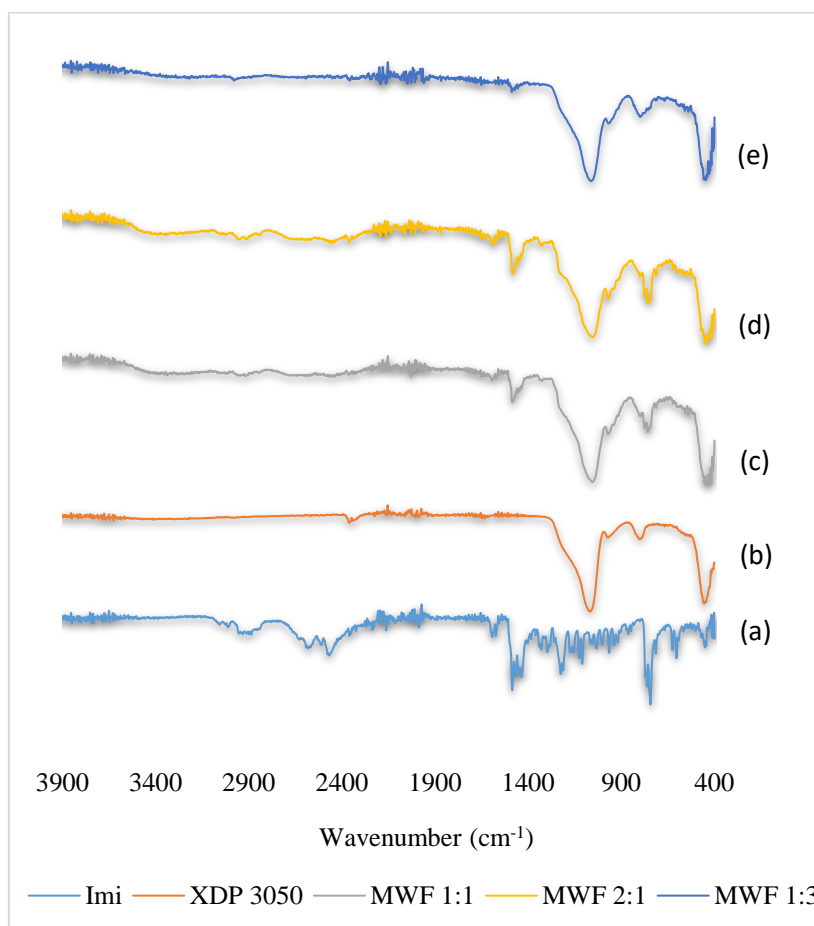


Figure 3. 36. FT-IR analysis of (a) Imi (b) XDP 3050, (c) MWF 1:1, (d) MWF 2:1, and (e) 1:3 drug-XDP 3050 formulations



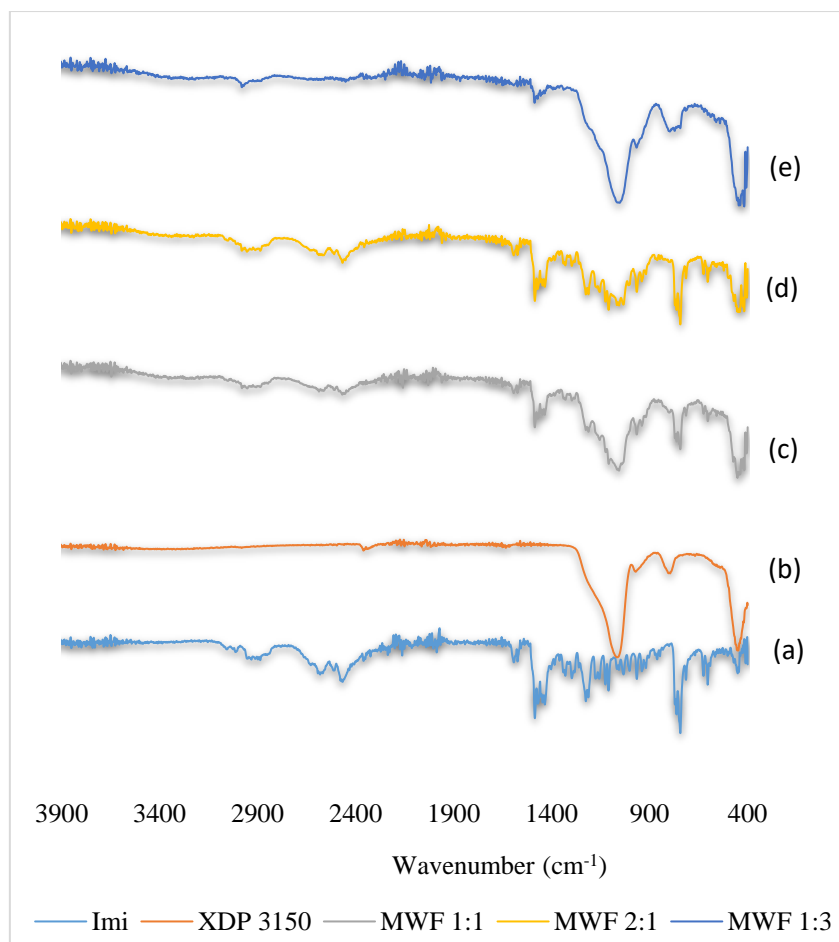


Figure 3. 37. FT-IR analysis of (a) Imi (b) XDP 3150, (c) MWF 1:1, (d) MWF 2:1, and (e) 1:3 drug-XDP 3150 formulations

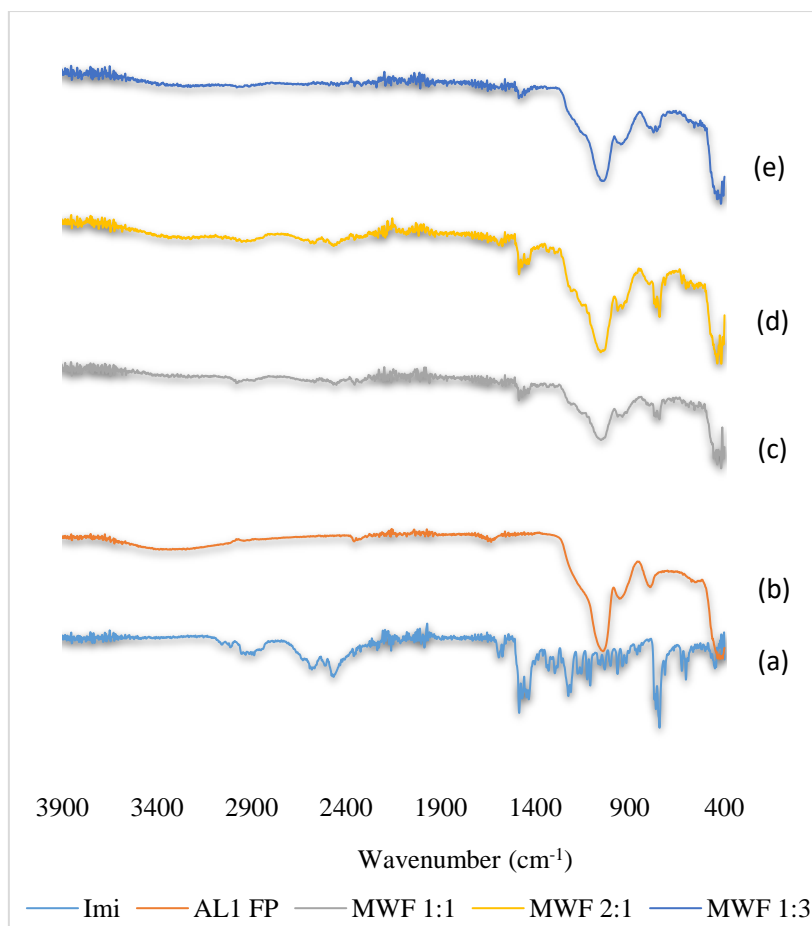


Figure 3. 38. FT-IR analysis of (a) Imi (b) AL1 FP, (c) MWF 1:1, (d) MWF 2:1, and (e) 1:3 drug-AL1 FP formulations

In this study, characteristics peaks of pure imipramine were observed at 3008.6 cm<sup>-1</sup> for C-H stretching, 742.5 cm<sup>-1</sup> for C-H bending, 2464.7 cm<sup>-1</sup> for C-N stretching and 1573.7 cm<sup>-1</sup> for C=C stretching vibrations. FT-IR for Syloid<sup>®</sup> XDP 3050, 3150 and AL1 FP have been previously discussed following Figure 3.22. The absorption bands of imipramine were evident in the 2:1 drug to silica ratio. For the three imipramine-silica formulated products, the results indicated a significant disappearance of the drug peaks, mainly displaying spectra corresponding to just each type of silica present. Furthermore, the spectra did not display any obvious additional peaks thus indicating there had been no significant changes in the chemical structure or drug-silica interactions.

### 3.2.5.4. Scanning electron microscopy (SEM)

SEM images of pure imipramine, physical mixtures and microwave-based formulations with Syloid® XDP 3050, XDP 3150 and AL1 FP at ratios of 1:1, 2:1 and 1:3 (x500 magnifications) were analysed to investigate changes in morphology.

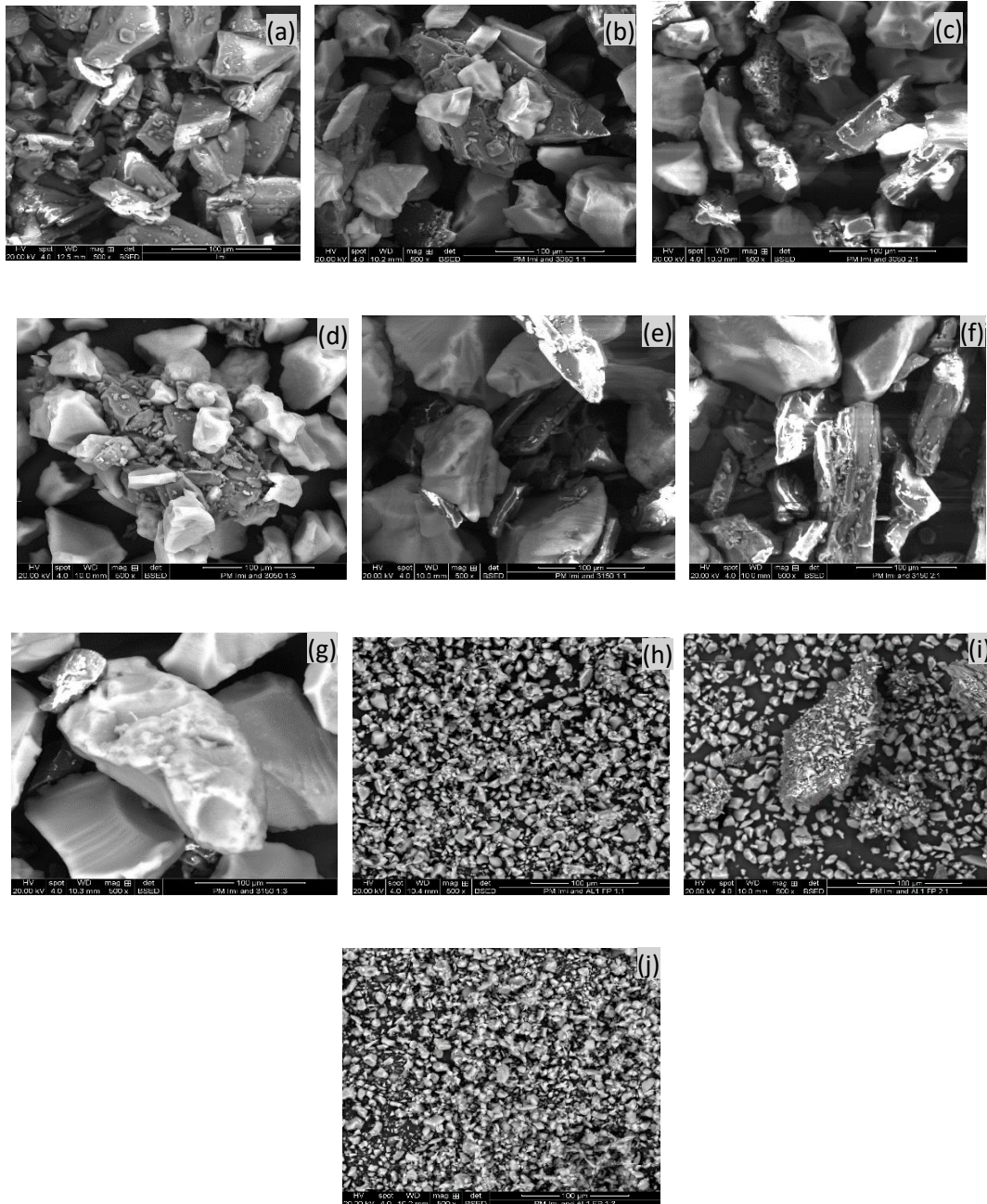
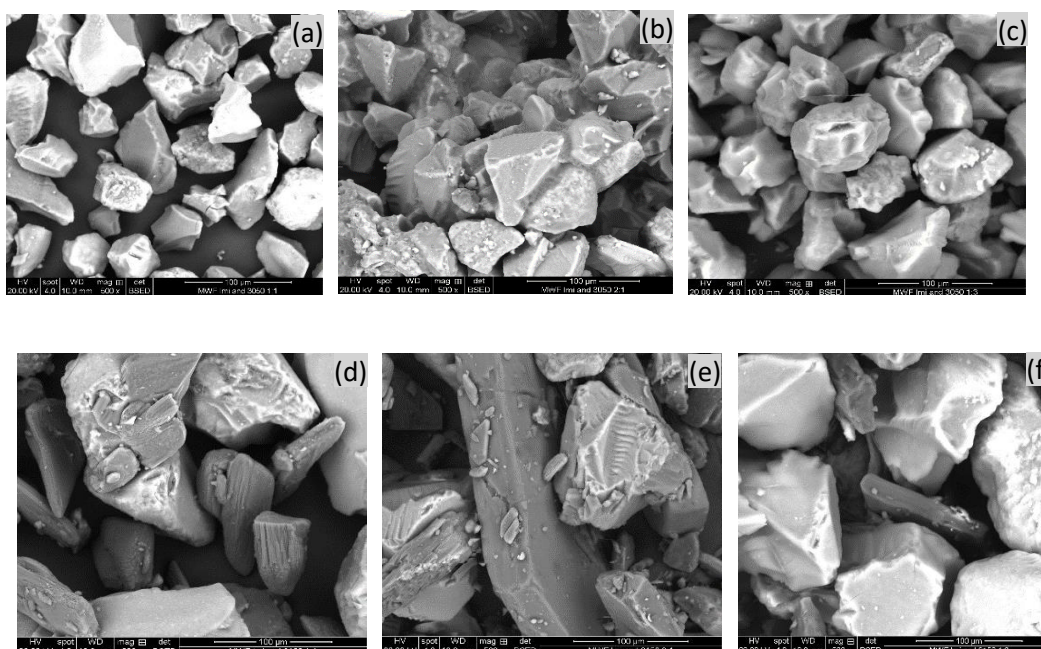


Figure 3.39. SEM images (x500) of (a) Imi (b) PM of Imi and XDP 3050 (1:1), (c) PM of Imi and XDP 3050 (2:1), (d) PM of Imi and XDP 3050 (3:1), (e), PM of Imi and XDP 3150 (1:1), (f) PM of Imi and XDP 3150 (2:1), (g) PM of Imi and XDP 3150 (1:3), (h) PM of Imi and AL1 FP (1:1), (i) PM of Imi and AL1 FP (2:1), and (j) PM of Imi and AL1 FP (1:3).

Images of imipramine and the silicas are shown in Figures 3.39 and 3.40. Imipramine particles (Figure 3.39a) have irregular morphology with some of them large and semi rectangular in shape while others are relatively small.

It can be clearly seen in the physical mixtures (Figure 3.39) that drug alone with three Syloid<sup>®</sup> silicas do not mix well together as the crystalline state of the drug was maintained. In microwave formulation of the drug with Syloid<sup>®</sup> 3050 and XDP 3150 at 1:1 and 1:3 drug to silica ratios, there is an even distribution of silica particles but imipramine particles are not visible possibly the particles are molecularly dispersed on the surface of the silicas after the formulation. It can be concluded that the imipramine is partially amorphous upon formulation with those two silicas, as confirmed with DSC and XRD findings. Small crystals of imipramine can be clearly seen on the surface of Syloid<sup>®</sup> AL1 FP 2:1 (Figure 3.40h) prepared by microwave formulation. This was attributed to the small pore volume and pore diameter ( $0.40 \text{ cm}^3 \text{ g}^{-1}$  and  $26 \text{ \AA}$ ) of the silica compared with Syloid<sup>®</sup> XDP 3050 and XDP 3150.



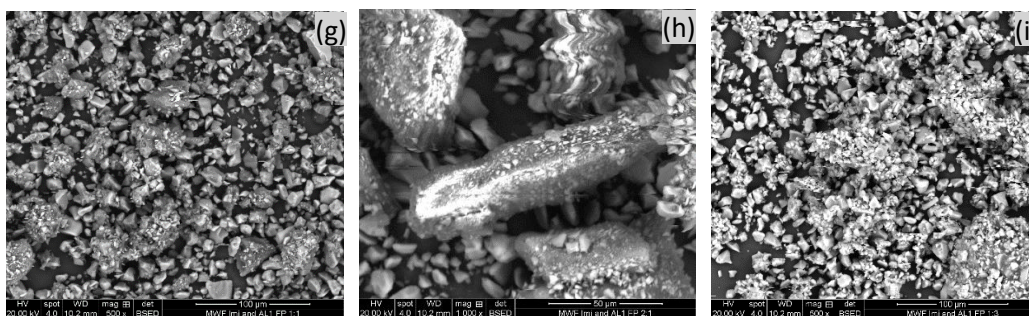


Figure 3. 40. SEM images x500 of (a) MWF of Imi and XDP 3050 (1:1), (b) MWF of Imi and XDP 3050 (2:1), (c) MWF of Imi and XDP 3050 (3:1), (d), MWF of Imi and XDP 3150 (1:1), (e) MWF of Imi and XDP 3150 (2:1), (f) MWF of Imi and XDP 3150 (1:3), (g) MWF of Imi and AL1 FP (1:1), (h) MWF of Imi and AL1 FP (2:1), and (i) MWF of Imi and AL1 FP (1:3).

Overall, SEM images confirmed uniform mixing of imipramine with Syloid® XDP 3050, XDP 3150 but the mixing with Syloid AL1 FP is not uniform as some crystalline drug was evident following the microwave formulation. Furthermore, modifying the formulation process such as that analysed in this study, can transform the extent of crystallinity in the sample and create a formulation that contains a uniform dispersion of imipramine within the silica matrix.

### 3.2.6. *In vitro* imipramine release

Dissolution profiles of imipramine loaded with Syloid® XDP 3050, XDP 3150 and AL1 FP materials at 1:1, 2:1 and 1:3 drug/silica ratios, along with imipramine itself (all containing an equivalent drug content), were investigated to determine the rate and extent of dissolution over a period of 45 minutes, as shown in Figures 3.41, 3.42 and 3.43. As shown in Figure 3.41, imipramine alone can be seen to rapidly undergo dissolution to reach 89.5 % ( $\pm 2.9\%$ ) drug release in the first 5 minutes yet only increase to a maximum of 91.2 % ( $\pm 2.4\%$ ) release after 45 minutes. This amount could have increased up to 100 % drug release over an extended period but about 10 % of the drug was not released from the medium due to lowest required sampling time.

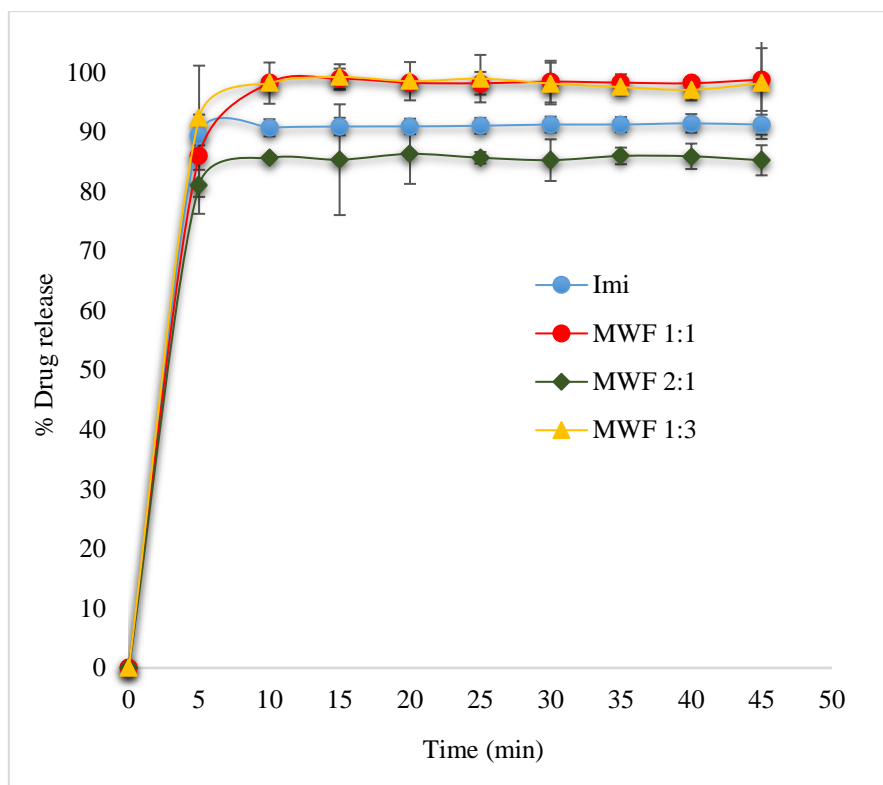


Figure 3. 41. Release profiles for pure imipramine (Imi) and imipramine Syloid<sup>®</sup> XDP 3050-based formulations at 1:1, 2:1 and 1:3. Each data point represents the mean of triplicate results ( $\pm$ SD).

This dramatic drug release can be explained by considering the physicochemical properties of the drug under analysis, i.e. imipramine alone is known to rapidly undergo dissolution due to its hydrophilic nature and aqueous solubility of 18.2 mg/L [199, 200], thus partially explaining the undesirable frequent dosing intervals required for patients with this drug [201].

For the Syloid<sup>®</sup> XDP 3050-based formulations investigated, the presence of the silica slightly modified the release profiles as illustrated in Figure 3.41 for 1:1 and 1:3 drug/silica ratios. The two ratios displayed a drug release of 86.0 % ( $\pm$ 6.9 %) and 92.4 % ( $\pm$  8.7 %) in 5 minutes whereas after 45 minutes, the products displayed a drug release of 98.8 % ( $\pm$  5.5 %) and 98.2 % ( $\pm$  9.4 %) for 1:1 and 1:3 respectively. Surprisingly, the 2:1 ratio did not provide such dramatic an increase but instead retarded drug release with a percentage of 81.1 % ( $\pm$  4.8 %) after 5 minutes, yet only increased to 85.2 % ( $\pm$  2.5 %) after 45 minutes. Hence, the drug may retain some parts of its crystalline state (as the DSC indicated in Figure 3.33f) which resulted

in less drug release. The surface chemistry of the XDP 3050 may be the reason for decreasing the imipramine release as a result of interactions between the drug and the functional group of the XDP 3050 mesopores [202]. Contrastingly, in 2:1 ratio the amount of drug is rather high and as a result, there could be a partial pore blockage during the release experiments due to the drug crystallisation on top of the pores as previously reported by Riikonen et al. [203], particularly for XDP 3050 with large pore diameter, which may also decrease the imipramine release [18].

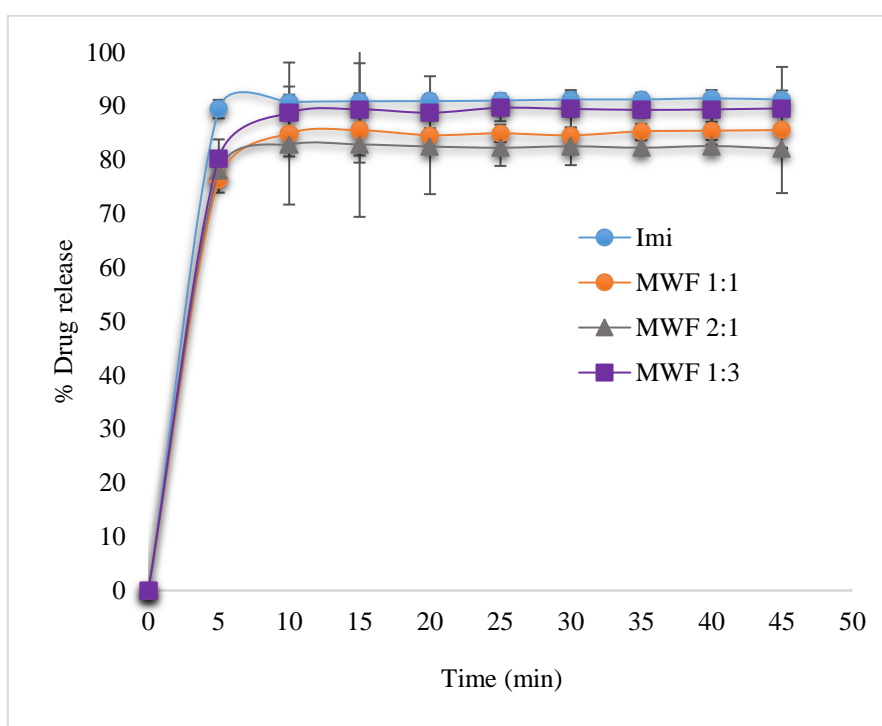


Figure 3. 42. Release profiles for pure imipramine (Imi) and imipramine Syloid<sup>®</sup> XDP 3150-based formulations at 1:1, 2:1 and 1:3. Each data point represents the mean of triplicate results ( $\pm$ SD).

Conversely, for the XDP 3150-based formulations analysed, it can be clearly seen that the rate and degree of drug release is dramatically reduced compared with pure drug. This deviation can be attributed to the difference in pore diameter of the XDP 3150 (200 Å) compared with the XDP 3050 (229 Å). The silica has a far smaller pore diameter which resulted in far less drug entering the pores during the microwave formulation process. The 1:3 ratio provided the greatest drug release of 80.3 % ( $\pm$ 3.5 %) after 5 minutes and 89.6 % ( $\pm$  1.4 %) of drug was

released after 45 minutes, while the 1:1 displayed a drug release of 76.4 % ( $\pm 2.4$  %) after 5 minutes and 85.6 % ( $\pm 6.7$  %) after 45 minutes. Conversely, the 2:1 product provided the slowest release of 77.9 % ( $\pm 1.3$  %) after 5 minutes and 82.1 % ( $\pm 0.2$  %) after 45 minutes respectively.

Comparing the dissolution profiles of imipramine from XDP 3050 and XDP 3150 samples with variation in their pore diameter, Figure 3.42 shows that the imipramine was clearly affected by the pore diameter of XDP 3150. The possible explanation for the different dissolution profiles between the 3050 and 3150 may emerge from the different pore structures of Syloid<sup>®</sup> XDP 3050 and 3150. These findings are in good agreement with previously published works [6, 150].

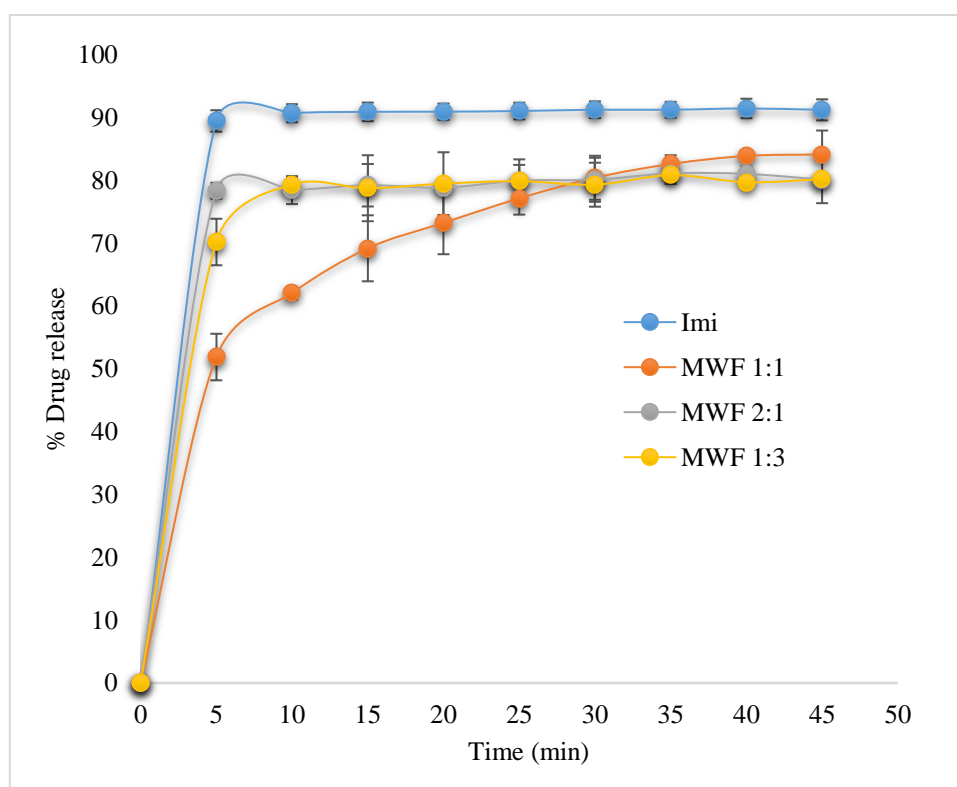


Figure 3. 43. Release profiles for pure imipramine (Imi) and imipramine Syloid<sup>®</sup> AL1 FP-based formulations at 1:1, 2:1 and 1:3. Each data point represents the mean of triplicate results ( $\pm$ SD).

Syloid AL1 FP (Fig. 3.43) did not follow this trend; the drug release for the three ratios was retarded compared with the drug alone, a 1:1 microwave formulation only achieved a



maximum drug release of 84.1 % ( $\pm 3.8$  %) after 45 minutes. The 2:1 product provided the maximum drug release of 80.1 % ( $\pm 4.8$  %) and 80.2 % ( $\pm 1.8$  %) drug was released for the 1:3 ratio after 45 minutes. This dramatic retardation in drug release can be explained by the physicochemical properties of the AL1 FP, specifically those identified in Table 2.1. For example, AL1 FP and XDP 3050 pore sizes are very different, in that AL1 FP has small mesopores, i.e. the silica has by far the smallest particle size (10  $\mu\text{m}$ ), smaller pore volume and pore diameter (0.40  $\text{cm}^3\text{g}^{-1}$  and 26  $\text{\AA}$ ) compared with other forms of silica analysed. Based on the pattern of increasing percentage release, i.e. from XDP 3150 to AL1 FP to XDP 3050, it would appear that two properties of the Syloid<sup>®</sup> silicas may play a key role in controlling the process, namely surface area and/or pore diameter. Interestingly, pore volume does not appear to be an influential factor for the rate and extent of dissolution, yet pore diameter is. In this work it appears that a large pore diameter, with a small surface area, maximises the extent of dissolution, which again, fits well with the findings of other studies with mesoporous microspheres [150, 204]. As a consequence of this, it is not only possible to dramatically enhance the rate and extent of dissolution, but also to vary the percentage depending upon the type of Syloid<sup>®</sup> silica used. Another potentially influential factor is the formation of complexes which may affect the drug release profile through the creation of particle aggregation. If this is the case, then it can be proposed that there are two unique structures within the formulation: drug within pores and aggregates between particles which can both contribute to drug release.

### **3.3. Conclusions**

In summary, all three Syloid<sup>®</sup> silicas have enhanced the percentage of dissolution following a microwave formulation technique, it would appear that the transformation from the crystalline to amorphous form (as evidenced by XRD and dissolution profiles of processed samples) plays a key role. This has been the conclusion of other researchers, when investigating alternative mesoporous materials [176], and fits well with the results from this research. However, when

considering why the three Syloid<sup>®</sup> silicas did not facilitate the same increase in percentage release, it is more appropriate to consider their relative physicochemical properties, specifically those identified in Table 2.1. For example, AL1 FP and XDP 3050 pore sizes are very different, in that AL1 FP has small mesopores, i.e. a smaller pore volume and diameter compared with XDP 3050. Based on the pattern of increasing percentage release, i.e. from XDP 3150 to AL1 FP to XDP 3050, it would appear that two properties of the Syloid<sup>®</sup> silicas might play a key role in controlling the process, namely surface area and/or pore diameter. In this study, it appears that a large pore diameter, with a small surface area, maximises the extent of dissolution, which again, fits well with the findings of other studies with mesoporous microspheres [205, 206]. As a consequence of this, it is not only possible to dramatically enhance the rate and extent of dissolution, but also to vary the percentage depending upon the type of Syloid<sup>®</sup> silica used. This finding can be of benefit for not only phenylbutazone, indomethacin or imipramine-based formulations but potentially a far wider range of compounds that exhibit poor aqueous solubility which will help alleviate bioavailability issues. Overall, a higher percentage release was achieved with the drug formulated with the microwave method in the presence of silica compared with pure drug.

## **Chapter 4. Microwave differential thermal analysis (MWDTA) of pharmaceutical compounds**

### **4.1. Introduction**

Almost twenty years ago a new analytical technique was described for the first time, namely microwave differential thermal analysis (MWDTA), that combined the advantages of microwave heating with the benefits of differential temperature measurement to probe the thermal properties of materials [90]. The limited thermal response using conventional heating is avoided using microwave heating as there is direct interaction of the material with the microwave energy. However, more importantly, microwave heating provides a unique means of investigating thermal transitions based on the associated changes in the dielectric properties of the sample. These thermally induced changes, such as melting or decomposition, are then analysed based on the microwave power profiles obtained. When a material is subjected to microwave radiation there are two important parameters that dictate the nature of the interaction, namely the dielectric constant and the dielectric loss factor. The former considers the way a material is polarised by the electric field and the latter the conversion from radiation to heat. This form of analysis has been successfully applied to a range of materials including decompositions, dehydrations and phase changes [207] and can provide qualitative and quantitative information of solid state processes [208]. Furthermore, MWDTA can make a valuable contribution to the investigation of the so-called ‘microwave effect’, these are anomalies that occur when certain materials are heated in a microwave field [209] as well as reveal fine detail through the use of derivative plots of either the applied power or temperature [210]. In recent years a variety of studies have investigated the application of MWDTA to both a range of materials, such as ceramics [211], and a range of more complex analytical systems [212].

In contrast to the use of microwave radiation as an analytical tool, a comparatively large volume of research has been undertaken to investigate the effects (and potential benefits) of using microwaves in a formulation capacity such as that carried out in one. This research has highlighted the benefits of using microwave processing for pharmaceutical compounds with the presence of excipients to create unique products. Furthermore, microwave processing has been applied for ibuprofen in combination with stearic acid and polyvinylpyrrolidone, along with fenofibrate and mesoporous silicas to create a unique formulation [87, 88]. An interesting, and very recent, application of microwave irradiation is the concept of amorphisation within the tablet, i.e. creating the amorphous form of the drug in its final dosage form directly before administration [89].

In summary, microwave radiation has been previously employed for the analysis of compounds through the use of MWDTA, and separately, to formulate products that possess unique physicochemical properties that can be advantageous, especially in the pharmaceutical industry. However, as yet there has been no consideration for the use of MWDTA to investigate pharmaceutical compounds that are to be subjected to microwave irradiation during formulation to fully comprehend if such a process will be suitable and to fully understand the interactions that will occur. This research considers the use of MWDTA on model pharmaceutical compounds to investigate the potential application of this form of thermal analysis on such compounds as an indicator of the suitability of microwave-based formulation methods.

## 4.2. Results and discussion

### 4.2.1. MWDTA of silicon carbide (SiC)

The MWDTA profile for the heating and cooling of silicon carbide (SiC) heated at 5 °C/min to 300 °C and then cooled at -5 °C min<sup>-1</sup> to 30 °C is shown in Figure 4.1. Silicon carbide (SiC) is relatively chemically inert over a wide temperature range [213], strongly absorbs microwave energy which makes it couple strongly and has high thermal conductivity. SiC has no chemical or physical changes over the temperature range investigated but was studied to provide information to illustrate the variation of phase change parameters which can be found as material is heated.

Figure 4.1(A) is in the form of calculated  $\Delta T$  as a function of temperature of the sample while Figure 4.1(B), shows the relationship between the temperature and power applied during the run. Apart from an initial variation at the onset of the experiment, the temperature control was smooth and featureless with a slow rise in microwave power, set to control the heating rate. No event was observed in both Figure 4.1(A) and 4.1(B) other than a switch upon cooling (X) as the fusion of SiC is around 2700 °C [103] and the minimum and maximum temperature used in this study was 160 °C and 200 °C depending upon the sample under analysis.

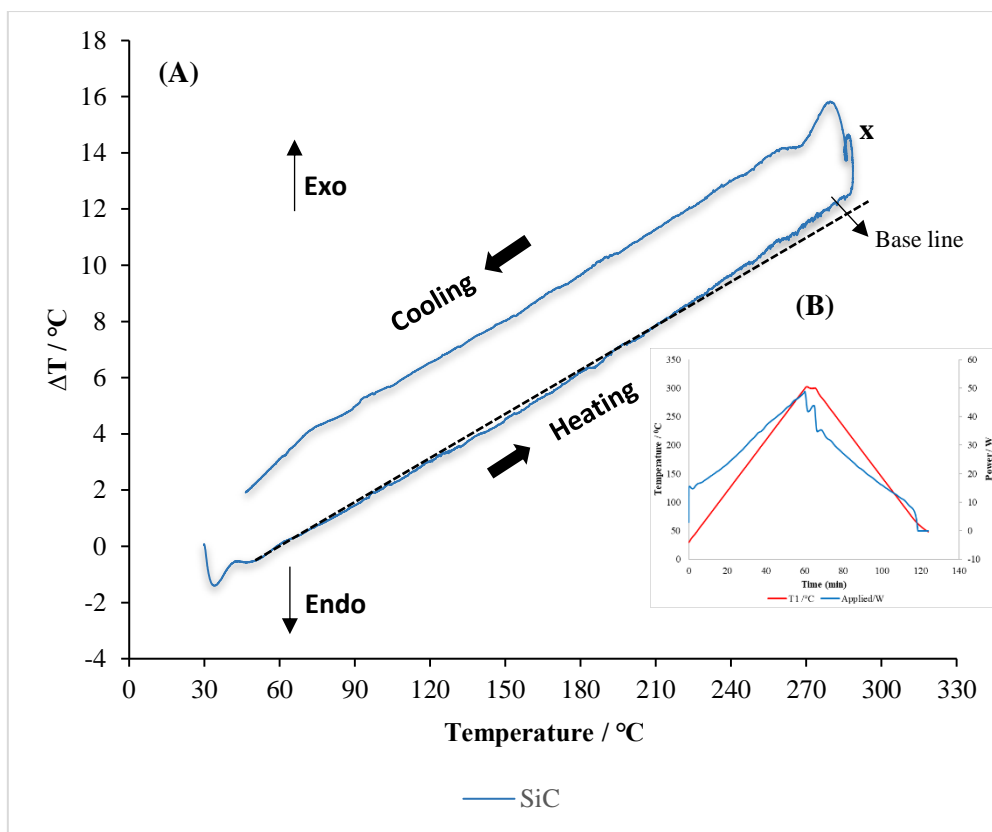


Figure 4. 1. Microwave differential thermal analysis (MWDTA) of silicon carbide (SiC) heated at 5 °C/min to 300 °C then cooled at -5 °C/min to 30 °C.

#### 4.2.2. MWDTA of pharmaceutical compounds

Eight model pharmaceutical compounds were analysed using MWDTA namely; benzocaine, haloperidol, ibuprofen, indomethacin, ketoprofen, naproxen, imipramine and phenylbutazone. These compounds were selected for their range of physicochemical properties thus covering the variety of types of compounds often encountered in the pharmaceutical industry. Firstly, benzocaine was investigated, as shown by the temperature and power-profile data in Figure 4.2.

Apart from an onset variation at 13.6 W (1.6 min) at the start of the experiment, it can be seen that temperature control was smooth and featureless with a slow rise in MW power to maintain the set heating rate. However, at around 92.8 °C the power rose to 21.0 W from 20.0 W, i.e. a 1 W difference required to maintain the heating rate as a result of the occurrence of fusion, thus

more energy was required to drive the endothermic process. At 97.1 °C the fusion of benzocaine was complete, and the temperature rose sharply to attain an equilibrium at 160 °C. The equilibrium was maintained for a further 5 min at which point the temperature was decreased from 160 °C to 40 °C.

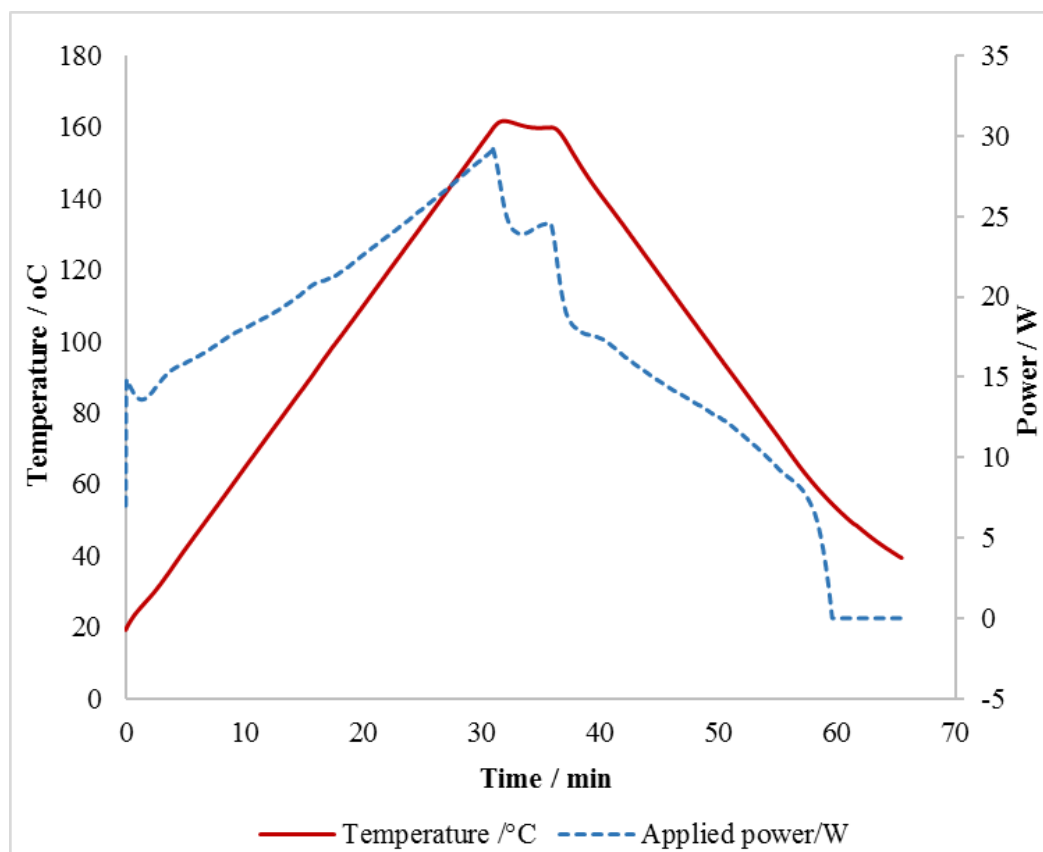


Figure 4. 2. Temperature and associated power profile for benzocaine heated at 5 °C/min to 160 °C and then cooled to 40 °C

There was a rapid decrease in power at the equilibrium stage from 29.3 W to 25.3 W, the stage was maintained for 5 min and then dropped again to 18.2 W with the overall change in power of 11.1 W. Initially, the applied MW power fell by 4.0 W and then decreased again by 7.1 W until the sample temperature returned to its set cooling rate where the power dropped back to 0 W without any change during the process. The dielectric change from solid to liquid revealed that less power was required to maintain the heating rate after the drug had become liquid, compared with before the transition. Results obtained for MWDTA of benzocaine (first and

second cycle) are displayed in Figure 4.3 in the form of calculated  $\Delta T$  ( $T_{\text{sample}} - T_{\text{reference}}$ ) plotted as a function of sample temperature.

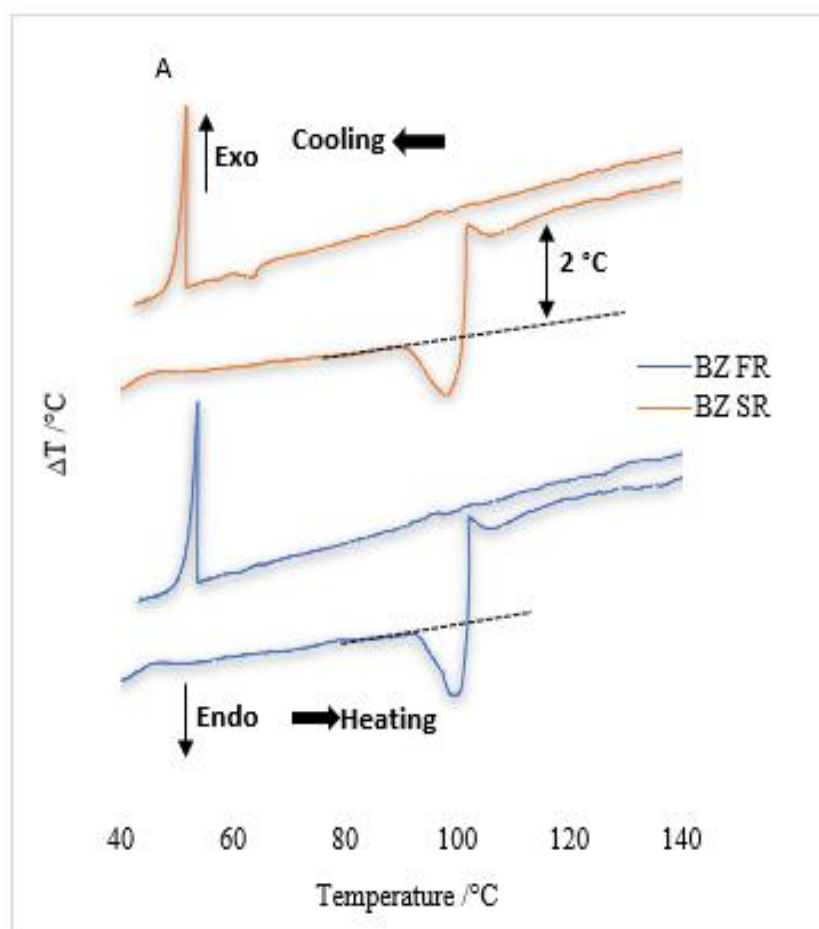


Figure 4. 3. Microwave differential thermal analysis (MWDTA) of benzocaine heated at 5 °C/min to 160 °C for the first and second run (FR and SR) and cooling at -5 °C/min to 40 °C in both cases.

From Fig. 4.3, there was an onset variation at the start of the experiment and a broad endothermic event at 91.2 °C corresponding to melting of the drug followed by a rise in  $\Delta T$  indicating an increase in  $\tan \delta$  going from solid to liquid. Upon cooling, a sharp exothermic event at 47.9 °C corresponding to recrystallisation has a slightly lower temperature, the fusion of the drug was slightly above that expected based on DSC data presented later in this study. The phase change of the drug due to the effect of temperature has been previously reported [214]. Many drugs decompose as a result of the effect of heat, oxygen, light, and moisture therefore based on these factors, the second cycle was carried out to an increased temperature



of 200 °C in an attempt to encourage decomposition of the compound. The second experimental cycle of the same sample showed an initial rise in  $\Delta T$  after the transition at 91.6 °C with recrystallisation occurring at 51.6 °C, i.e. only a slight shift was evident of the aforementioned transitions due to heating-cooling-reheating and re-cooling effects.

Changes observed in the profile of the drug obtained included a change in dielectric properties after the transition as the sample became molten which indicates that the sample was heating more efficiently than before the transition. This was also apparent in Figure 4.2 whereby the power increased and decreased as the sample coupled variably with the microwave energy. The resultant profile provided the expected behaviour of a fusion process accompanied by a large dielectric change. These changes were not observed during DSC (results discussed later) as a consequence of heat capacity.

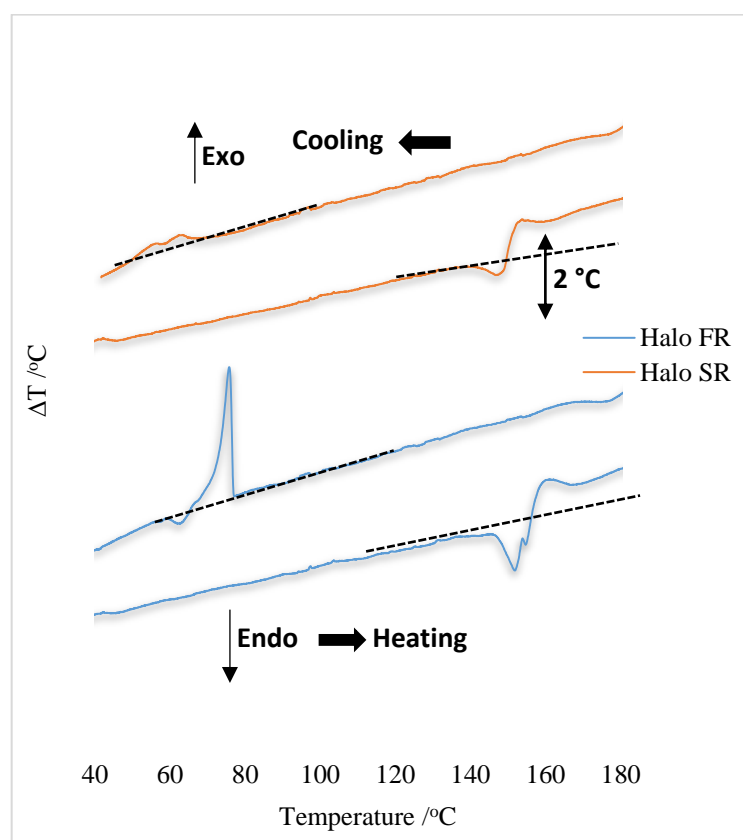


Figure 4. 4. Microwave differential thermal analysis (MWDTA) of haloperidol heated at 5 °C/min to 200 °C for the first (FR) and second (SR) run then cooling at 5 °C/min to 40 °C in both cases.

These changes demonstrate the sensitivity of this technique to materials that undergo thermal transitions. Secondly, haloperidol was analysed using MWDTA, as displayed in Fig. 4.4.

The MWDTA profiles of haloperidol (first and second run) shown in Figure 4.4 revealed a sharp transition at 151.8 °C corresponding to the melting point of the drug. The temperature at which the event takes place is in good agreement with the literature value of 153 °C found using a conventional thermal analysis technique [215], followed by a rise in  $\Delta T$  indicating an increase in  $\tan \delta$  going from solid to liquid. A dielectric change can be seen after the transition as the sample couples more strongly with the microwave energy, which again, suggests that the sample was heating more effectively than before the transition. When the temperature was changed from increasing to decreasing, a defined recrystallisation temperature was evident. In the second run, similar events were observed with a broadened, reduced intensity, and shifted to a lower temperature for the fusion of the drug, namely a 12.6 °C difference in comparison with the first run which further confirms the nature of crystallinity of the drug, although the changes in the latter are relatively small. Again, minor events observed were not thought to be 'real' transitions but merely artefacts of the method employed. Thirdly, indomethacin was analysed using MWDTA, as displayed in Figure 4.5.

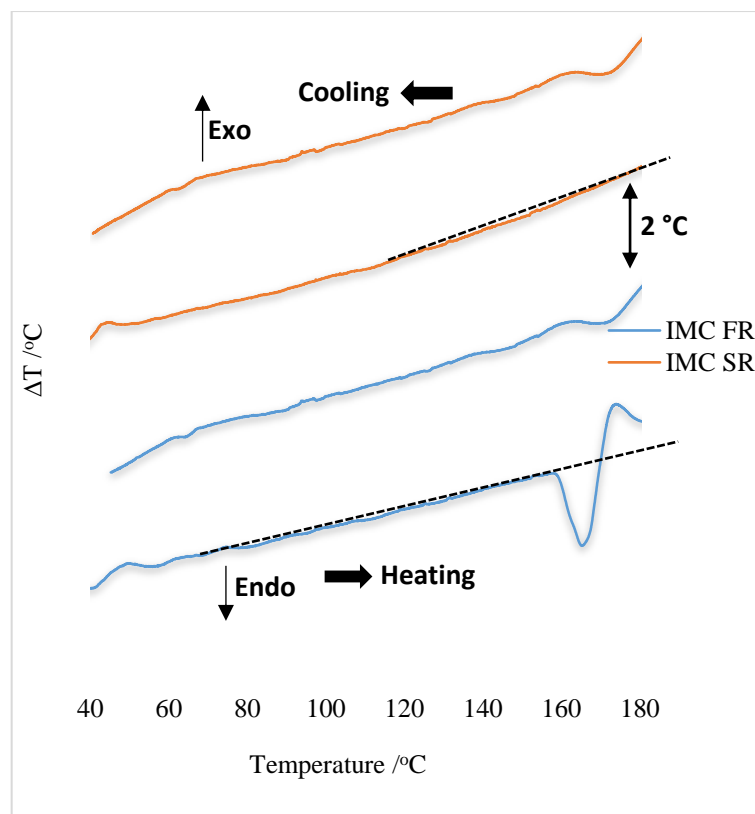


Figure 4. 5. Microwave differential thermal analysis (MWDTA) of indomethacin heated at 5 °C/min to 200 °C for the first (FR) and second (SR) run then cooled at 5 °C/min to 40 °C in both cases

Figure 4.5, displays a sharp transition with an extrapolated onset at 159.3 °C in the first run indicating fusion occurred: further evidenced at 165.2 °C, corresponding to the known melting point of this drug [216]. The transition was accompanied by a significant dielectric change, this change did not return to the baseline (as expected for this drug) as a consequence of the differing dielectric properties as the sample underwent melting. Upon subsequent cooling, no significant phase transition was observed, implying the drug did not recrystallise. No significant phase changes were observed in the second run (other than instrument recovery) further justifying the theory that the sample remained in an amorphous form. Fourthly, ketoprofen was analysed using MWDTA, as displayed in Figure 4.6.

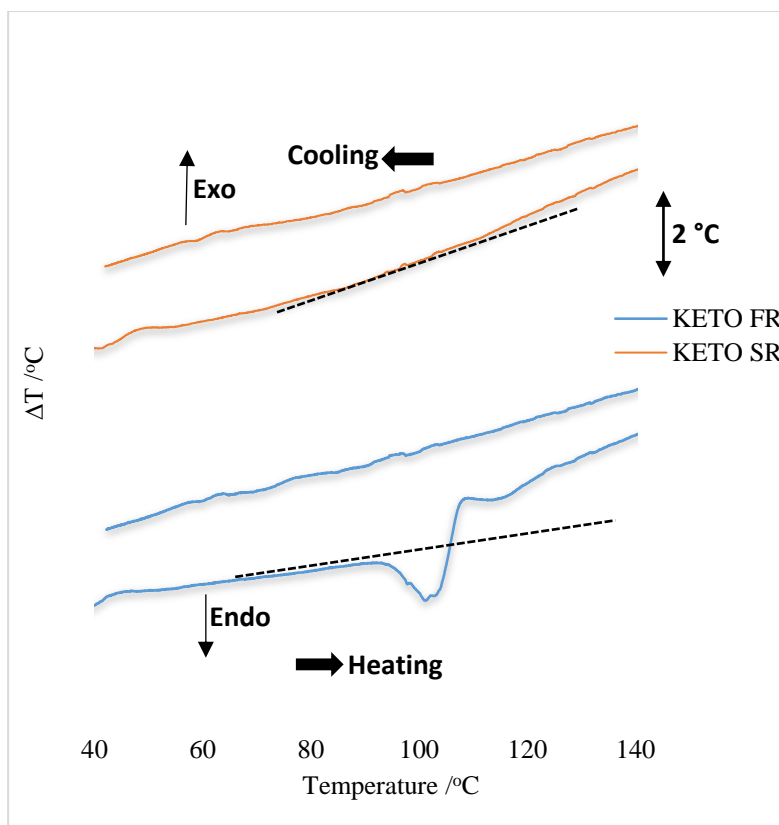


Figure 4. 6. Microwave differential thermal analysis (MWDTA) of ketoprofen heated at 5 °C/min to 160 °C then cooled to 40 °C for the first (FR) and second (SR) run.

In Figure 4.6, apart from an initial variation at the onset of the experiment, the differential temperature in the first run was smooth and featureless until a transition occurred at 94.7 °C, corresponding to the melting point of the drug in good agreement with what was previously reported [217]. The temperature was increased further which brought about a change in baseline as a consequence of the increased coupling of the sample with microwave energy as the sample underwent melting. Upon cooling, no significant transition event was observed, implying the sample remained in amorphous form, i.e. no recrystallisation. In the second run, there was no event observed other than a decrease in tangent in the region of 124.8 °C – 140.0 °C, which was brought about by a dielectric change. The tangent gave a good indication of how effectively the sample converted the applied microwaves into thermal energy, i.e. the greater the heating via polarisation the greater the thermal loss from the drug. The fifth pharmaceutical compound to be analysed using MWDTA was phenylbutazone, as shown in Figure 4.7.

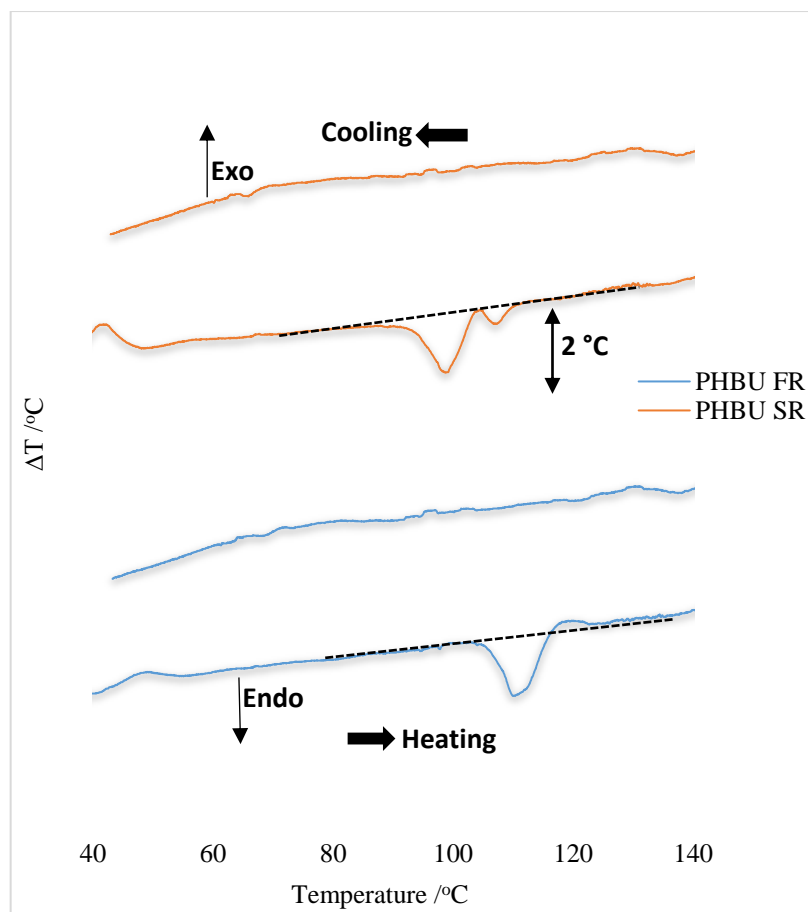


Figure 4. 7. Microwave differential thermal analysis (MWDTA) of phenylbutazone heated at 5 °C/min to 160 °C then cooled to 40 °C for the first (FR) and second run (SR).

The first run displayed in Figure 4.7 does not reveal a significant change in baseline following the transition corresponding to the known melting point of the drug at 109.8 °C [218]. This finding indicates that there was no change in the dielectric properties of the sample after the transition - in contrast with the previously analysed compounds. No observable event corresponding to recrystallisation was evident during the first cooling. The second cycle of phenylbutazone was characterised by a  $\beta$  polymorphic transition at 93.4 °C [173, 175]. Again, upon the second cooling no significant event occurred implying a lack of recrystallisation, as was the case with the first run. However, the presence of a small peak at 105.0 °C indicates that there was a small amount of partially crystalline compound present.

The sixth compound of pharmaceutical interest analysed using MWDTA was ibuprofen, as shown in Figure 4.8.

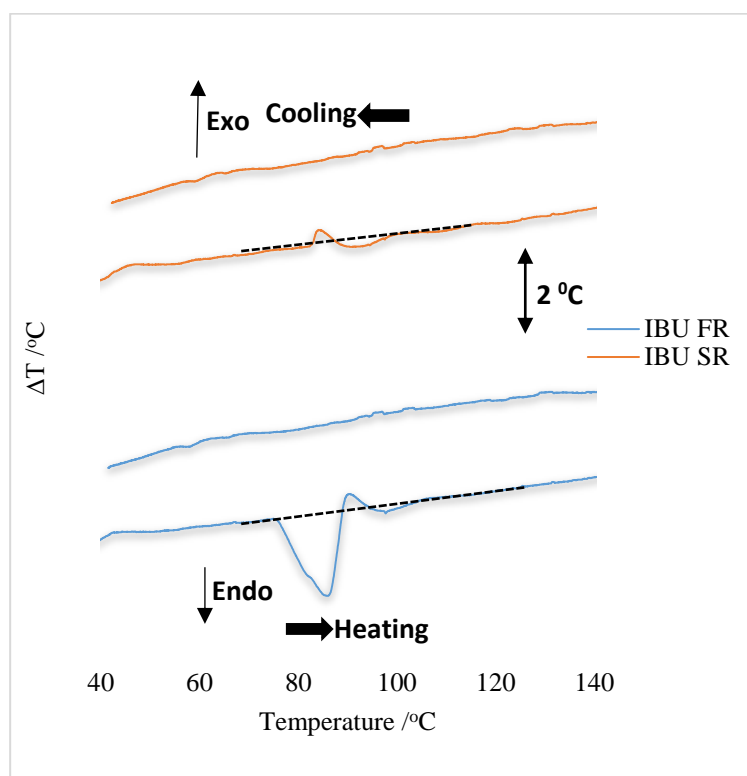


Figure 4. 8. Microwave differential thermal analysis (MWDTA) of ibuprofen heated at 5 °C min<sup>-1</sup> to 160 °C then cooled to 40 °C for the first (FR) and second (SR) run.

MWDTA (Figure 4.8) of ibuprofen indicated one transition occurring at 76.2 °C. The transition corresponds to the expected fusion of the drug in the first cycle [219] and no increased coupling was observed after the transition. Furthermore, no recrystallisation event was apparent upon cooling. In the second cycle, a transition at 83.1 °C was unexpectedly observed implying some recrystallisation had occurred during the previous cooling cycle and the sample was able to undergo a melting transition. The seventh compound of pharmaceutical interest analysed using MWDTA was naproxen, as shown in Figure 4.9.

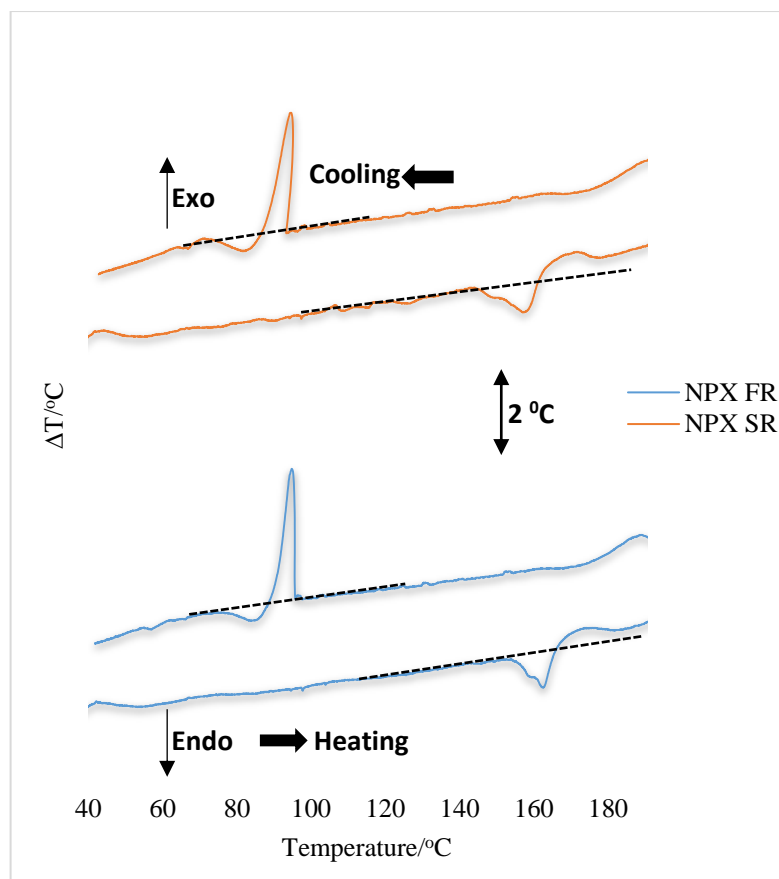


Figure 4. 9. Microwave differential thermal analysis (MWDTA) of naproxen heated at 5 °C/min to 200 °C for the first and second run (FR and SR) and cooling at 5 °C/min to 40 °C in both cases.

The MWDTA profile of naproxen in the form of calculated  $\Delta T$  as a function of temperature is shown in Figure 4.9 the endothermic fusion has an onset temperature of 154.6 C for the first run, which is in good agreement with the literature value of 152 °C found using conventional thermal analysis [220]. The transition was accompanied by a step change as the sample underwent melting. Upon cooling, a sharp exothermic recrystallisation had a slightly lower temperature of 95.6 °C. The second run of the sample showed an initial rise in  $\Delta T$  after the transition. All the phase changes observed in the first run were also observed in the second run. The eighth compound of pharmaceutical interest analysed using MWDTA was imipramine, as shown in Figure 4.10.

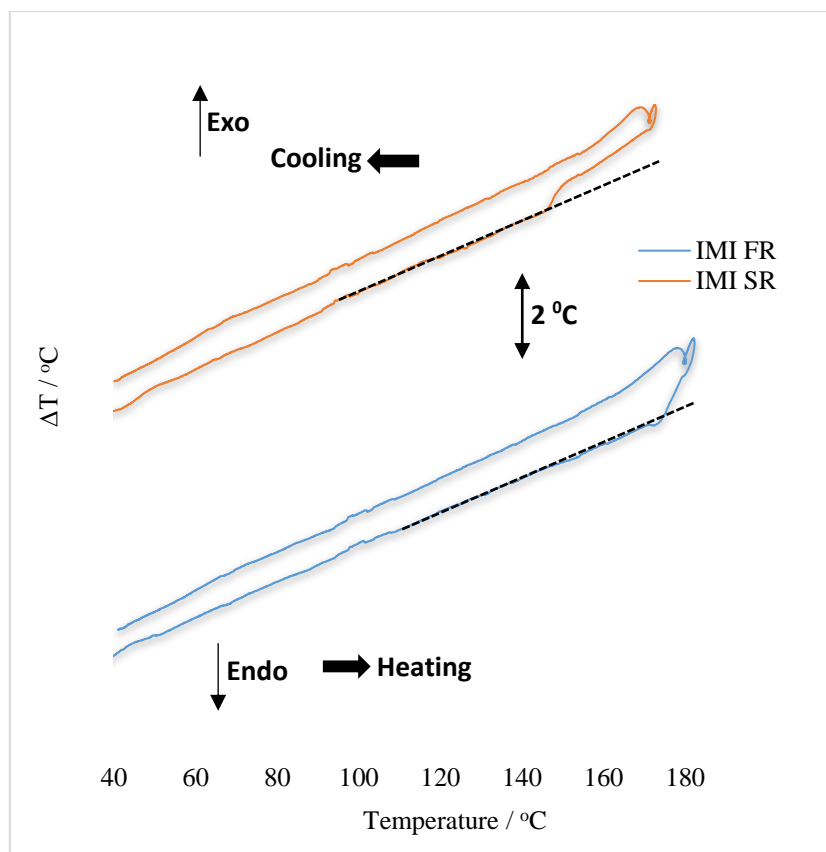


Figure 4. 10. Microwave differential thermal analysis (MWDTA) of imipramine heated at 5 °C/ min to 180 °C for the first and second run (FR and SR) and cooling at 5 °C/min to 40 °C in both cases.

The first run displayed in Figure 4.10 does not reveal a significant change in baseline following the transition corresponding to the known melting point of the drug at 173.7 °C [194]. This finding indicates that there was a small change in the dielectric properties of the sample after the transition - in contrast with the previously analysed compounds. The method did not observe any event corresponding to recrystallisation during the first cooling. The second cycle of the process was characterised by a transition at 145.4 °C, particularly surprising based upon data from the first run. Again, upon the second cooling no significant event occurred implying a lack of recrystallisation, as was the case with the first run. However, the presence of a small event at 145.4 °C indicates that there was a small amount of partially crystalline compound present.



#### 4.2.2. Differential scanning calorimetry (DSC) of pharmaceutical compounds

DSC analysis was undertaken for the eight model pharmaceutical compounds, a summary of the values obtained can be seen in Table 4.1.

Table 4. 1: Physicochemical data and DSC peak values for the melting ( $T_m$ ) and recrystallisation ( $T_r$ ) of eight compounds and four excipients

Material	$M_w/g.mol^{-1a}$	Crystalline/Amorphous	$T_m/^\circ C$	$T_r/^\circ C$
BZ	165.19	Crystalline	90.7	48.5
Halo	375.86	Crystalline	152.1	92.3
IBU	206.28	Crystalline	77.7	-
IMC	357.79	Crystalline	160.5	-
KETO	254.28	Crystalline	96.2	-
PHBU	308.37	Crystalline	107.5	-
NPX	230.26	Crystalline	156.4	112.6
IMI	316.87	Crystalline	174.9	-
$\beta$ -CD	1134.98	Crystalline	90-140	-
D-man	184.16	Crystalline	166.5	119.9
SA	284.48	Crystalline	70.1	61.2
XDP	-	Amorphous	-	-

<sup>a</sup> Average molecular weight ( $M_w$ ) according to the supplier

Benzocaine is a crystalline drug having a fusion temperature of 90.7 °C, as previously reported in literature [214]. In Figure 4.11(a), pure benzocaine (FR) displayed an endothermic peak at 91.2 °C followed by a sharp peak with high intensity appearing during cooling at 48.5 °C, corresponding to the exothermic recrystallisation event. The appearance of the fusion peak confirms the crystallinity of the drug during the first cycle. The second cycle (Figure 4.11b) exhibited a broader melting peak with a small shift to 91.5 °C, in comparison with the first

cycle. This result suggests that the drug molecules returned to a crystalline form after the first heating and cooling cycle, and again after the second cooling as a peak appeared at 51.3 °C.

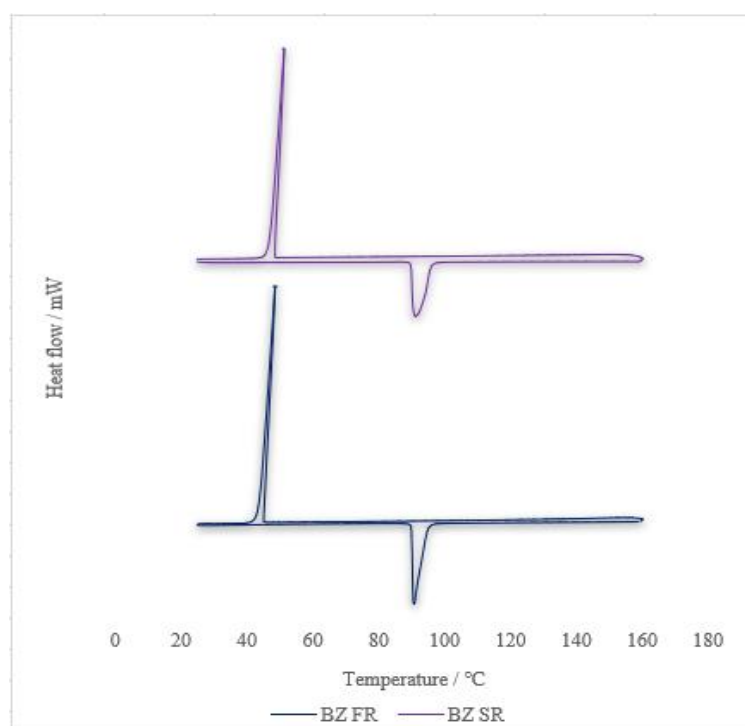


Figure 4. 11. DSC thermograms of; (a) Benzocaine first run (FR) and (b) Benzocaine second (SR)

Upon the first heating cycle for haloperidol (Figure 4.12 a), a sharp endothermic peak was observed at 152.0 °C, corresponding to the published melting point for the compound [215]. Subsequent cooling highlighted an exothermic event occurring at 92.5 °C corresponding to recrystallisation of the compound. In the second heating (Figure 4.12 b) and cooling cycle the initial peak temperature and subsequent exothermic event were observed at similar, but slightly lower, temperatures with an endothermic transition at 151.9 °C and recrystallisation at 88.9 °C.

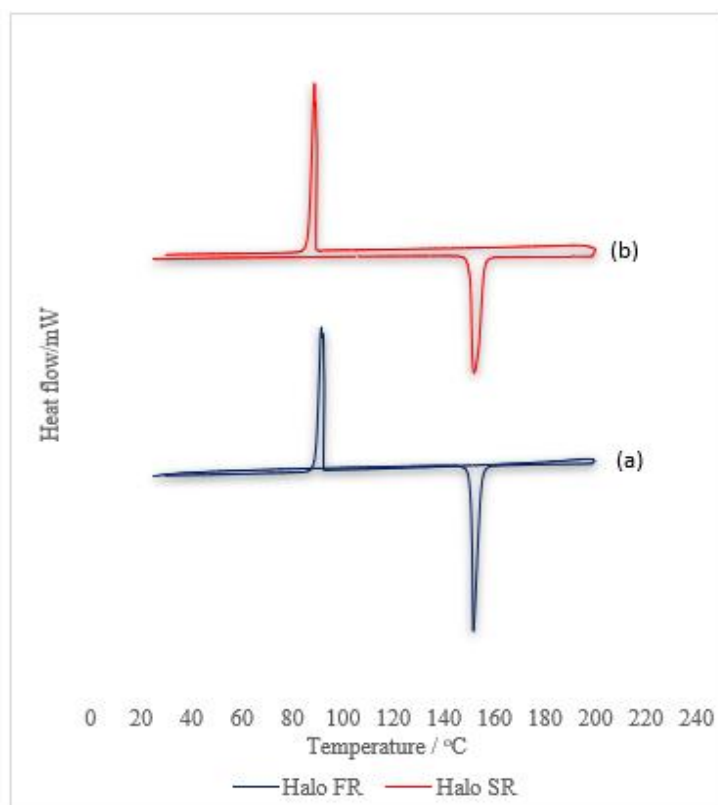


Figure 4. 12. DSC thermograms of; (a) Haloperidol first run (FR) and (b) Haloperidol second run (SR),

The thermal profile for indomethacin (Figure 4.13 a) was characterised by a well-defined sharp endothermic peak corresponding to the expected fusion process at 160.5 °C, in agreement with published data [216]. The drug did not appear to recrystallise upon cooling. Upon a second heating and cooling cycle (Figure 4.13b), an endothermic peak corresponding to glass transition was observed at 47.6 °C, melting and recrystallisation peaks were not observed, most likely to be a consequence of the drug remaining in amorphous form after fusion in the first heating cycle.

These findings agree with the XRD data to be discussed later. A summary of the DSC profiles for these three drugs is displayed in Table 4.1.

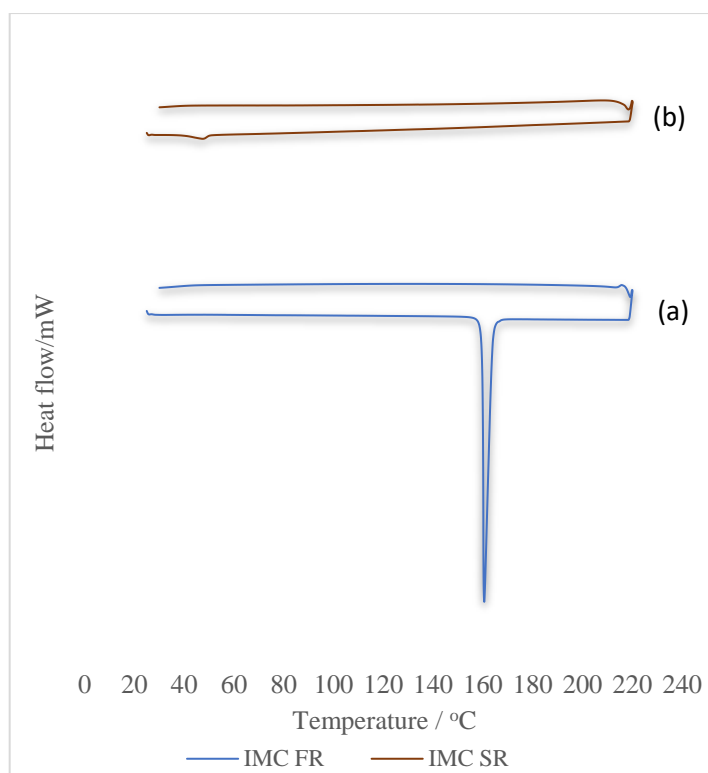


Figure 4. 13. DSC thermograms of; (a) indomethacin first run (FR), and (b) indomethacin second run (SR)

For the initial heating cycle of phenylbutazone a single sharp endothermic peak was observed at 109.3 °C implying melting of the compound, this value corresponded well with published data [218]. Upon cooling, no exothermic transition was observed, suggesting that there was no recrystallisation as the sample cooled. Upon the second heating and cooling cycle, a small and broad melting peak was observed at a slightly lower temperature than that seen in the first cycle, namely 99.2 °C. This small event suggests a  $\beta$  polymorphic transition of the drug as evidenced in the MWDTA experiment [173]. For ketoprofen only one transition was observed at 96.2 °C, in the first heating cycle, corresponding to the published fusion temperature for the compound [217].

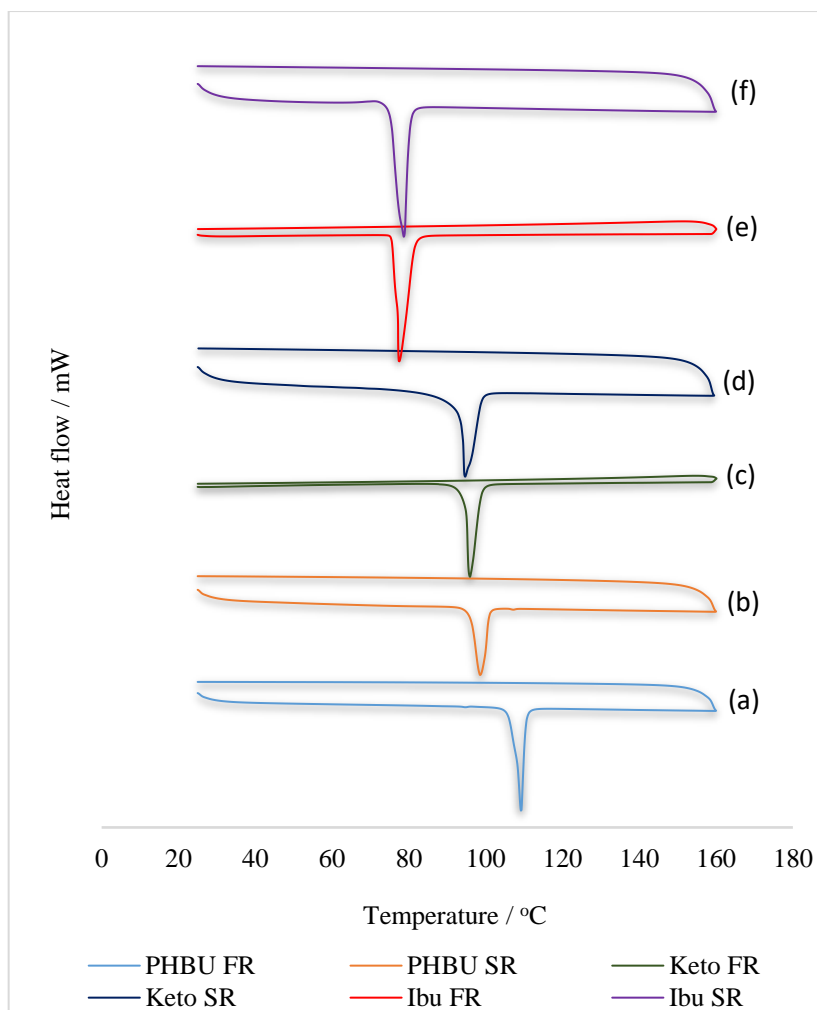


Figure 4. 14. DSC thermograms of; (a) phenylbutazone first run (FR), (b) phenylbutazone second (SR), (c) ketoprofen first run (FR), (d) ketoprofen second run (SR), (e) ibuprofen first run (FR), and (f) ibuprofen second run (SR)

However, a similar event was observed which shifted to a slightly lower temperature in the second cycle at 94.9 °C, suggesting that the compound has transformed into a partially amorphous form after the initial melt transition. In the case of ibuprofen, the DSC profiles are similar to those of ketoprofen. The only observable thermal event for ibuprofen was an endothermic peak at 77.4 °C indicating melting of the compound, only seen in the first cycle and closely related to that reported in the literature [219]. Once again, after cooling, an event at 78.2 °C was observed in the second cycle, implying the sample also melted after the initial transition was observed. These results fit well with the findings of the XRD to be discussed later. A summary of the DSC profiles for these three drugs is displayed in Figure 4.14.

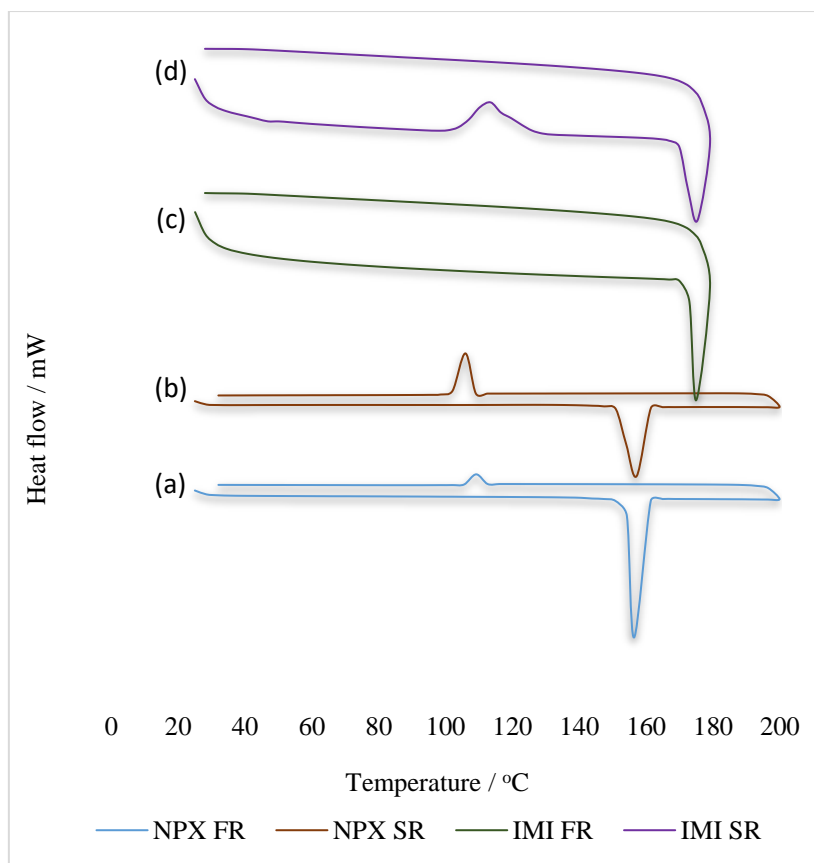


Figure 4. 15. DSC thermograms of; (a) naproxen first run (FR), (b) naproxen second (SR), (c) imipramine first run (FR), (d) imipramine second run (SR)

The comparable DSC profiles of naproxen and imipramine are shown in Figure 4.15. In the first run of naproxen, the endothermic fusion has an onset temperature of 156.4 °C which corresponds to the fusion of the compound while upon cooling, the corresponding exothermic recrystallisation has a slightly lower onset of 112.6 °C. The second run of the same sample shows a slightly broadened peak at 157.2 °C while after cooling, an event at 105.9 °C was observed in the second cycle, implying the sample also recrystallised after the initial transition was observed. In the case of imipramine, a single sharp endothermic peak was observed at 174.9 °C implying melting of the compound, this value corresponded well with published data [194]. Upon cooling, no exothermic transition was observed, suggesting that there was no recrystallisation as the sample cooled. In the second cycle, a transition at 113.5 °C was unexpectedly observed implying some recrystallisation had occurred during the previous

cooling cycle and the sample was able to undergo a melting transition at a slightly lower temperature of 175.4 °C.

#### 4.2.3. X-ray diffraction (XRD) of pharmaceutical compounds

The XRD patterns of benzocaine (FR and SR), haloperidol (FR and SR) and indomethacin (FR and SR) are illustrated in Figure 4.16. The diffraction patterns observed at 8.6°, 16.8°, 20.0°, 24.0°, and 27.2° correspond to powder diffraction patterns of pure benzocaine (FR) and were consistent with patterns reported in the literature for this drug [221].

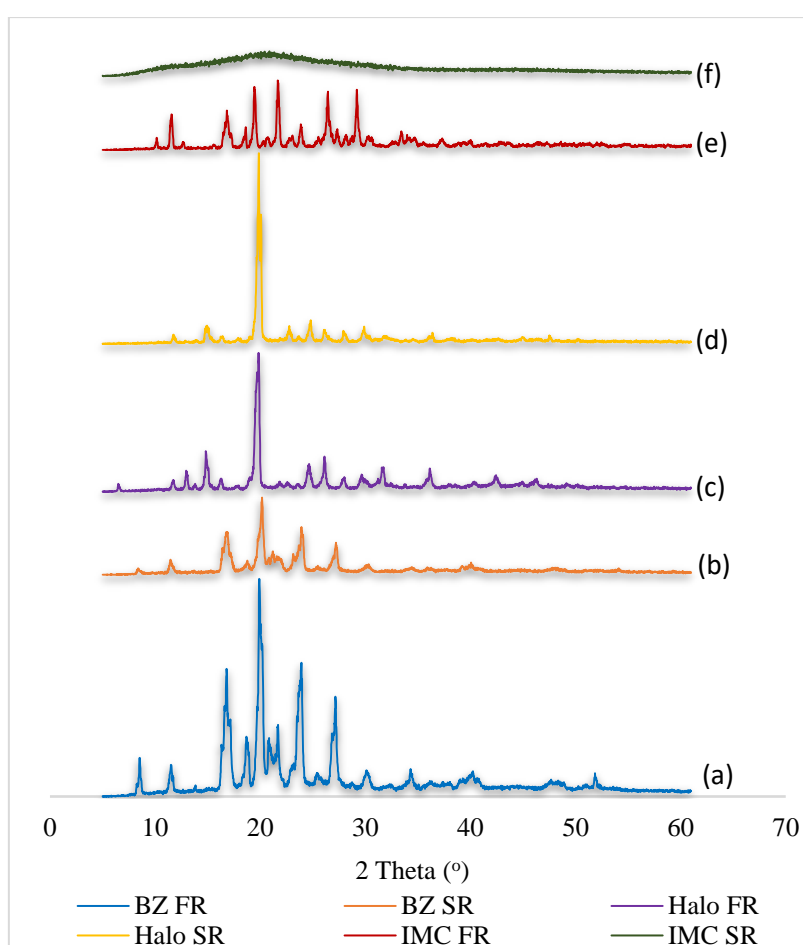


Figure 4. 16. XRD patterns of; (a) benzocaine first run (FR), (b) benzocaine second (SR), (c) haloperidol first run (FR), (d) haloperidol second run (SR), (e) indomethacin first run (FR) and (f) indomethacin second run (SR)

The patterns of benzocaine in the second run presented a different pattern from those of the first run. Less intense peaks for this drug in the second run (Figure 4.16b) were observed,

possibly due to changes in particle size and shape after the first run. The observed diffractions for haloperidol (FR) at  $14.9^\circ$ ,  $19.9^\circ$  and  $26.2^\circ$  confirm the crystalline nature of the drug is consistent with diffractograms reported in the literature [222] while the second run shows a less intense diffraction pattern due to the loss of some crystallinity of the drug after the first run. The diffractograms corresponding to the crystalline indomethacin (FR) were observed at  $17.0^\circ$ ,  $19.5^\circ$ ,  $21.8^\circ$ ,  $26.5^\circ$ , and  $29.3^\circ$  which suggest that indomethacin was  $\gamma$ -polymorph [223]. However, there was a complete disappearance of diffractograms in the second run of the drug which confirms the transformation from crystalline nature to amorphous form after the first run as previously evidenced in the DSC analysis.

The XRD patterns of PhB (FR and SR), Keto (FR and SR) and Ibu (FR and SR) are illustrated in Figure 4.17. Pure crystalline phenylbutazone can be seen in Figure 4.17(a) with sharp diffraction peaks at  $8.12^\circ$ ,  $12.95^\circ$ ,  $18.59^\circ$  and  $20.88^\circ$  and was in agreement with previously published data for the drug [11]. Phenylbutazone peaks are still evident in the second run with high intensity suggesting the drug is still in a partial-crystalline state. The patterns for ketoprofen in the first run were observed at  $14.6^\circ$ ,  $18.6^\circ$ , and  $23.0^\circ$  confirming the crystalline structure of the drug which fits in well with that reported previously [224]. However, the second run shows the diminishment of peak intensities confirming the loss of some crystalline structure of the drug after the first run. Characteristics peaks at  $16.7^\circ$ ,  $20.3^\circ$  and  $22.4^\circ$  suggests ibuprofen to be crystalline in the first run while the peak patterns are still maintained in the second run.



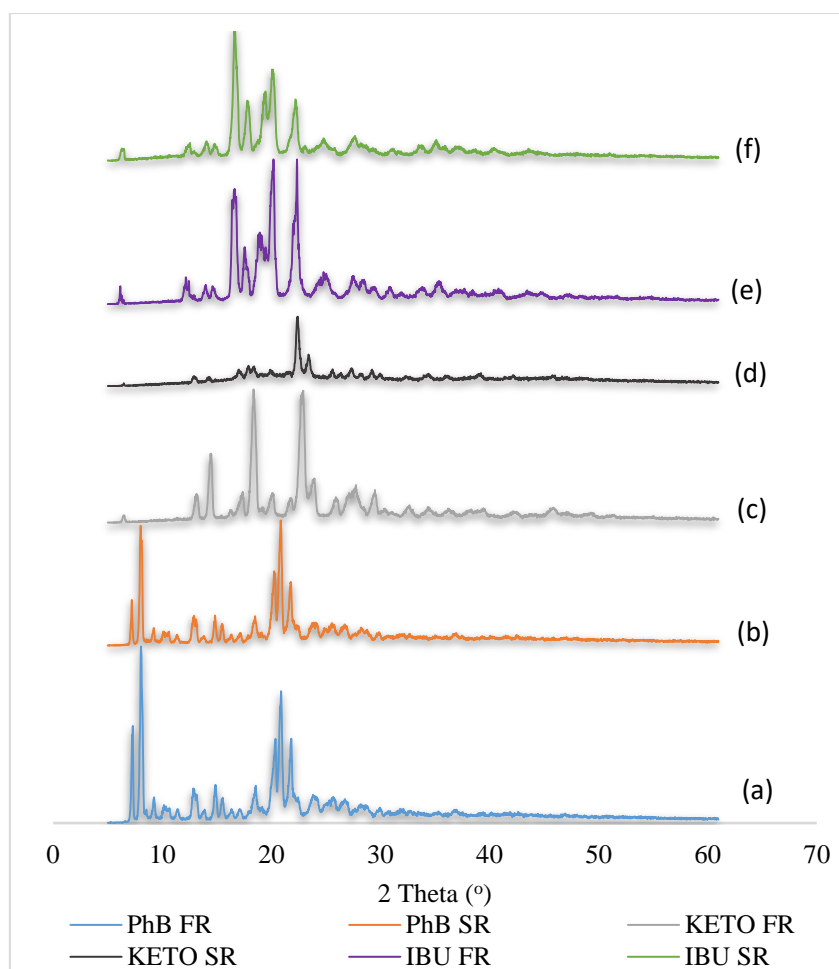


Figure 4. 17. XRD patterns of; (a) phenylbutazone first run (FR), (b) phenylbutazone second (SR), (c) ketoprofen first run (FR), (d) ketoprofen second run (SR), (e) ibuprofen first run (FR) and (f) ibuprofen second run (SR)

Figure 4.18 displays the XRD patterns of naproxen and imipramine. The diffraction pattern of naproxen (FR) was highly crystalline in nature with peaks appearing at  $12.6^\circ$ ,  $16.8^\circ$ ,  $18.8^\circ$  and  $22.5^\circ$  while in the second run, the peaks were still visible confirming the drug crystallinity which fits well with the previously published data for the drug [220]. In the case of imipramine first run (Figure 4.18c), the diffraction patterns were observed at  $12.2^\circ$ ,  $18.0^\circ$ ,  $19.8^\circ$  and  $23.6^\circ$  which confirmed the crystalline structure of the drug as expected based on MWDTA and DSC. The second run (after processing) can be seen in Figure 4.18d where the drug was converted to an amorphous form in contrast to what was observed in MWDTA and DSC discussed earlier. This could possibly be due to the conventional method employed in melting the compound.

Overall, these results are in good agreement with the DSC and MWDTA observations discussed earlier with the exception of the second run of imipramine.

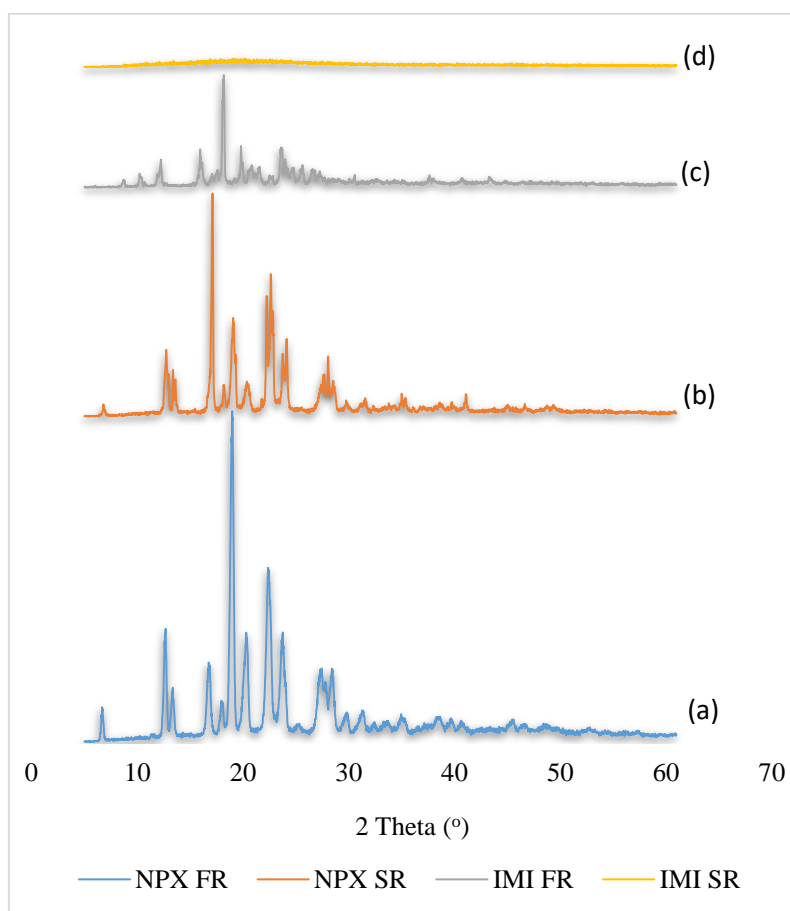


Figure 4. 18. XRD patterns of; (a) naproxen first run (FR), (b) naproxen second (SR), (c) imipramine first run (FR) and (d) imipramine second run (SR)

#### 4.2.4. Hot stage microscopy (HSM) of pharmaceutical compounds

HSM was utilised to follow the transformation of the eight compounds as a function of temperature to visibly observe changes. Optical images and reflected light intensity (RLI) values were recorded and are presented at selected temperatures in Figures 4.19 – 4.26.

Firstly, benzocaine (Figure 4.19) initially appeared as a white crystalline solid and, upon heating, a visible melting event occurred at an appropriate temperature to correspond with that previously seen using MWDTA and DSC. Observations during the analysis revealed a colourless liquid material suggestive of fusion of the drug at 90.2 °C followed by

recrystallisation having a lower temperature during the cooling at 48.1 °C, A gradual decrease in the sample RLI values was observed from 10.7 – 10.5 V, correlating with the gradual change in the sample temperature going from solid to liquid. Below 10.5 V, a slight decrease in the light intensity could be noted upon cooling when the sample began to recrystallise which is matched by a sharp decrease in the temperature profile.

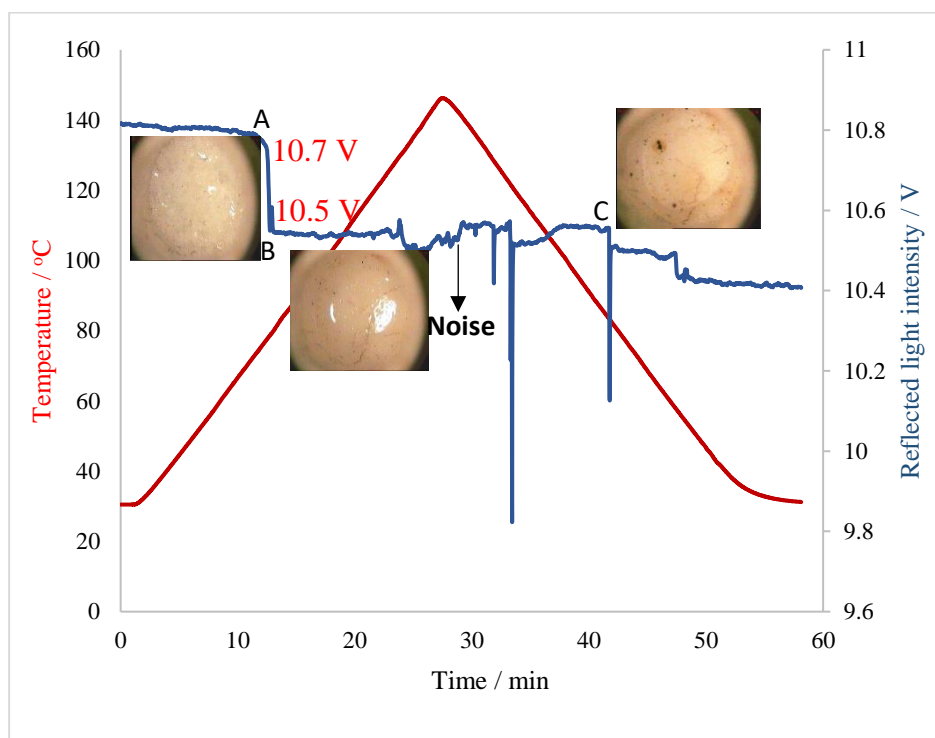


Figure 4. 19. Microscope images and optical data of a sample of benzocaine heated from 30 to 160 °C as a function of temperature

For haloperidol HSM analysis (Figure 4.20) revealed a white powder at 30 °C before the fusion, transforming to a liquid at 149.4 °C followed by recrystallisation at 90 °C during cooling, as expected based on MWDTA and DSC data. The sample decolourises around 200 °C after the fusion process as the sample begins to decompose due to differences between the furnace and sample temperatures. The furnace temperature was greater than the sample temperature as a result, the sample was heated at a faster rate when the analysis was carried out. There was a gradual decrease in the sample RLI values observed up to 7.1 V correlating with the gradual

fusion process. Upon decomposition, no change in RLI values was noted which is matched by the sample temperature.

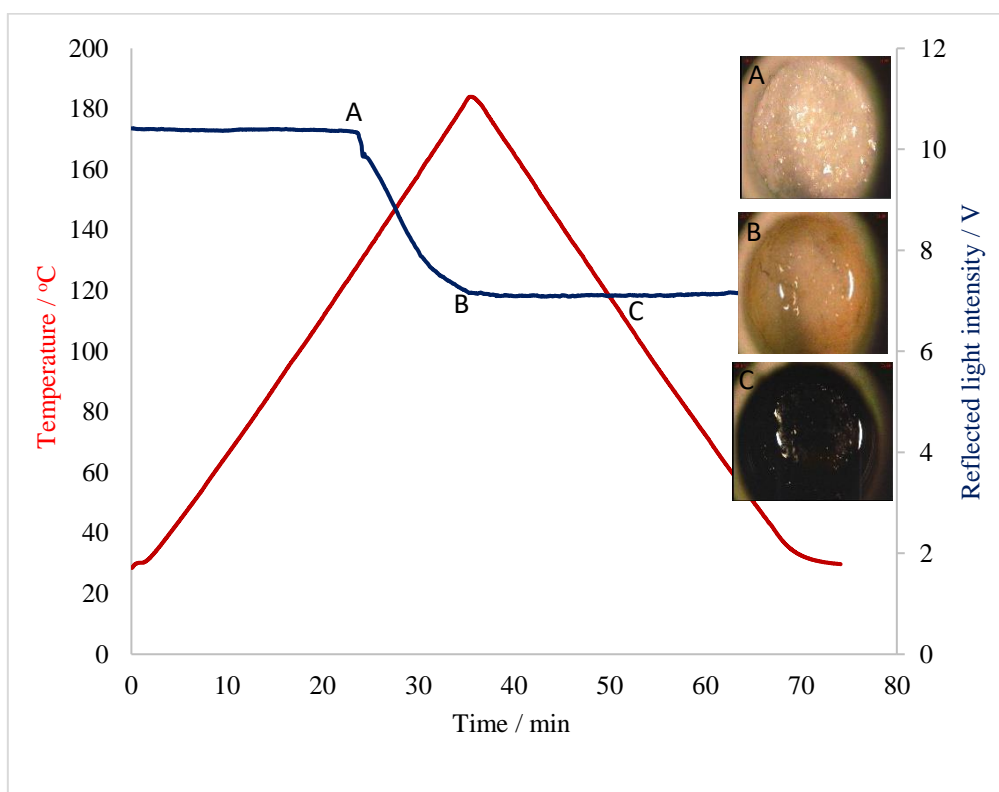


Figure 4. 20. Microscope images and optical data of a sample of haloperidol heated from 30 to 200 °C as a function of temperature

Figure 4.21 displays images of solid indomethacin before the melt at 30 °C then the transformation at 159.1 °C, indicating melting of the compound. Upon subsequent cooling to 30 °C, no transformation occurred as the sample stayed in an amorphous form after the initial phase change, in agreement with the previously presented MWDTA and DSC data. On looking at the RLI values, a gradual decrease could be observed going from solid to liquid from 10.5 to 9.5 V, correlating with the change in colour of the compound, followed by a sharp increase to 10.2 V and then decreased again to 9.9 V during cooling.

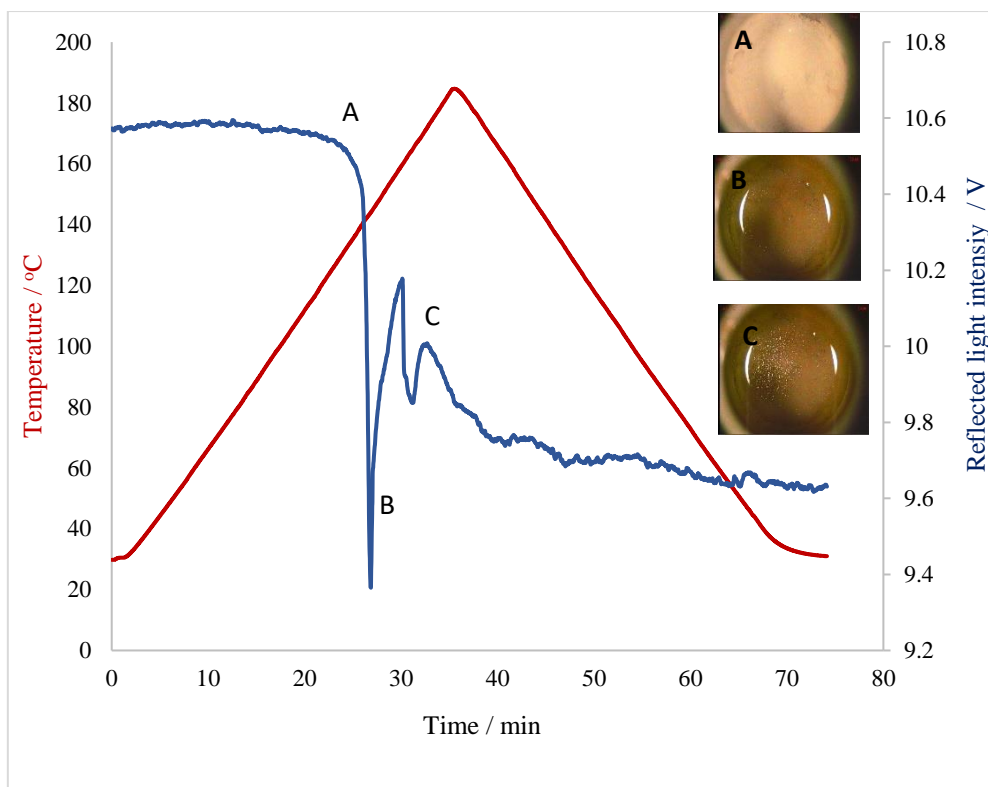


Figure 4. 21. Microscope images and optical data of a sample of indomethacin heated from 30 to 200 °C as a function of temperature

Optical images for phenylbutazone were recorded at 91.3 °C and 109.7 °C (Figure 4.22) and demonstrate that the compound underwent a solid-state transformation that started to occur at 91.3 °C and was complete at ~ 109.7 °C. Upon cooling the sample returned to a glassy form at 30 °C. These findings agree with those found using MWDTA and DSC analysis. From the optical data, a gradual decrease was observed for the compound from 10.4 to 9.8 V going from solid to liquid correlating with the phase transformation.

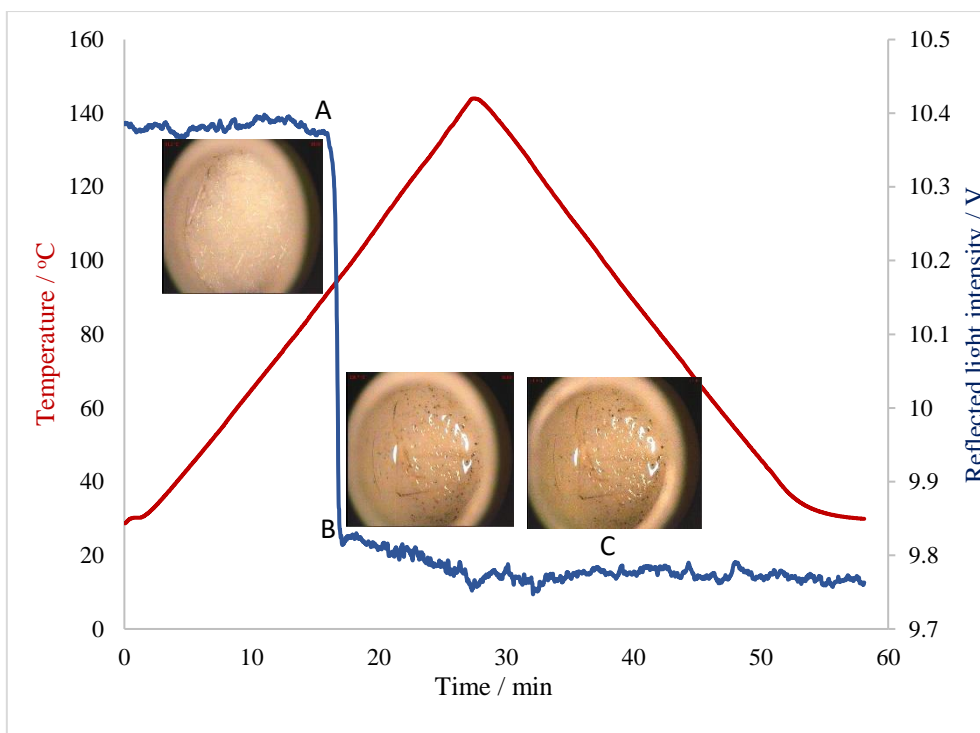


Figure 4. 22. Microscope images and optical data of a sample of phenylbutazone heated from 30 to 160 °C as a function of temperature

Figure 4.23 displays optical images of solid ketoprofen at 78.3 °C, upon melting at 96.7 °C and upon cooling to 30 °C. No observable transformation occurred after the initial melting, in agreement with findings previously presented using MWDTA and DSC. The optical data shows a gradual decrease of RLI values of the compound from 10.5 to 9.4 V going from solid to liquid, almost similar to what was observed in the case of phenylbutazone, correlating with the phase transformation.

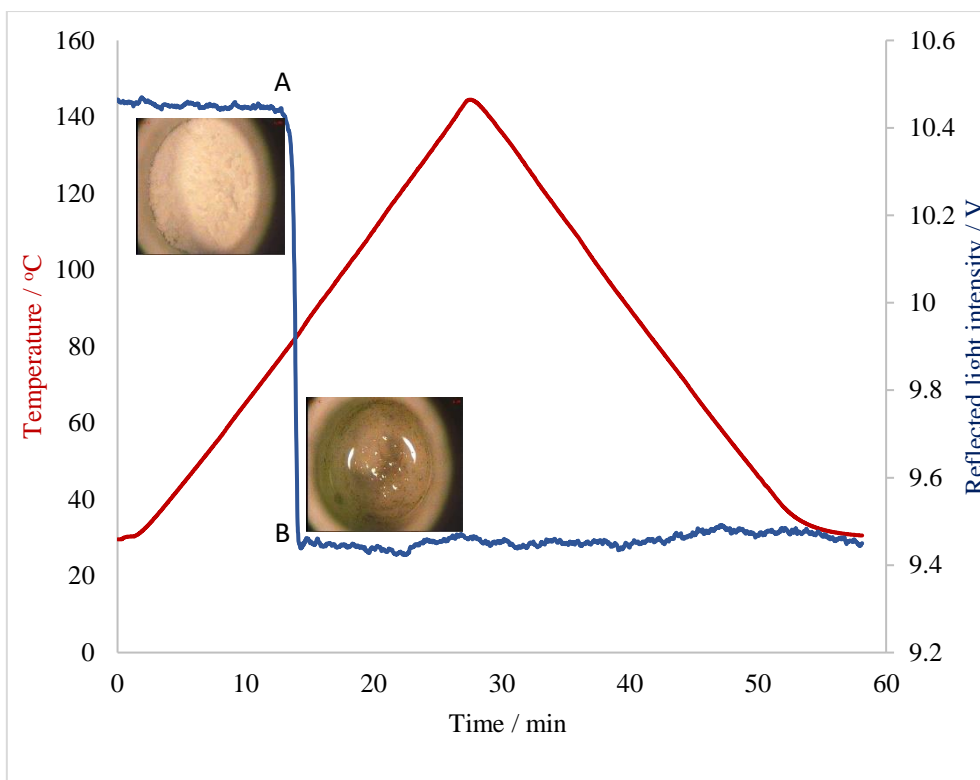


Figure 4. 23. Microscope images and optical data of a sample of ketoprofen heated from 30 to 160 °C as a function of temperature

Figure 4.24 displays images of the white powdered ibuprofen before the melt at 65.4 °C and upon melting at 78.5 °C. On cooling to 30 °C, no visible transformation occurred, in agreement with data evidenced from MWDTA and DSC analysis. The optical data shows a gradual decrease of RLI values of the compound from 10.2 to 9.2 V going from solid to liquid, correlating with the phase transformation.

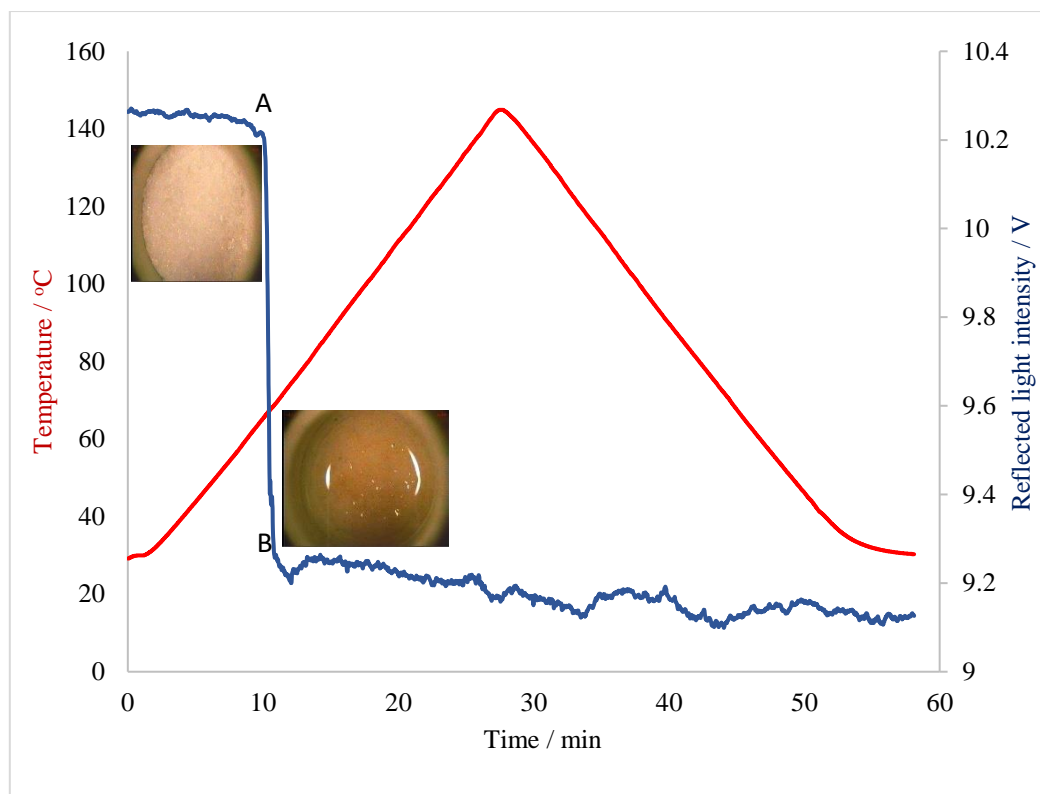


Figure 4. 24. Microscope images and optical data of a sample of ibuprofen heated from 30 to 160 °C as a function of temperature

Naproxen (Figure 4.25) initially appeared as a white crystalline solid and, upon heating, a visible melting event occurred at an appropriate temperature to correspond with that previously seen using MWDTA and DSC. Observations during analysis revealed a colourless liquid material suggestive of fusion of the drug at  $\sim 152.7$  °C followed by recrystallisation at a lower temperature during cooling at 109.6 °C. A gradual decrease in the sample RLI values was observed from 9.7 – 9.0 V, correlating with the gradual change in the sample temperature going from solid to liquid. Below 8.4 V, a slight decrease in the light intensity could be noted upon cooling when the sample began to recrystallise which is matched by a sharp decrease in the temperature profile.



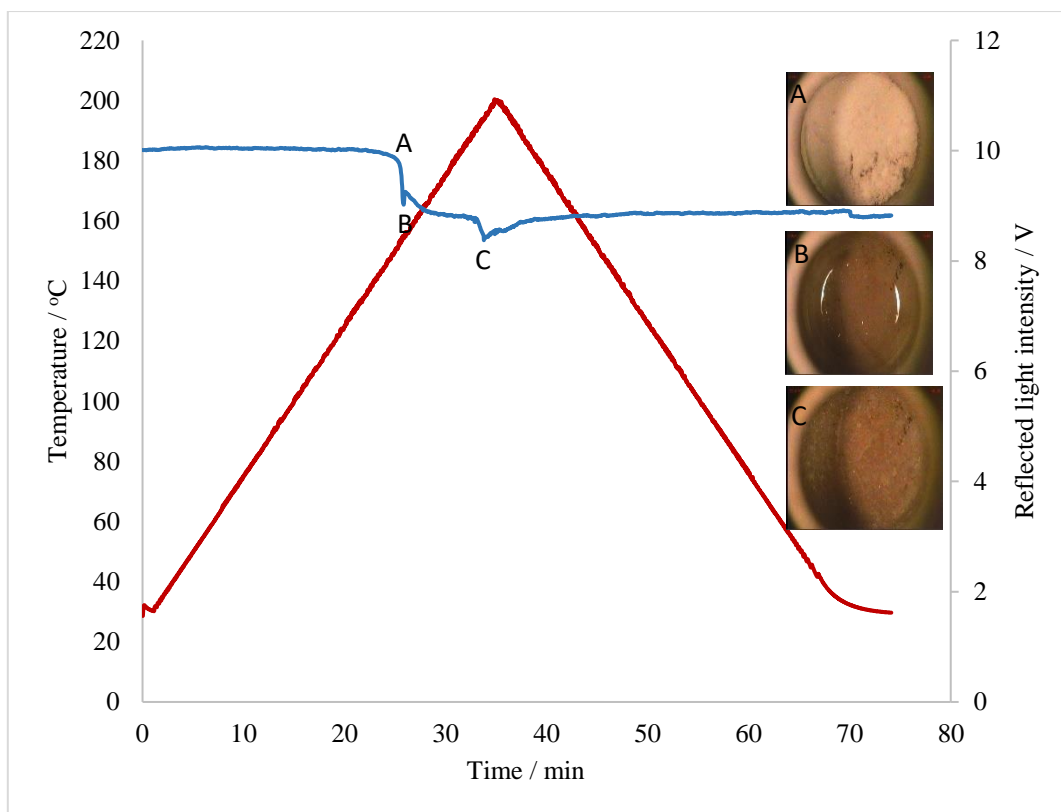


Figure 4. 25. Microscope images and optical data of a sample of naproxen heated from 30 to 200 °C as a function of temperature

Finally, imipramine (Figure 4.26) initially appeared as a white crystalline solid and upon heating, a visible melting event occurred at an appropriate temperature to correspond with that previously seen using MWDTA and DSC. Observations during analysis revealed a colourless liquid material suggestive of fusion of the drug at 170.7 °C without any recrystallisation during the cooling. Above 180 °C, the sample decomposed which is matched by the changes in colour of the sample. A gradual decrease in the sample RLI values was observed from 9.7 – 7.9 V, correlating with the gradual change in the sample temperature going from solid to liquid. A slight decrease in the light intensity was also noted at around 6.6 V, which occurred as the sample decomposed correlating with the images observed.

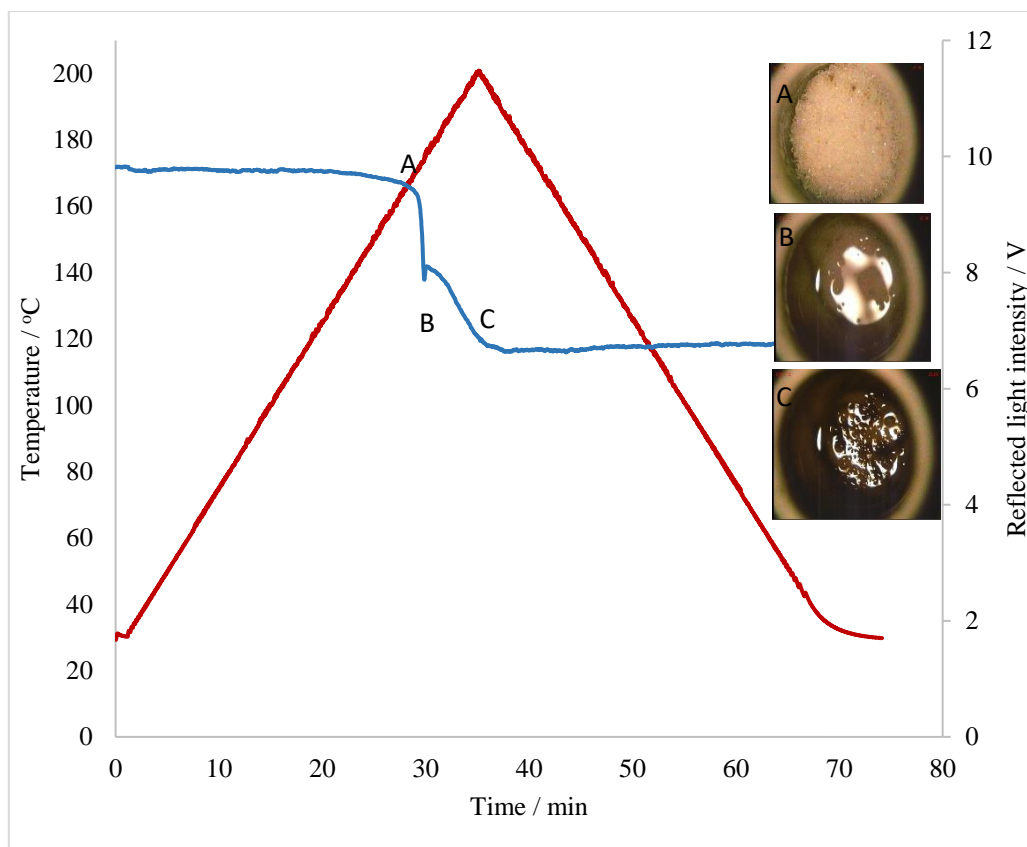


Figure 4. 26. Microscope images and optical data of a sample of imipramine heated from 30 to 200 °C as a function of temperature

### 4.3. MWDTA of excipients

Following on from analysis into eight pharmaceutical compounds, four excipients were selected for further investigations using MWDTA namely; D-mannitol, stearic acid, beta cyclodextrin and Syloid XDP 3050. Firstly, D-mannitol was analysed, as shown by  $\Delta T$  as a function of temperature in Figure 4.27.

The MWDTA profile of D-man is shown in Figure 4.27 in the form of calculated  $\Delta T$  ( $T_{\text{sample}} - T_{\text{reference}}$ ) as a function of sample temperature. In the first run of the compound, the endothermic fusion has an onset temperature of 163.8 °C, followed by a small rise in  $\Delta T$  indicating an increase in  $\tan \delta$  going from solid to liquid as the sample melted, while the corresponding decrease in  $\tan \delta$  on recrystallisation upon cooling has a slightly lower onset of 116.6 °C.

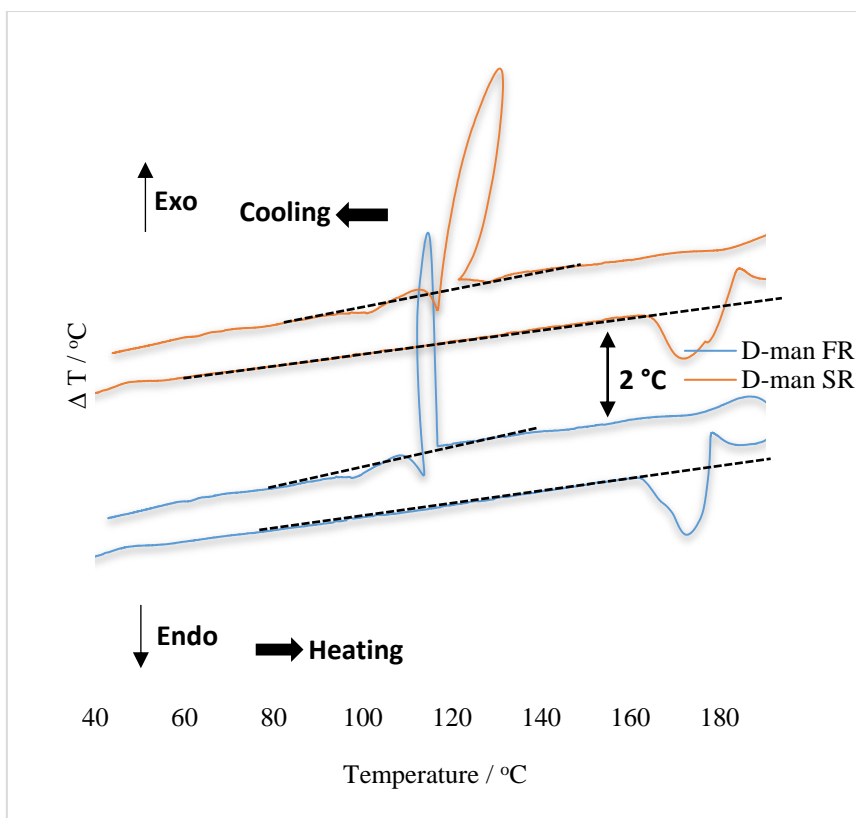


Figure 4.27. Microwave differential thermal analysis (MWDTA) of D-mannitol heated at 5 °C/min to 200 °C for the first and second run (FR and SR) and cooling at 5 °C/min to 40 °C in both cases.

A broad endothermic transition was observed in the second run of the same sample at 165.7 °C corresponding to fusion followed by a rise in  $\Delta T$  after the transition while upon cooling, exothermic recrystallisation of 124.9 °C was recorded which is consistent with the DSC and HSM data discussed later.

For stearic acid in Figure 4.28, the first profile results for the first run display a broad exothermic fusion with an onset temperature of 70.1 °C without any change in baseline or  $\Delta T$  after the transition possibly due to the compound having lower  $\tan \delta$  compared with D-mannitol. Upon cooling, the exothermic recrystallisation was recorded at 61.0 °C.

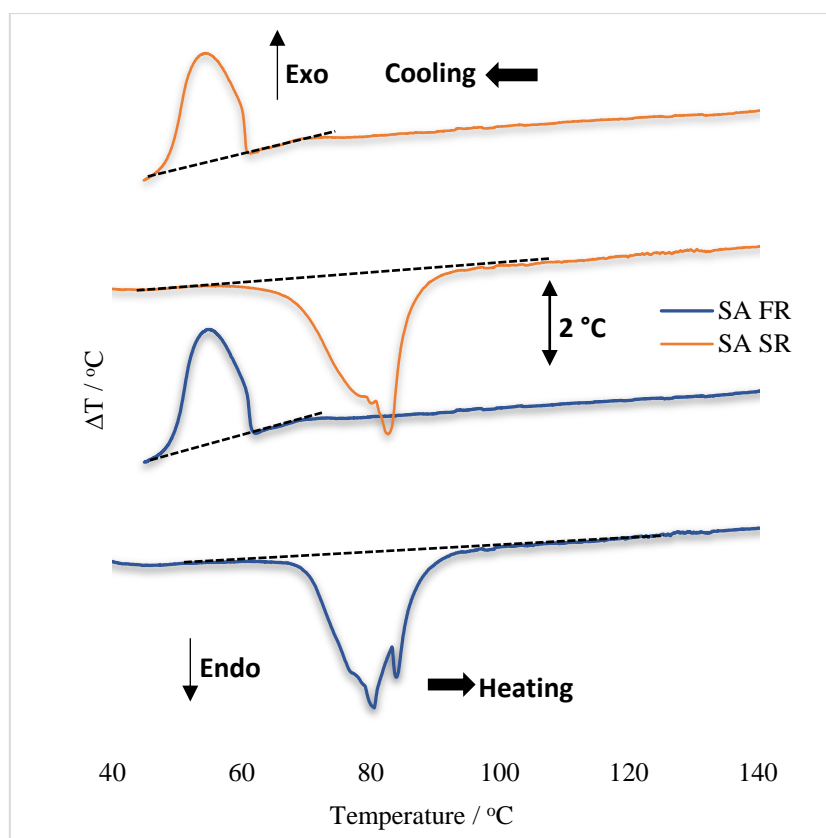


Figure 4.28. Microwave differential thermal analysis (MWDTA) of stearic acid heated at 5 °C/min to 160 °C for the first and second run (FR and SR) and cooling at 5 °C/min to 40 °C in both cases.

The second cycle of the excipients was characterised by a transition at 66.6 °C, and upon the second cooling exothermic recrystallisation was recorded at 66.5 °C further justifying the sample was still in a crystalline state after the second run.

Figure 4.29 displays a broad transition with an extrapolated onset of 100.0 °C to 140 °C, corresponding to dehydration of beta cyclodextrin. The exothermic fusion shows that the water is released in vapor form as expected and the peak extended to a higher temperature. Upon subsequent cooling, no significant phase transition was observed, as the sample did not recrystallise. No significant phase changes were observed in the second run further justifying the theory that the sample remained in an amorphous form.

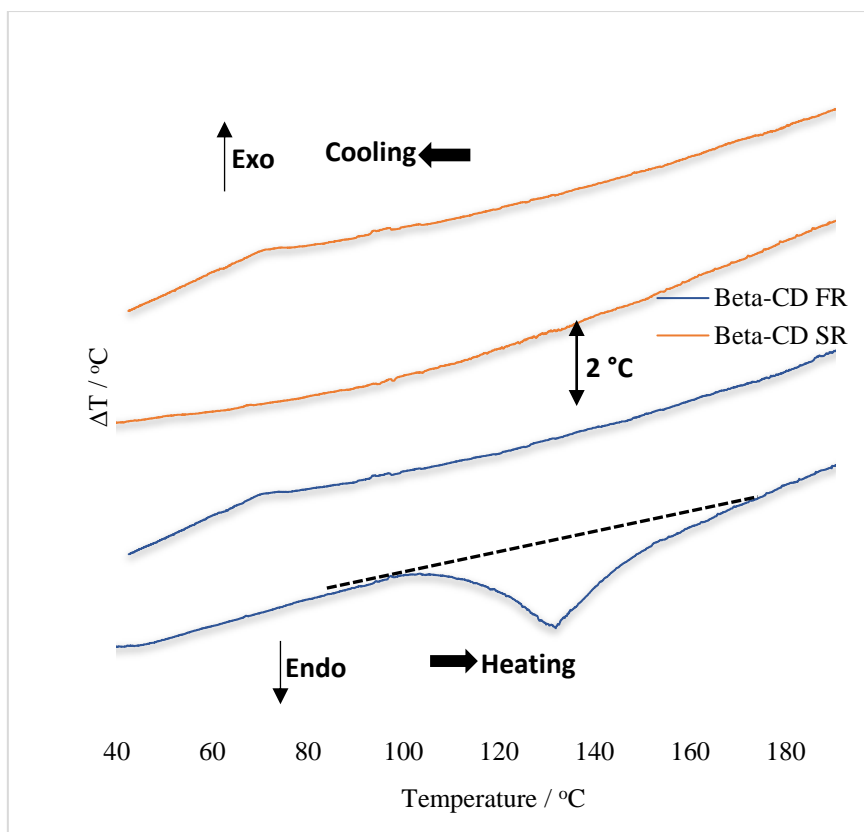


Figure 4.29. Microwave differential thermal analysis (MWDTA) of beta cyclodextrin heated at 5 °C/ min to 200 °C for the first and second run (FR and SR) and cooling at 5 °C/min to 40 °C in both cases.

Finally, Figure 4.30 displays the heating and cooling of XDP 3050, no significant phase transition was observed in the first and second run both upon heating and cooling due to the higher melting temperature of the excipient which further justifies the amorphous nature of the silica. These findings fit well with the results of DSC, XRD and HSM to be discussed later.

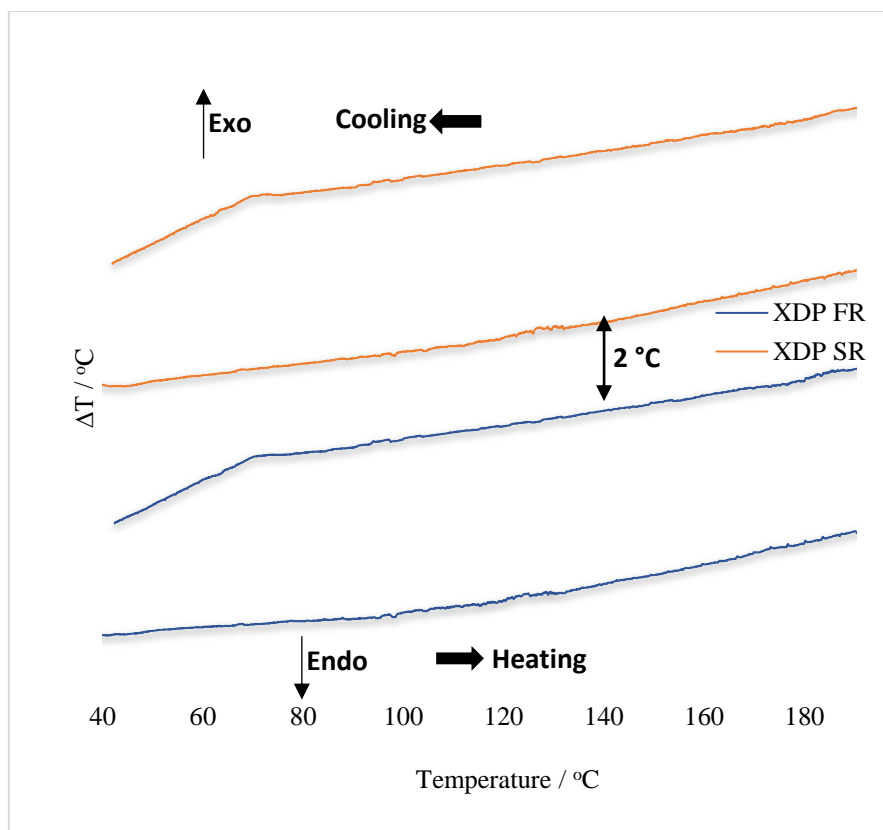


Figure 4.30. Microwave differential thermal analysis (MWDTA) of syloid XDP 3050 heated at 5 °C/ min to 200 °C for the first and second run (FR and SR) and cooling at 5 °C/min to 40 °C in both cases.

#### 4.3.1. DSC for excipients

Comparable DSC profiles for the fusion and recrystallisation of the excipients in aluminum pans heated at 10 °C/min to a maximum of 200 °C and then cooled at 10 °C/min to 25 °C are shown in Figures 4.31 – 4.32. The endothermic fusion of D-mannitol (Figure 4.31a) in the first run has an onset temperature of 166.5 °C while the corresponding exothermic recrystallisation of the compound has a slightly lower onset of 114.6 °C. The second run of the same sample did not reveal many changes other than a decreased intensity in the melting peak with a slight shift in the recrystallisation peak, possibly due to heating-cooling and reheating processes. The first run of stearic acid in Figure 4.31c, shows an endothermic fusion at 70.1 °C followed by a broad exothermic recrystallisation at 61.2 °C. The second run did not reveal any changes, all the phase transformations observed in the first run were also observed in the second run.

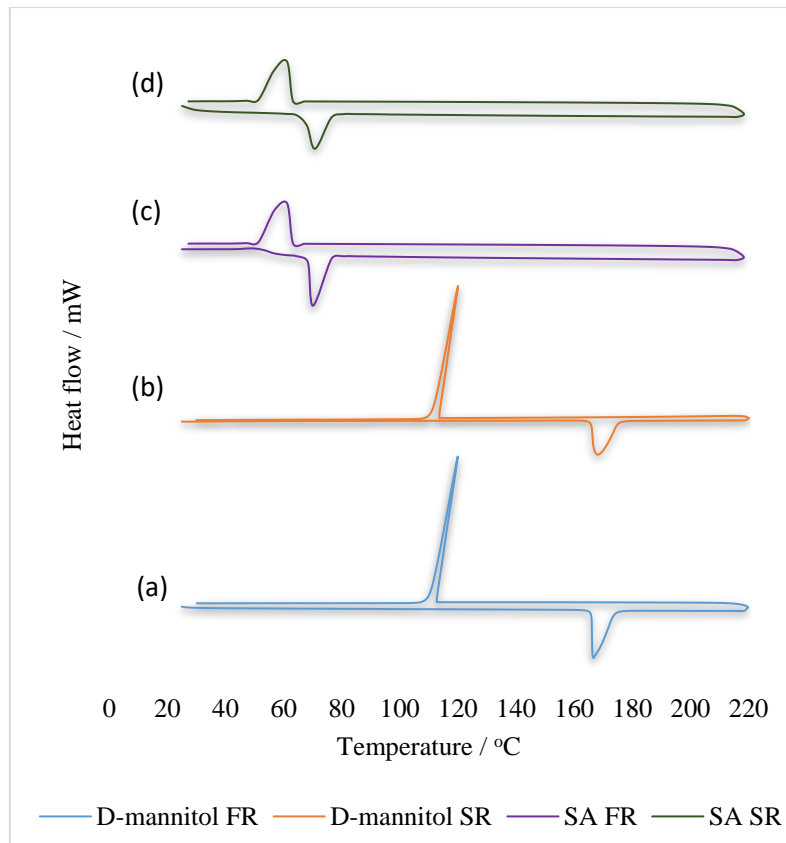


Figure 4.31. DSC thermograms of; (a) D-mannitol first run (FR), (b) D-mannitol second (SR), (c) stearic acid first run (FR), (d) stearic acid second run (SR)

The DSC profile for beta-cyclodextrin (Figure 4.32a) was characterised by a broad endothermic peak around 90 – 140 °C corresponding to dehydration while upon cooling no event was recorded as the sample doesn't recrystallise. The second run did not reveal any additional event as expected. For XDP 3050 in Figure 4.32c, no event was observed both in the first and second run due to the higher melting point of the silica. These findings agree with what was observed earlier in MWDTA for these excipients.

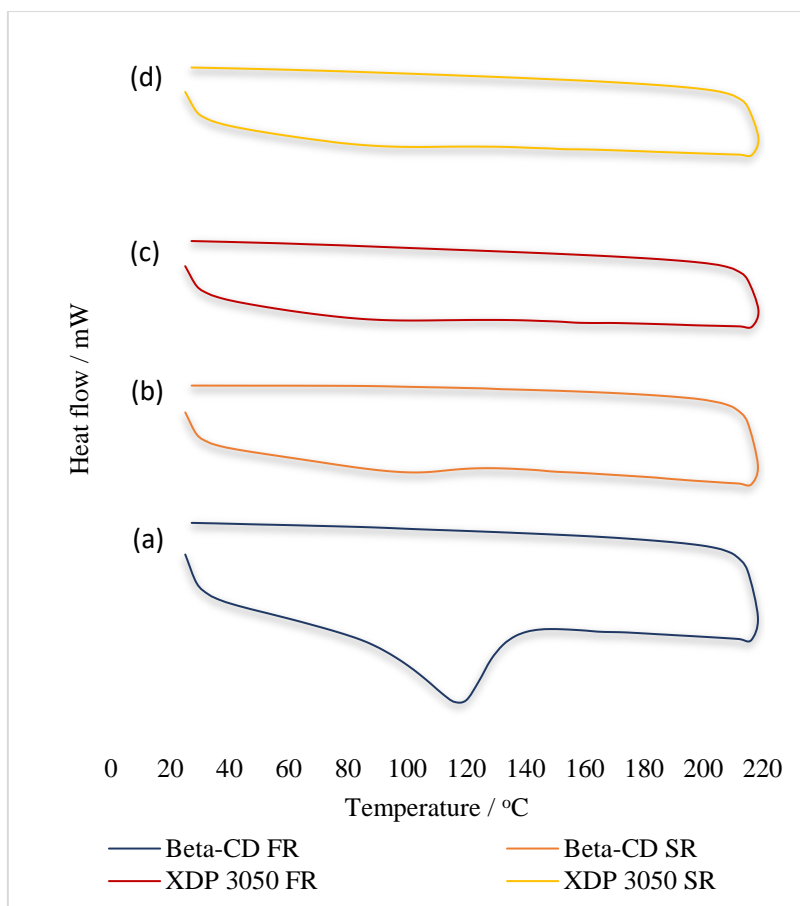


Figure 4.32. DSC thermograms of; (a) beta-cyclodextrin first run (FR), (b) beta-cyclodextrin second (SR), (c) XDP 3050 first run (FR), (d) XDP 3050 second run (SR)

#### 4.3.3. XRD for excipients

To follow the results of DSC, XRD was employed to confirm the crystalline or amorphous nature of the excipients. The characteristic diffraction peaks observed at  $10.7^\circ$ ,  $14.9^\circ$ ,  $18.9^\circ$ ,  $21.1^\circ$  and  $23.6^\circ$  correspond to the powder diffraction pattern for the first run of D-mannitol (Figure 4.33a) while in the second, the diffraction patterns were still observed but with reduced intensity attributed to loss of some crystalline structure of the D-mannitol after the first run of the same sample and is consistent with what was observed in DSC analysis. The first run of stearic acid (Figure 4.33c) was characterised by diffraction peaks appearing at  $10.2^\circ$ ,  $14.3^\circ$ ,  $24.0^\circ$ ,  $36.9^\circ$  and  $41.1^\circ$  confirming the crystalline structure while the second run was characterised by less intense diffraction patterns indicating a loss of some crystalline structure



after the first run of the same sample, consistent with the broadened peak observed in previous DSC analysis.

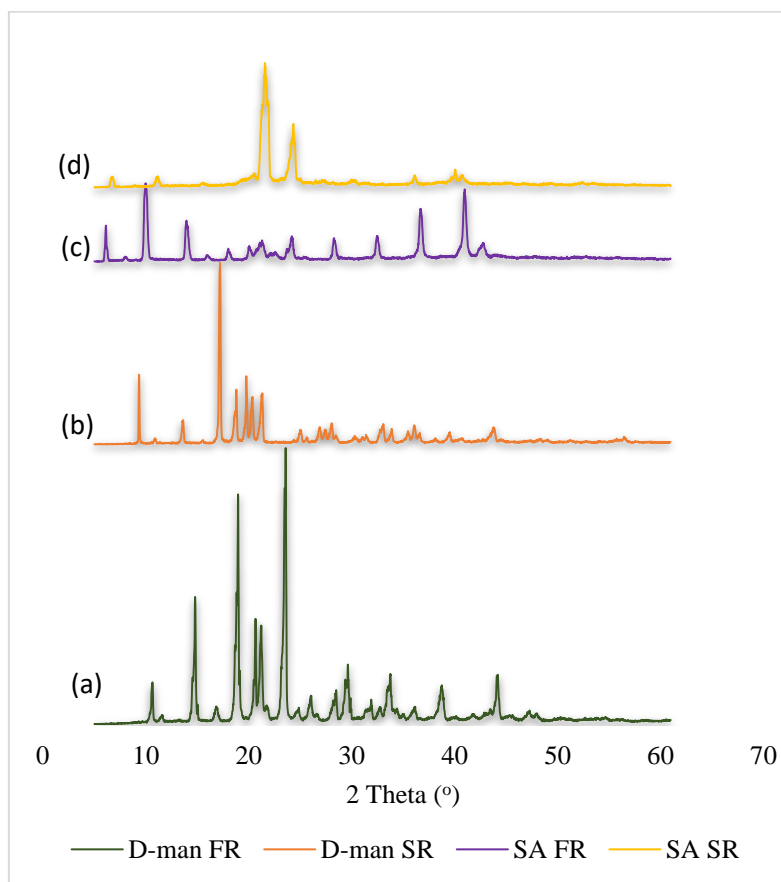


Figure 4.33. XRD patterns of; (a) D-mannitol first run (FR), (b) D-mannitol second run (SR), (c) stearic acid first run (FR) and (d) stearic acid second run (SR)

The XRD patterns of beta-cyclodextrin (FR and SR) and XDP 3050 (FR and SR) are illustrated in Figure 4.34. Beta-CD could be seen in Figure 4.34(a) with sharp diffraction peaks at 10.7°, 12.5°, 17.1° and 22.9° in agreement with previous data for the drug. Beta-CD peaks are still evident in the second run with reduced intensity attributed to the loss of some crystalline structure after the first run of the same sample, confirming the partial amorphous nature. The absence of diffraction patterns in XDP 3050 for the first and second run confirm their amorphous nature which fits in well with the results of MWDTA and DSC.

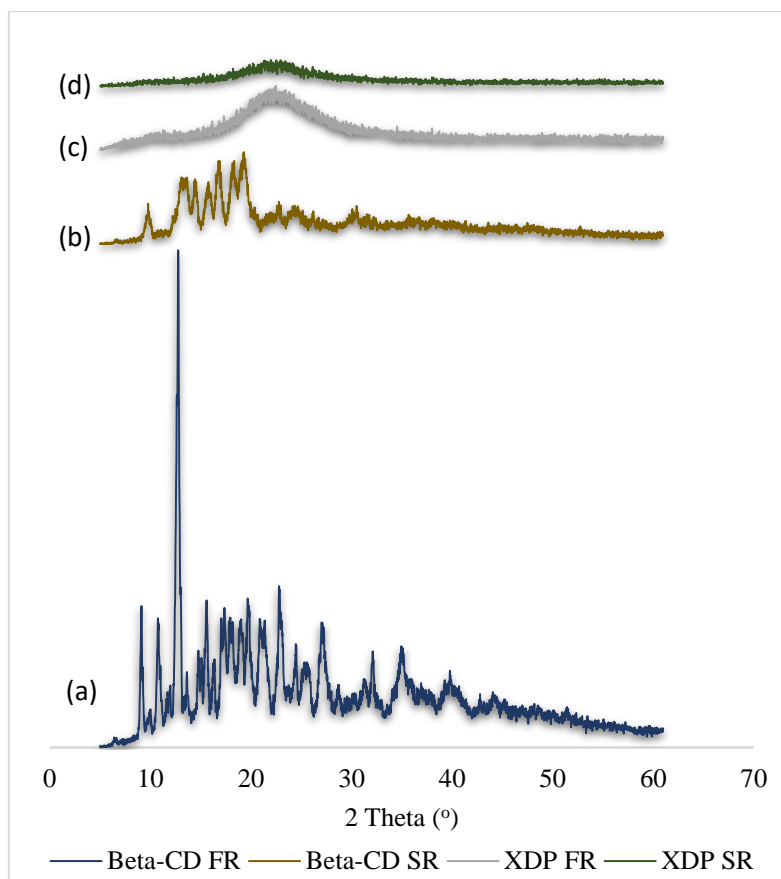


Figure 4.34. XRD patterns of; (a) beta-cyclodextrin first run (FR), (b) beta-cyclodextrin second run (SR), (c) XDP 3050 first run (FR) and (d) XDP 3050 second run (SR)

#### 4.3.4. HSM for excipients

HSM was used to follow the transformation of the four excipients as a function of temperature to visibly observe changes. Firstly, D-mannitol (Figure 4.35) appeared as a white crystalline solid at 30 °C, and upon heating a visible melting of the compound started to occur at around 155 °C, transforming to liquid at 165 °C followed by recrystallisation at 113 °C during cooling, as expected based on data obtained using MWDTA and DSC. For stearic acid (Figure 4.36), HSM revealed a white crystalline powder at 40 °C and complete transformation to liquid at 69 °C. These findings match those seen in the previously presented MWDTA and DSC data with recrystallisation upon cooling at 30 °C.

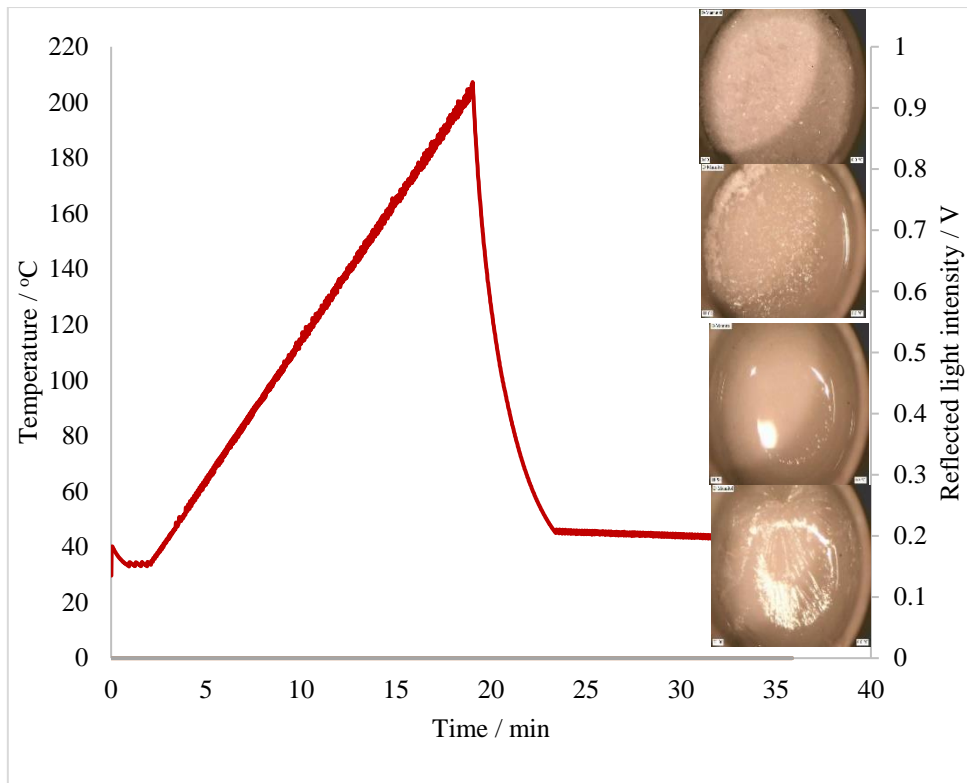


Figure 4.35. Microscope images and optical data of a sample of D-mannitol heated from 30 to 200 °C as a function of temperature

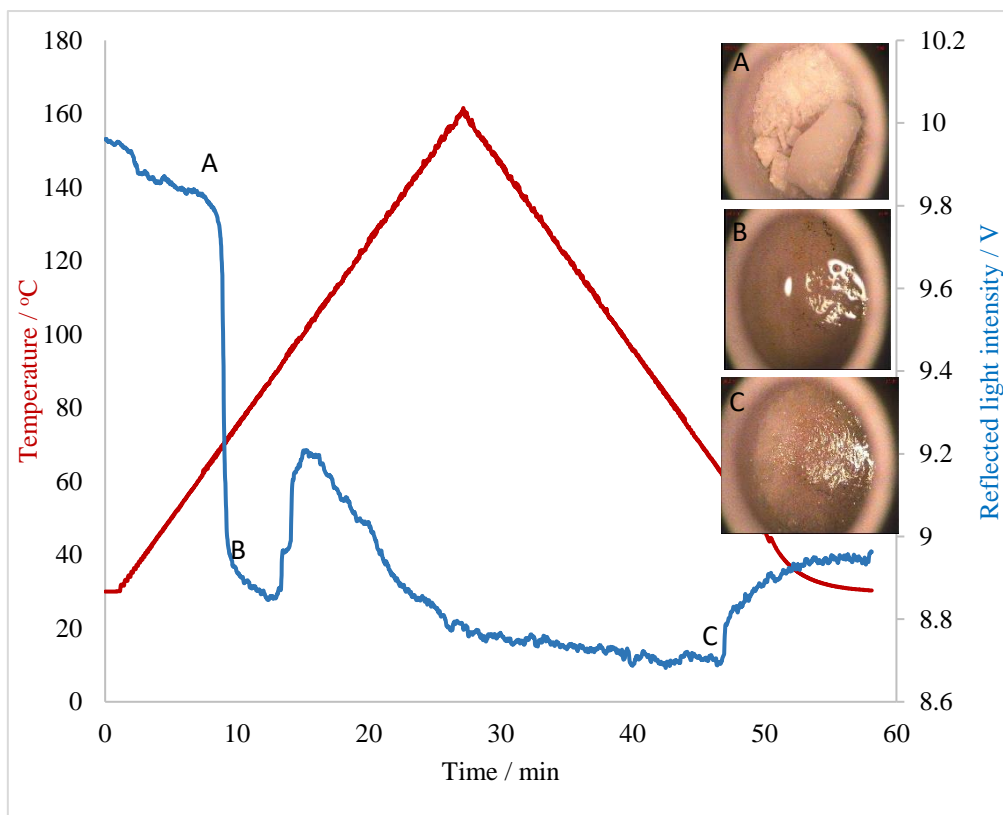


Figure 4.36. Microscope images and optical data of a sample of stearic acid heated from 30 to 160 °C as a function of temperature

HSM images for beta-cyclodextrin (Figure 4.37) and XDP 3050 (Figure 4.38) are hard to distinguish and did not appear to show any transformation during heating and cooling due to the higher melting points of the compounds.

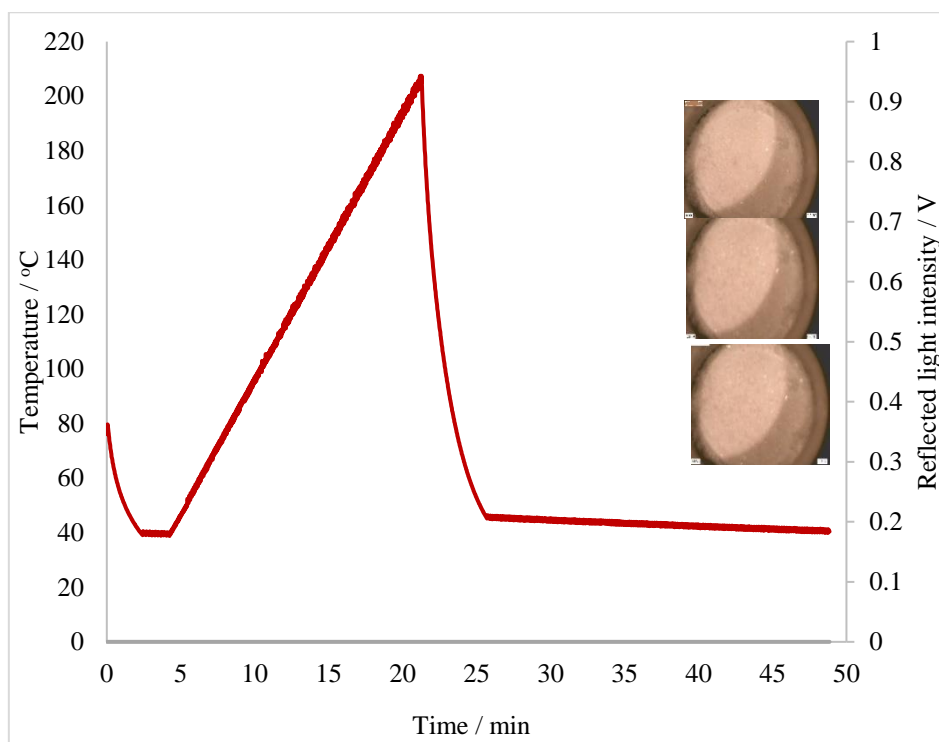


Figure 4.37. Microscope images and optical data of a sample of beta-cyclodextrin heated from 30 to 200 °C as a function of temperature

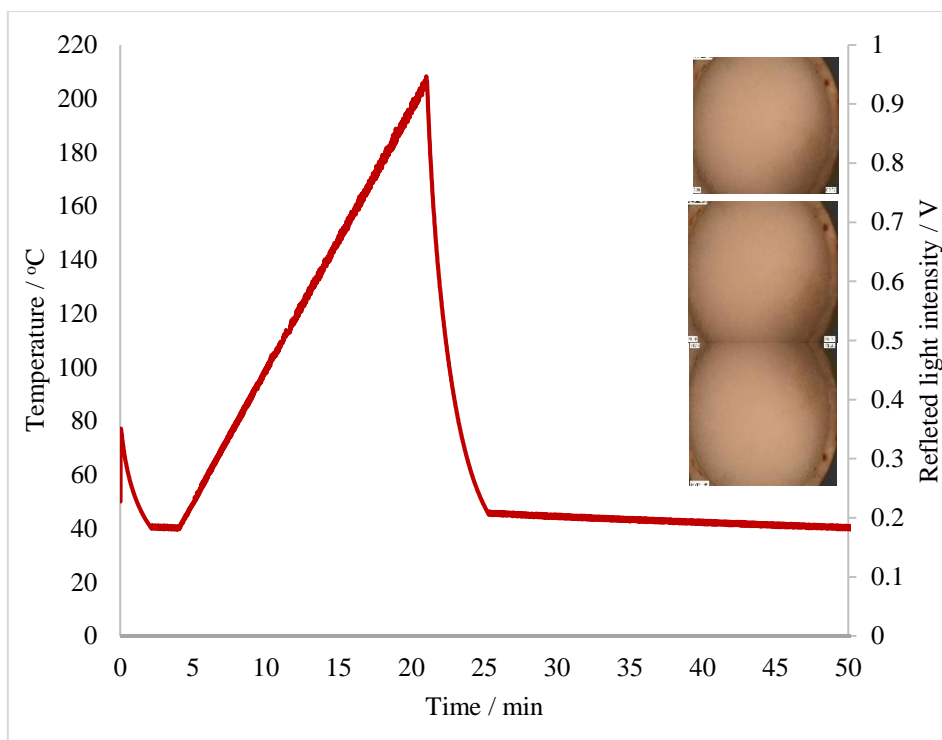


Figure 4.38. Microscope images and optical data of a sample of XDP 3050 heated from 30 to 200 °C as a function of temperature

#### 4.4. MWDTA of benzocaine and pharmaceutical excipients

Benzocaine was selected from the eight model compounds for further analysis in the presence of a selection of four pharmaceutical excipients, namely beta-cyclodextrin, D-mannitol, stearic acid and Syloid<sup>®</sup> silica (XDP 3050). Firstly, microwave thermal analysis of benzocaine with Syloid<sup>®</sup> silica, physically mixed at a 1:1 ratio was considered, and the resultant profile is shown in Figure 4.39.

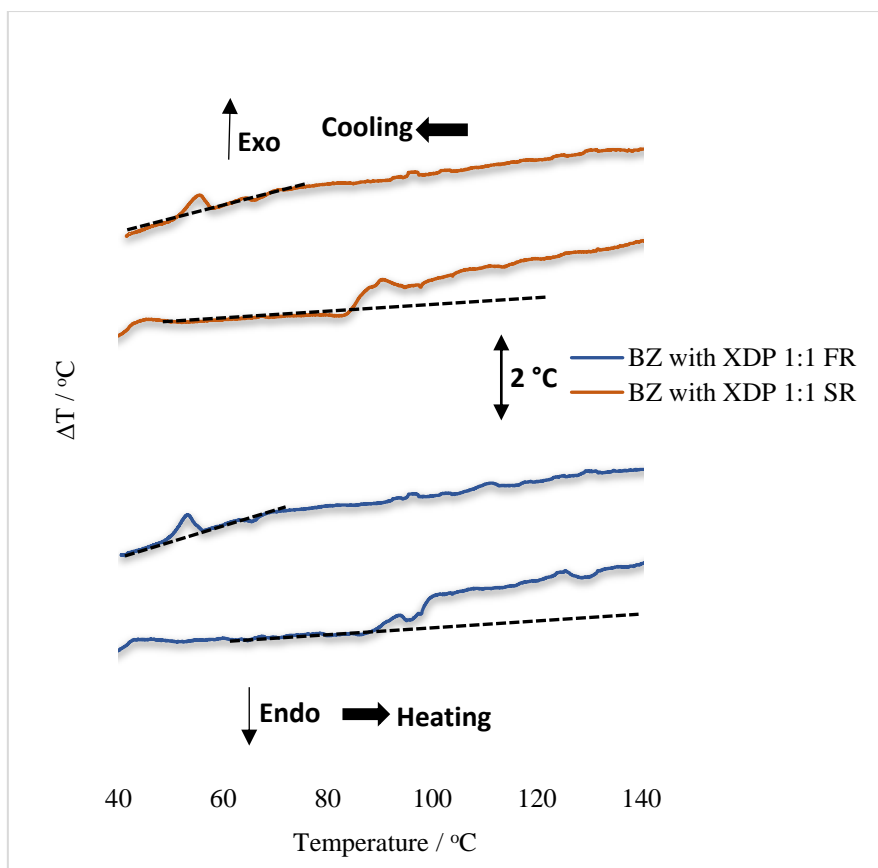


Figure 4.39. Microwave differential thermal analysis (MWDTA) of benzocaine (BZ) with Syloid<sup>®</sup> silica (XDP) heated at 5 °C min<sup>-1</sup> to 160 °C for both the first (FR) and second (SR) run, cooled in both cases to 40 °C

Figure 4.39 reveals a change in the baseline as the sample coupled more strongly with the microwave energy after the thermal transition of benzocaine at 88.3 °C, indicating a change in dielectric coupling. Compared with pure benzocaine (Figure 4.3), a reduction in the melting peak was observed, possibly indicating some loss of crystalline structure resulting from microwave energy interaction with the sample. Furthermore, this finding was interpreted as proof of some interaction between the drug and the XDP with recrystallisation observed upon cooling at 54.0 °C within the first heating-cooling cycle. In the second cycle, there was a slight shift to a lower temperature with transition occurring at 83.5 °C corresponding to an  $\alpha$ -polymorph of the drug in agreement with the studies conducted by Gana et al. [225] followed by a change in dielectric occurring from 82.7 – 91.6 °C and recrystallisation occurring at 56.3

°C. Secondly, MWDTA was undertaken for benzocaine formulated with  $\beta$ -cyclodextrin (beta-CD), as presented in Figure 4.40.

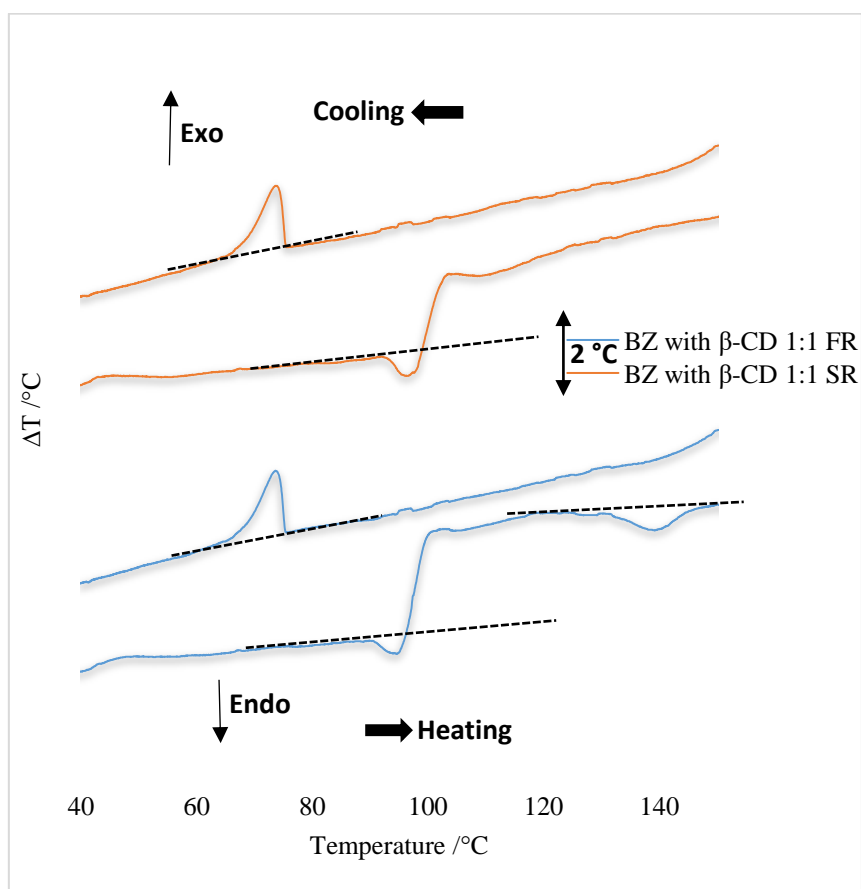


Figure 4.40. Microwave differential thermal analysis (MWDTA) of benzocaine (BZ) with  $\beta$ -cyclodextrin (beta-CD) heated at  $5\text{ }^\circ\text{C min}^{-1}$  to  $160\text{ }^\circ\text{C}$  for both the first (FR) and second (SR) run, cooled in both cases to  $40\text{ }^\circ\text{C}$ .

Fusion of benzocaine in  $\beta$ -cyclodextrin for the first heating cycle occurred at  $91.2\text{ }^\circ\text{C}$  with a large dielectric change after the transition suggesting that the sample then coupled more strongly. Dehydration of the  $\beta$ -CD occurred in the region of  $125.2\text{--}145.9\text{ }^\circ\text{C}$ . This is consistent with previous research where loss of solvation water from the  $\beta$ -CD cavity occurred at  $140\text{ }^\circ\text{C}$  [214]. This event appeared  $40\text{ }^\circ\text{C}$  higher than the standard boiling point of water, which indicated that water molecules are tightly held within the crystal lattice structure as a result of intermolecular forces such as hydrogen bonding and therefore, additional energy was required to overcome these forces [226]. Upon cooling, recrystallisation occurred at  $74.5\text{ }^\circ\text{C}$ . Data for the second cycle displayed an increase in  $\tan \delta$  after the transition with the melting peak

occurring at 92.3 °C, recrystallisation at 74.3 °C and no dehydration peak. Observations of the samples post-analysis revealed a white coloured material possibly suggestive of the absence of decomposition after both cycles.

Thirdly, MWDTA was undertaken for benzocaine formulated with stearic acid (SA), as presented in Figure 4.41

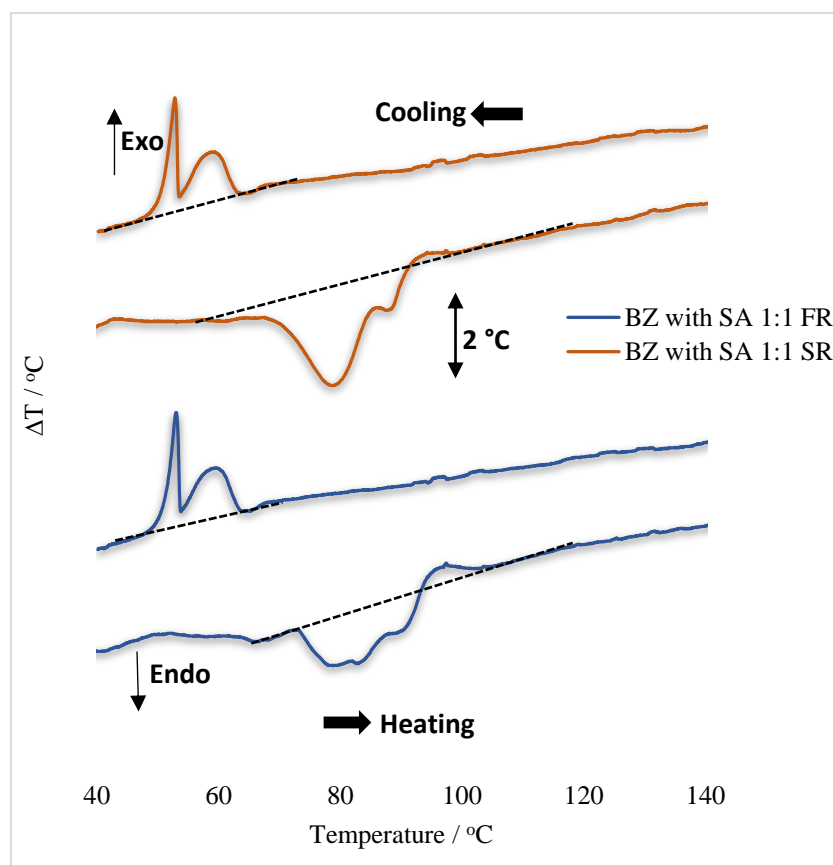


Figure 4.41. Microwave differential thermal analysis (MWDTA) of benzocaine (BZ) with stearic acid (SA) heated at 5 °C min<sup>-1</sup> to 160 °C for both the first (FR) and second (SR) run, cooled in both cases to 40 °C.

MWDTA (Figure 4.41) of benzocaine formulated with stearic acid was somewhat complex with two transitions occurring during the first heating cycle at 79.0 °C and 90.4 °C. It was assumed that the first transition corresponds to the melting of the stearic acid and the latter for benzocaine with two corresponding recrystallisation events upon cooling at 60.8 °C and 53.2 °C. There was a dielectric change after the transition yet little (or no) interaction between the two compounds had occurred. In the second heating and cooling cycle a sharp endothermic



peak was observed at 79.1 °C and another at 87.8 °C then upon cooling at 60.6 °C and 53.0 °C, i.e. somewhat similar to those temperatures observed during the first cycle.

Finally, benzocaine was analysed after formulation with D-mannitol, as shown in Figure 4.42

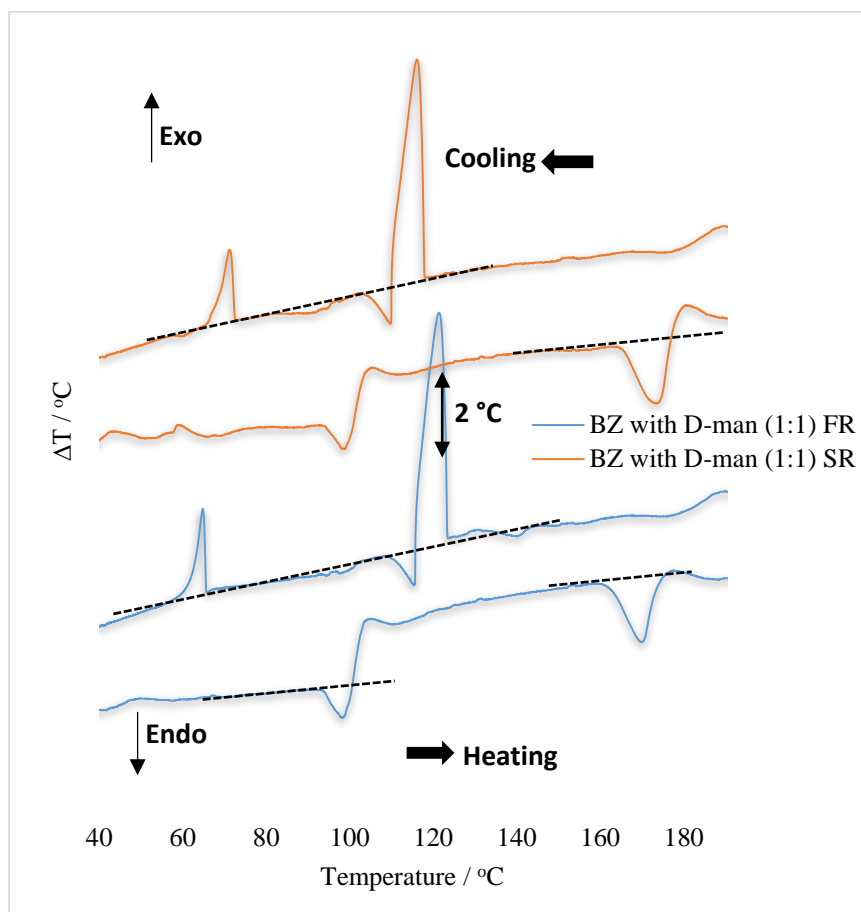


Figure 4.42. Microwave differential thermal analysis (MWDTA) of benzocaine (BZ) with D-mannitol (D-man) heated at 5 °C min<sup>-1</sup> to 200 °C for both the first (FR) and second (SR) run then cooled in both cases to 40 °C

MWDTA of benzocaine displayed a transition peak at 92.7 °C with a dielectric change occurring after the transition, suggesting the sample was heating more effectively after the transition. The event observed at 169.2 °C was deemed to be fusion of D-mannitol. Recrystallisation appeared to occur at 121.9 °C, with a high intensity peak and another with reduced intensity at 64.7 °C, corresponding to that of benzocaine. The second cycle displayed an endothermic transition at 95.6 °C followed by a dielectric change and a second transition at 166.0 °C, i.e. similar to values observed within the first heating and cooling cycle. Upon a

second cooling, recrystallisation was evident at slightly different temperatures compared with the first cycle, namely at 116.6 °C and at 71.5 °C.

#### 4.4.1. DSC of benzocaine and pharmaceutical excipients

Formulations of benzocaine with the four excipients under investigation were analysed using DSC, a data with peak values are displayed in Table 4.2.

Table 4. 2: A summary of DSC peak values for the melting ( $T_m$ ) and recrystallisation ( $T_r$ ) of benzocaine with four excipients.

Material (1:1)	$T_m$ / °C		$T_r$ / °C	
BZ with XDP	83.8 and 92.0	-	46.5	-
BZ with $\beta$ -CD	91.5	-	63.1	-
BZ with D-man	92.4	166.4	74.1	109.5
BZ with SA	84.6	69.9	57.9	54.9

Benzocaine is a crystalline drug undergoing fusion at 90.71 °C as reported in literature [214]. When benzocaine was formulated with Syloid<sup>®</sup> silica XDP 3050, two transitions were observed at 83.8 °C and 92.0 °C (Figure 4.43), potentially a reflection that some benzocaine was ‘bound’ and some ‘unbound’ within the formulation. Upon cooling, recrystallisation was observed at 46.5 °C with reduced intensity and a broadened peak, i.e. at a temperature lower than that seen for pure benzocaine. This phenomenon was attributed to the transition from a crystalline to partially amorphous state of benzocaine or that the drug was partially incorporated within the pores of the silica [81]. From a second heating cycle a peak at 77.6 °C was observed at a lower melting point than for benzocaine possibly due to an  $\alpha$ -polymorphic form of the drug [225]. Furthermore, the compound appeared to recrystallise at 45.8 °C, significantly lower than that observed for pure benzocaine. In the presence of  $\beta$ -cyclodextrin a small, broad endothermic peak was observed at 91.5 °C corresponding to fusion and almost a flat event in the region of 120 – 140 °C suggesting dehydration of  $\beta$ -CD with recrystallisation occurring at 63.1 °C. It

should be noted that the dehydration event was more noticeable using MWDTA, which further demonstrates the sensitivity of the microwave-based technique. These events were also observed in the second heating and cooling cycle (with the exception of the dehydration event). These reversible events suggested that there was a little interaction between benzocaine and  $\beta$ -cyclodextrin when compared with the melting temperature of the pure compound [227].

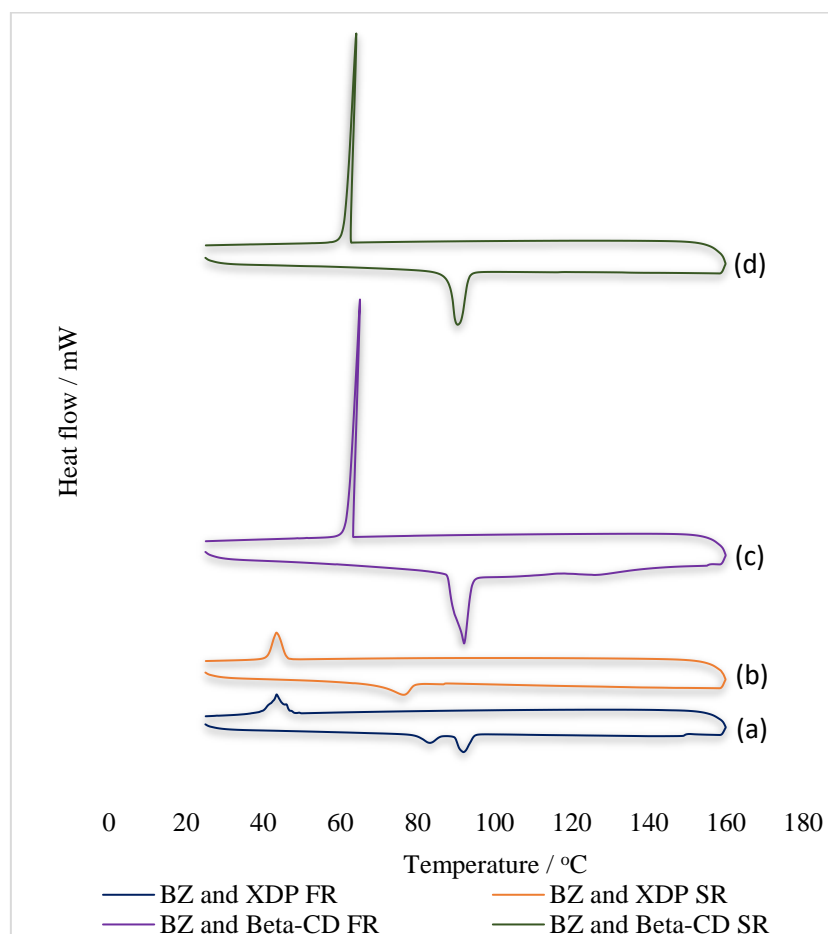


Figure 4.43. DSC profiles of (a) BZ with XDP 3050 first cycle, (b) BZ and XDP 3050 second cycle, (c) BZ and  $\beta$ -CD first cycle and (d) BZ and  $\beta$ -CD second cycle

For benzocaine formulated with stearic acid (Figure 4.44) during the first heating cycle a sharp endothermic peak was observed with an onset temperature of 69.9 °C and another at 84.6 °C, the former attributed to melting of the excipient and the latter to benzocaine. The reduction in the melting temperature of benzocaine, compared with pure drug, implies that some fraction of the molecules interacts with the excipient. Upon cooling two events occurred at 57.9 °C and

54.9 °C implying some lack of homogeneity in the mixture after heating. The second heating and cooling cycle displayed peak temperatures of 68.6 °C and 83.6 °C indicating the existence of some benzocaine-stearic acid interactions. Recrystallisation at 57.8 °C and at 40.1 °C suggest that both benzocaine and stearic acid recrystallised at lower temperatures during the second cooling. DSC profiles for D-mannitol (Figure 4.45) display endothermic peaks at 92.4 °C and at 166.4 °C. Upon cooling two peaks were observed at 109.5 °C and 74.1 °C, corresponding to recrystallisation of the excipient and benzocaine in the first cycle.

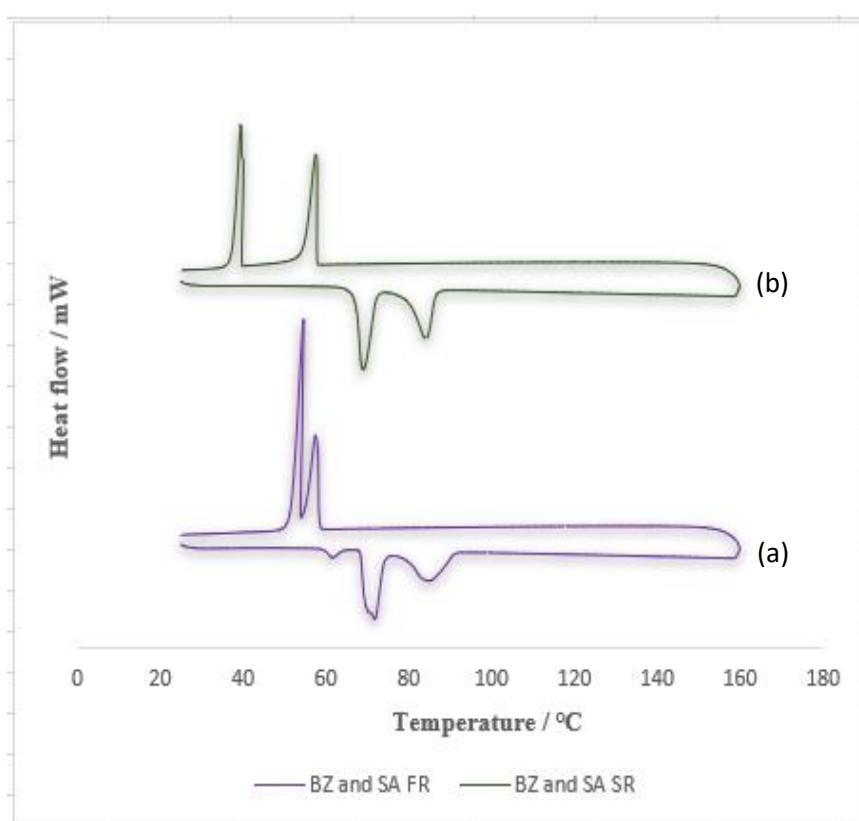


Figure 4.44. DSC profiles of (a) BZ with SA first cycle (FR) and (b) BZ with SA second cycle (SR)

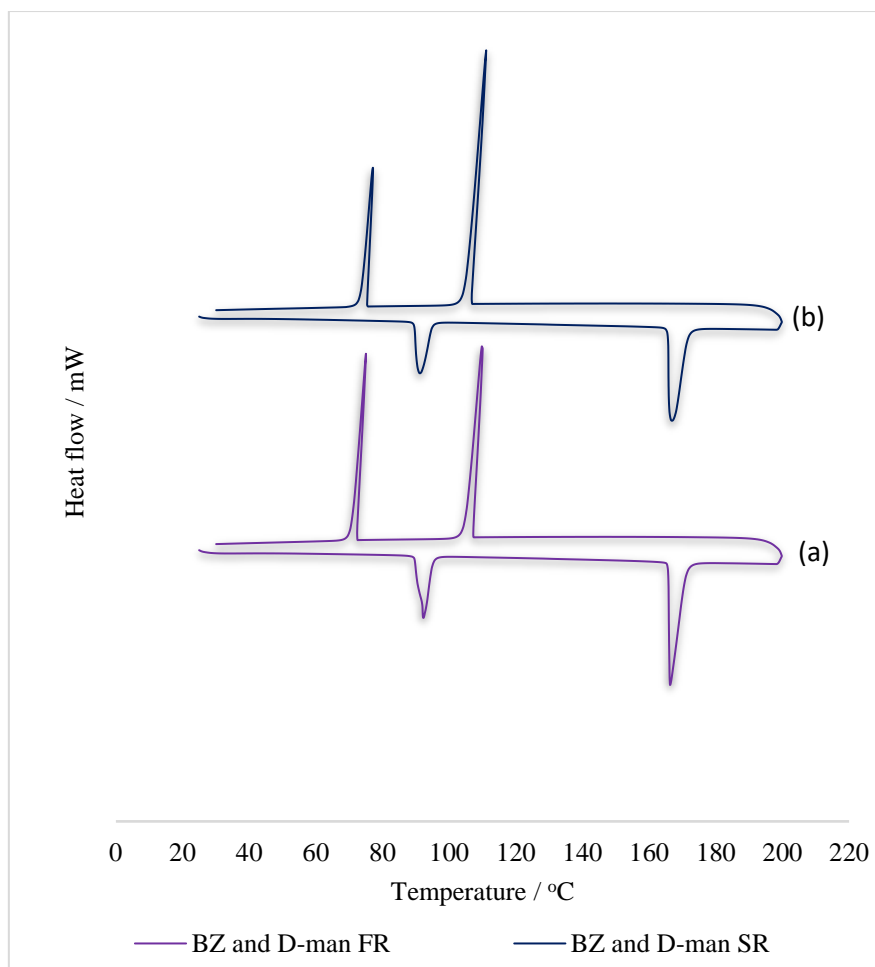


Figure 4.45. DSC profiles of (a) BZ with D-man first cycle (FR) and (b) BZ with D-man second cycle (SR).

In summary, all of the benzocaine-excipient formulations displayed no thermal transitions other than the fusion endotherm and exotherm of benzocaine, similar events for the excipients and, in one case, possibly dehydration of the  $\beta$ -CD, thus confirming thermal stability and absence of any polymorphic transitions.

#### 4.4.2. XRD of benzocaine and pharmaceutical excipients

To confirm the findings from DSC, i.e. the implication that the products had increased in amorphous content on formulation, X-ray powder diffraction (XRD) analysis of benzocaine with excipients was carried out. Figure 4.46(a) displays the XRD patterns of benzocaine with XDP 3050 (first run). Diffraction peaks with reduced intensity appear at  $8.9^\circ$ ,  $17.0^\circ$ ,  $20.2^\circ$ ,  $23.9^\circ$  and  $27.3^\circ$  thus confirming that the drug was still in a crystalline state in the first run while

in the second run (Figure 4.46b), almost complete disappearance of the peaks was observed in full agreement with the DSC, confirming that benzocaine was largely amorphous. The XRD pattern for BZ with beta-CD in Figure 4.46c and 4.46d (first and second run), showed that benzocaine diffraction patterns were maintained in both the runs, confirming that the drug was still present in a crystalline state with peaks appearing at 12.6°, 16.5°, 20.1°, 24.6° and 27.1°, this is consistent with the DSC results.

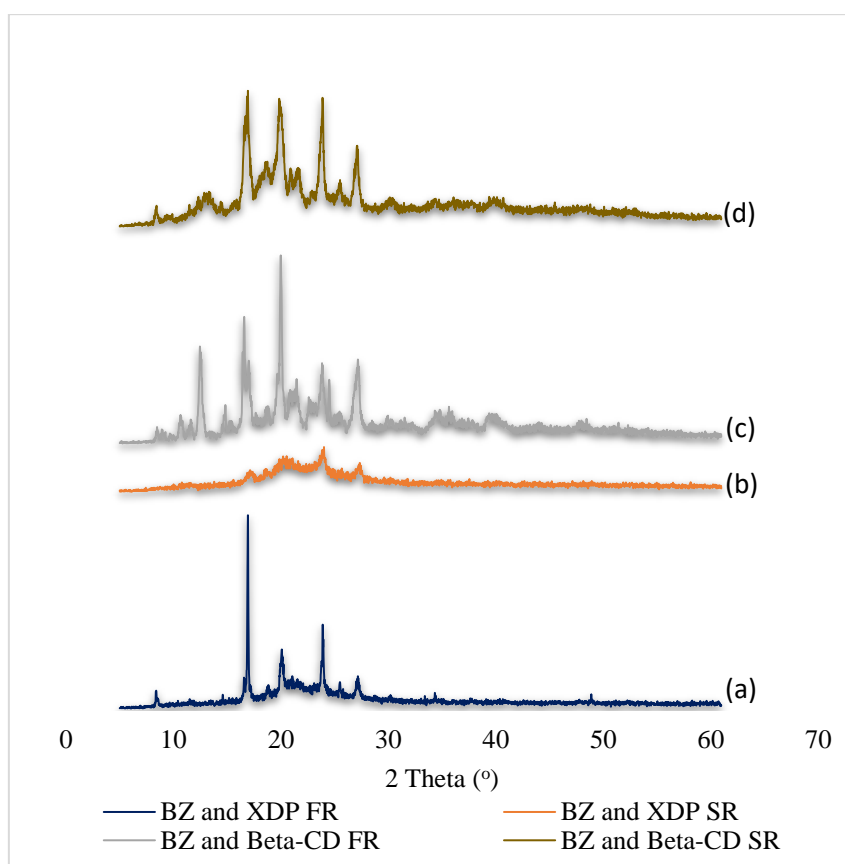


Figure 4.46. XRD patterns of; (a) BZ with XDP 3050 first run (FR), (b) BZ with XDP 3050 second run (SR), (c) BZ with Beta-CD first run (FR) and (d) BZ with Beta-CD second run (SR)

Figure 4.47a and 4.44b display the XRD diffraction patterns of benzocaine with stearic acid (first and second run). The diffraction patterns observed for the mixtures were with high intensities indicating little or no interaction between the compounds with diffraction peaks appearing at 6.3°, 10.4°, 17.1° and 20.0°. In the second run (Figure 4.47b), these peaks were still visible though with reduced intensities suggesting loss of some crystalline structure of the

stearic acid after the first run of the same sample. In the case of benzocaine with D-mannitol (first run) in Figure 4.47c, the diffraction patterns were observed at  $17.0^{\circ}$ ,  $18.9^{\circ}$ ,  $21.7^{\circ}$  and  $23.2^{\circ}$  which confirmed the presence of some crystalline structure of the drug while the second run (after processing) in Figure 4.47d, also displayed the diffraction patterns with reduced intensities suggesting loss of some crystalline structure of D-mannitol after the first run of the same sample. Overall, these results are in good agreement with the DSC and MWTA observations discussed earlier.

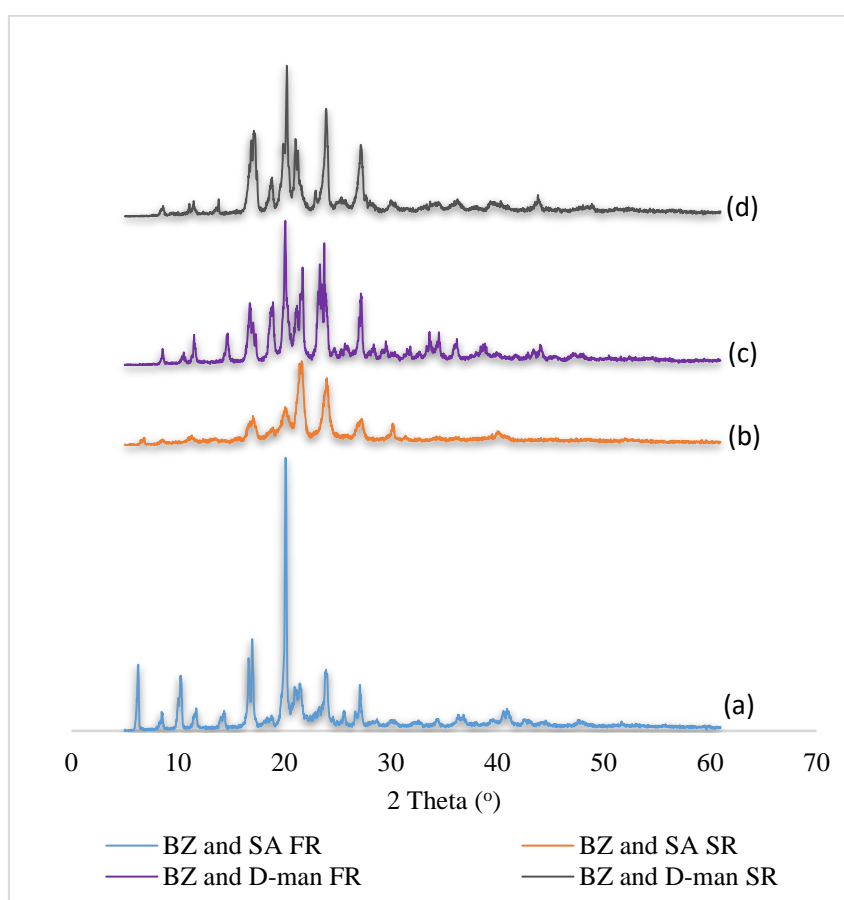


Figure 4.47. XRD patterns of; (a) BZ with SA first run (FR), (b) BZ with SA second run (SR), (c) BZ with D-man first run (FR) and (d) BZ with D-man second run (SR)

#### 4.4.3. HSM of benzocaine-excipient formulations

HSM was utilised to follow the transformation of benzocaine with the four excipients as a function of temperature to visibly observe changes. Photographic images were recorded and are presented at selected temperatures in Figures 4.48-4.51. Firstly, Syloid<sup>®</sup> silica XDP 3050

was analysed (Figure 4.48) and, although hard to distinguish, did appear to show partially melted benzocaine at 93.2 °C (Figure 4.48B), followed by recrystallisation when the sample was cooled down to 30 °C (Figure 4.48C). A small, gradual increase and decrease in the sample RLI values was observed, correlating with the gradual change in benzocaine temperature going from solid to liquid.

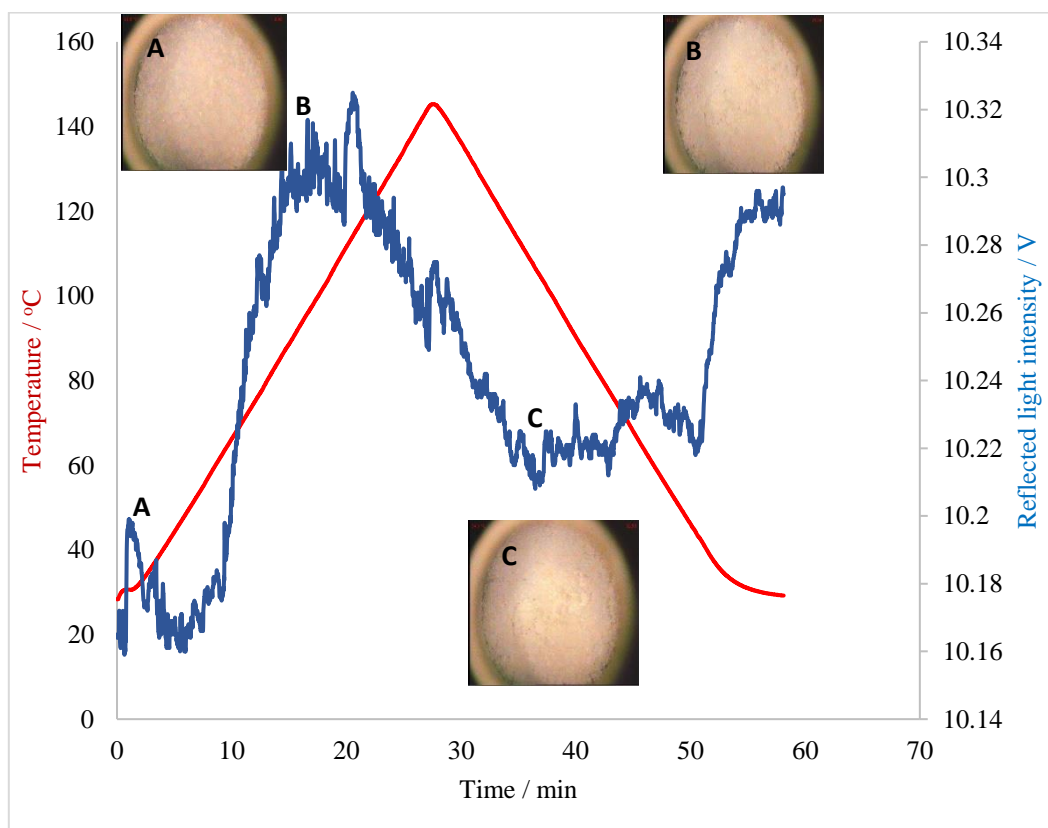


Figure 4.48. Microscope images and optical data of a sample of Benzocaine with XDP 3050 heated from 30 to 160 °C as a function of temperature

For benzocaine with  $\beta$ -cyclodextrin HSM (Figure 4.49) enabled observation of the fusion process of benzocaine at around 92.8 °C within  $\beta$ -cyclodextrin, confirming that benzocaine became molten, as evidenced during MWDTA and DSC profiles with dehydration occurring in the region of 120 – 140 °C. Furthermore, HSM confirmed that the drug recrystallised during the cooling process as expected based on previous analytical data. The RLI values decreased in the region of 10.4 – 9.5 V, correlating with the gradual change from solid to liquid. Upon



cooling, the RLI values gradually increased up to 10.1 V as the sample began to recrystallise which is matched in the temperature profile.

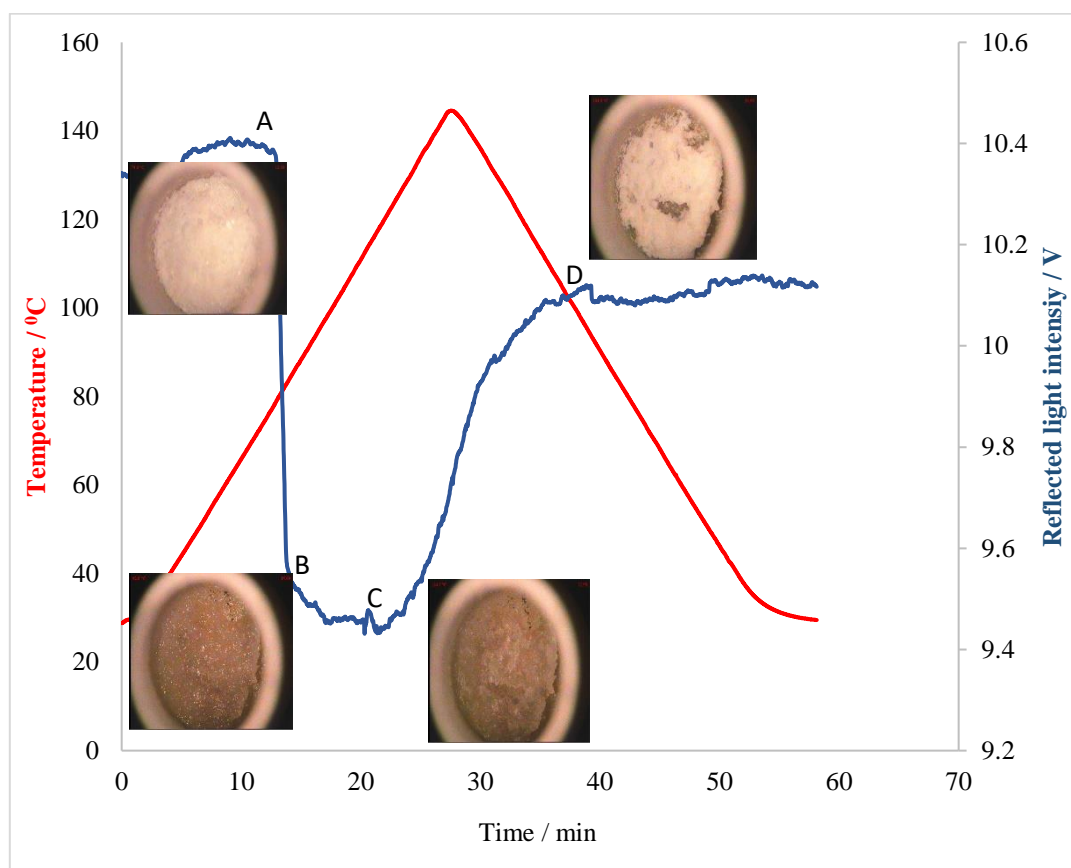


Figure 4.49. Microscope images and optical data of a sample of benzocaine with Beta-cyclodextrin heated from 30 to 160 °C as a function of temperature

HSM images for benzocaine formulated with stearic acid are shown in Figure 4.50. In conjunction with MWDTA and DSC data (shown earlier), it can be concluded that stearic acid loses its crystalline structure and undergoes a solid-state transformation near 71.2 °C, which corresponds to the melting point of the excipient. A second transformation at 89.4 °C was attributed to the fusion of benzocaine, followed by recrystallisation upon cooling. The RLI values decreased going from solid to liquid for the fusion of stearic acid from 10.3 – 9.8 then increased to 9.9 V for benzocaine melting, correlating with the gradual change in the sample temperature. A slight decrease in the light intensity was also noted at around 9.9 V, which occurred during the cooling correlating with the images observed.

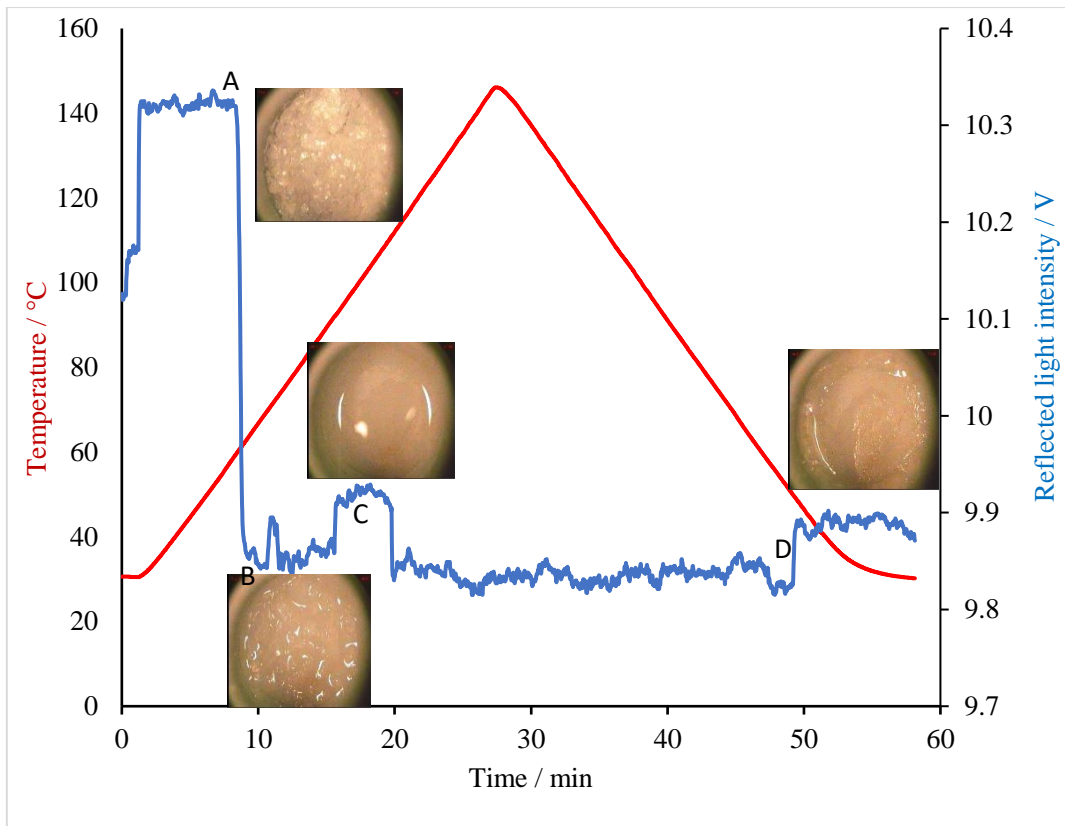


Figure 4.50. Microscope images and optical data of a sample of benzocaine with stearic acid heated from 30 to 160 °C as a function of temperature

For benzocaine formulated with D-mannitol (Figure 4.51) HSM revealed a white powder at 75.0 °C with some melting at ~ 93.2 °C corresponding to fusion of benzocaine and complete transformation at 167.8 °C for the fusion of D-mannitol. These findings match those seen in the previously presented MWDTA and DSC data with recrystallisation upon cooling at 30 °C. The RLI decreased going from solid to liquid for the fusion of benzocaine from 10.2 – 9.8 then increased to 9.9 V for D-mannitol melting, correlating with the gradual change in the sample temperature. Slight decreases in the light intensity were also noted at around 9.7 V, which occurred during cooling, correlating with the images observed.

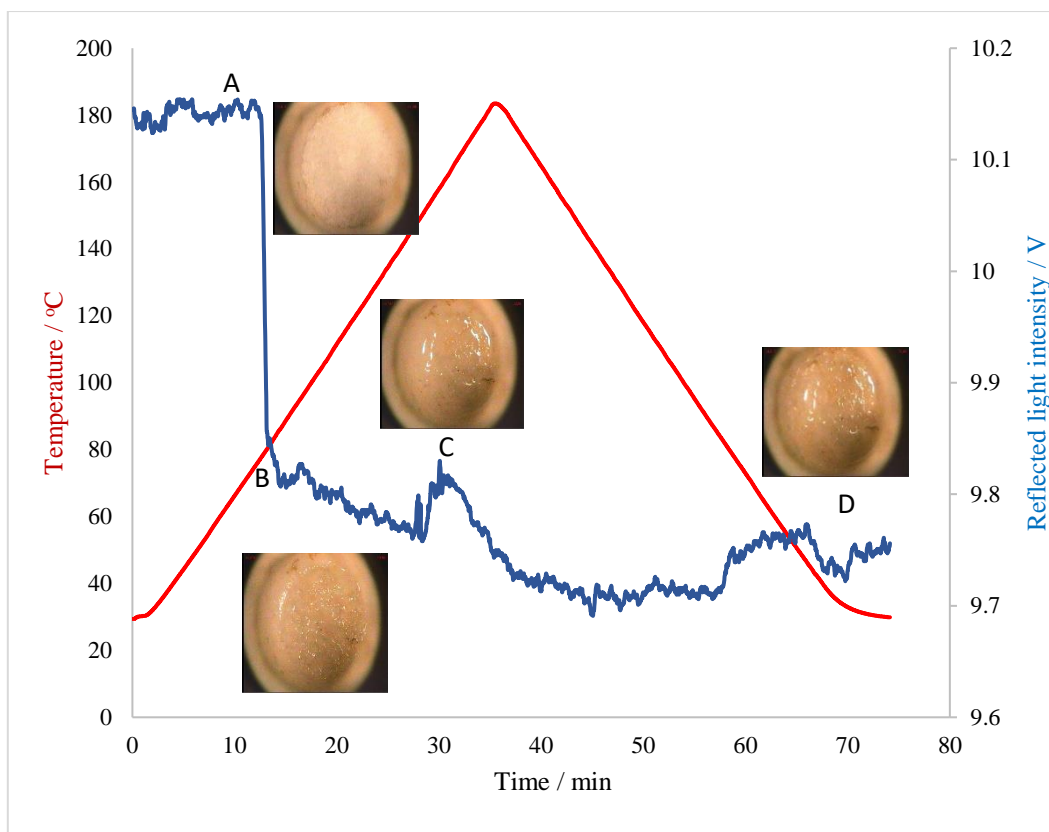


Figure 4.51. Microscope images and optical data of a sample of benzocaine with D-mannitol heated from 30 to 200 °C as a function of temperature

#### 4.5. MWDTA of indomethacin and pharmaceutical excipients

Indomethacin was another compound selected from the eight model compounds for analysis in the presence of a selection of four pharmaceutical excipients, namely  $\beta$ -cyclodextrin, D-mannitol, stearic acid and Syloid<sup>®</sup> silica (XDP 3050). Firstly, microwave thermal analysis of indomethacin with stearic acid, formulated at a 1:1 ratio was considered, and the resultant profile is shown in Figure 4.52. Apart from an initial variation at the start of the experiment, a broad transition could be observed for stearic acid (SA) with an onset temperature of 67.43 °C and peaking at 77.53 °C, which is higher by 6.8 °C compared with conventional DSC (Figure 4.56). Another phase change was observed around 161.9 °C corresponding to the fusion of IMC, which had shifted to a slightly lower temperature in comparison with fusion of pure drug (Figure 4.5), indicating an interaction between drug and SA. The phase change was followed with a change in baseline as drug was heating differently than before the transition due to

dielectric losses from the material, as a result of the microwave effect, a thermal effect that cannot be duplicated or achieved by conventional heating as previously reported [228]. Upon cooling, there was an event which was not thought to be a transition, it only occurred due to the instrument settling from heating to cooling. The crystallisation of SA was observed at 53.2 °C but the drug stayed in a glassy form and did not show any recrystallisation peak. This profile has a high tangent and heated much more rapidly in the microwave field when compared with IMC:  $\beta$ -CD profiles (Figure 4.54) with low tangent.

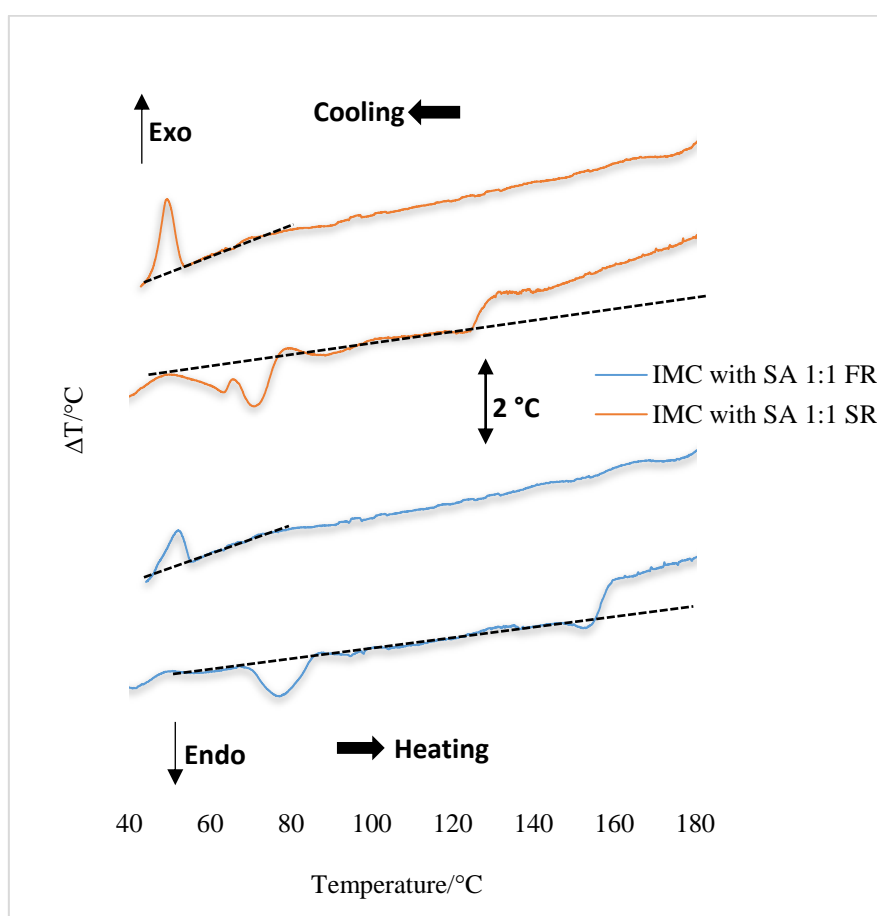


Figure 4.52. Microwave differential thermal analysis (MWDTA) of indomethacin (IMC) with stearic acid (SA) heated at 5 °C/min to 200 °C for both the first (FR) and second (SR) run then cooled in both cases to 40 °C

In the second profile, there was also a variation followed by a broad transition with an onset of 55.6 °C and peaking at 71.6 °C corresponding to fusion of SA. This had shifted to a lower temperature as the excipient lost some of its crystalline structure after the first run. Another

transition which had again shifted to lower temperature was recorded which could possibly be due to an  $\alpha$ -polymorph of the IMC around 135.3 °C [229]. This finding implies that there is not complete inclusion complexation between drug and excipient. This is contrary to what was observed in the second run between IMC:  $\beta$ -CD (Figure 4.54) and IMC: XDP (Figure 4.55) where there is complete disappearance of the drug melting peak as a result of drug conversion from crystalline to amorphous form by the microwave method and insertion of IMC molecules into the  $\beta$ -CD cavity and pore volume of XDP. Upon cooling there was a broad event that was not thought to be a transition which occurred due to settling down of the instrument followed by a well-defined sharp recrystallisation peak at 50.10 °C for SA. This suggested that even after the second run, SA recrystallised with no recrystallisation peak observed for drug or any thermal decomposition.

Figure 4.53 displays the MWDTA of IMC with D-man at a 1:1 ratio for the first run (FR) and second run (SR). The lower profile in the figure indicates the first cycle heating. Apart from an onset variation at the start of the experiment, the rise in temperature was smooth and featureless until a small transition occurred at 162.0 °C, the transition corresponds to the fusion of IMC in D-man, which was followed immediately with another at 169.5 °C corresponding to that of D-man. As expected, there was a change in baseline after the transitions were observed, which was due to the microwave effect as the samples were heating differently (and much more rapidly) in the microwave field than before the transition. On closer inspection of the profile, it was assumed that the dielectric losses from the mixtures were small in comparison with the previous analysis discussed (Figure 4.52) and it can be concluded that during heating, the thermal materials dielectric properties were responsible for the lower loss-tangent observed. On the cooling process, there was a sharp event at 113.86 °C which corresponds to the recrystallisation of D-man with no further events observed suggesting that the drug stayed in a glassy form after its fusion.

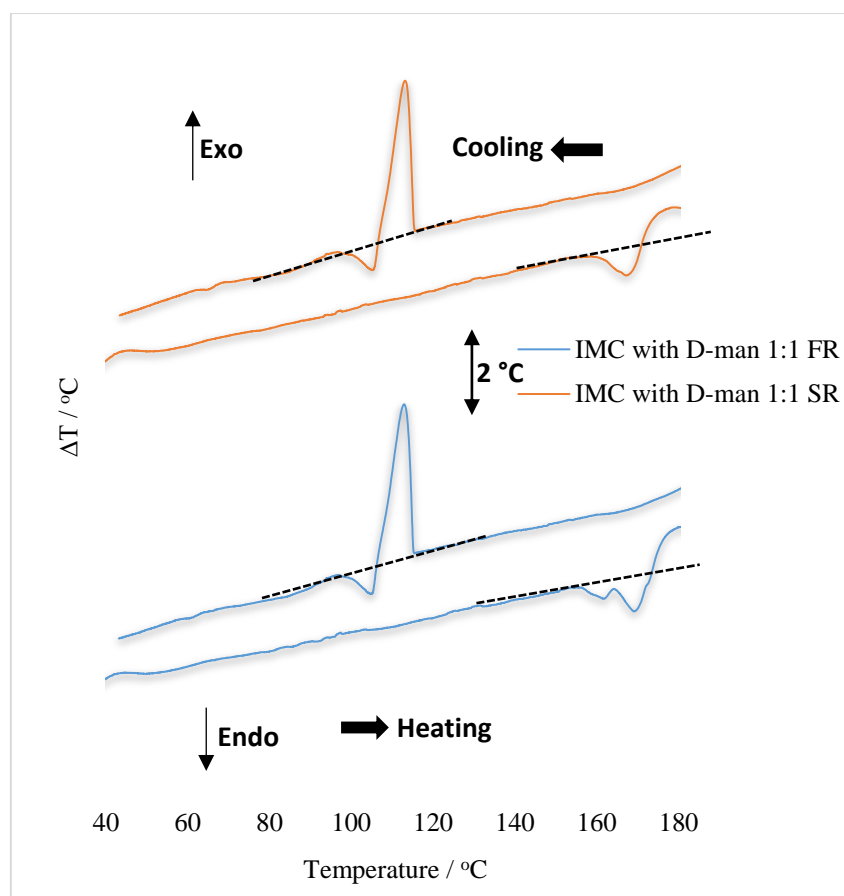


Figure 4.53. Microwave differential thermal analysis (MWDTA) of indomethacin (IMC) with D-mannitol (D-man) heated at 5 °C/min to 200 °C for both the first (FR) and second (SR) run then cooled in both cases to 40 °C

In the upper profile, it is important to note that the only transitions observed were those of D-man, with the first transition occurring at 167.7 °C for fusion of excipient and then upon cooling a sharp recrystallisation was observed at 113.6 °C. The transition for the drug was not reversible as expected as the drug stayed in an amorphous form. The change in baseline was small in comparison to the first run, which was due to a change in dielectric properties as drug was in an amorphous state. The loss tangent in comparison to the two profiles are almost similar between the first run and the second but are different in the previous experiment carried out due to the different variation in dielectric properties. This reflects the differing physical and chemical structures of the products, e.g. thermal conductivity, heat capacity, the aforementioned dielectric properties, particle size and density.

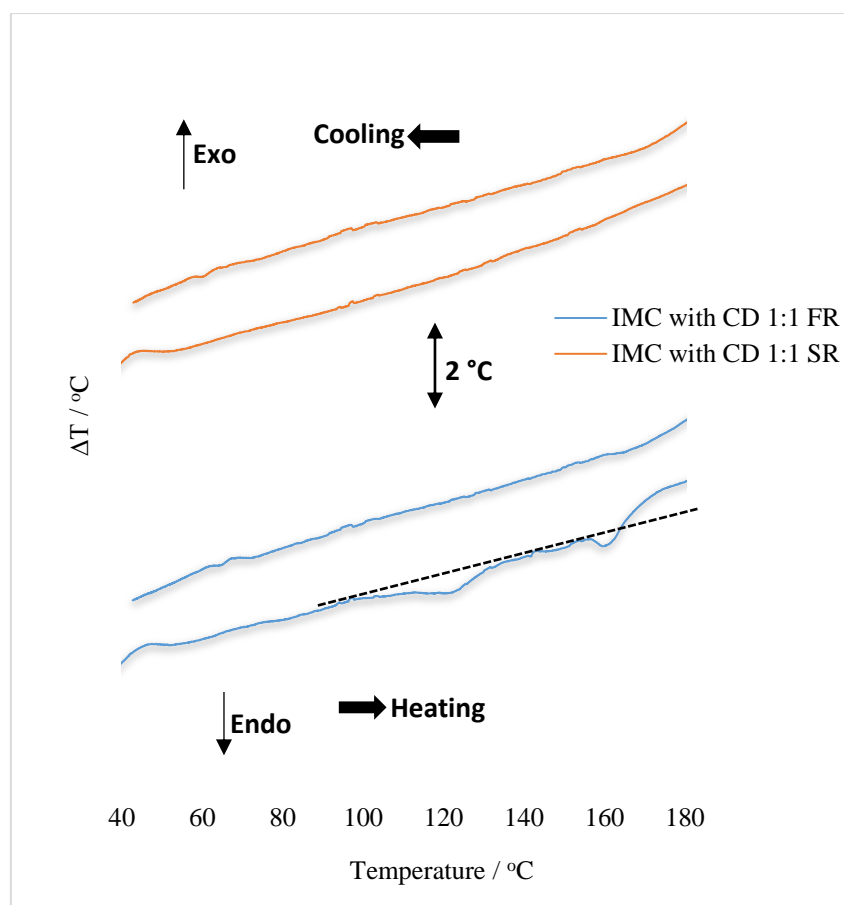


Figure 4.54. Microwave differential thermal analysis (MWDTA) of indomethacin (IMC) with beta-cyclodextrin (Beta-CD) heated at 5 °C/min to 200 °C for both the first (FR) and second (SR) run then cooled in both cases to 40 °C

MWDTA results with a linear heating and cooling rate of the physical mixture of 1:1 IMC with beta-CD first run (FR) and second (SR) heated at 5 °C/min under an air atmosphere are shown in Figure 4.54. The first profile result from the first heating of the mixture displays an initial variation at the onset of the experiment, followed by a broad event arising from the dehydration of the beta-CD in the region of 90 °C - 130 °C. The smaller event in the profile with an onset temperature of 157.42 °C and peaking at 160.56 °C was produced by a solid-liquid fusion of drug in beta-CD accompanied by a dielectric change, indicating that the molten drug couples to microwaves differently than before the transition. This is assumed to be a result of the difference in tangent that the sample possessed which brings about efficient absorption of the electromagnetic energy by the sample and, consequently, leading to rapid heating [228]. Upon

cooling, no transition was observed as drug remained in an amorphous state and did not recrystallise after fusion in beta-CD. In the second run, no transitions were observed both during the heating and cooling, demonstrating that all the thermal processes seen in the first run were irreversible. The result displayed a close correlation between the events observed with those of the DSC and HSM obtained in Fig. 4.57 and 4.62.

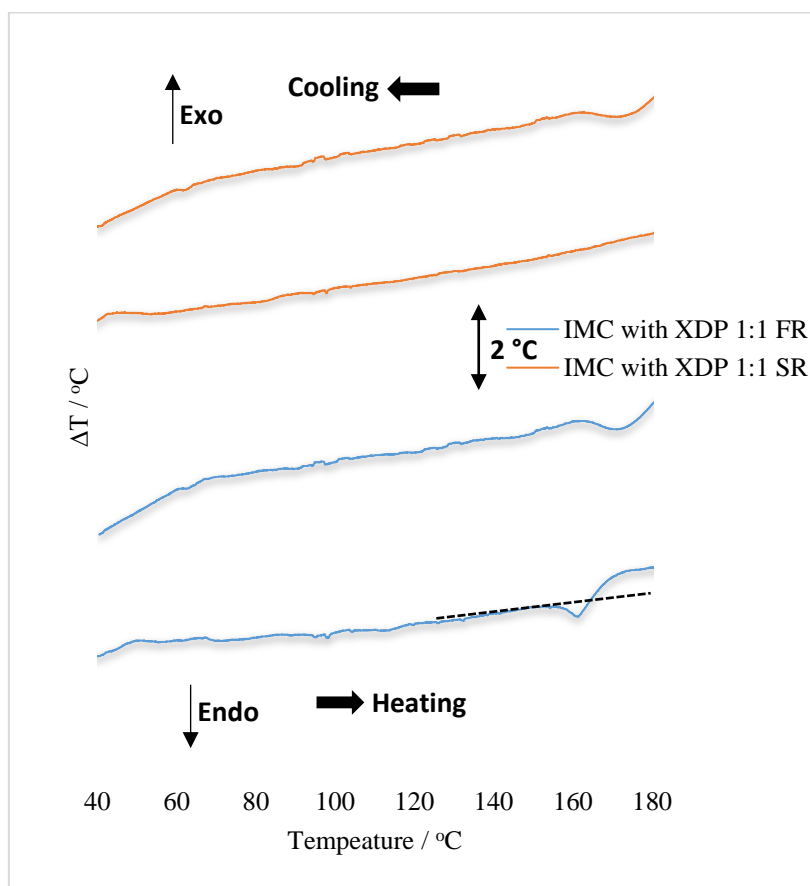


Figure 4.55. Microwave differential thermal analysis (MWDTA) of indomethacin (IMC) with XDP 3050 heated at  $5^\circ\text{C min}^{-1}$  to  $200^\circ\text{C}$  for both the first (FR) and second (SR) run then cooled in both cases to  $40^\circ\text{C}$

The MWDTA profiles from the linear heating and cooling of the physical mixture of a 1:1 IMC with XDP first run (FR) and second run (SR) heated at  $5^\circ\text{C}/\text{min}$  under an air atmosphere is shown in Figure 4.55 in the form of calculated  $\Delta T$  ( $T_{\text{sample}} - T_{\text{reference}}$ ) plotted as a function of sample temperature. Two profiles are displayed; the lower profile shows the first heating while the upper profile shows the second run. The first run shows an initial variation at the onset of



the experiment, fusion of drug can be seen at 164.2 °C. After the transition was observed, there was an increase in the baseline value (a microwave effect) as expected, which does not return as the sample was heating differently and couples more strongly with the microwave. The change in baseline (shown as a black dotted line) is the opposite of the DSC profiles (discussed later) where a negative sloping baseline was observed. Earlier analysis carried out on pure IMC in Figure 4.5, and on the mixture of drug with XDP, suggested that there was an interaction between the IMC and XDP during fusion. A size reduction, broadening and a shift of the drug peak to a lower temperature were observed as a result of the interaction between drug with XDP in comparison with pure IMC. DSC and HSM analysis (Fig. 4.5 and Fig. 4.21) undertaken on pure IMC and the mixture confirmed this interaction after fusion. This outcome further indicated that MWDTA can be a sensitive method for drugs that undergo transitions resulting in a large change in dielectric. Upon cooling, there was a broad event that was not thought to be a transition, it only occurred due to the instrument settling from heating to cooling. In cooling, there was no transition observed as drug stayed in an amorphous form and did not recrystallise after fusion in the XDP.

In contrast, the second heating of the mixture displayed no transition other than a small downward peak similar to the one observed during cooling at 173.16 °C. This event has been consistently observed during this research and was not thought to be a transition. There was a decrease in  $\tan \delta$  though in comparison to the first heating which occurred without any losses from the material. The drug stayed in amorphous form after the first heating, demonstrating that the thermal processes were irreversible.

#### **4.5.1. DSC for IMC and pharmaceutical excipients**

Formulations of indomethacin with the four excipients under investigation were analysed using DSC for comparison with MWDTA data with peak values displayed in Table 4.3.

Table 4. 3: A Summary of DSC peak values for melting ( $T_m$ ) and recrystallisation temperatures ( $T_r$ ) of indomethacin with four excipients.

Material (1:1)	$T_m / ^\circ\text{C}$		$T_r / ^\circ\text{C}$	
	IMC with SA	153.0	74.5	-
IMC with D-man	160.7	167.2	-	118.6
IMC with $\beta$ -CD	162.5	80-130	-	-
IMC with XDP	162.6	-	-	-

DSC thermograms of IMC with excipients at a 1:1 w/w ratio for the first and second run are displayed in Figures 4.56 – 4.58. IMC is a crystalline drug with a melting point of 159.8 °C as reported by Dalmoro [230]. In the thermal profile of the physical mixture of IMC with SA, there was a broad event observed in the first run (Figure 4.56a) with reduced intensity at 74.5 °C corresponding to the melting of SA followed by another at 153.0 °C with a reduced intensity corresponding to the melting of IMC.

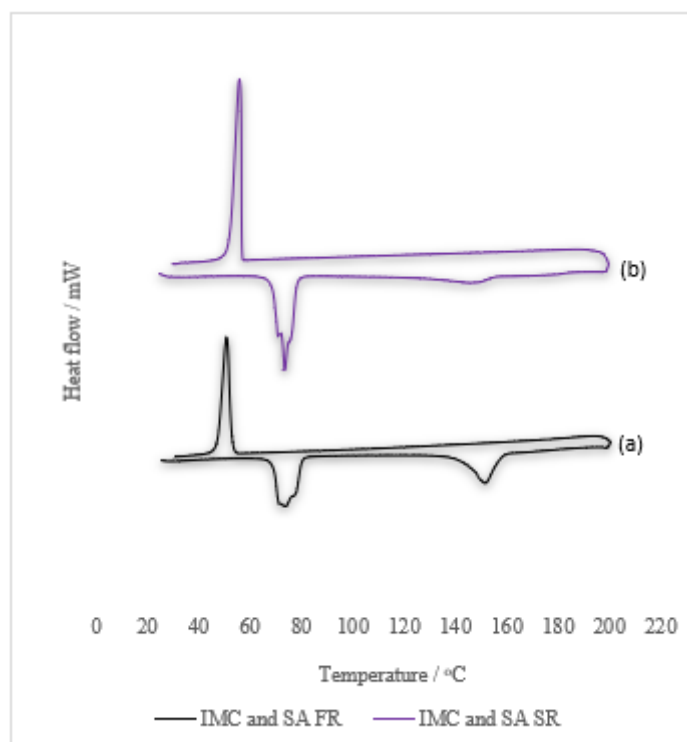


Figure 4.56. DSC thermograms of; (a) IMC with SA first run (FR) and (b) IMC with SA second run (SR)

Only a small shift of the melting peak of drug to a lower temperature was observed attesting to a decrease in drug crystallinity due to a minor reaction between drug and SA during heating. However, the appearance of an exothermic peak at 50.8 °C confirmed the recrystallisation of SA, indicating that SA recrystallised during cooling. A second heating of the physical mixture was also carried out (Figure 4.56b). The samples were cooled to room temperature and then reheated. During this process, there was a small shift to a lower melting point of the SA with a peak temperature recorded at 74.3 °C, which is an indicative loss of some SA crystalline structure as a consequence of the heating, cooling and reheating process. An event that appeared almost flat was evident at 151.9 °C for the drug indicating loss of drug crystalline structure. Recrystallisation of the drug was not evident (only for SA at 56.7 °C). In the thermal profile of the physical mixture of IMC with D-man in Figure 4.57a (FR), two events were recorded during heating. The first event was characterised by a melting peak of 160.7 °C with a reduced intensity corresponding to the fusion of IMC, followed by second event at 167.2 °C corresponding to the melting of D-man with high intensity. On cooling, a very sharp exothermic peak at 118.6 °C with a high-intensity (corresponding to recrystallisation of D-man) was observed with no other transition recorded. The second run of the physical mixture (Figure 4.57b) displayed two transitions during heating and cooling. The former at 167.8 °C was with reduced intensity also, broad when compared to the first run and corresponded to the fusion event, while the latter was at 116.1 °C and corresponded to recrystallisation of D-man. The fusion of drug was not observed due to the absence of the crystalline structure of drug in the second run.

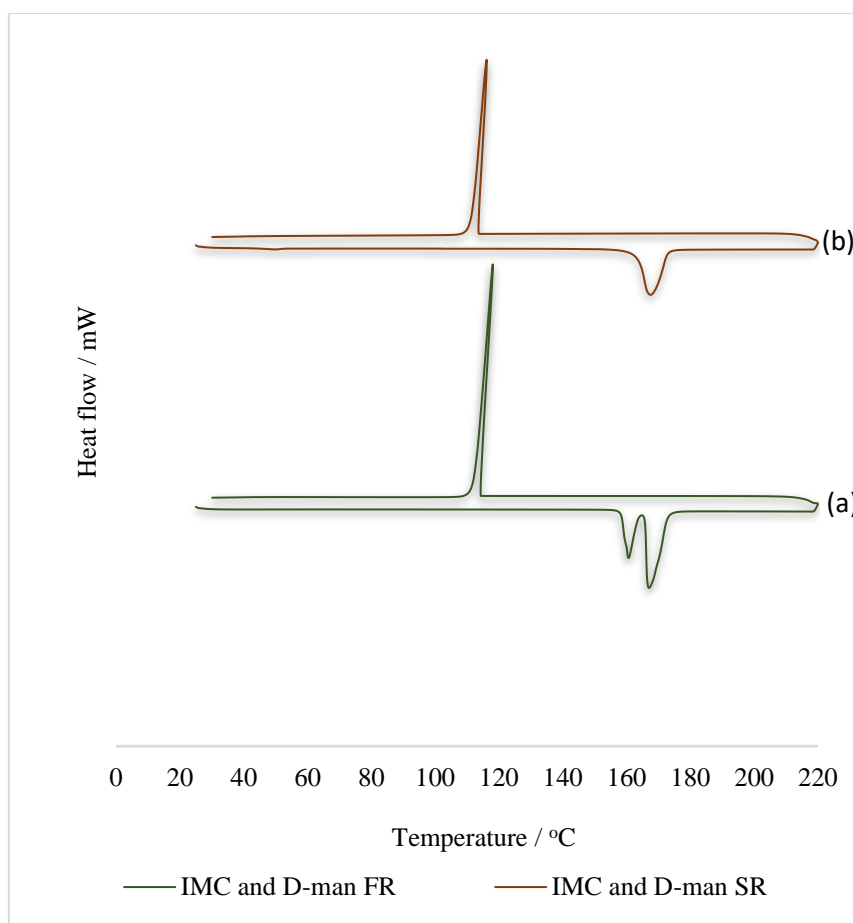


Figure 4.57. DSC thermograms of; (a) IMC with D-man first run (FR) and (b) IMC with D-man second run (SR)

The DSC thermogram of the physical mixture of IMC with beta-CD is shown in Figure 4.58a. The first event was broad and less intense in the temperature range of 80 – 130 °C indicating dehydration of  $\beta$ -CD followed by a sharp event at 162.5 °C corresponding to the melting of IMC. The endotherm was with reduced intensity in comparison to the melting endotherm of pure drug suggesting an interaction between IMC and  $\beta$ -CD. In the second run (Figure 4.58b), there was an event at 49.2 °C for IMC that looks almost flat, smaller and shifted to a lower temperature in comparison to the first run indicating a glass transition of the drug.

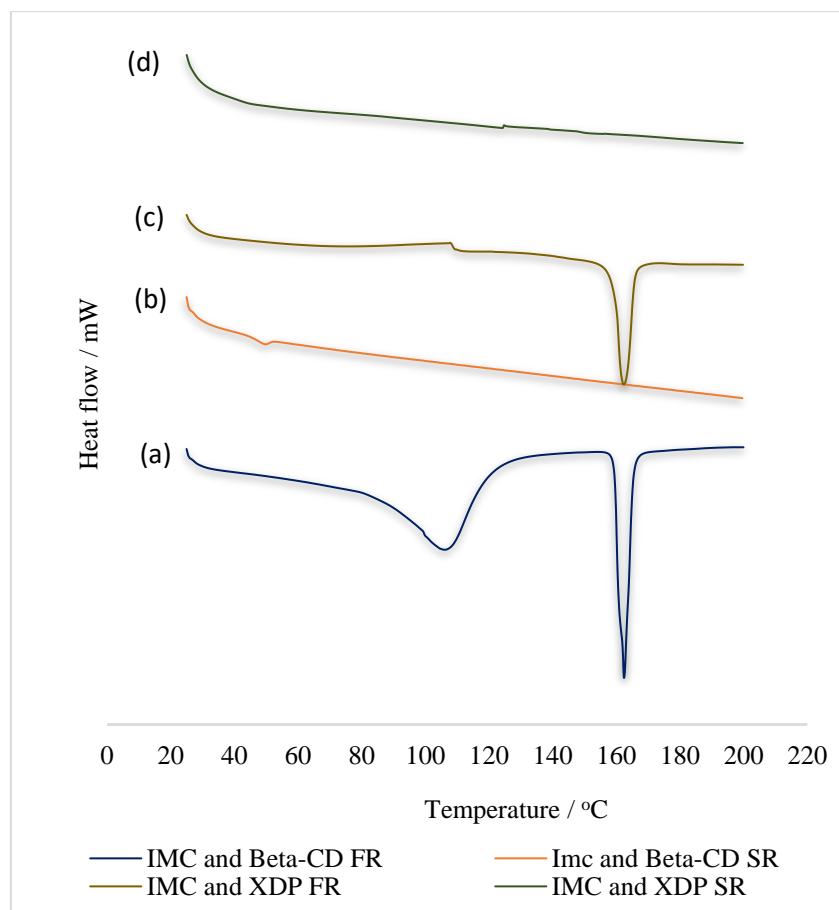


Figure 4.58. XRD patterns of; (a) IMC with Beta-CD first run (FR), (b) IMC with Beta-CD second run (SR), (c) IMC with XDP 3050 first run (FR) and (d) IMC with XDP 3050 second run (SR)

The result of the DSC in Figure 4.58c and 4.58d display the physical mixtures of IMC with XDP at 1:1 w/w ratio for a first and second run. The first run of the mixture shows an endothermic peak of the drug at 162.6 °C with size reduction in comparison to the endotherm of the pure drug suggesting some reaction between the drug and XDP during fusion. In the second run, no endotherm was observed as the drug stayed in amorphous form after the first run which is comparable to what was observed during the MWDTA (Figure 4.55) of the same mixture. The absence of drug endotherm in this run can be assumed as evidence of insertion of the drug molecules inside the pores of the silica. This effect can also be directly related to the conversion of the crystalline drug to amorphous form, which could be as a consequence of true

inclusion complexation. The DSC results showed a close relationship to the transition temperatures experienced during microwave thermal analysis (MWTDA) experiments.

#### 4.5.2. XRD of indomethacin and pharmaceutical excipients

Following on from DSC, i.e. the implication that the products had increased in amorphous content on formulation, X-ray powder diffraction (XRD) analysis of indomethacin with excipients was carried out. Figure 4.59(a) displays the XRD patterns of indomethacin with SA.

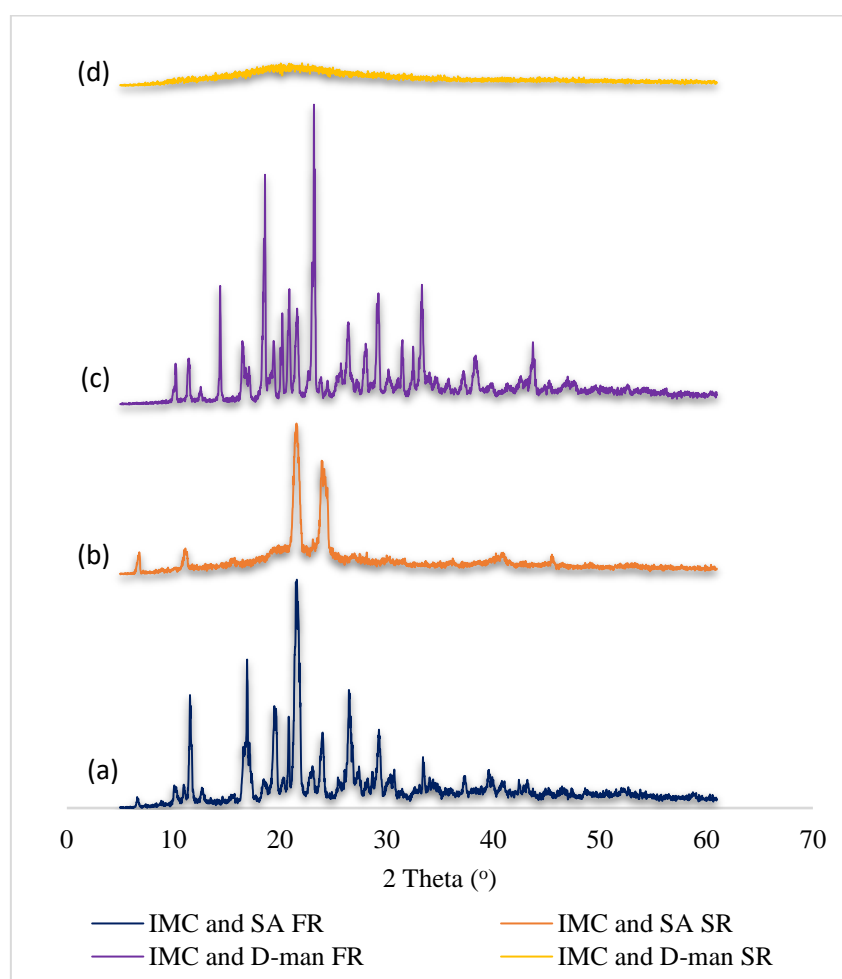


Figure 4.59. XRD patterns of; (a) IMC with SA first run (FR), (b) IMC with SA second run (SR), (c) IMC with D-mannitol first run (FR) and (d) IMC with D-mannitol second run (SR)

Diffraction peaks with a high intensity appeared at  $11.6^\circ$ ,  $16.9^\circ$ ,  $21.8^\circ$ ,  $26.6^\circ$  and  $29.4^\circ$  thus confirming that both the drug and excipient were still in a crystalline state after the first run while in the second run (Figure 4.59b), a few diffraction peaks with reduced intensity were

observed in full agreement with the DSC data confirming that indomethacin was partially amorphous.

The XRD pattern for indomethacin with D-mannitol in Figure 4.59c and 4.59d (first and second run), showed that indomethacin diffraction patterns were maintained in the first run, confirming that the physical mixtures were present in a crystalline state with peaks appearing at 14.3°, 18.5°, 23.2°, 29.3° and 33.4°, consistent with DSC data.

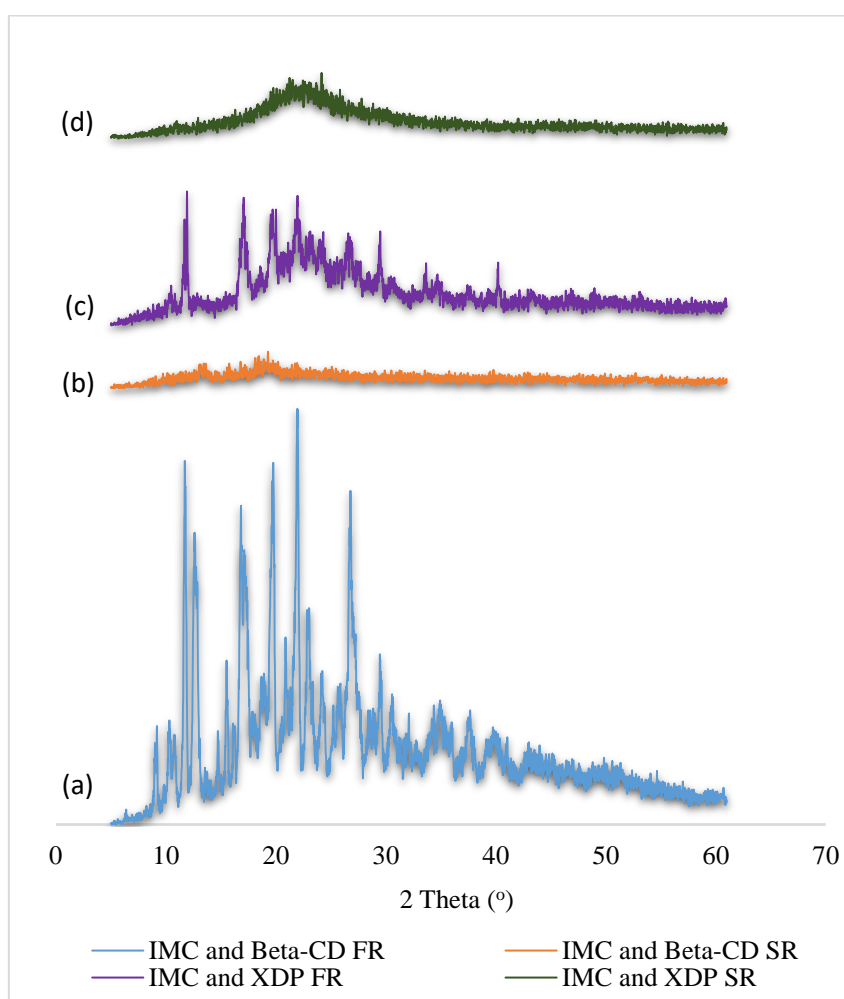


Figure 4.60. XRD patterns of; (a) IMC with Beta-CD first run (FR), (b) IMC with Beta-CD second run (SR), (c) IMC with XDP 3050 first run (FR) and (d) IMC with XDP 3050 second run (SR)

In the second run, diffraction peaks were not observed in contrast with what was observed in MWDTA and DSC discussed earlier which could possibly be due to the conventional method used in melting the mixture.

Figure 4.60a and 4.60b displayed the XRD diffraction patterns of indomethacin with beta-cyclodextrin (first and second run).

The diffraction patterns observed for the mixtures were of high intensity indicating little or no interaction between the compounds with diffraction peaks appearing at 11.8°, 17.4°, 19.5° and 26.9°, while in the second run, small peaks were still visible confirming that the sample was partially amorphous. In the case of indomethacin with XDP 3050 (first run) in Figure 4.60c, the diffraction patterns were observed at 11.9°, 17.2°, 20.0°, 22.0° and 29.4° which confirmed the presence of some crystalline structure of the drug while the second run (after processing) in Figure 4.60d, the sample was largely amorphous which displayed small diffraction patterns with reduced intensity. Overall, these results are in good agreement with the DSC and MWDTA observations discussed earlier.

#### **4.5.3. HSM for IMC with excipients**

HSM is mostly utilised with DSC to characterise the solid state of the drug in solid dispersions [231]. In Figure 4.61, for the physical mixture of IMC with SA, the mixture was not homogeneous, and crystals of the drug and SA were recognisable at around 30 °C. Going from solid to liquid, the SA melted completely at around 70 °C thereby leaving crystals of drug, which melted further at around 160 °C and turned into a homogeneous liquid because of the constant heating rate. Upon cooling, at around 50 °C, recrystallisation of the SA was evidenced. The RLI values decreased going from solid to liquid for the fusion of stearic acid from 10.8 – 10.4 V and decreased again to 10.3 V for indomethacin melting, correlating with the gradual change in the sample temperature. A slight decrease in light intensity was also noted at around 10.1 V, which occurred during cooling correlating with the images observed.



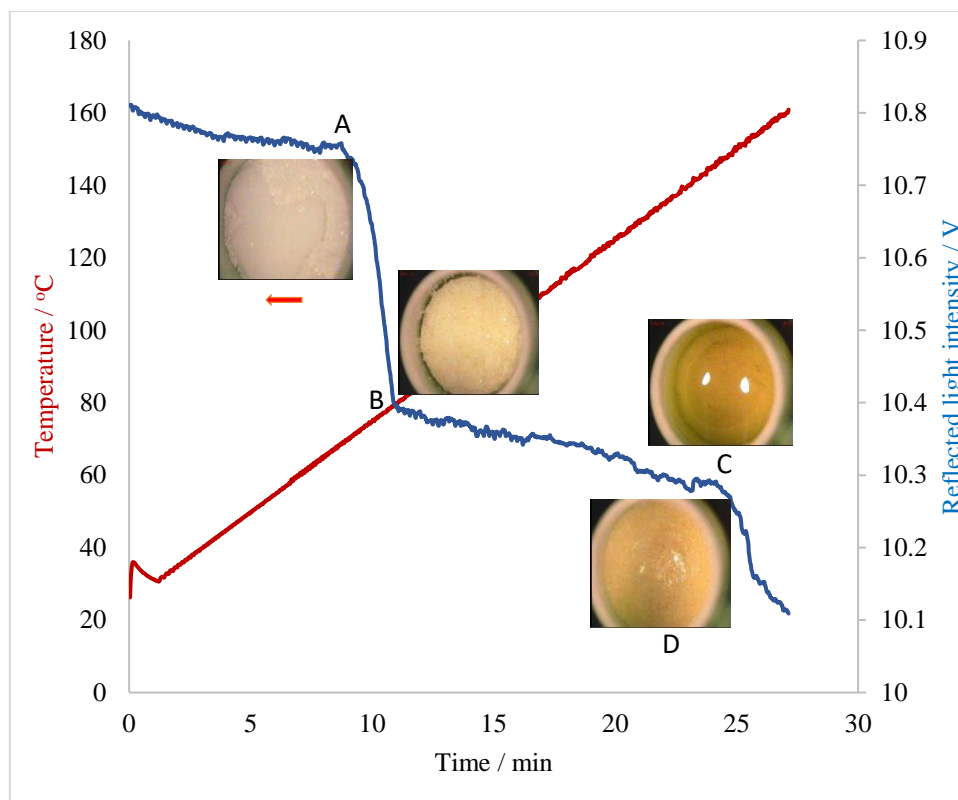


Figure 4.61. Microscope images and optical data of a sample of indomethacin with stearic acid heated from 30 to 200 °C as a function of temperature

The physical mixture of IMC with D-man (Figure 4.62) appeared as a homogeneous mixture at 30 °C. Heating of the mixture resulted in melting of indomethacin at around 160 °C that turned yellow as expected leaving D-man. At around 163 °C, the D-man gradually solubilised producing a homogenous liquid. On cooling, at around 116 °C, a recrystallisation of the D-man was evidenced which further confirms the result of the MWTA and DSC analysis discussed earlier. There was a gradual decrease in the sample RLI values observed from 10.8 to 9.3 V corresponding to the fusion of the indomethacin and a further decrease to 8.9 V for fusion of D-mannitol. Upon cooling, no change in RLI values was noted which is matched by the sample temperature.

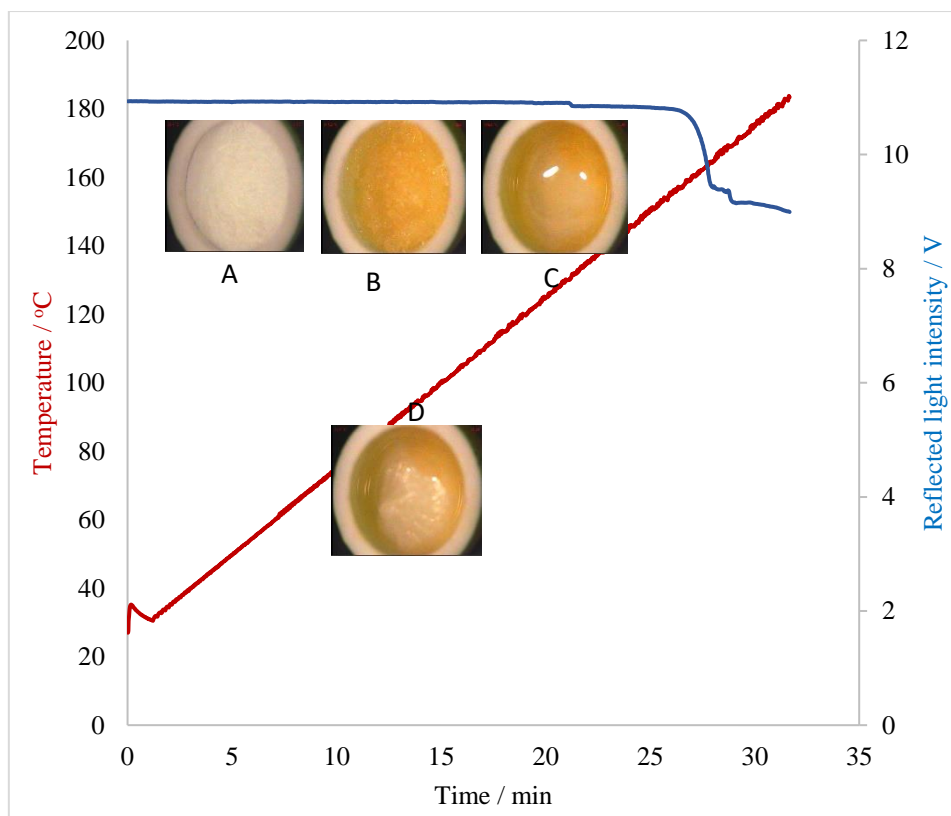


Figure 4.62. Microscope images and optical data of a sample of indomethacin with D-mannitol heated from 30 to 200 °C as a function of temperature

For indomethacin with beta-cyclodextrin in Figure 4.63, at 30 °C the physical mixture appeared homogeneous. During heating at around 160 °C, IMC melted completely in  $\beta$ -CD and turned to liquid with yellowish colouration as evidenced earlier for indomethacin with stearic acid (Figure 4.61). The RLI values decreased going from solid to liquid for the fusion of indomethacin from 10.8 – 9.9 V, correlating with the gradual change in the sample temperature. A slight decrease in the light intensity was also noted after the initial decrease, which occurred during the cooling correlating with the images observed.

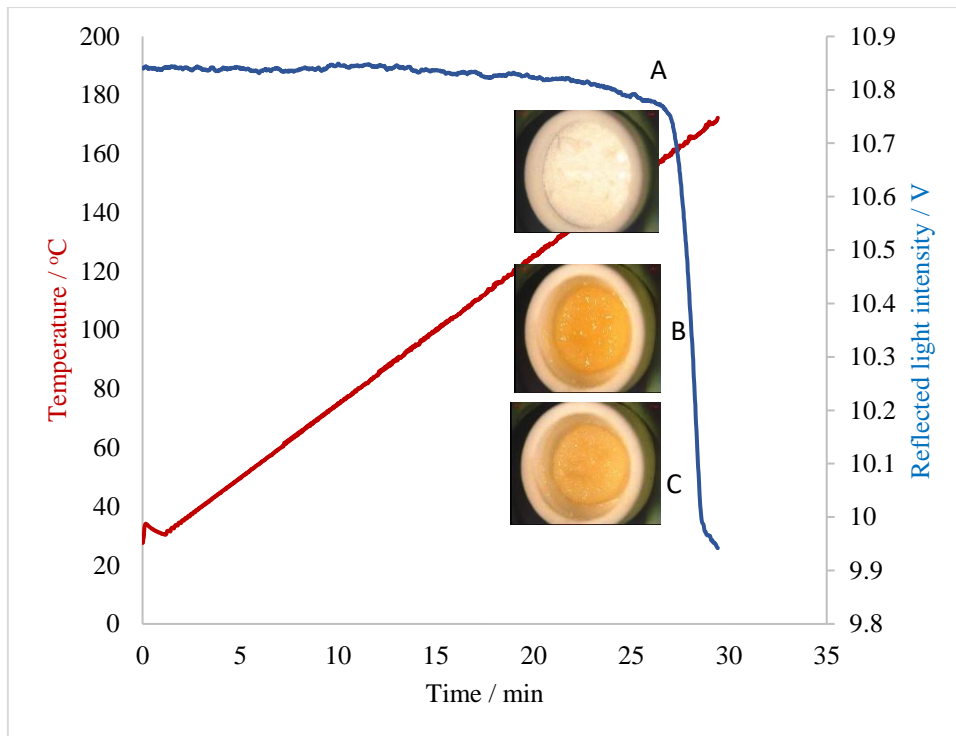


Figure 4.63. Microscope images and optical data of a sample of indomethacin with Beta-cyclodextrin heated from 30 to 200 °C as a function of temperature

Figure 4.64 displays data for IMC with XDP 3050:

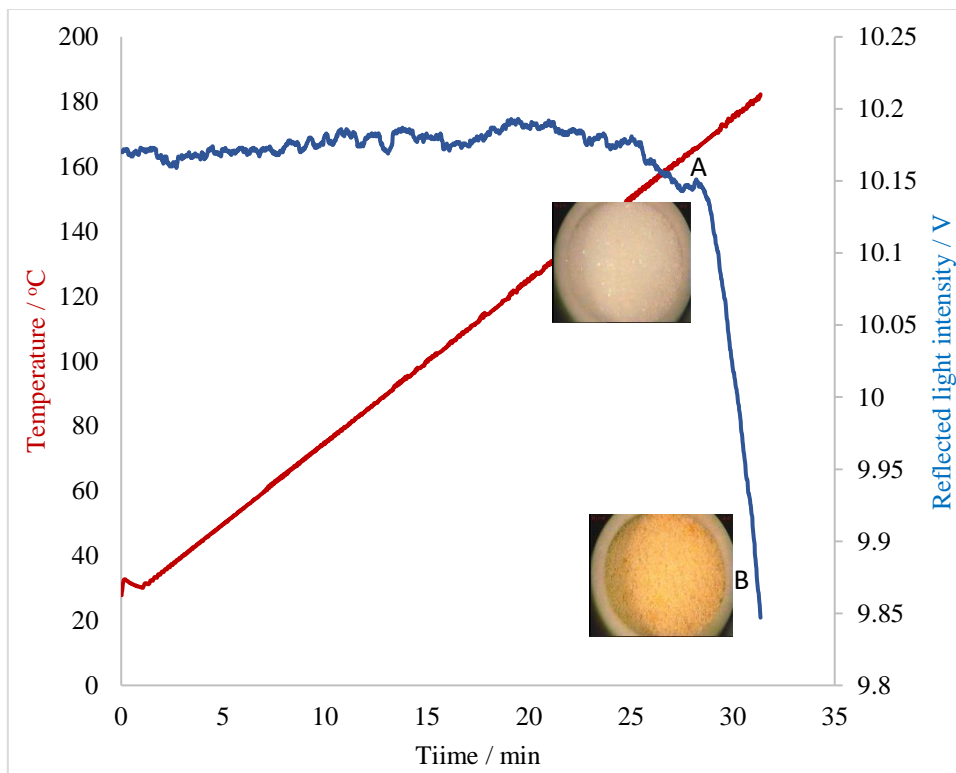


Figure 4.64. Microscope images and optical data of a sample of indomethacin with XDP 3050 heated from 30 to 200 °C as a function of temperature

The physical mixture of IMC with XDP at a temperature of 30 °C appeared as a seed crystal of the drug that completely melted at about 160 °C. There was a change in colour to yellow after the melting of the drug, which was not believed to be as a result of decomposition. This further confirms an interaction between the drug and the silica as evidenced in MWTA and DSC. Again, RLI values decreased going from solid to liquid for the fusion of indomethacin from 10.2 – 9.8 V, correlating with the gradual change in the sample temperature. It is important to state that the data provided by the hot-stage photomicrography experiments was essential in supporting the events observed in the MWDTA and DSC analysis.

#### **4.6. Conclusions**

In summary, the effect of microwave heating was studied through the application of microwave thermal analysis to eight model pharmaceutical compounds and a set of four model pharmaceutical excipients. The profiles were analysed and compared with the data generated using differential scanning calorimetry (DSC), X-ray diffraction (XRD) and hot stage microscopy (HSM). The results demonstrated that microwave thermal analysis (MWDTA) can be utilised to detect a wide range of thermal transitions including melting, recrystallisation, dehydration phase changes and dielectric change via changes in the materials ability to absorb microwave energy.

The dielectric change in some drugs analysed was significantly high, looking at the profiles generated while intermediate and low dielectric changes were observed in other drugs. The dielectric properties of a multicomponent mixture are dependent on the dielectric properties of the components. The thermal transition temperatures are slightly lower or higher in MWDTA than those observed with the conventional DSC method. This effect has been reported previously but has not received a complete explanation [213]. It should be recalled that the peaks seen in conventional techniques arise solely from the transformation enthalpy itself, while the temperature changes seen in MWDTA result primarily from the emergence of a

product or phase that has different dielectric properties. Overall, it was found that the process of microwave heating produced different thermal profiles to those seen using traditional, conductive heating. Investigating differences in thermal profiles can be a useful way to consider the effect of microwave-induced heating on formulations which can, in turn, help guide formulation choices.

## **Chapter 5: The DSC and TGA approach to study bound water restrained by polymer beads (DC Bead *MI*<sup>TM</sup>)**

### **5.1. Introduction**

An attempt was made to characterise the bound water restrained by polymer beads using microwave differential thermal analysis (MWDTA) but most of the water within the beads evaporated when the bead samples were introduced into the technique. The reason for this is that the MWDTA technique does not have a cooling system (e.g. chiller) attached to it, as the technique is still in development. Addition of a cooling system is another area where the MWDTA technique could be developed. The addition of a cooling system will provide several advantages including allowing the user to perform experiments at room /ambient temperatures. Furthermore, better temperature control could be achieved with cooling apparatus, particularly with samples tending to thermal runaway. However, for this study it was decided the most appropriate way forward with the time remaining was to focus on the beads and alternative forms of analysis.

DC Bead<sup>TM</sup> is a microspherical embolisation medium used for the treatment of arteriovenous malformations and hypervascular tumours [124, 232]. The bead consists of a poly (vinyl alcohol) (PVA) hydrogel polymer that has been modified by the addition of hydrophilic 2-acrylamido-2-methylpropane to contain sulfonate sodium salt components and is blue in colour to allow visualisation of drug loading [132, 233]. The presence of negatively charged sulfonate components on the beads (polymer chain) enables ionic interactions with positively charged drugs which is reversible in ion rich environments such as blood [137]. The beads are available in a range of sizes from 70 – 700  $\mu\text{m}$ . The water content in the beads is > 95 %, enabling diffusion of molecules in and out of the polymer structure [234]. The uptake of drug and rate of elution is dependent upon the size of the bead, as diffusion is inversely proportional to the diameter of the bead, attributed to the increase in the surface area to volume ratio [124].

Nevertheless, a couple of compounds can have a drug-drug interaction, which can affect the binding and elution of drug from the delivery device [132]. Initially, the beads increase in diameter as they are reconstituted with water, as the water is displaced from the bead, the diameter again decreases as the drug is concealed from the solution.

There are numerous factors affecting the biocompatibility of polymers including; ionic charge, chemical groups on the surface, morphological features, surface evenness among others, all of these factors have been examined [235, 236]. One factor that has received lots of interest is the structural changes of the water on the surface of the polymer, it is reasonable to expect that water molecules firmly restrained by biomaterials display distinctive behaviour which is different from bulk surface water [141, 235-237]. Water in hydrogels has been grouped into three main types by Hatakeyama [235] and Bertasa [238]: (1) free water which crystallises at approximately 0 °C and is slightly affected by the matrix polymer, (2) freezing bound water which crystallises during heating at a temperature lower than 0 °C and is strongly affected by the matrix polymer and finally (3) non-freezing water which is non-crystallisable due to strong intermolecular interactions with the matrix polymer. Both freezing bound water and non-freezing bound water are classified as bound water [239].

The state of water restrained by hydrogel systems have been investigated by various techniques, in particular thermal analysis since the phase transition of water behaviour can be identified by this method. Thermal analysis methods including thermogravimetric analysis (TGA) can be utilised to quantify the amount of different fractions of water in polymers through vaporisation as previously carried out by Hatakeyama [142], differential scanning calorimetry (DSC) was previously used to identify three kinds of water from temperature and enthalpy of transition peaks [238] and nuclear magnetic resonance (NMR) for identifying the amounts of water in polymers from relaxation time measurements i.e. correlation time ( $\tau_c$ ) calculated from

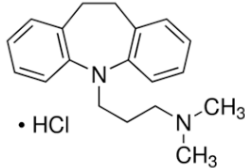
the spin-lattice ( $T_1$ ) and spin-spin relaxation times ( $T_2$ ) of water restrained by biomaterials [235].

## 5.2. Results and discussion

### 5.2.1. Drug loading evaluations

Beads containing imipramine were formulated and analysed as described in the methods section. Drug loading studies permitted calculation of the amount of imipramine hydrochloride loaded per mL of hydrated beads from the three different drug concentration solutions (Table 5.1). For the 10  $\text{mgmL}^{-1}$ , 25  $\text{mgmL}^{-1}$  and 50  $\text{mgmL}^{-1}$  drug concentrations, beads were found to yield 95.2 %, 92.5 % and 61.5 % of the drug respectively. Drug interaction is presumed to be *via* an ion exchange process as for other reported hydrochloride salts [136] through the tertiary amine group pendent to the ring structure. At lower concentrations (10 & 25 mg), loading yield was relatively high (> 90 %) as the number of cationic charged binding groups on the drug was less than the number of anionic sulfonate groups in the bead structure. For the 50  $\text{mgmL}^{-1}$  loading, the number of drug binding groups is in excess and loading is saturated at 62 % loading, where all binding sites are occupied by drug molecules. This equates to around 30  $\text{mgmL}^{-1}$  maximum loading potential for imipramine hydrochloride.

Table 5. 1: Drug structure and loading amount and efficiency in 1 mL of DC Bead *MI* (n=3)

	Target loading ( $\text{mgmL}^{-1}$ )	Loading ( $\text{mgmL}^{-1}$ )	Loading yield (%)
	10	$9.52 \pm 0.01$	$95.19 \pm 0.09$
	25	$23.13 \pm 0.27$	$92.54 \pm 1.09$
	50	$30.76 \pm 2.65$	$61.53 \pm 5.29$

### 5.2.2 Optical microscopy

Optical microscopy analysis of the beads indicated that their average size decreased when drug loading was greater than 10  $\text{mgmL}^{-1}$  (Figure 5.1 and 5.2), with the greatest change seen from  $121 \pm 19 \mu\text{m}$  to  $79 \pm 17 \mu\text{m}$  following loading with the highest concentration of drug (see Table



5.2). This is consistent with what has been observed previously with other cationically charged drugs, where bulky drugs with hydrophobic components enter the hydrogel matrix and bind to the anionic sulfonate moieties, resulting in water being displaced from the interstitial spaces between polymer chains, decreasing the water content and causing the beads to shrink in diameter [124, 138].

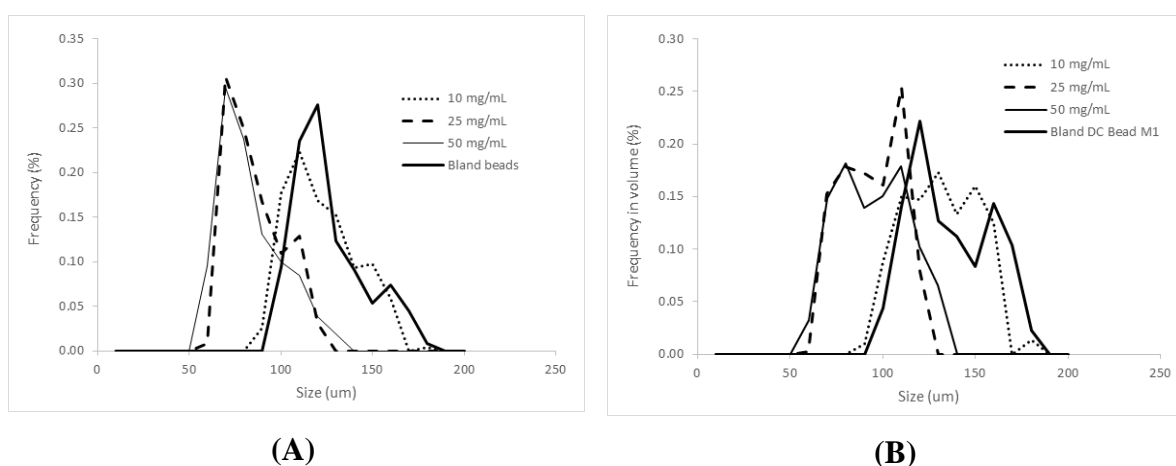


Figure 5. 1. Size (A) and volume (B) distribution of bland DC Bead *MI*, 10 mgmL<sup>-1</sup>, 25 mgmL<sup>-1</sup>, and 50 mgmL<sup>-1</sup> drug loaded beads.

Table 5. 2: Data for bead sizes and estimated water fraction in beads

	Bland	10 mgmL <sup>-1</sup>	25 mgmL <sup>-1</sup>	50 mgmL <sup>-1</sup>
Bead size range (µm)	91.1-175.5	84.4-178.9	57.4-118.2	52.3-124.9
Average diameter of beads ± SD (µm)	121.4 ± 19.4	117.4 ± 18.9	80.9 ± 14.9	78.5 ± 16.8
Estimated water content in beads (v/v)	96.30 % *	95.90 %	87.48 %	86.30 %

\* Data based on a weight measurement previously published by Ashrafi et al. [240].

Figure 5.2 shows optical micrographs of DC Bead *MI* before and after drug loading at different concentrations. The drug loaded beads remain a spherical shape with no signs of deformation or fragmentation. The blue colour is due to the presence of the Reactive Blue 4 tint on the bead structure and the beads loaded with >25 mgmL<sup>-1</sup> drug appear more intense in colour as the bead shrinkage intensifies the appearance of the dye.

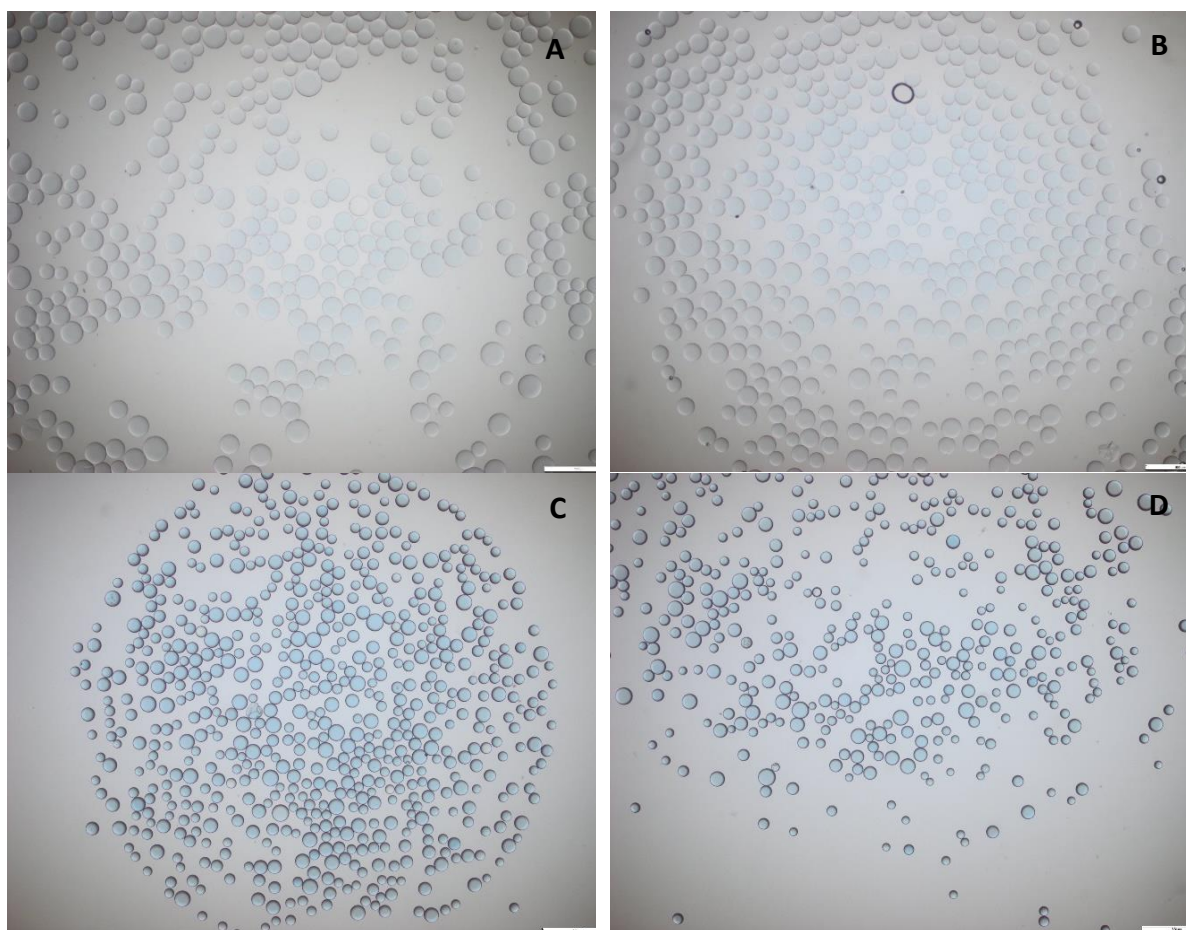


Figure 5. 2. Microscope images of DC Bead *MI* after loading overnight. A) Bland beads. B) 10 mgmL<sup>-1</sup> loading. C) 25 mgmL<sup>-1</sup> loading. D) 50 mgmL<sup>-1</sup> loading. The scale bar is 500 μm.

### 5.2.3 Water content analysis

#### 5.2.3.1 Thermogravimetric analysis (TGA)

TGA was undertaken for three samples of beads with a mass loss of 97.2, 95.6 and 97.5 % indicating the beads to contain an average of 3.2 % solid content and 96.8 % water. Previous research has indicated a percentage of water content of 96.3 % using centrifuged mass loss analysis [240]. This is the first published result using TGA to analyse this type of beads and it is reassuring to see that the values from this work and that published previously are very similar, thus confirming the suitability of TGA as a technique to determine total water content within such beads. Following drug loading, three samples of beads were analysed with a mass loss of 94.6, 95.6 and 96.1 % indicating the beads contained an average of 95.4 % water, i.e. a

1.4 % reduction in water content compared with beads without drug present. This finding correlates well with the results observed regarding bead size in that water content decreased as the beads reduced in size. An example of TGA data obtained for the beads in the absence and presence of drug is shown in Figure 5.3.

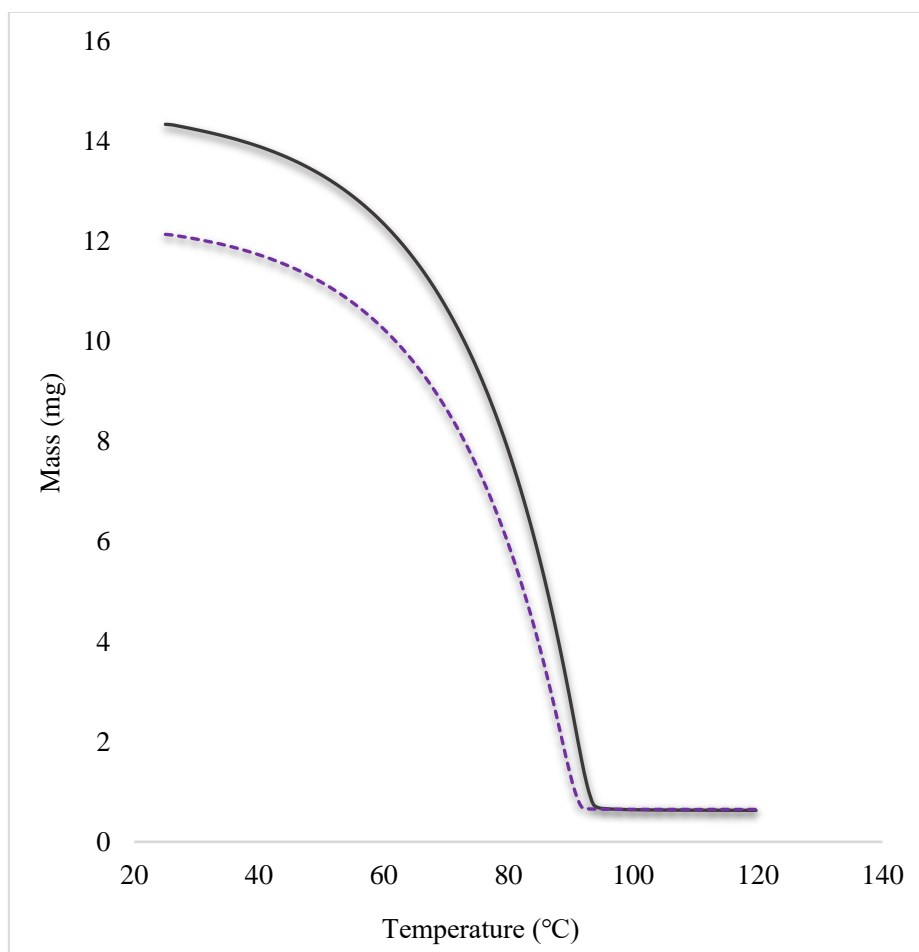


Figure 5. 3. A TGA sample profile for beads alone (solid line) and imipramine with beads (dashed line) indicating the associated mass loss from water.

### 5.2.3.2 Differential scanning calorimetry (DSC)

DSC analysis was completed for the bead samples, both with and without drug present, and also for water, to quantify the extent of the water within the beads that could undergo the freezing process. Examples of the data obtained for water alone and a sample of beads are presented in Figure 5.4.

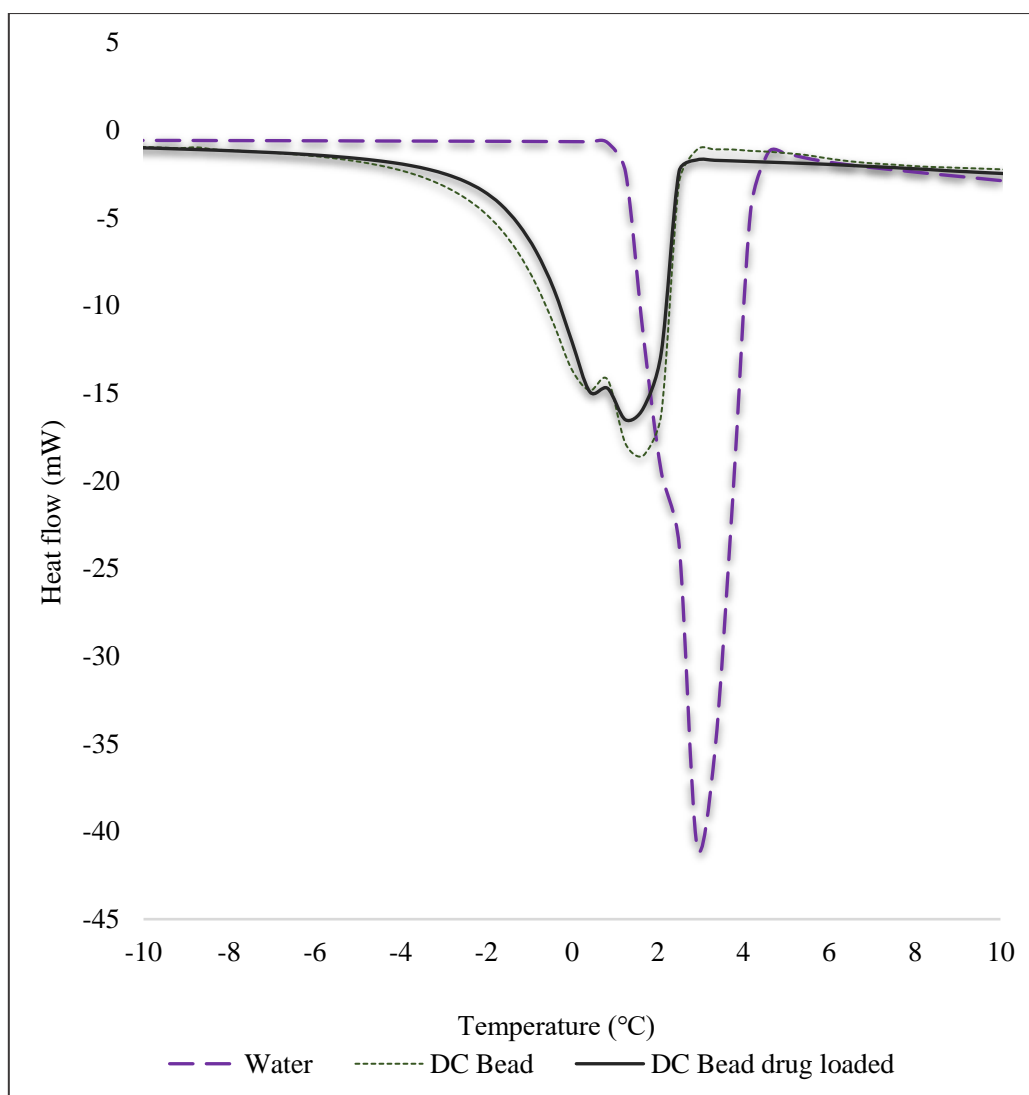


Figure 5. 4. DSC profiles for water, DC Bead *MI* and DC Bead *MI* drug loaded.

Analysis of the data acquired resulted in an average total area for water of  $376.8 \pm 9.2 \text{ Jg}^{-1}$  per mg,  $317.3 \pm 0.6.2 \text{ Jg}^{-1}$  per mg for beads without drug (assuming an average water content of 96.8 %) and  $314.1 \pm 9.3 \text{ Jg}^{-1}$  per mg for the beads with drug (assuming an average water content of 95.4 %). As the error associated with the two bead profiles is greater than the difference between the values it can be concluded that there was no significant difference in the data, thus implying a similar percentage of water within the beads was available to undergo the freezing process. However, these values are lower than that recorded for water alone, thus a proportion of the water within the beads was so tightly bound that it was unable to freeze (known as non-freezing), as seen in other similar systems [241-243]. Through subtracting the normalised

integral for the beads from that of pure water it was possible to calculate the percentage of non-freezing water present within the beads, with a value for beads alone of 15.8 % ( $\pm 3.2$  %) and beads with drug of 16.7 % ( $\pm 2.9$  %). These findings indicate that the presence of drug did not affect the non-freezing water content of the beads with both values being similar within experimental error. Interestingly, the peaks observed for the beads alone, and with drug, were not symmetrical, implying that DSC was able to differentiate between the two remaining types of water within the beads, i.e. that which is loosely bound (known as freezing bound) and the remainder which is unbound (known as free water). Through deconvolution of the peaks and subsequent integration of the areas it was possible to determine the percentages of the two within the bead. For beads without drug present the 81.0 % water content that was not non-freezing can be further subdivided into 25.1 % loosely bound with the remaining 55.9 % unbound. For beads with drug present the 78.7 % water content that was not non-freezing can be further subdivided into 20.5 % loosely bound with the remaining 58.2 % unbound, indicating that the presence of drug more significantly decreased the freezing bound water within the bead rather than the unbound water. This finding infers that the drug is binding within the beads by replacing some of the freezing bound water rather than unbound water, explaining the modified release within dissolution analysis as some of the drug is initially bound within the sulfonate moieties in the bead before releasing more slowly over time.

### **5.3. Conclusions**

In summary, previous studies had focussed on the application of such beads purely for embolisation purposes, in conjunction with drug delivery. In this analysis, significant differences in the overall water content was demonstrated by DC Bead™ and in the properties of water and imipramine concentration loaded into beads. Thermogravimetric analysis of mass loss as a function of temperature provided a constant decrease in mass as the temperature

increased. In particular, an average of 3.2 % beads solid content and 96.8 % total water content were recorded due to evaporation.

Estimates on the amount of bound water and non-bound water were obtained by DSC measurements. The analysis of DSC data provided the enthalpy of melting, area in  $\text{Jg}^{-1}$  per mg for water, beads with drug and the beads without drug. It was found that for beads without drug the amount of non-freezing water was approximately 81.0 % in which 25.1 % was loosely bound with the remaining 55.9 % unbound. For beads with drug present the 78.7 % water content that was not non-freezing can be further subdivided into 20.5 % loosely bound with the remaining 58.2 % unbound, indicating that the presence of drug more significantly decreased the freezing bound water within the bead rather than the unbound water.

These results provide an insight into the binding behaviour of water within the beads and how this is affected by the presence of the drug

## **Chapter 6: Conclusions and Future work**

### **6.1. Conclusions**

The objectives of this thesis as highlighted in Chapter One were successfully achieved and are summarised as follows;

The first objective was to investigate the suitability of using three types of Syloid<sup>®</sup> silica-based excipients to quantify their potential to enhance the rate of dissolution of drugs and determine the causes of any enhancements observed. It has been confirmed that it is possible to formulate Syloid<sup>®</sup> silica-based formulations to enhance the dissolution of poorly soluble drugs using a microwave formulation method, in this case, phenylbutazone, indomethacin and imipramine which is more soluble compared to the former two.

The formulations were prepared first by simple physical mixing at different ratios and second a highly developed microwave method and finally, the resultant products were subsequently analysed utilising a variety of analytical techniques. The resultant products from the microwave method exhibited improved drug release compared with the pure drugs in agreement with other analysis [148]. Solid-state characterisation of the samples implies that there are transformations of the drugs from a crystalline state to a more amorphous form as confirmed by DSC and XRD. Furthermore, data obtained implies this enhancement is a result of a change in crystallinity and the ability of the drug to enter pores within the Syloid<sup>®</sup> silica structure.

For functional group identification and also to ensure that long term stability is not a limiting factor for formulation possibilities, FT-IR analysis was carried before and after formulation and no interactions were observed other than the drugs used and the three Syloid<sup>®</sup> silicas under analysis. All Syloid<sup>®</sup> silicas analysed demonstrated a dramatic increase in percentage release with their final percentage values linked to the Syloid<sup>®</sup> silica pore diameter and/or surface area.

SEM images demonstrated that at the highest drug to silica ratio investigated, it was possible to achieve a uniformly distributed mixed product.

This finding can be of benefit for not only phenylbutazone, indomethacin and imipramine-based formulations but potentially a far wider range of compounds that exhibit poor aqueous solubility which will help alleviate bioavailability issues.

The second objective was to use MWDTA on model pharmaceutical compounds to investigate the potential application of this form of thermal analysis on such compounds as an indicator of the suitability of microwave-based formulation methods. The effect of microwave heating was studied through the application of microwave differential thermal analysis to different model pharmaceutical compounds and a set of four model pharmaceutical excipients. The profiles were analysed and compared with the data generated using differential scanning calorimetry (DSC), X-ray powder diffraction (XRD) and hot stage microscopy (HSM). The results demonstrated that microwave differential thermal analysis (MWDTA) can be utilised to detect a wide range of thermal transitions including melting, recrystallisation, dehydration phase changes and dielectric change via changes in the materials ability to absorb microwave energy.

For some drugs, the dielectric change was significantly high from looking at the profiles generated while intermediate and low dielectric changes were observed in other drugs analysed. The dielectric properties of a multicomponent mixture are dependent on the dielectric properties of the components. The thermal transition temperatures are slightly lower or higher in MWDTA than those observed with the conventional DSC method. This effect has been reported previously but has not received a complete explanation [213]. It should be recalled that the peaks seen in conventional techniques arise solely from the transformation enthalpy itself, while the temperature changes seen in MWDTA result primarily from the emergence of a product or phase that has different dielectric properties.



Overall, it was found that the process of microwave heating produced different thermal profiles to those seen using traditional, conductive heating. Investigating differences in thermal profiles can be a useful way to consider the effect of microwave-induced heating on formulations.

The final objective was to portray the potential of TGA and DSC to quantify and characterise the water present within beads, including the incorporation of imipramine to exemplify the effect of drugs on the relative water profiles. The investigations carried out on beads revealed significant differences in the overall water content and in the properties of water. TGA analysis of weight loss as a function of temperature showed a constant decline in weight of the sample as the temperature increased. The technique facilitated a simple and rapid form of analysis to determine the total water content within beads alone or in the presence of three model compounds. Furthermore, DSC was successfully employed to look into the water content in more detail, to identify the tightly bound, loosely bound and unbound percentages within the samples analysed. The values obtained provided the heat of melting of loosely bound and unbound water in the beads.

The results presented in this study confirm the suitability of TGA and DSC to investigate such beads with respect to their water content and could potentially be applicable to an even wider variety of bead types available commercially. Knowledge of how drugs interact with the polymers is incredibly useful when trying to understand the nature of the drug-bead interactions.

## 6.2. Future work

This work can be improved further in many areas of potential opportunity to develop the scope of the techniques including:

### (I) Optimisation of the microwave method

Drugs with a variable melting point range could be processed to evaluate possible effects of heating on the resultant formulations. Moreover, rather than using syloid silicas, the work could be expanded further using other excipients like D-mannitol, stearic acid, cyclodextrin, natural and synthetic polymers such as chitosan, pectin and gelucire. This could ultimately lead to a large range of formulation possibilities.

Microwave dielectric thermal analysis (MWDTA), dielectric constant, dielectric loss factor, and dielectric loss tangent of all the studied compounds can be measured directly as a function of temperature using a dielectric spectrometer. It would be interesting to link the results obtained with MWDTA to fundamental dielectric measurements.

An area where the MWDTA technique itself could be developed is through the addition of cooling apparatus. The addition of a cooling system will provide several advantages including allowing the user to perform experiments at room /ambient temperatures. This will also enable the characterisation of different proportions of water within polymer beads which will be interesting to link the results obtained with DSC and TGA measurements to MWDTA. Furthermore, better temperature control could be achieved with cooling apparatus, particularly with samples tending to thermal runaway.

The ability to compare directly the MWDTA responses with DSC calculations of the energy of transitions should be investigated further, along with profiles of transitions types.

In conventional techniques like differential thermal analysis (DTA) and DSC analysis, increasing the heating rate often leads to sharper transitions and it would be interesting to see

whether the same style is achievable using MWDTA. Rapid heating rates such as 10 or 20 °C/min were generally avoided during the current research as they adversely affected temperature control.

## (II) Expansion of analytical techniques

Techniques including DSC, XRD, FTIR and SEM were used to investigate crystallinity, surface morphologies and thermal transitions as well as the stability of resultant products. However, other techniques such as transmission electron microscopy (TEM) could help in investigating the physical state of the drug within a formulation.

## (III) Bound water analysis

Other types and sizes of DC beads such as 100 – 300, 300 – 500 and 500 – 700 µm should be analysed to explore the state of water and the types of water (the tightly bound, loosely bound and unbound) within such beads. Other drugs such as doxorubicin and irinotecan could be incorporated into such beads for identification and quantification of the influence of drug concentrations on the water behaviour.

Techniques such as proton nuclear magnetic resonance (<sup>1</sup>H NMR) could be used to investigate the water mobility and localisation surrounding the hydrogel network. <sup>1</sup>H NMR could provide an in-depth analysis about the hydrogel deformation due to water release and to evaluate the ability of the hydrogel in controlling the water release into a porous substance.

## References

1. Bukara, K., L. Schueller, J. Rosier, M.A. Martens, T. Daems, L. Verheyden, S. Eelen, M. Van Speybroeck, C. Libanati, and J.A. Martens, *Ordered mesoporous silica to enhance the bioavailability of poorly water-soluble drugs: Proof of concept in man*. European Journal of Pharmaceutics and Biopharmaceutics, 2016. **108**: p. 220-225.
2. Ke, J., Y. Wang, L. Wang, B. Yang, K. Gou, Y. Qin, S. Li, and H. Li, *Synthesis and characterization of core-shell mesoporous silica nanoparticles with various shell thickness as indomethacin carriers: In vitro and in vivo evaluation*. Microporous and Mesoporous Materials, 2020. **297**: p. 110043.
3. Zhu, M., H. Wang, J. Liu, H. He, X. Hua, Q. He, L. Zhang, X. Ye, and J. Shi, *A mesoporous silica nanoparticulate/ $\beta$ -TCP/BG composite drug delivery system for osteoarticular tuberculosis therapy*. Biomaterials, 2011. **32**(7): p. 1986-1995.
4. Zhou, T., N. Song, S.H. Xu, B. Dong, and Y.W. Yang, *Dual-Responsive Mechanized Mesoporous Silica Nanoparticles Based on Sulfonatocalixarene Supramolecular Switches*. ChemPhysChem, 2016. **17**(12): p. 1840-1845.
5. Eren, Z.S., S. Tunçer, G. Gezer, L.T. Yildirim, S. Banerjee, and A. Yilmaz, *Improved solubility of celecoxib by inclusion in SBA-15 mesoporous silica: Drug loading in different solvents and release*. Microporous and Mesoporous Materials, 2016. **235**: p. 211-223.
6. Waters, L.J., T. Hussain, G. Parkes, J.P. Hanrahan, J.M.J.E.J.o.P. Tobin, and Biopharmaceutics, *Inclusion of fenofibrate in a series of mesoporous silicas using microwave irradiation*. 2013. **85**(3): p. 936-941.
7. Gullapalli, R.P. and C.L. Mazzitelli, *Gelatin and non-gelatin capsule dosage forms*. Journal of pharmaceutical sciences, 2017. **106**(6): p. 1453-1465.
8. Peralta, M.E., S.A. Jadhav, G. Magnacca, D. Scalarone, D.O. Mártire, M.E. Parolo, and L. Carlos, *Synthesis and in vitro testing of thermoresponsive polymer-grafted core-shell magnetic mesoporous silica nanoparticles for efficient controlled and targeted drug delivery*. Journal of colloid and interface science, 2019. **544**: p. 198-205.
9. Mahajan, M. and S. Rajput, *Development of mesoporous silica nanoparticles of ritonavir with enhanced bioavailability potential: formulation optimization, in-vitro and in-vivo evaluation*. drug delivery system, 2018. **22**: p. 23.
10. Maleki, A., H. Kettiger, A. Schoubben, J.M. Rosenholm, V. Ambroggi, and M. Hamidi, *Mesoporous silica materials: From physico-chemical properties to enhanced dissolution of poorly water-soluble drugs*. Journal of Controlled Release, 2017. **262**: p. 329-347.
11. Waters, L.J., J.P. Hanrahan, J.M. Tobin, C.V. Finch, G.M. Parkes, S.A. Ahmad, F. Mohammad, and M. Saleem, *Enhancing the dissolution of phenylbutazone using Syloid® based mesoporous silicas for oral equine applications*. Journal of pharmaceutical analysis, 2018. **8**(3): p. 181-186.
12. Manna, S., Y. Wu, Y. Wang, B. Koo, L. Chen, P. Petrochenko, Y. Dong, S. Choi, D. Kozak, and B. Oktem, *Probing the mechanism of bupivacaine drug release from multivesicular liposomes*. Journal of controlled release, 2019. **294**: p. 279-287.

13. Budai-Szűcs, M., E.L. Kiss, B.Á. Szilágyi, A. Szilágyi, B. Gyarmati, S. Berkó, A. Kovács, G. Horvát, Z. Aigner, and J. Soós, *Mucoadhesive cyclodextrin-modified thiolated poly (aspartic acid) as a potential ophthalmic drug delivery system*. *Polymers*, 2018. **10**(2): p. 199.
14. Wersig, T., R. Krombholz, C. Janich, A. Meister, J. Kressler, and K. Mäder, *Indomethacin functionalised poly (glycerol adipate) nanospheres as promising candidates for modified drug release*. *European Journal of Pharmaceutical Sciences*, 2018. **123**: p. 350-361.
15. Dey, M., M. Das, A. Chowhan, and T.K. Giri, *Breaking the barricade of oral chemotherapy through polysaccharide nanocarrier*. *International journal of biological macromolecules*, 2019.
16. Biopharma-asia. *Syloid® XDP Silicas Oil Adsorption Capacity*. 2020 23/05/2014 [cited 2020 01/04/2020]; Available from: <https://biopharma-asia.com/technical-papers/syloid-xdp-silica-optimized-for-liquisolid-and-lipid-based-formulations/>.
17. Linnell, T., H.A. Santos, E. Mäkilä, T. Heikkilä, J. Salonen, D.Y. Murzin, N. Kumar, T. Laaksonen, L. Peltonen, and J. Hirvonen, *Drug delivery formulations of ordered and nonordered mesoporous silica: Comparison of three drug loading methods*. *Journal of Pharmaceutical Sciences*, 2011. **100**(8): p. 3294-3306.
18. Kinnari, P., E. Mäkilä, T. Heikkilä, J. Salonen, J. Hirvonen, and H.A. Santos, *Comparison of mesoporous silicon and non-ordered mesoporous silica materials as drug carriers for itraconazole*. *International Journal of Pharmaceutics*, 2011. **414**(1-2): p. 148-156.
19. Linnell, T., H.A. Santos, E. Mäkilä, T. Heikkilä, J. Salonen, D.Y. Murzin, N. Kumar, T. Laaksonen, L. Peltonen, and J.J.J.o.p.s. Hirvonen, *Drug delivery formulations of ordered and nonordered mesoporous silica: comparison of three drug loading methods*. 2011. **100**(8): p. 3294-3306.
20. Heikkilä, T., J. Salonen, J. Tuura, N. Kumar, T. Salmi, D.Y. Murzin, M. Hamdy, G. Mul, L. Laitinen, and A.M. Kaukonen, *Evaluation of mesoporous TCPSi, MCM-41, SBA-15, and TUD-1 materials as API carriers for oral drug delivery*. *Drug delivery*, 2007. **14**(6): p. 337-347.
21. Mellaerts, R., J.A. Jammaer, M. Van Speybroeck, H. Chen, J.V. Humbeeck, P. Augustijns, G. Van den Mooter, and J.A. Martens, *Physical state of poorly water soluble therapeutic molecules loaded into SBA-15 ordered mesoporous silica carriers: a case study with itraconazole and ibuprofen*. *Langmuir*, 2008. **24**(16): p. 8651-8659.
22. Saffari, M., A. Ebrahimi, and T. Langrish, *A novel formulation for solubility and content uniformity enhancement of poorly water-soluble drugs using highly-porous mannitol*. *European Journal of Pharmaceutical Sciences*, 2016. **83**: p. 52-61.
23. Van Nguyen, H., C. Park, E. Oh, and B.-J. Lee, *Improving the dissolution rate of a poorly water-soluble drug via adsorption onto pharmaceutical diluents*. *Journal of Drug Delivery Science and Technology*, 2016. **35**: p. 146-154.
24. Savjani, K.T., A.K. Gajjar, and J.K. Savjani, *Drug solubility: importance and enhancement techniques*. *ISRN pharmaceutics*, 2012. **2012**.
25. Blagden, N., M. de Matas, P.T. Gavan, and P. York, *Crystal engineering of active pharmaceutical ingredients to improve solubility and dissolution rates*. *Advanced drug delivery reviews*, 2007. **59**(7): p. 617-630.

26. Nacsá, A., R. Ambrus, O. Berkesi, P. Szabo-Revesz, and Z. Aigner, *Water-soluble loratadine inclusion complex: analytical control of the preparation by microwave irradiation*. Journal of pharmaceutical and biomedical analysis, 2008. **48**(3): p. 1020-1023.
27. Khan, S., H. Batchelor, P. Hanson, Y. Perrie, and A.R. Mohammed, *Physicochemical characterisation, drug polymer dissolution and in vitro evaluation of phenacetin and phenylbutazone solid dispersions with polyethylene glycol 8000*. Journal of pharmaceutical sciences, 2011. **100**(10): p. 4281-4294.
28. Mendonsa, N., B. Almutairy, V.R. Kallakunta, S. Sarabu, P. Thipsay, S. Bandari, and M.A. Repka, *Manufacturing strategies to develop amorphous solid dispersions: An overview*. Journal of Drug Delivery Science and Technology, 2020. **55**: p. 101459.
29. Crowley, M.M., F. Zhang, M.A. Repka, S. Thumma, S.B. Upadhye, S. Kumar Battu, J.W. McGinity, and C. Martin, *Pharmaceutical applications of hot-melt extrusion: part I*. Drug development and industrial pharmacy, 2007. **33**(9): p. 909-926.
30. Repka, M.A., S.K. Battu, S.B. Upadhye, S. Thumma, M.M. Crowley, F. Zhang, C. Martin, and J.W. McGinity, *Pharmaceutical applications of hot-melt extrusion: Part II*. Drug development and industrial pharmacy, 2007. **33**(10): p. 1043-1057.
31. Ye, X., H. Patil, X. Feng, R.V. Tiwari, J. Lu, A. Gryczke, K. Kolter, N. Langley, S. Majumdar, and D. Neupane, *Conjugation of hot-melt extrusion with high-pressure homogenization: a novel method of continuously preparing nanocrystal solid dispersions*. Aaps Pharmscitech, 2016. **17**(1): p. 78-88.
32. Kallakunta, V.R., R. Tiwari, S. Sarabu, S. Bandari, and M.A. Repka, *Effect of formulation and process variables on lipid based sustained release tablets via continuous twin screw granulation: A comparative study*. European Journal of Pharmaceutical Sciences, 2018. **121**: p. 126-138.
33. Mendonsa, N.S., A. Pradhan, P. Sharma, R.M. Prado, S.N. Murthy, S. Kundu, and M.A. Repka, *A quality by design approach to develop topical creams via hot-melt extrusion technology*. European Journal of Pharmaceutical Sciences, 2019. **136**: p. 104948.
34. Patil, H., V. Kulkarni, S. Majumdar, and M.A. Repka, *Continuous manufacturing of solid lipid nanoparticles by hot melt extrusion*. International journal of pharmaceutics, 2014. **471**(1-2): p. 153-156.
35. Zhang, J., L. Wu, H.-K. Chan, and W. Watanabe, *Formation, characterization, and fate of inhaled drug nanoparticles*. Advanced drug delivery reviews, 2011. **63**(6): p. 441-455.
36. Chiou, H., H.-K. Chan, R.K. Prud'homme, and J.A. Raper, *Evaluation on the use of confined liquid impinging jets for the synthesis of nanodrug particles*. Drug development and industrial pharmacy, 2008. **34**(1): p. 59-64.
37. Wang, S., S. Devahastin, and A. Mujumdar, *Effect of temperature difference on flow and mixing characteristics of laminar confined opposing jets*. Applied Thermal Engineering, 2006. **26**(5-6): p. 519-529.
38. Scholz, A., B. Abrahamsson, S.M. Diebold, E. Kostewicz, B.I. Polentarutti, A.-L. Ungell, and J.B. Dressman, *Influence of hydrodynamics and particle size on the absorption of felodipine in labradors*. Pharmaceutical research, 2002. **19**(1): p. 42-46.
39. Kawabata, Y., K. Wada, M. Nakatani, S. Yamada, and S. Onoue, *Formulation design for poorly water-soluble drugs based on biopharmaceutics classification system: basic approaches and practical applications*. International journal of pharmaceutics, 2011. **420**(1): p. 1-10.

40. Vasconcelos, T., B. Sarmiento, and P. Costa, *Solid dispersions as strategy to improve oral bioavailability of poor water soluble drugs*. Drug discovery today, 2007. **12**(23-24): p. 1068-1075.
41. Tachibana, T. and A. Nakamura, *A methode for preparing an aqueous colloidal dispersion of organic materials by using water-soluble polymers: Dispersion of  $\beta$ -carotene by polyvinylpyrrolidone*. Kolloid-Zeitschrift und Zeitschrift für Polymere, 1965. **203**(2): p. 130-133.
42. Vo, C.L.-N., C. Park, and B.-J. Lee, *Current trends and future perspectives of solid dispersions containing poorly water-soluble drugs*. European journal of pharmaceutics and biopharmaceutics, 2013. **85**(3): p. 799-813.
43. Desai, J., K. Alexander, and A. Riga, *Characterization of polymeric dispersions of dimenhydrinate in ethyl cellulose for controlled release*. International journal of pharmaceutics, 2006. **308**(1-2): p. 115-123.
44. Hussain, T., *The application of microwave formulation and isothermal titration calorimetry for pharmaceutical compounds*. 2014, University of Huddersfield.
45. Desai, P.P., A.A. Date, and V.B. Patravale, *Overcoming poor oral bioavailability using nanoparticle formulations—opportunities and limitations*. Drug Discovery Today: Technologies, 2012. **9**(2): p. e87-e95.
46. Fasinu, P., V. Pillay, V.M. Ndesendo, L.C. du Toit, and Y.E. Choonara, *Diverse approaches for the enhancement of oral drug bioavailability*. Biopharmaceutics & drug disposition, 2011. **32**(4): p. 185-209.
47. Amidon, G.L., H. Lennernäs, V.P. Shah, and J.R. Crison, *A theoretical basis for a biopharmaceutic drug classification: the correlation of in vitro drug product dissolution and in vivo bioavailability*. Pharmaceutical research, 1995. **12**(3): p. 413-420.
48. Date, A.A., N. Desai, R. Dixit, and M. Nagarsenker, *Self-nanoemulsifying drug delivery systems: formulation insights, applications and advances*. Nanomedicine, 2010. **5**(10): p. 1595-1616.
49. Alam, M.A., F.I. Al-Jenoobi, and A.M. Al-mohizea, *Commercially bioavailable proprietary technologies and their marketed products*. Drug Discovery Today, 2013. **18**(19-20): p. 936-949.
50. Langham, Z.A., *Design and performance of felodipine-based solid dispersions*. 2011, University of Nottingham.
51. Silva, F.V., S. Resende, A.N. Araújo, and J.A. Prior, *Determination of  $pK_a$  (s) of nilutamide through UV-visible spectroscopy*. Microchemical Journal, 2018. **138**: p. 303-308.
52. Babić, S., A.J. Horvat, D.M. Pavlović, and M. Kaštelan-Macan, *Determination of  $pK_a$  values of active pharmaceutical ingredients*. TrAC Trends in Analytical Chemistry, 2007. **26**(11): p. 1043-1061.
53. Hörter, D. and J. Dressman, *Influence of physicochemical properties on dissolution of drugs in the gastrointestinal tract*. Advanced drug delivery reviews, 2001. **46**(1-3): p. 75-87.
54. Avdeef, A., *pH-metric log P. II: Refinement of partition coefficients and ionization constants of multiprotic substances*. Journal of pharmaceutical sciences, 1993. **82**(2): p. 183-190.
55. Shore, P.A., B.B. Brodie, and C.A.M. Hogben, *The gastric secretion of drugs: a pH partition hypothesis*. Journal of Pharmacology and Experimental Therapeutics, 1957. **119**(3): p. 361-369.
56. Shalaeva, M., J. Kenseth, F. Lombardo, and A. Bastin, *Measurement of dissociation constants ( $pK_a$  values) of organic compounds by multiplexed capillary electrophoresis using aqueous and cosolvent buffers*. Journal of pharmaceutical sciences, 2008. **97**(7): p. 2581-2606.

57. Gaisford, S. and M. Saunders, *Essentials of pharmaceutical preformulation*. 2012: John Wiley & Sons.
58. Bedford, S., *The Application of Microwave Heating Methods in Pharmaceutical Formulations*. 2011, University of Huddersfield.
59. Lin, S.-Y., H.-L. Lin, Y.-T. Chi, Y.-T. Huang, C.-Y. Kao, and W.-H. Hsieh, *Thermoanalytical and Fourier transform infrared spectral curve-fitting techniques used to investigate the amorphous indomethacin formation and its physical stability in Indomethacin-Soluplus® solid dispersions*. *International journal of pharmaceutics*, 2015. **496**(2): p. 457-465.
60. Separovic, L., A.M. Saviano, and F.R. Lourenço, *Using measurement uncertainty to assess the fitness for purpose of an HPLC analytical method in the pharmaceutical industry*. *Measurement*, 2018. **119**: p. 41-45.
61. Miao, Q., Y. Cui, J. Zhang, Y. Mi, W. Tan, Q. Li, G. Gu, F. Dong, and Z. Guo, *Determination of chitosan content with ratio coefficient method and HPLC*. *International Journal of Biological Macromolecules*, 2020. **164**: p. 384-388.
62. Nasuno, R., S. Shino, Y. Yoshikawa, N. Yoshioka, Y. Sato, K. Kamiya, and H. Takagi, *Detection system of the intracellular nitric oxide in yeast by HPLC with a fluorescence detector*. *Analytical Biochemistry*, 2020: p. 113707.
63. Chemistry, R.S.O. *High Performance Liquid Chromatography HPLC*. 2008 [cited 2020 26/10/2020]; Available from: [https://www.youtube.com/watch?v=kz\\_egMtdnL4](https://www.youtube.com/watch?v=kz_egMtdnL4).
64. Mondal, B., M. Kote, C. Lunagariya, and M. Patel, *Development of a simple high performance liquid chromatography (HPLC)/evaporative light scattering detector (ELSD) method to determine Polysorbate 80 in a pharmaceutical formulation*. *Saudi Pharmaceutical Journal*, 2020.
65. Pavia, D.L., G.M. Lampman, G.S. Kriz, and J.A. Vyvyan, *Introduction to spectroscopy*. 2008: Cengage Learning.
66. Chemistry, R.S.O. *Ultraviolet/Visible Spectroscopy (UV-Vis)*. 2008 [cited 2020 26/10/2020]; Available from: <https://www.youtube.com/watch?v=O39avevqndU>.
67. Passos, M.L. and M.L.M. Saraiva, *Detection in UV-visible spectrophotometry: Detectors, detection systems, and detection strategies*. *Measurement*, 2019. **135**: p. 896-904.
68. Ferreira, C.P., F.T.T. Antunes, I.N. Rebelo, C.A. da Silva Junior, F.N. Vilanova, D.S. Corrêa, and A.H. de Souza, *Application of the UV-Vis Spectrophotometry Method for the Determination of Glutamate in the Cerebrospinal Fluid of Rats*. *Journal of Pharmaceutical and Biomedical Analysis*, 2020: p. 113290.
69. Stam, D.M., D. Banfield, P.J. Gierasch, P.D. Nicholson, and K. Matthews, *Near-IR spectrophotometry of saturnian aerosols—Meridional and vertical distribution*. *Icarus*, 2001. **152**(2): p. 407-422.
70. Chemistry, R.S.O. *Infrared spectroscopy (IR)*. 2008 [cited 2020 27/10/2020]; Available from: <https://www.youtube.com/watch?v=DDTIJgIh86E>.
71. Staniloae, D., B. Petrescu, and C. Patroescu, *Pattern recognition based software for oil spills identification by gas-chromatography and IR spectrophotometry*. *Environmental Forensics*, 2001. **2**(4): p. 363-366.
72. Leng, J., J. Sidorowich, M. Senko, and J. Opsal, *Simultaneous measurement of six layers in a silicon on insulator film stack using visible-near-IR spectrophotometry and single-wavelength beam profile reflectometry*. *Thin solid films*, 1998. **313**: p. 270-275.



73. Colman, T.A.D., I.M. Demiate, and E. Schnitzler, *The effect of microwave radiation on some thermal, rheological and structural properties of cassava starch*. Journal of Thermal Analysis and Calorimetry, 2014. **115**(3): p. 2245-2252.
74. Singh, S., K.K. Gaikwad, M. Lee, and Y.S. Lee, *Microwave-assisted micro-encapsulation of phase change material using zein for smart food packaging applications*. Journal of Thermal Analysis and Calorimetry, 2017: p. 1-9.
75. Kersting, D.F., H. Wiebeck, and F.J. Esper, *Processing and Characterization of Composites Curing by Microwave Irradiation*. Macromolecular Symposia, 2016. **367**(1): p. 49-54.
76. Lewis, D.A., J.D. Summers, T.C. Ward, and J.E. McGrath, *Accelerated imidization reactions using microwave radiation*. Journal of Polymer Science Part A: Polymer Chemistry, 1992. **30**(8): p. 1647-1653.
77. Wu, L., H. Zhu, and K. Huang, *Thermal analysis on the process of microwave-assisted biodiesel production*. Bioresource Technology, 2013. **133**: p. 279-284.
78. Otsuka, M., Y. Maeno, T. Fukami, M. Inoue, T. Tagami, and T. Ozeki, *Solid dispersions of efonidipine hydrochloride ethanolate with improved physicochemical and pharmacokinetic properties prepared with microwave treatment*. European Journal of Pharmaceutics and Biopharmaceutics, 2016. **108**: p. 25-31.
79. Fuliaş, A., G. Vlase, T. Vlase, L.M. Şuta, C. Şoica, and I. Ledeti, *Screening and characterization of cocrystal formation between carbamazepine and succinic acid*. Journal of Thermal Analysis and Calorimetry, 2015. **121**(3): p. 1081-1086.
80. Bergese, P., I. Colombo, D. Gervasoni, and L.E. Depero, *Microwave generated nanocomposites for making insoluble drugs soluble*. Materials Science and Engineering C, 2003. **23**(6-8): p. 791-795.
81. Hussain, T., L.J. Waters, G.M.B. Parkes, and Y. Shahzad, *Microwave processed solid dispersions for enhanced dissolution of gemfibrozil using non-ordered mesoporous silica*. Colloids and Surfaces A: Physicochemical and Engineering Aspects, 2017. **520**: p. 428-435.
82. Wong, T.W., *Use of microwave in processing of drug delivery systems*. Current Drug Delivery, 2008. **5**(2): p. 77-84.
83. Solanki, H.K., V.D. Prajapati, and G.K. Jani, *Microwave technology-A potential tool in pharmaceutical science*. International Journal of PharmTech Research, 2010. **2**(3): p. 1754-1761.
84. Bonde, M.N., A.C. Sohani, A.S. Daud, and N.P. Sapkal, *Microwave: An emerging trend in pharmaceutical processes and formulations*. International Journal of Pharmacy and Technology, 2011. **3**(4): p. 3499-3520.
85. Moneghini, M., B. Bellich, P. Baxa, and F. Princivale, *Microwave generated solid dispersions containing ibuprofen*. International journal of pharmaceutics, 2008. **361**(1-2): p. 125-130.
86. McLoughlin, C., W. McMinn, and T. Magee, *Microwave drying of pharmaceutical powders*. Food and bioproducts processing, 2000. **78**(2): p. 90-96.
87. Waters, L.J., S. Bedford, and G.M.B. Parkes, *Controlled microwave processing applied to the pharmaceutical formulation of ibuprofen*. AAPS PharmSciTech, 2011. **12**(4): p. 1038-1043.
88. Waters, L.J., T. Hussain, G. Parkes, J.P. Hanrahan, and J.M. Tobin, *Inclusion of fenofibrate in a series of mesoporous silicas using microwave irradiation*. European Journal of Pharmaceutics and Biopharmaceutics, 2013. **85**(3 PART B): p. 936-941.

89. Doreth, M., M.A. Hussein, P.A. Priemel, H. Grohganz, R. Holm, H. Lopez de Diego, T. Rades, and K. Löbmann, *Amorphization within the tablet: Using microwave irradiation to form a glass solution in situ*. International Journal of Pharmaceutics, 2017. **519**(1-2): p. 343-351.
90. Parkes, G.M.B., P.A. Barnes, E.L. Charsley, and G. Bond, *Microwave differential thermal analysis in the investigation of thermal transitions in materials*. Analytical Chemistry, 1999. **71**(22): p. 5026-5032.
91. Kappe, C.O., A. Stadler, and D. Dallinger, *Microwave theory*. Microwaves in Organic and Medicinal Chemistry, Second Edition, 2012: p. 9-39.
92. Kostas, E.T., D. Beneroso, and J.P. Robinson, *The application of microwave heating in bioenergy: A review on the microwave pre-treatment and upgrading technologies for biomass*. Renewable and Sustainable Energy Reviews, 2017. **77**: p. 12-27.
93. Motasemi, F. and F. Ani, *A review on microwave-assisted production of biodiesel*. Renewable and Sustainable Energy Reviews, 2012. **16**(7): p. 4719-4733.
94. von Hippel, A.R. and S. Morgan, *Dielectric materials and applications*. Journal of The Electrochemical Society, 1955. **102**(3): p. 68C-68C.
95. Parkes, G., P. Barnes, E. Charsley, and G. Bond, *Microwave thermal analysis-A new approach to the study of the thermal and dielectric properties of materials*. Journal of thermal analysis and calorimetry, 1999. **56**(2): p. 723-731.
96. Remya, N. and J.-G. Lin, *Current status of microwave application in wastewater treatment—a review*. Chemical Engineering Journal, 2011. **166**(3): p. 797-813.
97. Lidström, P., J. Tierney, B. Wathey, and J. Westman, *Microwave assisted organic synthesis—a review*. Tetrahedron, 2001. **57**(45): p. 9225-9283.
98. Kerč, J., S. Srčić, and B. Kofler, *Alternative solvent-free preparation methods for felodipine surface solid dispersions*. Drug development and industrial pharmacy, 1998. **24**(4): p. 359-363.
99. Taherzadeh, M.J. and K. Karimi, *Pretreatment of lignocellulosic wastes to improve ethanol and biogas production: a review*. International journal of molecular sciences, 2008. **9**(9): p. 1621-1651.
100. Karmazsin, E., *Use of low-and high-power microwave energy for thermal analysis*. Thermochemica Acta, 1987. **110**: p. 289-295.
101. Parkes, G., G. Bond, P. Barnes, and E. Charsley, *Development of a new instrument for performing microwave thermal analysis*. Review of Scientific Instruments, 2000. **71**(1): p. 168-175.
102. Nesbitt, A., P. Navabpour, B. Degamber, C. Nightingale, T. Mann, G. Fernando, and R. Day, *Development of a microwave calorimeter for simultaneous thermal analysis, infrared spectroscopy and dielectric measurements*. Measurement Science and Technology, 2004. **15**(11): p. 2313.
103. Hamilton, I., *The Development of Microwave Thermal Analysis (MWTA) and its application to the study of Carbons and other materials*. 2009, University of Huddersfield.
104. Parkes, G., P. Barnes, G. Bond, and E. Charsley, *Qualitative and quantitative aspects of microwave thermal analysis*. Thermochemica Acta, 2000. **356**(1-2): p. 85-96.
105. Solhy, A., W. Amer, M. Karkouri, R. Tahir, A. El Bouari, A. Fihri, M. Bousmina, and M. Zahouily, *Bi-functional modified-phosphate catalyzed the synthesis of  $\alpha$ - $\alpha'$ -(EE)-bis (benzylidene)-cycloalkanones: Microwave versus conventional-heating*. Journal of Molecular Catalysis A: Chemical, 2011. **336**(1-2): p. 8-15.

106. Yin, C., *Microwave-assisted pyrolysis of biomass for liquid biofuels production*. Bioresource technology, 2012. **120**: p. 273-284.
107. Nair, B.K.S., G. Parkes, P. Barnes, M. Sibley, and G. Bond, *Development of a novel instrument for microwave dielectric thermal analysis*. Review of scientific instruments, 2006. **77**(4): p. 045108.
108. Savu, S.V. *Microwave Differential Thermal Analysis Technique of the Fe<sub>2</sub>O<sub>3</sub>+ BaCO<sub>3</sub> homogeneous mixture*. in *Advanced Materials Research*. 2014. Trans Tech Publ.
109. Wagner, M., *Thermal Analysis in Practice: Collected Applications*. 2013: Mettler-Toledo.
110. Rabel Riley, S.R., *An integrated approach to thermal analysis of pharmaceutical solids*. Journal of Chemical Education, 2014. **92**(5): p. 932-935.
111. Tian, Y., X. Xu, Z. Xie, J. Zhao, and Z. Jin, *Starch retrogradation determined by differential thermal analysis (DTA)*. Food hydrocolloids, 2011. **25**(6): p. 1637-1639.
112. Martínez, L.M., M. Videa, and J. Mesquita, *Design, construction and calibration of a portable multi sample DTA setup*. Thermochimica acta, 2013. **560**: p. 89-94.
113. Morita, H., *Characterization of starch and related polysaccharides by differential thermal analysis*. Analytical Chemistry, 1956. **28**(1): p. 64-67.
114. DeBoyace, K., C. Zdaniewski, and P.L. Wildfong, *Differential scanning calorimetry isothermal hold times can impact interpretations of drug-polymer dispersability in amorphous solid dispersions*. Journal of pharmaceutical and biomedical analysis, 2018. **150**: p. 43-50.
115. Skoog, D.A., F.J. Holler, and S.R. Crouch, *Principles of instrumental analysis*. 2017: Cengage learning.
116. Robinson, J.W., E.S. Frame, and G.M. Frame II, *Undergraduate instrumental analysis*. 2014: CRC press.
117. Gabbott, P., *Principles and applications of thermal analysis*. 2008: John Wiley & Sons.
118. Bach, Q.-V. and W.-H. Chen, *Pyrolysis characteristics and kinetics of microalgae via thermogravimetric analysis (TGA): A state-of-the-art review*. Bioresource technology, 2017.
119. Sanchez-Silva, L., D. López-González, A. Garcia-Minguillan, and J. Valverde, *Pyrolysis, combustion and gasification characteristics of Nannochloropsis gaditana microalgae*. Bioresource technology, 2013. **130**: p. 321-331.
120. Warrington, S. and E. Charsley, *Thermal analysis: techniques and applications*. 1992: Royal Society of Chemistry.
121. McCrone, W. and I. Stewart, *American Laboratory*. 1996, June.
122. Dash, A.K. and P. Tyle, *Solid-state characterization of AG337 (thymitaq), a novel antitumor drug*. Journal of pharmaceutical sciences, 1996. **85**(10): p. 1123-1127.
123. Vitez, I.M., A.W. Newman, M. Davidovich, and C. Kiesnowski, *The evolution of hot-stage microscopy to aid solid-state characterizations of pharmaceutical solids*. Thermochimica Acta, 1998. **324**(1-2): p. 187-196.
124. Lewis, A.L., M.V. Gonzalez, S.W. Leppard, J.E. Brown, P.W. Stratford, G.J. Phillips, and A.W. Lloyd, *Doxorubicin eluting beads– I: Effects of drug loading on bead characteristics and drug distribution*. Journal of Materials Science: Materials in Medicine, 2007. **18**(9): p. 1691-1699.
125. Llovet, J.M., *Updated treatment approach to hepatocellular carcinoma*. Journal of gastroenterology, 2005. **40**(3): p. 225-235.

126. Bruix, J., M. Sala, and J.M. Llovet, *Chemoembolization for hepatocellular carcinoma*. Gastroenterology, 2004. **127**(5): p. S179-S188.
127. Llovet, J.M., M.I. Real, X. Montaña, R. Planas, S. Coll, J. Aponte, C. Ayuso, M. Sala, J. Muchart, and R. Solà, *Arterial embolisation or chemoembolisation versus symptomatic treatment in patients with unresectable hepatocellular carcinoma: a randomised controlled trial*. The Lancet, 2002. **359**(9319): p. 1734-1739.
128. Lewis, A.L., M.R. Dreher, V. O'Byrne, D. Grey, M. Caine, A. Dunn, Y. Tang, B. Hall, K.D. Fowers, and C.G. Johnson, *DC BeadMI™: towards an optimal transcatheter hepatic tumour therapy*. Journal of Materials Science: Materials in Medicine, 2016. **27**(1): p. 13.
129. Brown, D.B., J.E. Gould, D.A. Gervais, S.N. Goldberg, R. Murthy, S.F. Millward, W.S. Rilling, J.-F.S. Geschwind, R. Salem, and S. Vedantham, *Transcatheter therapy for hepatic malignancy: standardization of terminology and reporting criteria*. Journal of Vascular and Interventional Radiology, 2009. **20**(7): p. S425-S434.
130. Carugo, D., L. Capretto, B. Roy, M. Carboni, M. Caine, A.L. Lewis, M. Hill, S. Chakraborty, and X. Zhang, *Spatiotemporal dynamics of doxorubicin elution from embolic beads within a microfluidic network*. Journal of Controlled Release, 2015. **214**: p. 62-75.
131. Fuchs, K., R. Duran, A. Denys, P.E. Bize, G. Borchard, and O. Jordan, *Drug-eluting embolic microspheres for local drug delivery—State of the art*. Journal of Controlled Release, 2017. **262**: p. 127-138.
132. Lewis, A.L. and M.R. Dreher, *Locoregional drug delivery using image-guided intra-arterial drug eluting bead therapy*. Journal of controlled release, 2012. **161**(2): p. 338-350.
133. Liapi, E. and J.-F.H. Geschwind, *Transcatheter arterial chemoembolization for liver cancer: is it time to distinguish conventional from drug-eluting chemoembolization?* Cardiovascular and interventional radiology, 2011. **34**(1): p. 37-49.
134. Swaine, T., *Drug-Excipient Interaction Investigation using Calorimetry and Related Techniques*. 2018, University of Huddersfield.
135. Forster, R.E., S.A. Small, Y. Tang, C.L. Heaysman, A.W. Lloyd, W. Macfarlane, G.J. Phillips, M.D. Antonijevic, and A.L. Lewis, *Comparison of DC Bead-irinotecan and DC Bead-topotecan drug eluting beads for use in locoregional drug delivery to treat pancreatic cancer*. Journal of Materials Science: Materials in Medicine, 2010. **21**(9): p. 2683-2690.
136. Lewis, A.L., *DC Bead™: a major development in the toolbox for the interventional oncologist*. Expert review of medical devices, 2009. **6**(4): p. 389-400.
137. Gonzalez, M.V., Y. Tang, G.J. Phillips, A.W. Lloyd, B. Hall, P.W. Stratford, and A.L. Lewis, *Doxorubicin eluting beads—2: methods for evaluating drug elution and in-vitro: in-vivo correlation*. Journal of Materials Science: Materials in Medicine, 2008. **19**(2): p. 767-775.
138. Taylor, R.R., Y. Tang, M.V. Gonzalez, P.W. Stratford, and A.L. Lewis, *Irinotecan drug eluting beads for use in chemoembolization: in vitro and in vivo evaluation of drug release properties*. european journal of pharmaceutical sciences, 2007. **30**(1): p. 7-14.

139. Jordan, O., A. Denys, T. De Baere, N. Boulens, and E. Doelker, *Comparative study of chemoembolization loadable beads: in vitro drug release and physical properties of DC bead and hepasphere loaded with doxorubicin and irinotecan*. *Journal of vascular and interventional radiology*, 2010. **21**(7): p. 1084-1090.
140. Hatakeyama, T. and H. Hatakeyama, *Molecular relaxation of cellulosic polyelectrolytes with water*. 1992, ACS Publications.
141. Hatakeyama, H. and T. Hatakeyama, *Interaction between water and hydrophilic polymers*. *Thermochimica acta*, 1998. **308**(1-2): p. 3-22.
142. Hatakeyama, T., K. Nakamura, and H. Hatakeyama, *Vaporization of bound water associated with cellulose fibres*. *Thermochimica acta*, 2000. **352**: p. 233-239.
143. Průšová, A., P. Conte, J. Kučerík, and G. Alonzo, *Dynamics of hyaluronan aqueous solutions as assessed by fast field cycling NMR relaxometry*. *Analytical and bioanalytical chemistry*, 2010. **397**(7): p. 3023-3028.
144. Gocho, H., H. Shimizu, A. Tanioka, T.-J. Chou, and T. Nakajima, *Effect of polymer chain end on sorption isotherm of water by chitosan*. *Carbohydrate Polymers*, 2000. **41**(1): p. 87-90.
145. Maréchal, Y., M. Milas, and M. Rinaudo, *Hydration of hyaluronan polysaccharide observed by IR spectrometry. III. Structure and mechanism of hydration*. *Biopolymers: Original Research on Biomolecules*, 2003. **72**(3): p. 162-173.
146. Hunger, J., A. Bernecker, H.J. Bakker, M. Bonn, and R.P. Richter, *Hydration dynamics of hyaluronan and dextran*. *Biophysical journal*, 2012. **103**(1): p. L10-L12.
147. Mráček, A., J. Varhaníková, M. Lehocký, L. Gründelová, A. Pokopcová, and V. Velebný, *The influence of Hofmeister series ions on Hyaluronan swelling and viscosity*. *Molecules*, 2008. **13**(5): p. 1025-1034.
148. Mazeau, K. and M. Rinaudo, *The prediction of the characteristics of some polysaccharides from molecular modeling. Comparison with effective behavior*. *Food Hydrocolloids*, 2004. **18**(6): p. 885-898.
149. Xu, W., J. Riikonen, and V.-P.J.I.j.o.p. Lehto, *Mesoporous systems for poorly soluble drugs*. 2013. **453**(1): p. 181-197.
150. Hu, Y., J. Wang, Z. Zhi, T. Jiang, S.J.J.o.c. Wang, and i. science, *Facile synthesis of 3D cubic mesoporous silica microspheres with a controllable pore size and their application for improved delivery of a water-insoluble drug*. 2011. **363**(1): p. 410-417.
151. Grace, W.R. *Multifunctional Excipients for the Pharmaceutical Industry*. September, 2015 09/2015 03/03/2020]; Available from: [https://grace.com/pharma-and-biotech/en-us/Documents/Syloid/M309c\\_Syloid\\_FP\\_XDP\\_Tech\\_Note\\_0915.pdf](https://grace.com/pharma-and-biotech/en-us/Documents/Syloid/M309c_Syloid_FP_XDP_Tech_Note_0915.pdf).
152. Chemistry, R.S.o. 2020 04/12/2019]; ChemSpider | Search and Share Chemistry]. Available from: <http://www.chemspider.com/>.
153. Medicine, N.L.o. *Explore Chemistry*. 2020 [cited 2020 30/10/2020]; Available from: <https://pubchem.ncbi.nlm.nih.gov/>.
154. Saeedi, M., J. Akbari, K. Morteza-Semnani, R. Enayati-Fard, S. Sar-Reshteh-dar, and A. Soleymani, *Enhancement of dissolution rate of indomethacin: using liquisolid compacts*. *Iranian journal of pharmaceutical research: IJPR*, 2011. **10**(1): p. 25.

155. Zhang, J., R. Thakkar, Y. Zhang, and M. Maniruzzaman, *Microwave induced dielectric heating for the on-demand development of indomethacin amorphous solid dispersion tablets*. *Journal of Drug Delivery Science and Technology*, 2020: p. 102109.
156. Choudhari, Y., H. Hoefler, C. Libanati, F. Monsuur, and W. McCarthy, *Mesoporous silica drug delivery systems*, in *Amorphous Solid Dispersions*. 2014, Springer. p. 665-693.
157. Shen, S.-C., W. Kiong Ng, L. Sze Onn Chia, Y.-C. Dong, and R.J.C.p.d. Beng Hee Tan, *Applications of mesoporous materials as excipients for innovative drug delivery and formulation*. 2013. **19**(35): p. 6270-6289.
158. McCarthy, C.A., R.J. Ahern, R. Dontireddy, K.B. Ryan, and A.M.J.E.o.o.d.d. Crean, *Mesoporous silica formulation strategies for drug dissolution enhancement: a review*. 2016. **13**(1): p. 93-108.
159. Cheng, S.-H., W.-N. Liao, L.-M. Chen, and C.-H.J.J.o.M.C. Lee, *pH-controllable release using functionalized mesoporous silica nanoparticles as an oral drug delivery system*. 2011. **21**(20): p. 7130-7137.
160. Hu, Y., X. Dong, L. Ke, S. Zhang, D. Zhao, H. Chen, and X.J.J.o.m.s. Xiao, *Polysaccharides/mesoporous silica nanoparticles hybrid composite hydrogel beads for sustained drug delivery*. 2017. **52**(6): p. 3095-3109.
161. Wen, H. and Y. Qiu, *Adsorption of small drug particles at the surface of large excipients*. 2006.
162. Kiwilsza, A., A. Pajzderska, J. Mielcarek, J. Jencyk, and J.J.C.P. Wąsicki, *Dynamical properties of nimodipine molecules confined in SBA-15 matrix*. 2016. **475**: p. 126-130.
163. Murillo-Cremaes, N., A.M. López-Periago, J. Saurina, A. Roig, and C.J.T.J.o.S.F. Domingo, *Nanostructured silica-based drug delivery vehicles for hydrophobic and moisture sensitive drugs*. 2013. **73**: p. 34-42.
164. Patil, A., U. Chirmade, V. Trivedi, D. Lamprou, A. Urquhart, D.J.J.o.N. Douroumis, and Nanotechnology, *Encapsulation of water insoluble drugs in mesoporous silica nanoparticles using supercritical carbon dioxide*. 2011. **2**(3).
165. Ahern, R.J., A.M. Crean, and K.B.J.I.j.o.p. Ryan, *The influence of supercritical carbon dioxide (SC-CO<sub>2</sub>) processing conditions on drug loading and physicochemical properties*. 2012. **439**(1-2): p. 92-99.
166. Kankala, R.K., Y.S. Zhang, S.B. Wang, C.H. Lee, and A.Z.J.A.h.m. Chen, *Supercritical fluid technology: An emphasis on drug delivery and related biomedical applications*. 2017. **6**(16): p. 1700433.
167. Choudhari, Y., U. Reddy, F. Monsuur, T. Pauly, H. Hoefler, and W.J.O.M.S. McCarthy, *Comparative evaluation of porous silica based carriers for lipids and liquid drug formulations*. 2014. **1**(1).
168. Monsuur, F., Y. Choudhari, U. Reddy, W. McCarthy, I. Sadek, H. Grohgan, T. Rades, and K.J.I.J.o.P. Löbmann, *Solvent free amorphisation for pediatric formulations (minitablets) using mesoporous silica*. 2016. **511**(2): p. 1135-1136.
169. McCarthy, C.A., W. Faisal, J.P. O'Shea, C. Murphy, R.J. Ahern, K.B. Ryan, B.T. Griffin, and A.M.J.J.o.C.R. Crean, *In vitro dissolution models for the prediction of in vivo performance of an oral mesoporous silica formulation*. 2017. **250**: p. 86-95.
170. Kankala, R.K., C.-G. Liu, A.-Z. Chen, S.-B. Wang, P.-Y. Xu, L.K. Mende, C.-L. Liu, C.-H. Lee, Y.-F.J.A.B.S. Hu, and Engineering, *Overcoming multidrug resistance through the synergistic effects of hierarchical pH-sensitive, ROS-generating nanoreactors*. 2017. **3**(10): p. 2431-2442.

171. Kankala, R.K., Y. Kuthati, C.-L. Liu, C.-Y. Mou, and C.-H.J.R.A. Lee, *Killing cancer cells by delivering a nanoreactor for inhibition of catalase and catalytically enhancing intracellular levels of ROS*. 2015. **5**(105): p. 86072-86081.
172. Waters, L.J., S.A. Ahmad, G.M.J.J.o.T.A. Parkes, and Calorimetry, *Predicting the suitability of microwave formulation using microwave differential thermal analysis (MWDTA)*. 2019: p. 1-10.
173. Ibrahim, H., F. Pisano, and A. Bruno, *Polymorphism of phenylbutazone: properties and compressional behavior of crystals*. *Journal of Pharmaceutical Sciences*, 1977. **66**(5): p. 669-673.
174. Mura, P.J.J.o.P. and B. Analysis, *Analytical techniques for characterization of cyclodextrin complexes in aqueous solution: a review*. 2014. **101**: p. 238-250.
175. MATSUNAGA, J., N. NAMBU, and T. NAGAI, *Polymorphism of phenylbutazone*. *Chemical and Pharmaceutical Bulletin*, 1976. **24**(6): p. 1169-1172.
176. Guo, Z., X.M. Liu, L. Ma, J. Li, H. Zhang, Y.P. Gao, and Y. Yuan, *Effects of particle morphology, pore size and surface coating of mesoporous silica on Naproxen dissolution rate enhancement*. *Colloids and Surfaces B: Biointerfaces*, 2013. **101**: p. 228-235.
177. Hussain, T., L.J. Waters, G.M. Parkes, Y.J.C. Shahzad, S.A. Physicochemical, and E. Aspects, *Microwave processed solid dispersions for enhanced dissolution of gemfibrozil using non-ordered mesoporous silica*. 2017. **520**: p. 428-435.
178. Al-Oweini, R. and H.J.J.o.M.S. El-Rassy, *Synthesis and characterization by FTIR spectroscopy of silica aerogels prepared using several Si (OR)<sub>4</sub> and R'' Si (OR)<sub>3</sub> precursors*. 2009. **919**(1-3): p. 140-145.
179. Bertoluzza, A., C. Fagnano, M.A. Morelli, V. Gottardi, and M.J.J.o.N.-C.S. Guglielmi, *Raman and infrared spectra on silica gel evolving toward glass*. 1982. **48**(1): p. 117-128.
180. Xia, X., C. Zhou, L. Ballell, and A.E. Garcia-Bennett, *In vivo Enhancement in Bioavailability of Atazanavir in the Presence of Proton-Pump Inhibitors using Mesoporous Materials*. *ChemMedChem*, 2012. **7**(1): p. 43-48.
181. Hussain, T., L.J. Waters, G.M. Parkes, and Y. Shahzad, *Microwave processed solid dispersions for enhanced dissolution of gemfibrozil using non-ordered mesoporous silica*. *Colloids and Surfaces A: Physicochemical and Engineering Aspects*, 2017. **520**: p. 428-435.
182. Guo, Z., X.-M. Liu, L. Ma, J. Li, H. Zhang, Y.-P. Gao, Y.J.C. Yuan, and S.B. Biointerfaces, *Effects of particle morphology, pore size and surface coating of mesoporous silica on Naproxen dissolution rate enhancement*. 2013. **101**: p. 228-235.
183. Lin, S.-Y., H.-L. Lin, Y.-T. Chi, Y.-T. Huang, C.-Y. Kao, and W.-H.J.I.j.o.p. Hsieh, *Thermoanalytical and Fourier transform infrared spectral curve-fitting techniques used to investigate the amorphous indomethacin formation and its physical stability in Indomethacin-Soluplus® solid dispersions*. 2015. **496**(2): p. 457-465.
184. Li, J., L. Xu, H. Wang, B. Yang, H. Liu, W. Pan, S.J.M.S. Li, and E. C, *Comparison of bare and amino modified mesoporous silica@ poly (ethyleneimine) s xerogel as indomethacin carrier: Superiority of amino modification*. 2016. **59**: p. 710-716.
185. Palazi, E., E. Karavas, P. Barmpalexis, M. Kostoglou, S. Nanaki, E. Christodoulou, and D.N.J.E.J.o.P.S. Bikiaris, *Melt extrusion process for adjusting drug release of poorly water soluble drug felodipine using different polymer matrices*. 2018. **114**: p. 332-345.

186. Kaffash, E., A. Badiee, A. Akhgari, N.A. Rezayat, M. Abbaspour, F.J.J.o.D.D.S. Saremnejad, and Technology, *Development and characterization of a multiparticulate drug delivery system containing indomethacin-phospholipid complex to improve dissolution rate*. 2019: p. 101177.
187. Zeleňák, V., D. Halamová, M. Almáši, L. Žid, A. Zeleňáková, and O.J.A.S.S. Kapusta, *Ordered cubic nanoporous silica support MCM-48 for delivery of poorly soluble drug indomethacin*. 2018. **443**: p. 525-534.
188. Van Speybroeck, M., V. Barillaro, T. Do Thi, R. Mellaerts, J. Martens, J. Van Humbeeck, J. Vermant, P. Annaert, G. Van Den Mooter, and P.J.J.o.p.s. Augustijns, *Ordered mesoporous silica material SBA-15: a broad-spectrum formulation platform for poorly soluble drugs*. 2009. **98**(8): p. 2648-2658.
189. Li, Y., J. Rantanen, M. Yang, and A. Bohr, *Molecular structure and impact of amorphization strategies on intrinsic dissolution of spray dried indomethacin*. *European Journal of Pharmaceutical Sciences*, 2019. **129**: p. 1-9.
190. McCarthy, C.A., W. Faisal, J.P. O'Shea, C. Murphy, R.J. Ahern, K.B. Ryan, B.T. Griffin, and A.M. Crean, *In vitro dissolution models for the prediction of in vivo performance of an oral mesoporous silica formulation*. *Journal of Controlled Release*, 2017. **250**: p. 86-95.
191. Aerts, C.A., E. Verraedt, R. Mellaerts, A. Depla, P. Augustijns, J. Van Humbeeck, G. Van den Mooter, and J.A. Martens, *Tunability of pore diameter and particle size of amorphous microporous silica for diffusive controlled release of drug compounds*. *The Journal of Physical Chemistry C*, 2007. **111**(36): p. 13404-13409.
192. Böttcher, H., P. Slowik, and W. Süß, *Sol-gel carrier systems for controlled drug delivery*. *Journal of sol-gel science and technology*, 1998. **13**(1-3): p. 277-281.
193. Qu, F., G. Zhu, S. Huang, S. Li, J. Sun, D. Zhang, and S. Qiu, *Controlled release of Captopril by regulating the pore size and morphology of ordered mesoporous silica*. *Microporous and Mesoporous Materials*, 2006. **92**(1-3): p. 1-9.
194. Kender, D.N. and R.E. Schiesswohl, *Imipramine hydrochloride*, in *Analytical Profiles of Drug Substances*. 1985, Elsevier. p. 37-75.
195. Tahir, H., Y. Shahzad, L.J. Waters, T. Hussain, A.M. Yousaf, T. Mahmood, and R. Sheikh, *Impact of processing methods on the dissolution of artemether from two non-ordered mesoporous silicas*. *European Journal of Pharmaceutical Sciences*, 2018. **112**: p. 139-145.
196. Shahzad, Y., S. Sohail, M.S. Arshad, T. Hussain, and S.N.H. Shah, *Development of solid dispersions of artemisinin for transdermal delivery*. *International journal of pharmaceutics*, 2013. **457**(1): p. 197-205.
197. Waters, L.J., T. Hussain, G. Parkes, J.P. Hanrahan, and J.M. Tobin, *Inclusion of fenofibrate in a series of mesoporous silicas using microwave irradiation*. *European Journal of Pharmaceutics and Biopharmaceutics*, 2013. **85**(3): p. 936-941.
198. Zhang, Y., Z. Zhi, T. Jiang, J. Zhang, Z. Wang, and S. Wang, *Spherical mesoporous silica nanoparticles for loading and release of the poorly water-soluble drug telmisartan*. *Journal of Controlled Release*, 2010. **145**(3): p. 257-263.
199. Srivastava, R. and A. Nagappa, *Surface activity in drug action*. Vol. 21. 2005: Elsevier.
200. Yalkowsky, S. and R.J.C.o.P. Dannenfelser, Univ. of Ariz, Tucson, Az, *Aquasol database of aqueous solubility, Version 5*. 1992.

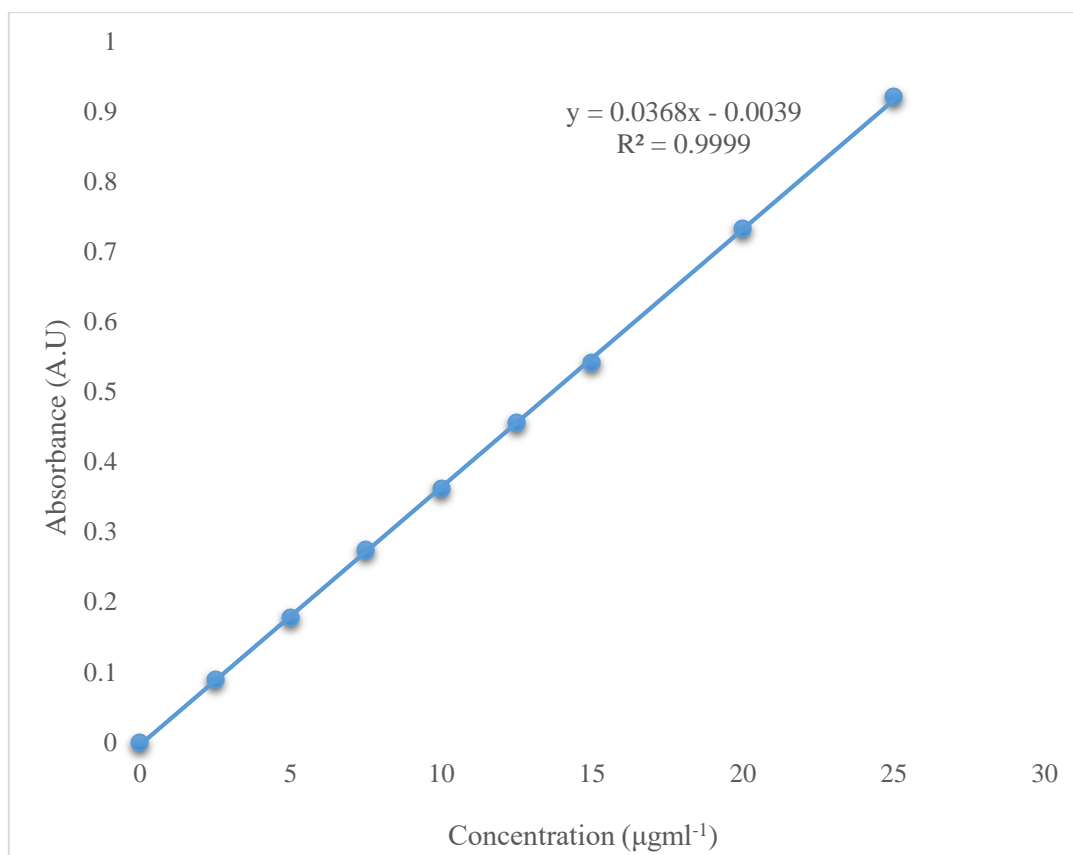


201. Ramey, K., J.D. Ma, B.M. Best, R.S. Atayee, and C.M.J.J.o.a.t. Morello, *Variability in metabolism of imipramine and desipramine using urinary excretion data*. 2014. **38**(6): p. 368-374.
202. Linnell, T., J. Riikonen, J. Salonen, A.M. Kaukonen, L. Laitinen, J. Hirvonen, and V.-P. Lehto, *Surface chemistry and pore size affect carrier properties of mesoporous silicon microparticles*. International journal of pharmaceutics, 2007. **343**(1-2): p. 141-147.
203. Riikonen, J., E. Mäkilä, J. Salonen, and V.-P. Lehto, *Determination of the physical state of drug molecules in mesoporous silicon with different surface chemistries*. Langmuir, 2009. **25**(11): p. 6137-6142.
204. Martín, A., R. García, D.S. Karaman, and J.J.J.o.m.s. Rosenholm, *Polyethyleneimine-functionalized large pore ordered silica materials for poorly water-soluble drug delivery*. 2014. **49**(3): p. 1437-1447.
205. Hu, Y., J. Wang, Z. Zhi, T. Jiang, and S. Wang, *Facile synthesis of 3D cubic mesoporous silica microspheres with a controllable pore size and their application for improved delivery of a water-insoluble drug*. Journal of Colloid and Interface Science, 2011. **363**(1): p. 410-417.
206. Martín, A., R.A. García, D.S. Karaman, and J.M. Rosenholm, *Polyethyleneimine-functionalized large pore ordered silica materials for poorly water-soluble drug delivery*. Journal of Materials Science, 2014. **49**(3): p. 1437-1447.
207. Parkes, G.M.B., P.A. Barnes, E.L. Charsley, and G. Bond, *Microwave thermal analysis - a new approach to the study of the thermal and dielectric properties of materials*. Journal of Thermal Analysis and Calorimetry, 1999. **56**(2): p. 723-731.
208. Parkes, G.M.B., P.A. Barnes, G. Bond, and E.L. Charsley, *Qualitative and quantitative aspects of microwave thermal analysis*. Thermochemica Acta, 2000. **356**(1-2): p. 85-96.
209. Nair, B.K.S., G.M.B. Parkes, P.A. Barnes, M.J.N. Sibley, and G. Bond, *Development of a novel instrument for microwave dielectric thermal analysis*. Review of Scientific Instruments, 2006. **77**(4).
210. Parkes, G.M.B., G. Bond, P.A. Barnes, and E.L. Charsley, *Development of a new instrument for performing microwave thermal analysis*. Review of Scientific Instruments, 2000. **71**(1): p. 168-175.
211. Savu, S.V., *Microwave differential thermal analysis technique of the  $Fe_2O_3 + BaCo_3$  homogeneous mixture*, in *Advanced Materials Research*. 2014. p. 24-29.
212. Nesbitt, A., P. Navabpour, B. Degamber, C. Nightingale, T. Mann, G. Fernando, and R.J. Day, *Development of a microwave calorimeter for simultaneous thermal analysis, infrared spectroscopy and dielectric measurements*. Measurement Science and Technology, 2004. **15**(11): p. 2313-2324.
213. Parkes, G., P. Barnes, E. Charsley, and G. Bond, *Microwave differential thermal analysis in the investigation of thermal transitions in materials*. Analytical Chemistry, 1999. **71**(22): p. 5026-5032.
214. Pinto, L.M.A., L.F. Fraceto, M.H.A. Santana, T.A. Pertinhez, S. Oyama Jr, and E. De Paula, *Physico-chemical characterization of benzocaine- $\beta$ -cyclodextrin inclusion complexes*. Journal of Pharmaceutical and Biomedical Analysis, 2005. **39**(5): p. 956-963.
215. Avula, S.G.C., K. Alexander, and A. Riga, *Thermal analytical characterization of mixtures of antipsychotic drugs with various excipients for improved drug delivery*. Journal of Thermal Analysis and Calorimetry, 2016. **123**(3): p. 1981-1992.

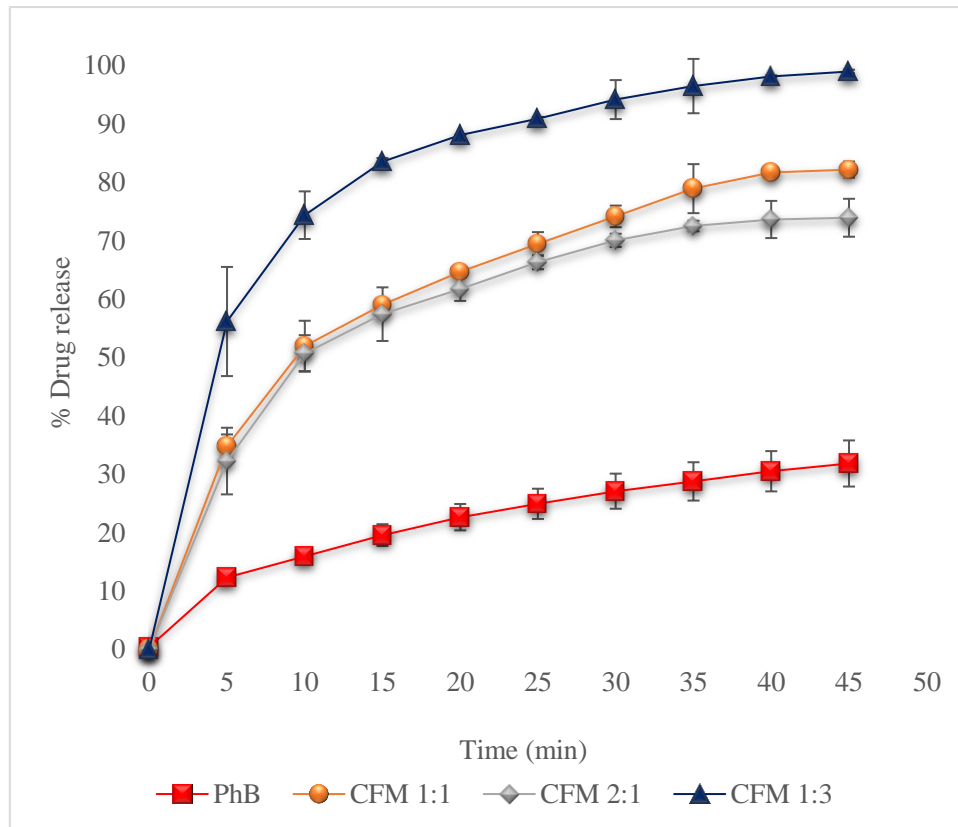
216. Lin, H.L., G.C. Zhang, and S.Y. Lin, *Real-time co-crystal screening and formation between indomethacin and saccharin via DSC analytical technique or DSC-FTIR microspectroscopy*. Journal of Thermal Analysis and Calorimetry, 2015. **120**(1): p. 679-687.
217. Oliveira, L.J., N.C.F. Stofella, A. Veiga, S. Féderle, M. da Graça T. Toledo, L.S. Bernardi, P.R. Oliveira, M.A.S. Carvalho Filho, I.F. Andrezza, and F.S. Murakami, *Physical–chemical characterization studies of ketoprofen for orodispersible tablets*. Journal of Thermal Analysis and Calorimetry, 2018. **133**(3): p. 1521-1533.
218. Forni, F., G. Coppi, V. Iannuccelli, and R. Cameroni, *Thermal behaviour of melt crystallized phenylbutazone*. Journal of Thermal Analysis, 1990. **36**(1): p. 35-44.
219. Maswadeh, H.M., *Incompatibility study of ibuprofen in ternary interactive mixture by using differential scanning calorimetry*. Journal of Thermal Analysis and Calorimetry, 2016. **123**(3): p. 1963-1971.
220. Guo, Z., X.-M. Liu, L. Ma, J. Li, H. Zhang, Y.-P. Gao, and Y. Yuan, *Effects of particle morphology, pore size and surface coating of mesoporous silica on Naproxen dissolution rate enhancement*. Colloids and Surfaces B: Biointerfaces, 2013. **101**: p. 228-235.
221. Zhu, Q., M.T. Harris, and L.S. Taylor, *Modification of crystallization behavior in drug/polyethylene glycol solid dispersions*. Molecular pharmaceutics, 2012. **9**(3): p. 546-553.
222. Greco, K. and R. Bogner, *Solution-mediated phase transformation of haloperidol mesylate in the presence of sodium lauryl sulfate*. AAPS PharmSciTech, 2011. **12**(3): p. 909-916.
223. Asare-Addo, K., M. Alshafiee, K. Walton, A. Ward, A.-M. Totea, S. Taheri, N. Mawla, A.O. Adebisi, S. Elawad, and C. Diza, *Effect of preparation method on the surface properties and UV imaging of indomethacin solid dispersions*. European Journal of Pharmaceutics and Biopharmaceutics, 2019. **137**: p. 148-163.
224. Kaushik, S. and K. PATHAK, *Development and evaluation of monolithic osmotic tablet of Ketoprofen: Using solid dispersion technique*. Int J Pharm Pharm Sci, 2016. **8**: p. 41-7.
225. Gana, I., M. Barrio, B. Do, J.-L. Tamarit, R. Céolin, and I.B. Rietveld, *Benzocaine polymorphism: pressure–temperature phase diagram involving forms II and III*. International journal of pharmaceutics, 2013. **456**(2): p. 480-488.
226. Rabel Riley, S.R., *An integrated approach to thermal analysis of pharmaceutical solids*. Journal of Chemical Education, 2015. **92**(5): p. 932-935.
227. Mura, P., *Analytical techniques for characterization of cyclodextrin complexes in the solid state: A review*. Journal of Pharmaceutical and Biomedical Analysis, 2015. **113**: p. 226-238.
228. Kappe, C.O., A. Stadler, and D. Dallinger, *Microwaves in organic and medicinal chemistry*. 2012: John Wiley & Sons.
229. Van Duong, T., D. Lüdeker, P.-J. Van Bockstal, T. De Beer, J. Van Humbeeck, and G. Van den Mooter, *Polymorphism of indomethacin in semicrystalline dispersions: Formation, transformation, and segregation*. Molecular pharmaceutics, 2018. **15**(3): p. 1037-1051.
230. Dalmoro, A., S. Bochicchio, S.F. Nasibullin, P. Bertocin, G. Lamberti, A.A. Barba, and R.I. Moustafine, *Polymer-lipid hybrid nanoparticles as enhanced indomethacin delivery systems*. European Journal of Pharmaceutical Sciences, 2018.

231. Moneghini, M., G. Zingone, and N. De Zordi, *Influence of the microwave technology on the physical–chemical properties of solid dispersion with Nimesulide*. Powder technology, 2009. **195**(3): p. 259-263.
232. Waters, L.J., T.S. Swaine, and A.L. Lewis, *A calorimetric investigation of doxorubicin–polymer bead interactions*. International journal of pharmaceutics, 2015. **493**(1-2): p. 129-133.
233. Lewis, A.L., M.V. Gonzalez, A.W. Lloyd, B. Hall, Y. Tang, S.L. Willis, S.W. Leppard, L.C. Wolfenden, R.R. Palmer, and P.W. Stratford, *DC bead: in vitro characterization of a drug-delivery device for transarterial chemoembolization*. Journal of vascular and interventional radiology, 2006. **17**(2): p. 335-342.
234. Namur, J., M. Wassef, J. Pelage, A. Lewis, M. Manfait, and A. Laurent, *Infrared microspectroscopy analysis of ibuprofen release from drug eluting beads in uterine tissue*. Journal of controlled release, 2009. **135**(3): p. 198-202.
235. Hatakeyama, T., M. Tanaka, and H. Hatakeyama, *Studies on bound water restrained by poly (2-methacryloyloxyethyl phosphorylcholine): comparison with polysaccharide–water systems*. Acta Biomaterialia, 2010. **6**(6): p. 2077-2082.
236. Tanaka, M. and A. Mochizuki, *Effect of water structure on blood compatibility—thermal analysis of water in poly (meth) acrylate*. Journal of Biomedical Materials Research Part A, 2004. **68**(4): p. 684-695.
237. Tanaka, M., T. Motomura, N. Ishii, K. Shimura, M. Onishi, A. Mochizuki, and T. Hatakeyama, *Cold crystallization of water in hydrated poly (2-methoxyethyl acrylate)(PMEA)*. Polymer international, 2000. **49**(12): p. 1709-1713.
238. Bertasa, M., T. Poli, C. Riedo, V. Di Tullio, D. Capitani, N. Proietti, C. Canevali, A. Sansonetti, and D. Scalarone, *A study of non-bounded/bounded water and water mobility in different agar gels*. Microchemical Journal, 2018. **139**: p. 306-314.
239. Hatakeyama, T. and H. Hatakeyama, *Lignin. Thermal properties of green polymers and biocomposites*. 2004, Kluwer Academic Publishers, Netherlands.
240. Ashrafi, K., Y. Tang, H. Britton, O. Domenge, D. Blino, A.J. Bushby, K. Shuturminska, M. den Hartog, A. Radaelli, and A.H. Negussie, *Characterization of a novel intrinsically radiopaque drug-eluting bead for image-guided therapy: DC Bead LUMI™*. Journal of Controlled Release, 2017. **250**: p. 36-47.
241. Talik, P. and U. Hubicka, *The DSC approach to study non-freezing water contents of hydrated hydroxypropylcellulose (HPC)*. Journal of Thermal Analysis and Calorimetry, 2018. **132**(1): p. 445-451.
242. Hatakeyama, H. and T. Hatakeyama, *Thermal properties of freezing bound water restrained by sodium lignosulfonate-based polyurethane hydrogels*. Journal of Thermal Analysis and Calorimetry, 2019. **135**(4): p. 2039-2048.
243. Mlčoch, T. and J. Kučerík, *Hydration and drying of various polysaccharides studied using DSC*. Journal of thermal analysis and calorimetry, 2013. **113**(3): p. 1177-1185.

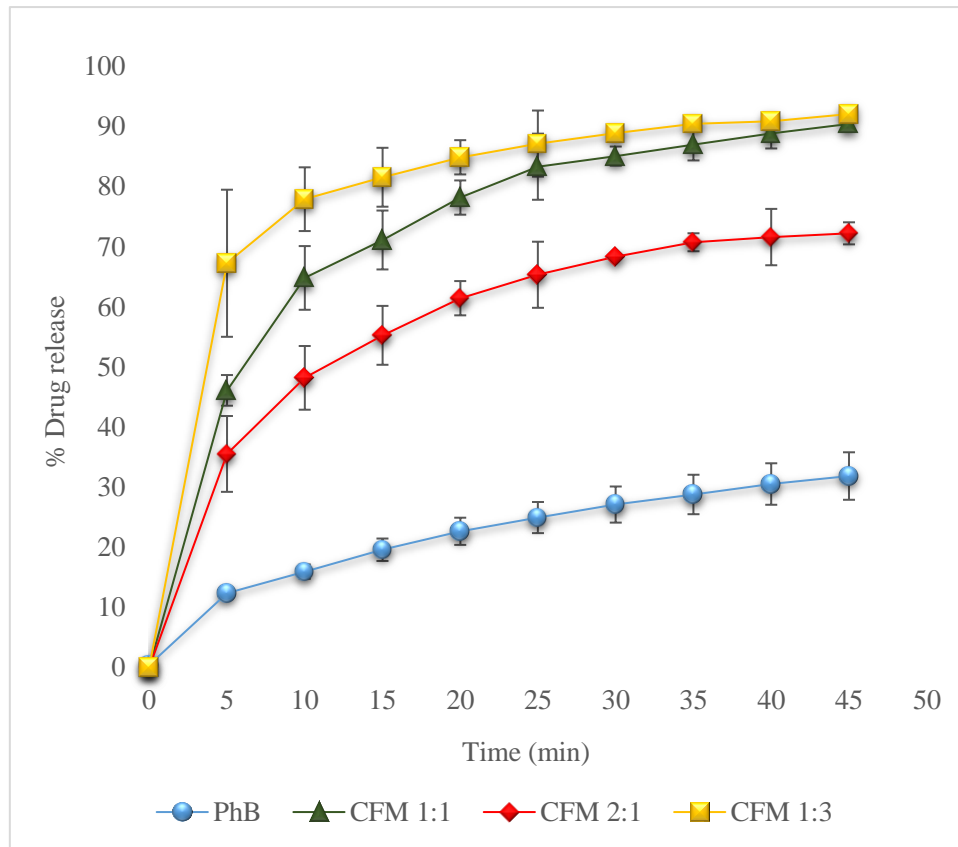
**Appendix 1:** Graph of Absorbance (A.U) versus Concentration ( $\mu\text{gml}^{-1}$ ) of Phenylbutazone



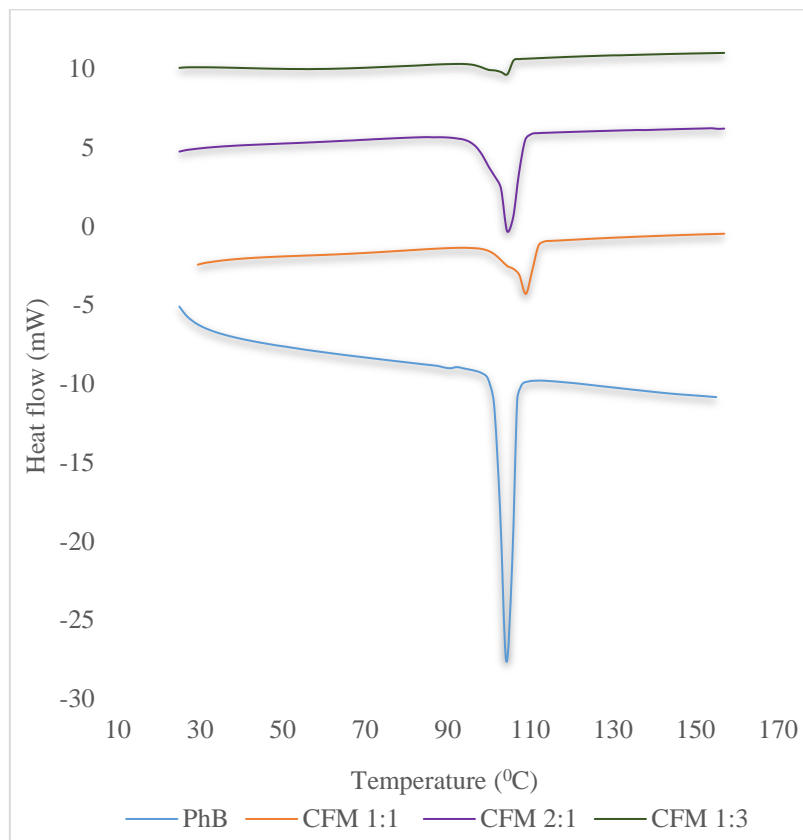
**Appendix 2:** Release profiles for phenylbutazone (PhB), Syloid® XDP 3050 based formulations using conventional method at 1:1, 2:1 and 1:3 drug to silica ratios. Each data point represents the mean of triplicate results ( $\pm$ SD).



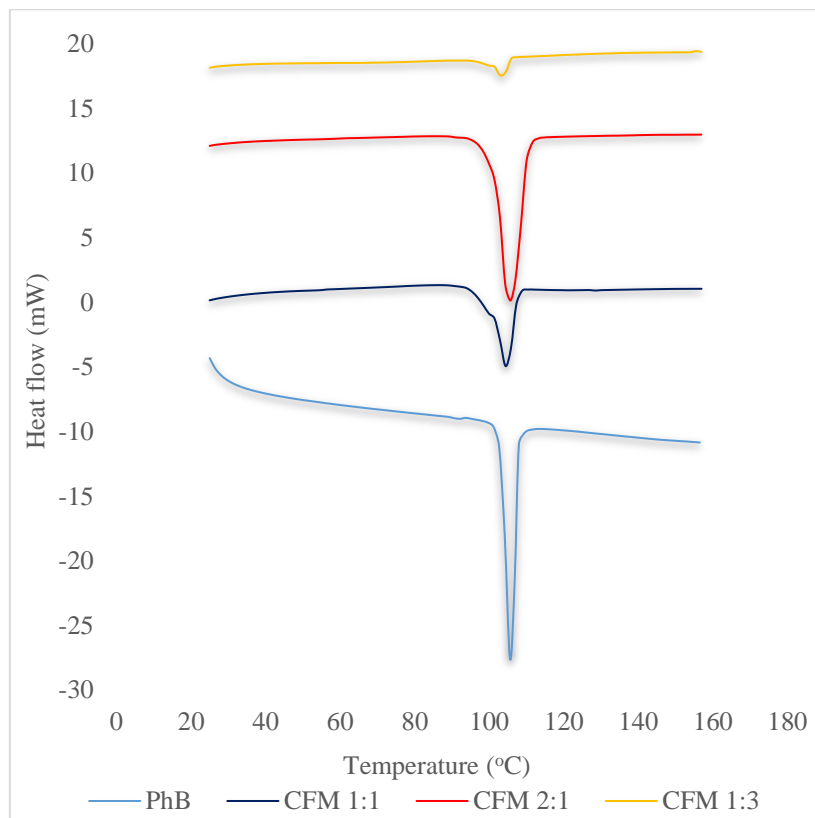
**Appendix 3:** Release profiles for phenylbutazone (PhB), Syloid® XDP 3150 based formulations using conventional method at 1:1, 2:1 and 1:3 drug to silica ratios. Each data point represents the mean of triplicate results ( $\pm$ SD).



**Appendix 4:** DSC profiles for phenylbutazone (PhB), and conventional formulation (CFM) of PhB: XDP 3050 at 1:1, 2:1 and 1:3 drug to silica ratios

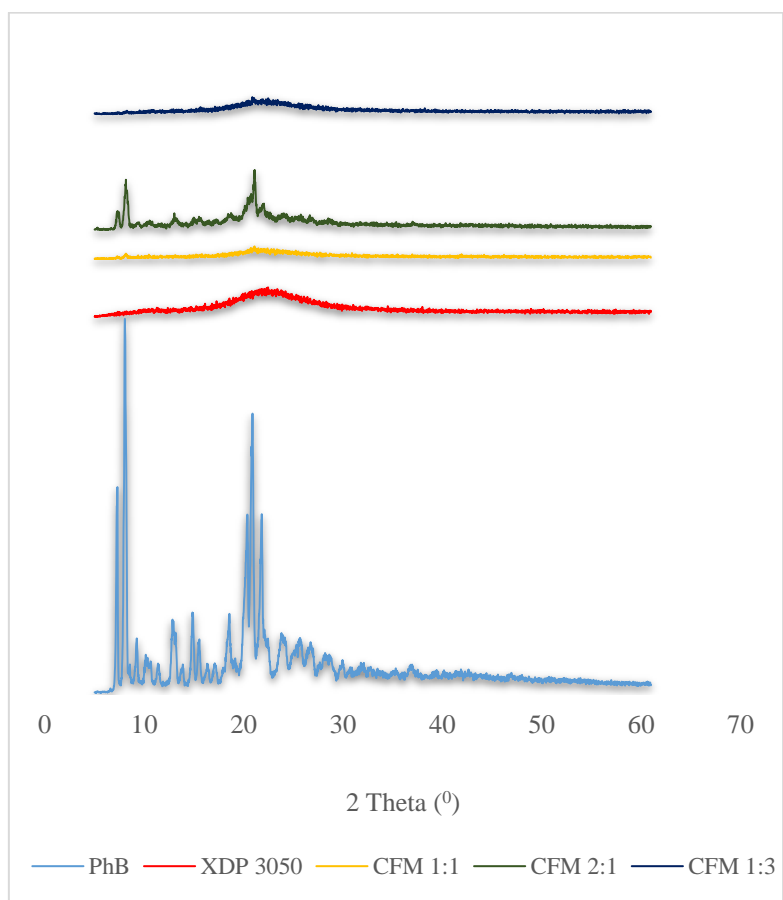


**Appendix 5:** DSC profiles for phenylbutazone (PhB), and conventional formulation (CFM) of PhB:XDP 3150 at 1:1, 2:1 and 1:3 drug to silica ratios

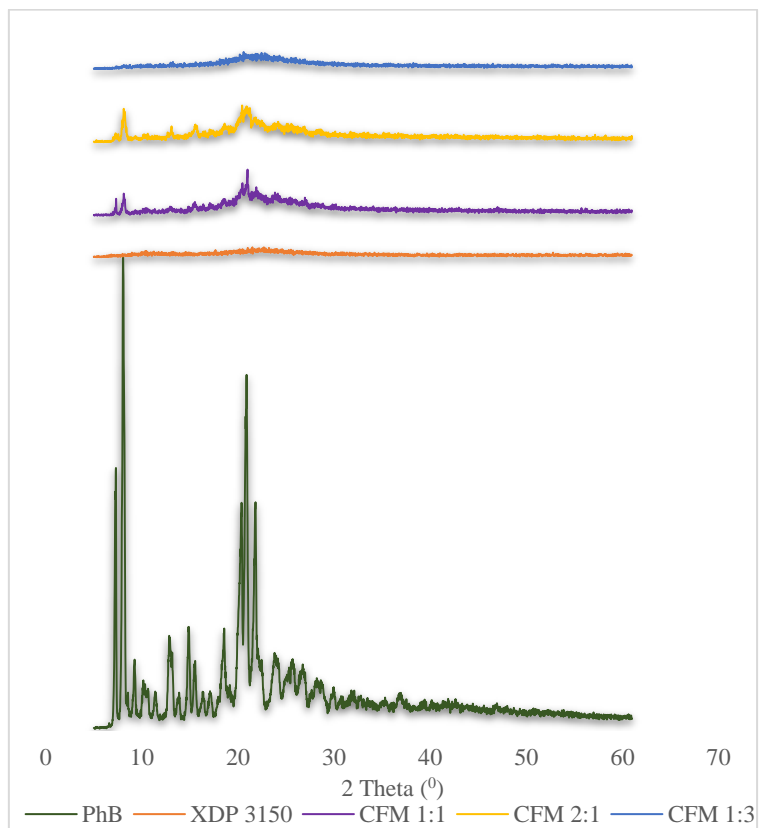




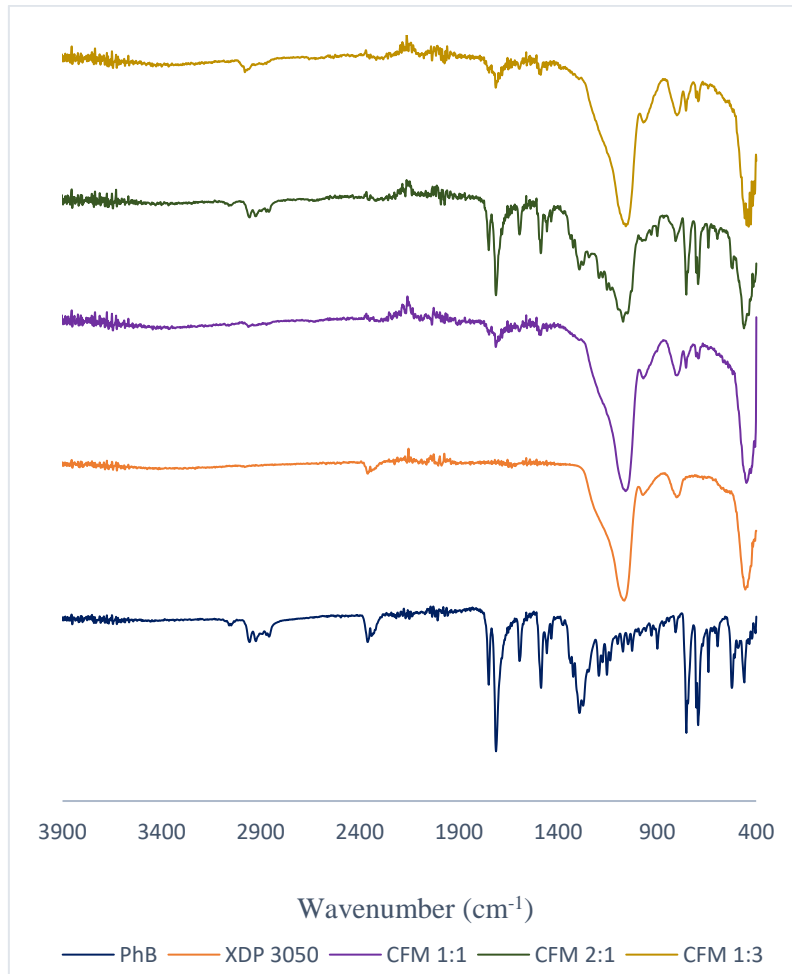
**Appendix 6:** XRD patterns for (a) PhB, (b) XDP 3050, (c) CFM 1:1, (d) CFM 2:1 and (e) CFM 1:3.



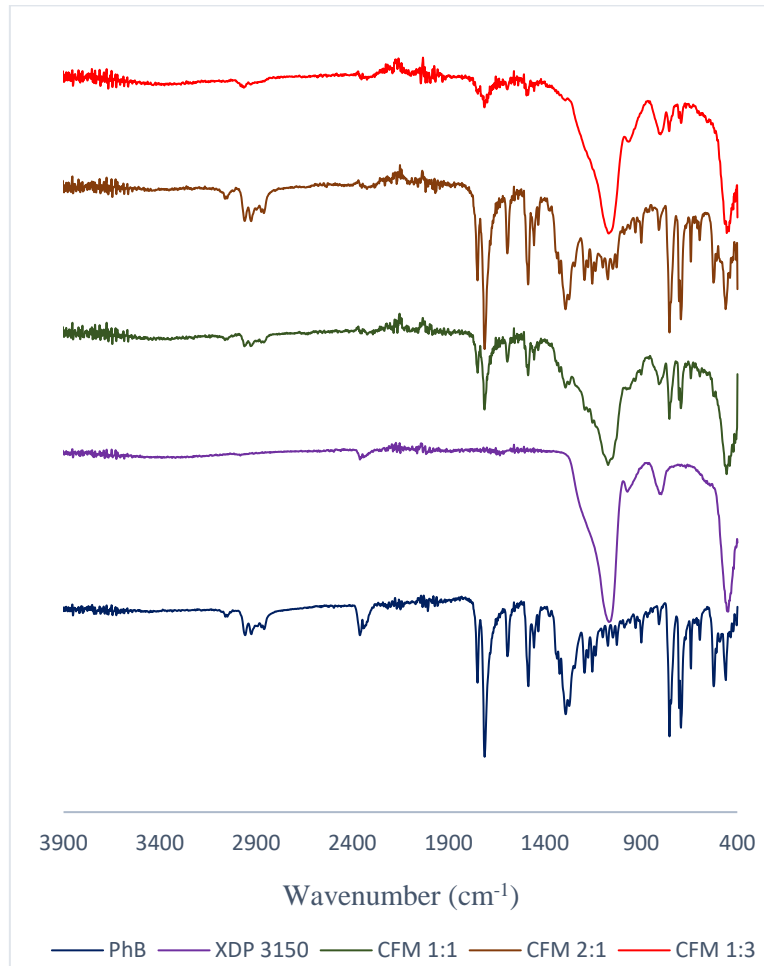
**Appendix 7:** XRD patterns for (a) PhB, (b) XDP 3150, (c) CFM 1:1, (d) CFM 2:1 and (e) CFM 1:3.



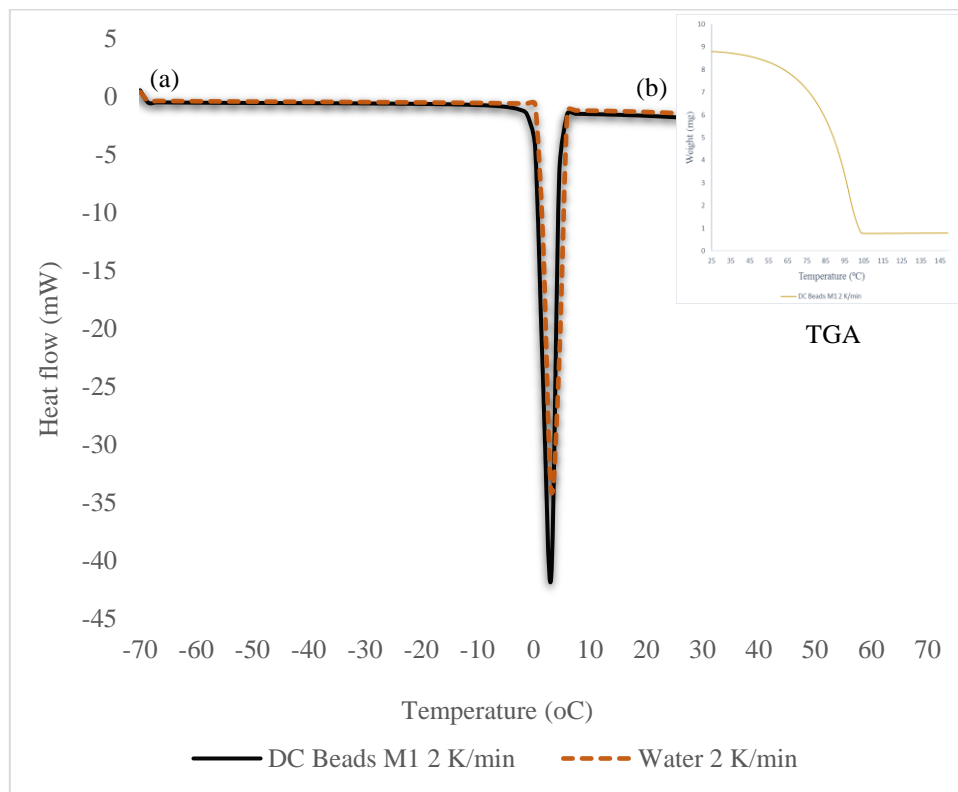
**Appendix 8:** FT-IR analysis of (a) PhB (b) XDP 3050, (c) CFM 1:1, (d) CFM 2:1, and (e) CFM 1:3 drug-XDP 3050 formulations



**Appendix 9:** FT-IR analysis of (a) PhB (b) XDP 3150, (c) CFM 1:1, (d) CFM 2:1, and (e) CFM 1:3 drug-XDP 3050 formulations



**Appendix 10:** DSC profiles of (a) DC beads M1, water and (b) TGA of DC beads M1 heated at a rate of 2 K/min from -70 to 70 °C.



## **Appendix 11**

### **Conference attended**

PGR Conference 2016, University of Huddersfield, Huddersfield, UK, 2016.

10<sup>th</sup> International conference and exhibition on pharmaceuticals and novel drug delivery systems, London, UK, 2017